THE DEPOSITIONAL HISTORY AND EVALUATION OF TWO LATE QUATERNARY, DIAMONDIFEROUS POCKET BEACHES, SOUTH - WESTERN NAMIBIA

Michael George Millad

January 2004

THE DEPOSITIONAL HISTORY AND EVALUATION OF TWO LATE QUATERNARY, DIAMONDIFEROUS POCKET BEACHES, SOUTH-WESTERN NAMIBIA

by

Michael George Millad

Thesis submitted in partial fulfilment of the requirements
for the degree of Master of Science in Economic Geology

Department of Geology
Rhodes University
January 2004

THESIS DECLARATION

The material contained in this thesis is the result of my own research, except where otherwise acknowledged or referenced in the text. The work was carried out between November 1997 and December 2003 at Oranjemund, Namibia and in Cape Town, South Africa.

M.G. Millad

ACKNOWLEDGEMENTS

First and foremost, I would like to thank the Namdeb Diamond Corporation (Pty) Ltd. for providing the funding and equipment necessary to conduct this study, and for generously granting permission for some of the results of the pocket beach evaluation to be written up. I would particularly like to single out Mr. Bob Burrell, the Mineral Resource Manager at Namdeb, for his kind support in this regard. I would also like to take this opportunity to thank Namdeb and Mr. Burrell for allowing me the time off work to go to Grahamstown and complete the block modules for this degree. I am hugely indebted to both of the aforementioned, and sincerely hope that the findings of this thesis can contribute meaningfully to the knowledge base of Namdeb.

This thesis was co-supervised by Dr. John Ward of De Beers, Prof. Brian Bluck of the University of Glasgow, and Prof. John Moore of Rhodes University. Myself and this thesis have benefited greatly from the knowledge imparted by Professors Bluck and Moore during numerous field trips, talks and debates over the course of the last few years; many thanks to you gentlemen for all your help. A very special word of thanks must go to Dr. John Ward, who, in many ways, was the person who most inspired me to initiate this study. Dr. Ward is filled with a level of enthusiasm for the subject of geology that buoys up all those around him, myself included, and he has freely shared his remarkable knowledge on the subject of alluvial diamonds with me. Dr. Ward gave generously of his time, mostly after work hours, to assist me with this thesis, and his insightful and thorough reviews of drafts of this text are particularly appreciated.

The successful completion of the pocket beach evaluation programme involved numerous people, without whose splendid efforts this study would not have been possible. A very special word of thanks to Keith Childs and his team, who looked after the logistics of this remote project under difficult conditions, the severe winds of the Sperrgebiet not being the least of these! I will carry to my grave the fond memories of the time I spent in the field with you fellows. Thanks to Colin Britz for seeing to it that the GB50 sampling was of a high quality. To the Rosond contractors, under the able leadership of Paul Coetzee, Bertie and Wimpie, who operated the delineation drill rigs and GB50, a great word of thanks. Renato Spaggiari and Leonard Apollus logged most of the delineation drill holes at Site 2 and some of those at Site 3 prior to the author's arrival on the pocket beach project; many thanks to you gentlemen. Thank you too to Andre Fourie, who did the pocket beach surveying, as well as to Annette, Wimpie, Johan W and all the other guys

in the drawing office. Tony Goosen, chief surveyor, is thanked for arranging the flying of the very useful Airborne Laser Survey. Many thanks to Ralph Scholz, who always found the time to help me with the GIS and 3-D modeling software packages, both of which played a large role in the completion of this study. A special word of thanks must go to Marais Loubser and Kai-Uwe Molzahn, and the rest of their team, who managed the X-Ray unit that recovered the pocket beach diamonds, and who delivered great support to the remote sampling operations. Thanks to some of the other sections at Namdeb, who from time to time provided vital logistical support – I would like to single out electricians Christie and Henk, instrumentation specialist Mark Kemp, town garage foreman Dave Hockney and security officer Kevin Bam. To Antonie, Wayne and Lourens – thanks for doing the tough job of conducting gravel screening analyses. Thanks to Elana Groenewald and her team of ladies at the Namdeb Geolab, who sorted the pocket beach samples. I want to thank my ex-colleagues, with whom I had many fruitful and thought-stimulating discussions, especially Jana and Jurgen Jacob, Renato Spaggiari and Marais Loubser. I would also like to thank Dawn Jones, Christa Keyser, Colleen Parkins and Ronel van der Merwe, all of whom played a role in the pocket beach project. My deep appreciation to John Pether, for expertly identifying and interpreting the shell assemblages; his work had an important bearing on some of the main findings of this thesis. Thanks to Dr. Iain Robertson and his team at the Council for Scientific and Industrial Research for dating the shells. To Ashley Goddard, who helped me with many queries and administrative matters at Rhodes University, thank you for your assistance. I would also like to thank my new colleagues, Sean Duggan and Dr. Andy Grills, for their input into the estimation of the pocket beach deposits, and for generously allowing me to print this thesis using De Beers' resources. Thanks to Chris Prins and Clyde Mallinson for some helpful discussions around the subject of lognormal distributions and lognormal estimators.

Last, but by no means least, I would like to thank my wife, Georgia, for her unwavering support and encouragement during the writing of this thesis and for putting up with a husband who disappeared into the black hole of his study almost every week-end over the course of this last year.

CONTENTS

LIST OF FIGURES

Figure 2.5. The stratigraphic framework for important Tertiary and Quaternary deposits of the Sperrgebiet and the coast of Namaqualand. Sources are Hallam, C.D. (1964), Stocken (1978), Siesser and Salmon, (1979), Haq *et al*, (1987), Corbett (1989; 1996), Pickford and Senut (1999), Ward and Bluck (1997), Ward (2000), Pether, (2000) and J.S. Marsh (pers. comm., 2002).

Figure 2.6. A marine gravel layer at Buntfeldschuh, showing the clast assemblage that typifies the Eocene succession in the Sperrgebiet. Clast Types: yc=yellow chalcedony, rj=red jasper, bi=banded ironstone, ag=agate and rvq=well rounded vein quartz. Scale is 150mm long.

Figure 2.7. A schematic cross-section of the gravel beach deposits on MA1 (modified after C.D. Hallam, 1964 and J. Jacob, 2001).

Figure 2.8. The positions of current aeolian transport corridors in the deflation basin (after Corbett, 1989).

Figure 3.1. The positions of Frankipile holes, small-diameter delineation drill holes, GB50 sample clusters and the bulk sampling trench at Site 2.

Figure 3.2. The positions of Frankipile holes, small-diameter delineation drill holes and GB50 sample clusters at Site 3.

Figure 3.3. The mud drill rig used to conduct small diameter delineation drilling at pocket beach Sites 2 and 3. This drilling constituted the first phase of a recent (1997 to 2002) evaluation programme. The inset shows a hollow-core bit that was used.

Figure 3.4. A three-dimensional view from the southwest, in Vuloan©, of the bedrock surface and buried marine gravel body at Site 2. The green crosses at the top of the borehole traces are the positions of the hole collars. Vertical exaggeration is 10x. Width of view is approximately 1 km.

Figure 3.5. Taking a GB50 sample - i) Digging in of the standpipe, pumping a mud medium of attapulgite and sea water into the hole and beginning excavation. ii) Discarding the sand and grit overburden. iii) Careful placing of the marine gravel sample in a 12 ton multibucket. iv) Transport of the gravel to the heavy mineral separation treatment plant.

Figure 3.6. Heavy Mineral (HM) Separation process for the Site 2 Trench and GB50 samples - i) Tipping bin, 90 mm grizzly and 2 mm de-sanding screen (-2 mm and +90 mm material removed). ii) The scrubber and 16 mm trommel (+16 mm material removed). iii) +2-16 mm feed to 200 mm cyclone (HM separator – using ferrosilicon medium). iv) Discharge chute for floats and +16-90 mm material from scrubber. The orange

Figure 4.24. The imbricate zone of Gravel Unit 3, as seen in the Site 2 trench. Note the abundance of small, tightly-packed discoidal clasts which define the imbrication. View is towards the north. Scale is 30 cm.

Figure 4.25. The washover deposit associated with Gravel Unit 3. The washover zone thins seaward towards the berm crest, where it is superseded by the large disc zone. Note the landward-dipping laminae and discoidal cobbles, with long and intermediate axes in the plane of the laminae. View is towards the north. Scale is 30 cm.

Figure 4.26. Unit E, as exposed in the Site 2 trench. The planar, parallel, seaward-dipping laminae represent a sandy beachface which has prograded seaward over trough cross-bedded sediments of the upper shoreface. View is towards the north. Scale is 30 cm.

Figure 4.27. A glacio-eustatic sea level curve, derived using oxygen isotope measurements from deep-sea cores, for the last 130 000 years. Note the sea level highstand at around 120 000 to 130 000 BP, which is believed to be represented at pocket beach Sites 2 and 3 by Gravel Unit 1. The curve also shows that Gravel Unit 1 would have been subaerially exposed for at least 100 000 years (after Shackleton and Opdyke, 1973).

Figure 4.28. The Barbados glacio-eustatic sea level curve, as compared to the dated indicators from Gravel Unit 3 and Unit D. Error bars for age and sea level are shown for the pocket beach indicators. The uncalibrated ^{14}C ages of the indicators have been corrected for the mean age of sea water by subtracting 550 years, so that they are compatible with the data used to define the curve. Agreement between the two data sets is good, although the Barbados curve does not resolve a Middle Holocene highstand (after Fairbanks, 1989).

Figure 4.29. Sea level curves from the Queensland coast in Australia and the southwest coast of South Africa as compared to the dated indicators from Gravel Unit 3 and Unit D. Both curves define a Middle Holocene highstand, which is represented by Gravel Unit 3 at pocket beach Sites 2 and 3. Compton's (2001) curve is slightly displaced towards older ages, a fact which he attributes to neotectonic activity. Agreement between the data sets is, nevertheless, reasonably good if one considers the error ranges associated with these measurements (after Larcombe and Carter, 1998 and Compton, 2001).

Figure 4.30a. Deposition of Unit A by ephemeral streams, activated by a sea level lowstand.

Figure 4.30b. Deposition of Gravel Unit 1 during a +4 mamsl highstand between 120 000 and 130 000 BP.

Figure 4.30c. Ephemeral stream action and deflation of the pre-existing valley fill results in the deposition of Unit B between 120 000 and 9 000 BP, which was a period of

directly adjacent to each other, compressed into a narrow zone; *G3Sub* – subtidal gravels of G3; *G2Int* – intertidal gravels of G2.

Figure 5.12. The variation in average stone size at Site 2, as measured by GB50 and Site 2 trench paddock evaluation samples. Subdivisions of the marine gravels are as follows : *G1Int* – intertidal gravels of G1; *G3Int/G1Sub* – intertidal gravels of G3 overlapping subtidal gravels of G1; *G3IntA* and *G3IntB* – intertidal gravels of G3; *G3Sub* – subtidal gravels of G3; *G2Int* – intertidal gravels of G2.

Figure 5.13. The variation in average stone size at Site 3, as measured by GB50 evaluation samples. Geological subdivisions of the marine gravels are as follows : *G3IntA* and *G3IntB* – intertidal gravels of G3; *G2+G3* – intertidal and subtidal gravels of G2 and G3 directly adjacent to each other, compressed into a narrow zone; *G3Sub* – subtidal gravels of G3; *G2Int* – intertidal gravels of G2.

Figure 5.14. A cross-section showing the results of the Site 2 trench paddock evaluation samples of the marine gravels at Site 2. Subdivisions of the marine gravels are as follows : *G1Int* – intertidal gravels of G1; *G3Int/G1Sub* – intertidal gravels of G3 overlapping subtidal gravels of G1; *G3IntB* – intertidal gravels of G3; *G3Sub* – subtidal gravels of G3.

Figure 5.15. The diminution in average stone size northward from the Orange River mouth. The sudden drop in stone size from Site 2 to Site 3, over only 6 km, is, however, difficult to account for by longshore sorting alone. Sources are C.D. Hallam (1964) and stone size data from this study.

Figure 5.16. The fluvial terrace at the northern end of Marmora Valley. The terrace is raised some 20m above the level of the modern streams. The view in the inset photograph is towards the north.

Figure 5.17. The clast assemblage in the fluvial terrace at the northern end of Marmora Valley. Clast Types: yc=yellow chalcedony, rj=red jasper, ag=agate, avq=angular vein quartz and rvq=well rounded vein quartz. The exotic clast assemblage is good evidence that the exotics were derived from the Sperrgebiet's Eocene marine succession.

Figure 5.18. Stone size-frequency distribution curves from the GB50 and Site 2 trench samples at Sites 2 and 3. Note that while the modes of the two distributions are similar, the Site 3 population has a greater proportion of small diamonds and smaller proportion of large diamonds than Site 2.

Figure 6.1. The marine gravel resource blocks and positions of GB50 samples at Site 3. Note the overlap of sample sets for G3Int1 and G3Int2 near their common boundary.

Explanation of resource blocks : *G2+G3* – zone of high stone density and size at south-eastern headland, with G2 and subtidal gravels of G3 adjacent to each other, compressed into a narrow zone. *G3Int1* – zone of high stone density and size, decreasing towards the north, intertidal gravels of G3. *G3Int2* – zone of low stone density and size, increasing towards boundary with G3Int1, intertidal gravels of G3. *G3Int3* – zone of low-to-moderate stone density and size, intertidal gravels of G3. *G3Sub1* – zone of low-to-moderate stone density and size, subtidal gravels of G3. *G3Sub2* – zone of very low stone density and moderate stone size, subtidal gravels of G3. *G2Int* – zone of very high stone density and low-to-moderate stone size, intertidal gravels of G2.

Figure 6.2. A sketch showing the shape of a sample frequency distribution curve in the case where there are a few, large sample values. The arithmetic mean estimator sometimes tends to overestimate the mean of the true population in such instances.

Figure 6.3. A plot of the data from Table 6.4, showing the spread of distribution parameters and mean estimates for the GB50 sample sets at Site 3.

Figure 6.4. A simple flow diagram showing the simulation method employed in this study.

LIST OF TABLES

Table 6.4. The values of μ ($n > 50$) , Sichel T ($n \leq 50$) and σ^2, as determined by the graphical method. The values of ā are the same as those in Table 6.1.

ABSTRACT

The two Late Quaternary, diamondiferous pocket beach deposits studied here are situated along a 10 km stretch of the storm-dominated, Atlantic coastline of the Sperrgebiet, south-western Namibia. The pocket beaches are approximately 130 km north of the Orange River mouth, which is widely accepted as a long-lived point source for diamonds sourced from the interior of southern Africa. A total of fourteen pocket beach deposits were recently evaluated in this area, but only two of these, namely Site 2 (to the south) and Site 3 (to the north), are considered here. The main diamond-bearing horizons are beach gravels, which occur within, and form part of, the pocket beach sequences. The beach gravels are mostly blanketed by sand overburden, meaning that exposures available for study were limited, and much reliance was placed on borehole logging and observations of evaluation sample tailings.

The main aims are to unravel the depositional history of the pocket beach sequences, identify the controls on diamond mineralisation in the beach gravels, and critically examine two different methods of estimating average diamond size for the deposits. In pursuit of these aims, sedimentological characteristics of the unconsolidated pocket beach deposits were recorded using small diameter drill holes, hydraulic grab bulk samples, trench exposures and surface outcrops. The surface geology, geomorphology and modern wave patterns were mapped using high-resolution, Airborne Laser Survey imagery coupled with extensive field checking. Three-dimensional geological modeling software was used to gain insight into the subsurface morphology of the deposits. Fossil shell samples were used to aid interpretation of ancient depositional environments and to date parts of the pocket beach sequences. Variations in diamond concentration and the size of diamonds were recorded using bulk samples, some of which were taken from a trench, but most of which were excavated using a hydraulic grab tool called the GB50. Finally, by using diamond size data from Site 3, sample data from diamondiferous beach gravels to the south of the study area and sample campaign simulations, two alternative methods of evaluating average diamond size in marine gravel deposits were appraised.

The pocket beach sequences occur within north-south trending valleys of a major deflation basin and are separated from one another by rocky headlands. The ridge-and-valley topography of the deflation basin has resulted from differential erosion of Late Proterozoic basement rock units, alternating layers of which differ greatly in their resistance to the long-lived, local denudational

processes. On the basis of the stratigraphic information collected from the unconsolidated pocket beach valley fills, interpreted within the context of global, Late Pleistocene sea level records, the following depositional history is deduced :

a) Deposition of sheetflood gravels by ephemeral streams, activated during a regressive phase.
b) Transgression, culminating in the deposition of a gravel beach, representing a sea level highstand of +4 metres above mean sea level (mamsl) at between 120 000 and 130 000 BP.
c) A regressive phase, resulting in deflation of former valley fills to the bedrock valley floor and accompanied by re-activation of ephemeral stream activity to form sheetflood deposits; this represents a protracted period of subaerial exposure of the +4 m gravel beach deposit.
d) Deposition of a great volume of sediment in the valleys during the latter stages of the transgression from the Last Glacial Maximum (LGM). The sequence generated during this phase, which started at ca. 9 000 BP, contains :
    i) pan/coastal sabkha sediments,
    ii) shallow, sheltered bay sediments,
    iii) back-barrier lagoonal sediments,
    iv) a gravel beach deposit representing a sea level stillstand at –5 mamsl, laid down between 7 600 and 5 600 BP,
    v) another gravel beach deposit representing the well-known Middle Holocene sea level highstand at +2 to +3 mamsl, laid down at ca. 5 000 BP, and which terminated the transgression from the LGM.
e) A minor regression to the current sea level, accompanied by progradation of the shoreline to its current position. This progradational marine unit consists almost entirely of sand and grit, reflecting the lack of gravel supply to this part of the coastline in the most recent past.
f) Deposition of modern coastal dunes, which cap the pocket beach sequence and are the youngest sediments in the study area.

Using trench and hydraulic grab evaluation sample results, in combination with analysis of wave patterns and field observations, the following local controls on the density distribution (ie. concentration) and size distribution of diamonds in the gravel beach deposits (+4, -5 and +2 to +3 mamsl stands) are recognised :

a) Gravel beach depositional processes, which are responsible for clast sorting on the beach, have influenced the density and size distribution of diamonds. The infill zone, or beach toe,

favours maximum diamond concentration while diamond size decreases from the imbricate zone (intertidal) to the infill zone (subtidal).

b) Wave energy is identified as the dominant local control on diamond size distribution, but has also influenced diamond concentration to a limited degree. Larger diamonds are intimately associated with coarser beach gravels, both of which are a reflection of increased wave energy. Higher concentrations of diamonds are sometimes associated with zones of coarser gravel and therefore greater wave energy.

c) The time of deposition of the host gravel beach is seen to be the dominant controlling factor with respect to diamond concentration. This is seen as evidence of significant temporal variation in the availability of diamonds in the littoral evironment.

A significant reduction (20%) in average diamond size from Site 2 to Site 3, over a distance of only 6 km, is evident. The following were identified as reasons for this reduction in diamond size :

a) Longshore sorting processes, of which the long-lived northerly littoral drift is a key part, are known to have played a role in the diminution of diamond size northwards from the Orange River mouth point source. However, it is believed that this can only partly account for the observed 20% reduction in diamond size.

b) Input of sediment and smaller diamonds at Site 3, reworked out of an older, Eocene-aged marine succession in the hinterland, is recognised as a possible additional reason for the large reduction in diamond size from Site 2 to Site 3. It is also speculated that the large size of the pocket beach at Site 3, relative to Site 2, may have resulted in lower average wave energy at Site 3, with consequent reduced average diamond size.

Diamond size in the beach gravels of Site 3, as well as in beach gravels elsewhere in the Sperrgebiet, is seen to be lognormally-distributed within geologically homogeneous zones. In theory, lognormal mean estimators represent the best method of estimating average diamond size in such cases, whereas the arithmetic mean estimator has the tendency to overestimate when large outlier values occur. Lognormal mean estimators have the added benefit of providing for the calculation of confidence limits, which are becoming increasingly more important as financial lending institutions insist on better quantification of the risk involved in resource estimates. Sample campaign simulations demonstrate, for the kinds of diamond size-frequency distributions typical of beach gravel deposits at Site 3, that there is no significant improvement in the accuracy of average diamond size estimates when lognormal mean estimators are used instead of the arithmetic mean

estimator. This is because the variance (σ^2) of the diamond populations is low, and large outlier values are extremely unlikely to occur. However, simulation of a diamond population with high variance, drawn from a sample of beach gravels near the Orange River mouth, shows that lognormal estimators produce significantly more accurate results when σ^2 is large. Since individual diamond weights were not recorded during evaluation sampling of Site 3, numerical solution of lognormal estimators is not possible, and these would need to be solved using a less accurate graphical method. It is therefore recommended that individual diamond weights are recorded in future sampling campaigns, allowing for the use of lognormal mean estimators, and the calculation of confidence limits for average diamond size estimates.

CHAPTER 1 – INTRODUCTION

This study considers the depositional history and evaluation of two diamondiferous pocket beaches on the southwest coast of Namibia. These two beaches lie within the Mining Area No. 1 mining licence held by the Namdeb Diamond Corporation (Pty) Ltd. (but outside the fence surrounding the currently active mining areas). The study stems from the exploration programme run by the Mineral Resource Department of Namdeb, which included the prospecting of pocket beach deposits along the Atlantic coast between the Orange River mouth and Lüderitz. A pocket beach is a sediment-filled embayment situated between rocky headlands, and typically covers between 1 km and 4 km of coastline in the study region (Figure 1.1).

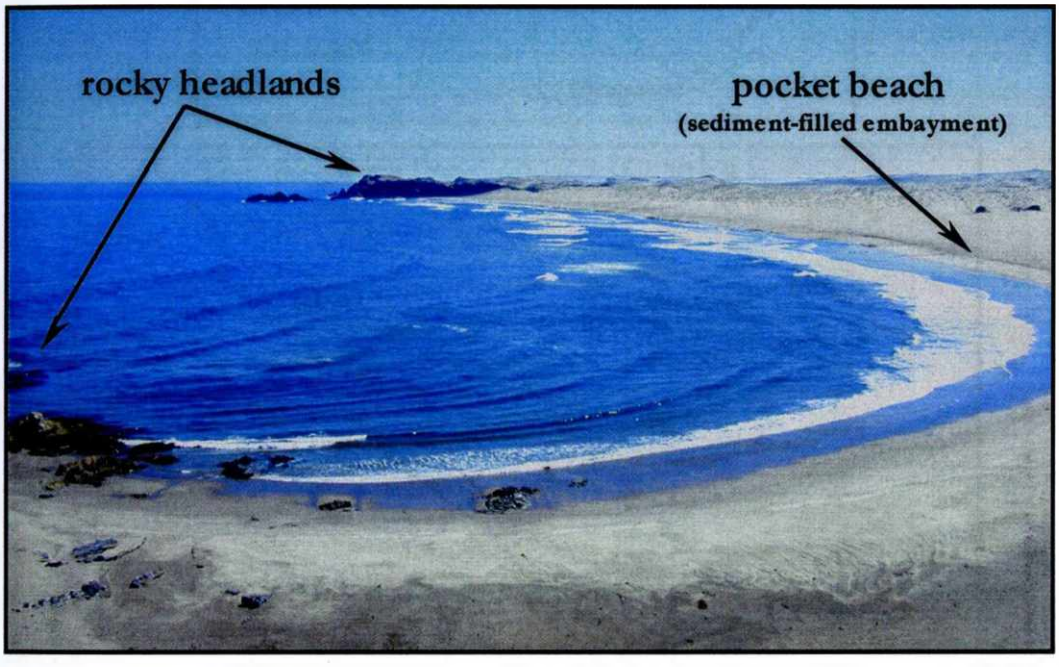

Figure 1.1. A typical example of a pocket beach along the southwest coast of Namibia. Distance between headlands is approximately 2 km.

1.1 LOCATION OF THE STUDY AREA

The study area, situated within Namibia's Sperrgebiet or "forbidden territory", is located in the southern portion of the Namib Desert, along the Atlantic coast of southern Africa (Figure 1.2). This area lies between latitudes 27° 47' S and 27° 52' S, and is situated some 130 km north of the Orange River mouth. The coastline from just south of Chameis Bay to Lüderitz is characterised by the existence of numerous embayments, most of which host unconsolidated pocket beach sediments

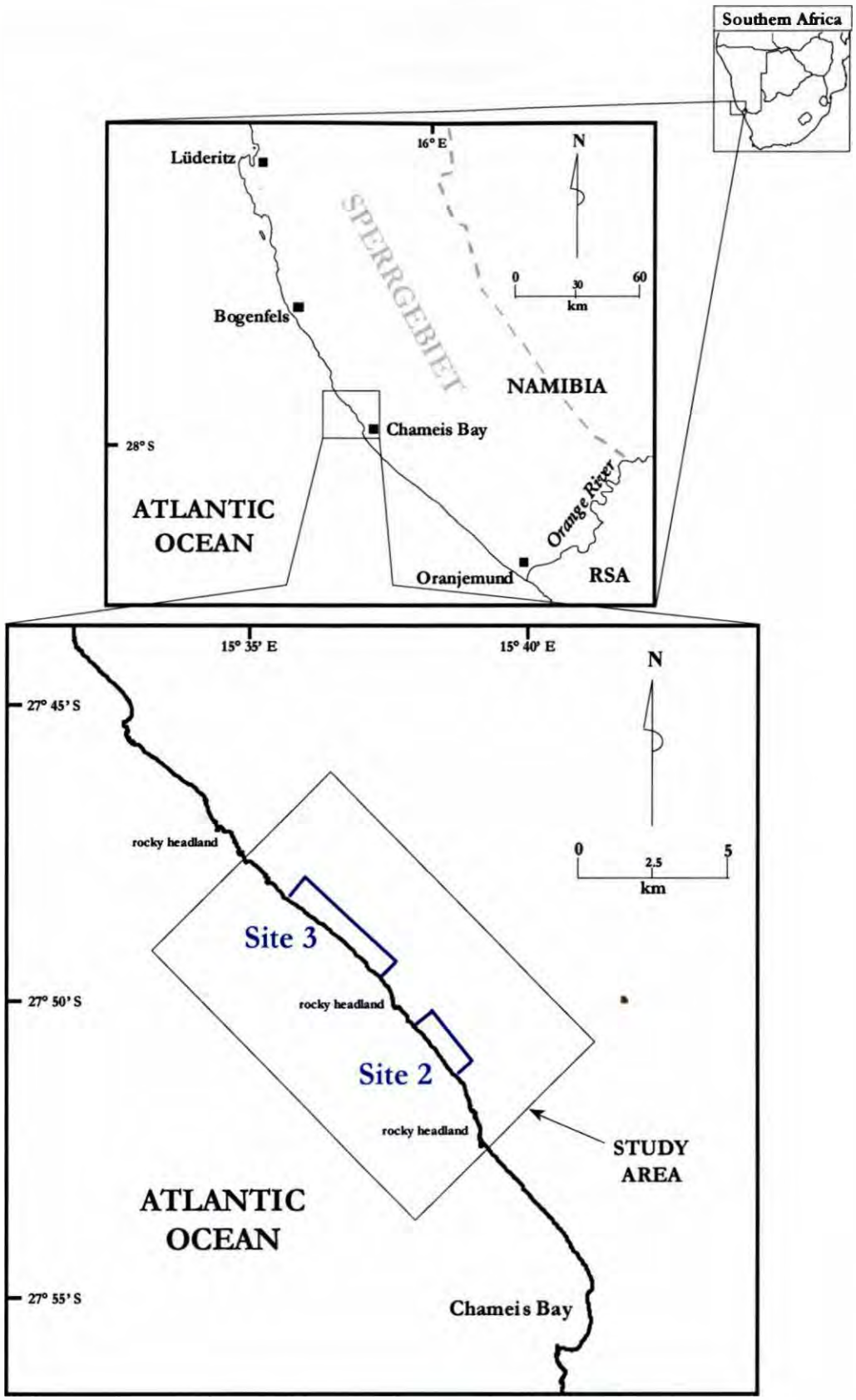

Figure 1.2. A locality map of the study area, showing the positions of pocket beach Sites 2 and 3 within the Sperrgebiet, Namibia.

of Late Quaternary age. Diamondiferous marine gravels occur within the pocket beach sequences, and these form part of the Sperrgebiet's suite of world-class, alluvial diamond placers (Figure 1.3). The marine gravels are mostly buried by overburden sands of aeolian and marine origin. Consequently, they occur mostly below sea level, reaching elevations as low as –8 metres above mean sea level (mamsl) in the study area. The Sperrgebiet diamond placers are characterised by the presence of Orange River-derived "exotic" clasts, which have been sourced from the interior of southern Africa (Stocken, 1978; Ward, 2000). Two pocket beach sites, referred to as Sites 2 and 3, were selected for study because they were extensively drilled and sampled as part of a recent (1997 to 2002) evaluation programme (Figures 1.4 and 1.5). This recent evaluation programme was aimed at estimating the diamond resources contained within the marine gravels of fourteen pocket beach placers, which included pocket beach Sites 2 and 3.

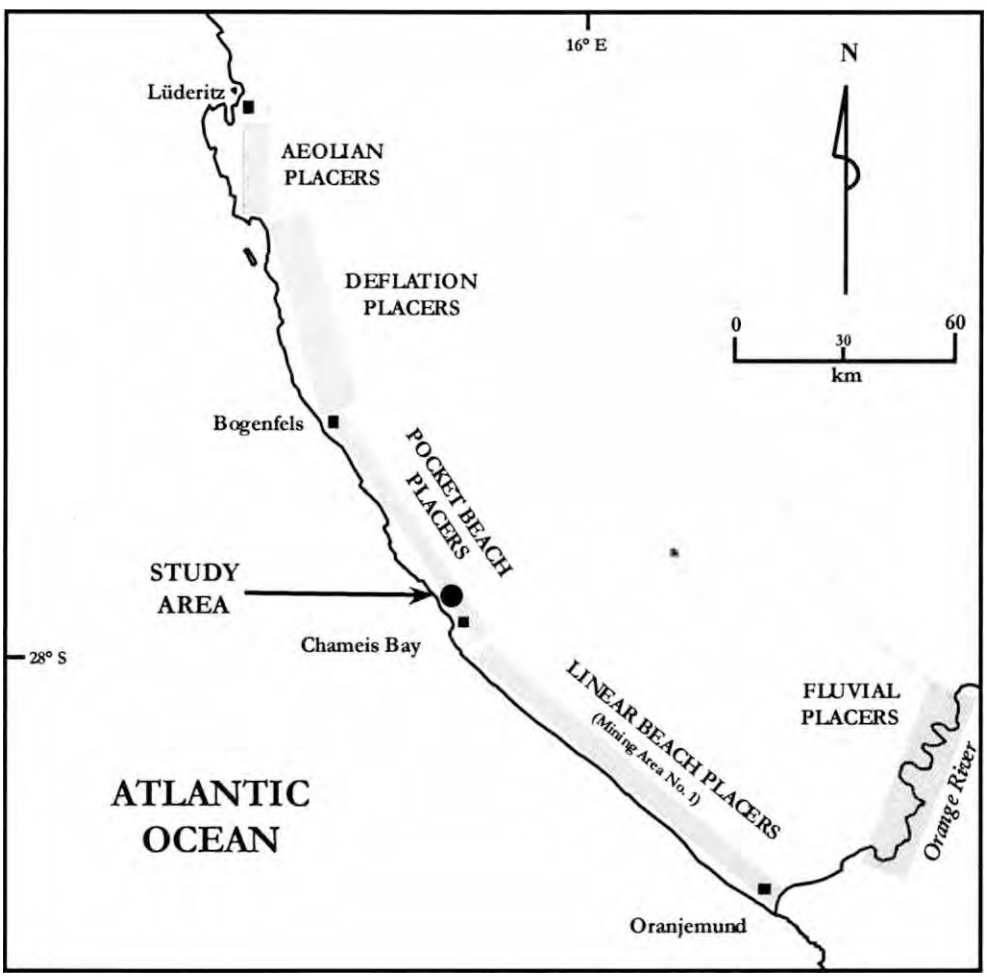

Figure 1.3. The position of the study area in relation to the spectrum of diamond placer types found within the Sperrgebiet (sources are J. Jacob, 2001; Corbett and Burrell, 2001).

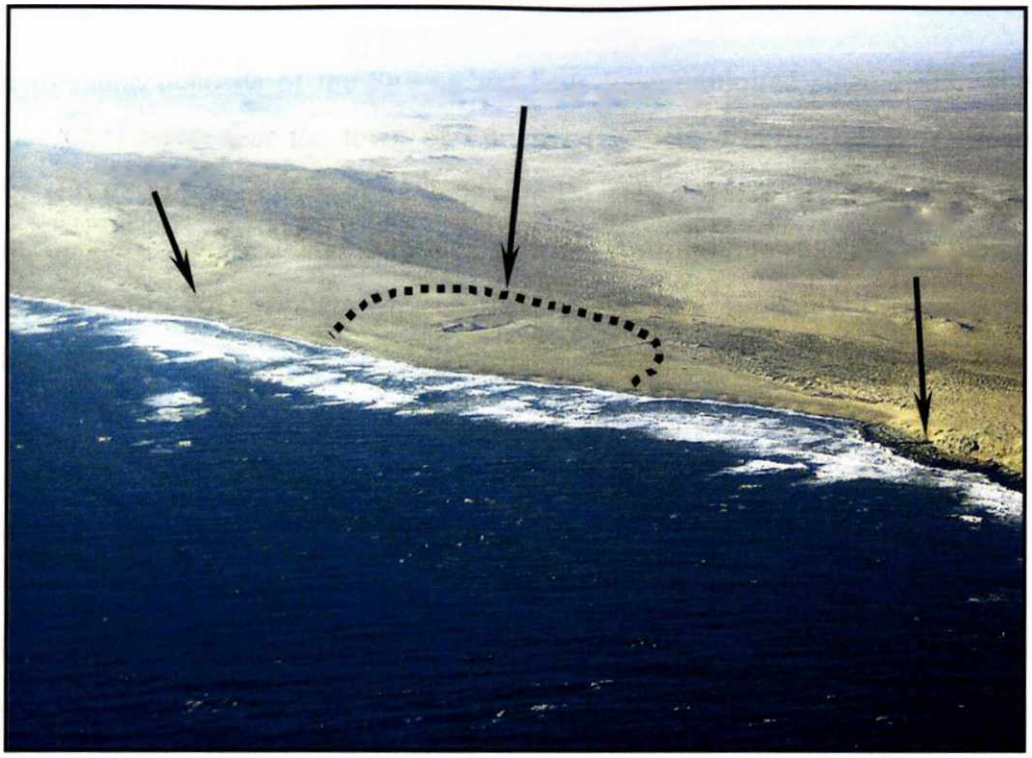

Figure 1.4. An oblique aerial view, from the southwest, of pocket beach Site 2. The approximate position of the buried, diamondiferous, Late Quaternary marine gravels are shown (pocket beach is approximately 1 km wide between headlands).

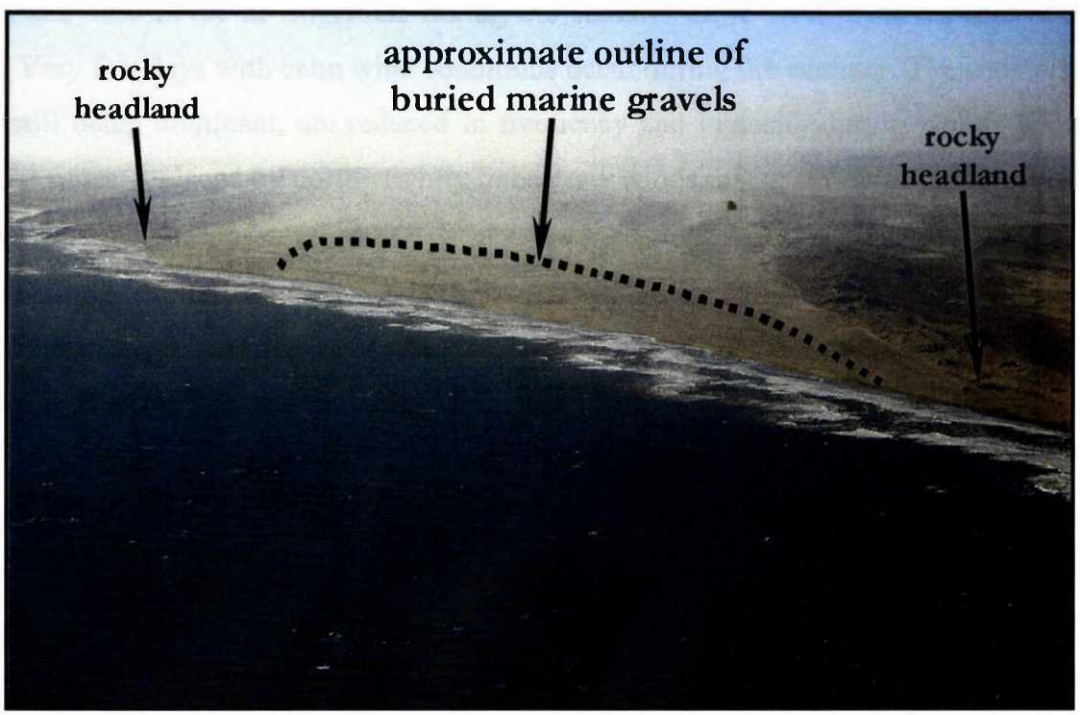

Figure 1.5. An oblique aerial view of Site 3, with the position of the buried, diamondiferous marine gravels illustrated (pocket beach approximately 4 km wide). View is from the southwest.

The diamond deposits of the Sperrgebiet have been exploited since 1908, when the first diamond was discovered near the town of Lüderitz (Corbett, 1989). Today, Namdeb Diamond Corporation (Pty) Ltd., a joint venture between De Beers Centenary AG and the Namibian government, operates several diamond mining operations in the Sperrbgebiet, of which the linear beach gravel deposits of Mining Area No. 1 (MA1) are probably the most well-known (C.D. Hallam, 1964).

1.2 CLIMATE AND COASTAL REGIME

The southern, coastal portion of the Namib Desert has an average annual rainfall of 40 to 50 mm, most of which falls in the winter months. Ocean water temperatures average 10°C, thus moderating the coastal climate. The average maximum daily air temperature is 23°C (Murray *et al.*, 1970). Advective fog formation is common along the coastal strip, and is believed to have played an important role in the formation of gypsum crusts and in salt weathering processes (Rogers, 1977; Corbett, 1989). A southerly quadrant wind direction prevails, peaking both in terms of its frequency and intensity in the summer months. Corbett (1989) recorded average wind velocities of between 9.8 m/sec and 18.0 m/sec at Bogenfels during the summer days, with gusts capable of reaching 25 m/sec. Very few days with calm wind conditions occur during the summer. The southerly winds, although still being dominant, are reduced in frequency and intensity during winter (Figure 1.6). They are, at times, replaced by northwesterly or easterly winds that occur mostly between April and September.

The tidal range along the Sperrgebiet coastline falls within the micro-tidal (< 2 m) range. Measurements made by de Decker (1988) at a water depth of 15 m, and at a position roughly 6 km south of the Orange River mouth, demonstrate that median wave heights range from 1.5 m in summer to 1.9 m in winter. Maximum wave heights can exceed 4.75 m throughout the year. East-southeasterly to southerly wave approach angles dominate during summer with a significant secondary south-southwesterly to westerly component also evident. During winter, the incidence of longer period waves from the southwest increases markedly in response to the passage of cyclones in the South Atlantic. These wave patterns result in a northerly littoral drift, which increases in intensity in winter (de Decker, 1988).

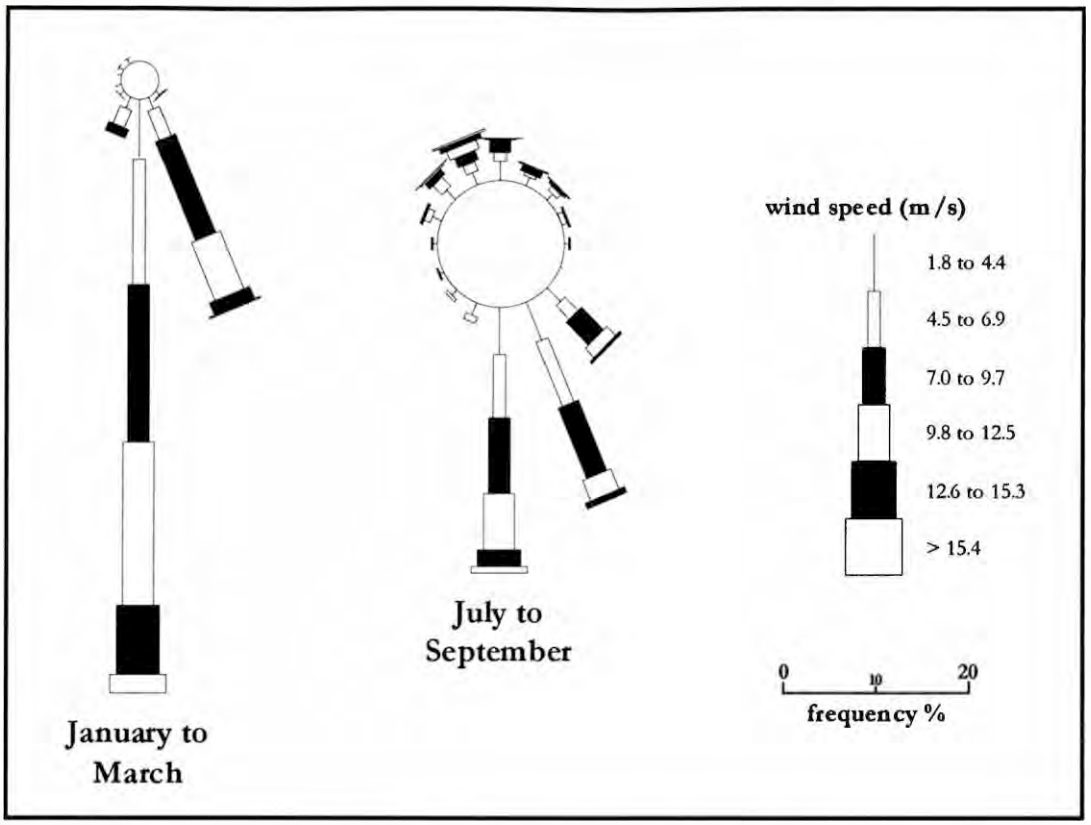

Figure 1.6. 16-point wind roses showing summarised, hourly wind data from Bogenfels for 1987. Note the dominance of the southerly wind regime in the summer months (January to March) and the much higher percentage of calm days (open circles at centre of wind roses) during the winter months (July to September). Strong northwesterly winds in the winter reflect the passage of cyclones in the South Atlantic (after Corbett, 1989).

Using the wave data presented above, de Decker (1988) has calculated, using the median values, that quartz pebbles 10.5 mm in diameter would be transported at 15 m water depth, while coarse sand could be mobilised at 30 m water depth. Wave heights exceed 3.25 m approximately 5 % of the time; under these conditions, quartzose cobbles 100 mm in diameter can be mobilised at 15 m water depth and pebbles 10 mm in diameter will move at 30 m water depth. The present wave regime is thus quite capable of transporting diamonds, especially during storm events. Since a northward littoral drift prevails along most of the Namib coastline, the net displacement of coarser sediment is towards the north (Rogers, 1977). The dominant southerly wind regime and northerly littoral drift is believed to have operated since Early Tertiary times, resulting in the almost exclusively northward transport of diamondiferous sediment from the Orange River mouth, to form the marine and deflation placers of the Sperrgebiet (Corbett, 1989; 1996; Ward, 2000).

1.3 PREVIOUS WORK

This section summarises the most relevant elements of previous studies related to the geology and diamond content of pocket beach deposits along the Namibian coast. Previous work relating to the evaluation of diamondiferous gravel beach deposits is also discussed. The body of work related to pocket beaches in general and the Sperrgebiet pocket beaches in particular is relatively limited.

1.3.1 Geology

Merensky (1909), Kaiser (1926), C.D. Hallam (1964), amongst others, have studied and reviewed the diamondiferous coastal deposits of the west coast of southern Africa. C.D. Hallam's (1964) treatise is an excellent overview of these deposits as a whole, and makes brief mention of the pocket beach placers of the Sperrgebiet.

During a previous (1979 to 1981) evaluation sampling campaign at Sites 2 and 3, which pre-dates the most recent one by almost twenty years, Stocken (1980) and Elford (1980a; 1980b) briefly described the geology at these localities. They note that each of the pocket beach sequences, both of which occupy the mouths of drowned deflation valleys, contain a seaward-thickening wedge of marine sediments. They identified diamondiferous marine gravel horizons at the base of the marine wedge, and these typically rest on a platform incised into various other types of unconsolidated sediments. They showed that the pocket beach sequences as a whole overlie Proterozoic bedrock, which forms the floors of the drowned deflation valleys.

More recently, Apollus (1995) considered a single diamondiferous pocket beach deposit situated just several kilometres to the south of the current study area (Figure 1.7). Apollus (1995) identifies an older red unit and a younger grey unit in his pocket beach. Both of these units are interpreted as beach and nearshore sediments composed of both sand and gravel. Importantly, the red and grey units rest mostly on a gullied Proterozoic bedrock footwall, which differs considerably from the unconsolidated sedimentary footwalls to the marine gravels at pocket beach Sites 2 and 3. The study also shows that the red unit was subaerially exposed for a considerable period of time, as evidenced by oxidation of the sediments and incipient pedogenesis/calcretisation at the upper contact. Grain size data and the distribution of clasts of differing densities from both units clearly

demonstrate that higher wave energy conditions prevailed at the northern end of the pocket beach during deposition. Apollus (1995) attributes the deposition of the red unit to a sea level highstand which reached elevations of +3 to +6 mamsl at ca. 130 000 BP (Eemian). The red unit is correlated with C.D. Hallam's (1964) intermediate terrace, which he identified on MA1. Deposition of the grey unit is correlated with the well-known Middle Holocene (ca. 5 000 BP) highstand, which reached a maximum elevation of +2 to +3 mamsl (Miller *et al.*, 1993; Compton, 2001). The grey unit is correlated with C.D. Hallams' (1964) advanced terrace.

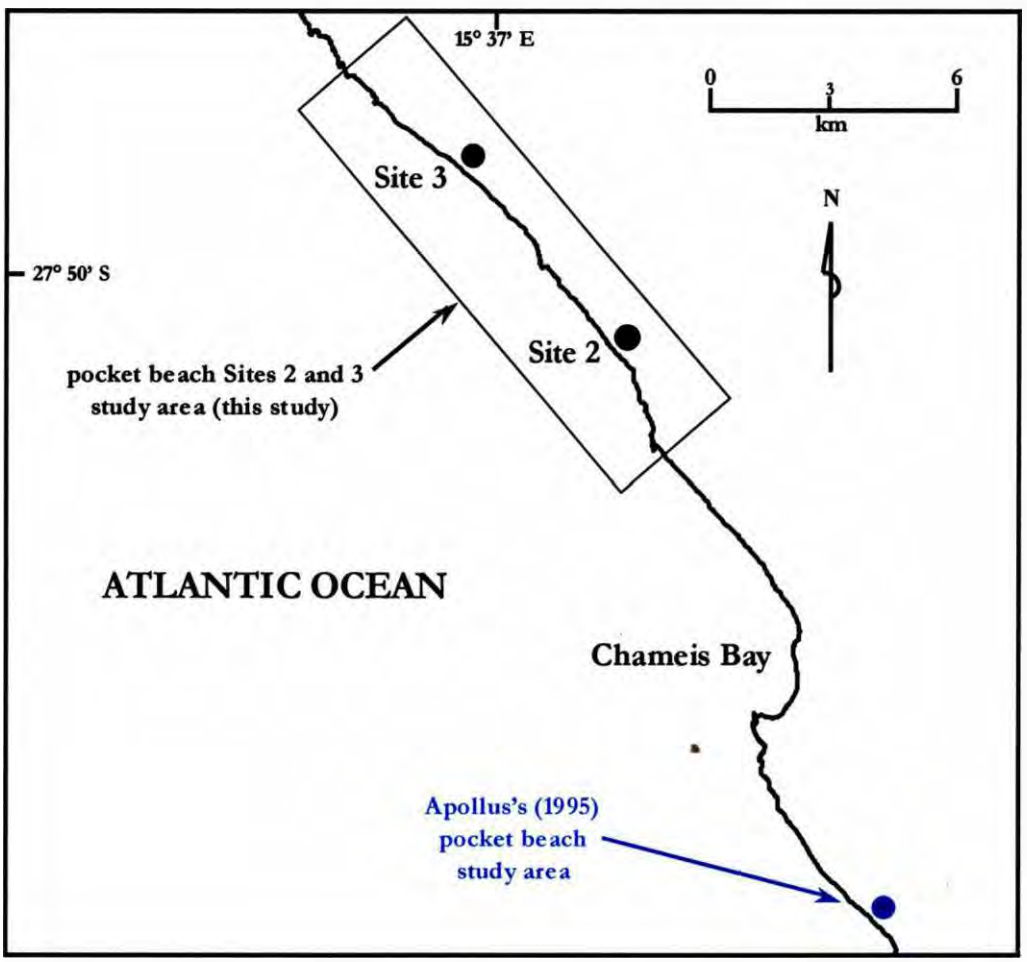

Figure 1.7. The position of Apollus's (1995) pocket beach study area in relation to the two pocket beaches, Sites 2 and 3, which form the subject of this study.

Elsewhere, Hobday and Banks (1971) described a coarse-grained pocket beach complex in Tanafjord, Norway, where they noted that the gravel beach deposits exhibit clast size and shape sorting as described by Bluck (1967).

1.3.2 Diamonds

C.D. Hallam (1964) notes that diamonds tend to concentrate on the north side of south-opening bays, on the southern side of headlands and in pocket beaches with steep beaches. Within the gravel beach units, he reports that diamonds are concentrated preferentially at the top and bottom of the beach and on marine erosion platforms.

Apollus (1995) concludes that diamonds are concentrated best in the red unit at the northern end of his southwest-facing pocket beach, where wave energy was highest at the time of deposition. He also notes that diamond concentration is more greatly influenced by processes of beach accretion than by the grain size of the gravel (which he equates to wave energy). However, he does point out that there is some relationship between wave energy and diamond concentration in the red unit. For the grey unit, Apollus (1995) concludes that maximum diamond concentration is associated with the subtidal facies in areas having the highest density of bedrock-incised gullies. He could find no obvious trend with respect to the size distribution of diamonds across his pocket beach.

Elford (1980a, 1980b) and Stocken (1980), using a limited data set, conclude that the marine gravel deposits at Site 2 and 3 are the most important diamond carriers. The limitations of the sampling technique used prevented any detailed interpretations of diamond distribution at pocket beach Site 2 and 3 by these workers.

1.3.3 Evaluation of Diamondiferous Gravel Beach Deposits

Previous work on the evaluation of diamondiferous gravel beach deposits is limited, with only two studies being directly applicable. The first study was conducted by Sichel (1972), who notes that the evaluation of a diamondiferous deposit depends on i) the diamond or stone density distribution through the deposit, ii) the size distribution of the stones through the deposit and iii) the selling price structure prevailing at a given time. He found, using sample data from the linear beaches of MA1, that the density distribution of stones (ie. distribution of number of stones per sample unit) was best modeled by a compound Poisson distribution. He then went on to provide methods for the estimation of a mean and confidence limits for this distribution. With regard to stone size-frequency

1.3.2 Diamonds

C.D. Hallam (1964) notes that diamonds tend to concentrate on the north side of south-opening bays, on the southern side of headlands and in pocket beaches with steep beaches. Within the gravel beach units, he reports that diamonds are concentrated preferentially at the top and bottom of the beach and on marine erosion platforms.

Apollus (1995) concludes that diamonds are concentrated best in the red unit at the northern end of his southwest-facing pocket beach, where wave energy was highest at the time of deposition. He also notes that diamond concentration is more greatly influenced by processes of beach accretion than by the grain size of the gravel (which he equates to wave energy). However, he does point out that there is some relationship between wave energy and diamond concentration in the red unit. For the grey unit, Apollus (1995) concludes that maximum diamond concentration is associated with the subtidal facies in areas having the highest density of bedrock-incised gullies. He could find no obvious trend with respect to the size distribution of diamonds across his pocket beach.

Elford (1980a, 1980b) and Stocken (1980), using a limited data set, conclude that the marine gravel deposits at Site 2 and 3 are the most important diamond carriers. The limitations of the sampling technique used prevented any detailed interpretations of diamond distribution at pocket beach Site 2 and 3 by these workers.

1.3.3 Evaluation of Diamondiferous Gravel Beach Deposits

Previous work on the evaluation of diamondiferous gravel beach deposits is limited, with only two studies being directly applicable. The first study was conducted by Sichel (1972), who notes that the evaluation of a diamondiferous deposit depends on i) the diamond or stone density distribution through the deposit, ii) the size distribution of the stones through the deposit and iii) the selling price structure prevailing at a given time. He found, using sample data from the linear beaches of MA1, that the density distribution of stones (ie. distribution of number of stones per sample unit) was best modeled by a compound Poisson distribution. He then went on to provide methods for the estimation of a mean and confidence limits for this distribution. With regard to stone size-frequency

distributions in MA1, Sichel (1972) found that they follow a two-parameter lognormal distribution for a sample or samples taken close to each other within the same beach deposit. Importantly, Sichel (1972) also recognized that stone density and stone size-frequency distributions remain constant within geologically homogeneous zones. Therefore, the modern practice is that average stone density and average stone size estimates typically take place for each geologically homogeneous zone. Sichel (1972) concluded that average stone size within a geologically homogeneous zone should be estimated using either a simple arithmetic mean estimator, or lognormal estimators, such as the Sichel-T estimator (Sichel, 1952; 1966). The lognormal estimators are theoretically more suited to lognormally-distributed sample populations. A second study by Oosterveld *et al.* (1987), applied Sichel's (1952; 1966; 1972) methods for the estimation of average stone density and average stone size in the evaluation of the linear beach deposits on MA1. Oosterveld *et al.* (1987) paid more attention to the estimation of average stone density and made very little mention of the results of their average stone size estimates, which were conducted using the Sichel T estimator. It is worth noting that Sichel's (1952; 1966; 1972) estimation techniques involve the use of conventional statistics. Alluvial diamond placers often do not lend themselves to the use of geostatistical estimation techniques because of the high "nugget effect" (Oosterveld, 2003) and the limited number of samples that are usually taken. Evaluation of alluvial diamond placers typically requires the taking of very large samples, which places financial limits on the number of samples that can be taken. The successful modeling of variograms in geostatistics usually requires the availability of many sample values, a situation seldom found in alluvial diamond evaluation projects due to cost and logistical constraints.

1.4 AIMS OF THE STUDY

This study aims to :

a) Unravel the lithostratigraphy and depositional history of the pocket beach sequences at Sites 2 and 3. A detailed reconstruction of the depositional history at these localities has never been undertaken before.

b) Identify the controls on i) *the density distribution of diamonds*, and ii) *the size distribution of diamonds*, within the marine gravels at pocket beach Sites 2 and 3. Recognition of these controls is important economically, in that they facilitate the evaluation of alluvial diamond

placers and provide a predictive mineralisation model that can be applied to similar deposits elsewhere.

c) Determine the more effective method of estimating average stone size in diamondiferous beach gravel deposits by comparing arithmetic and lognormal mean estimators, primarily using evaluation sample results obtained at Site 3 but also with an example from MA1. Average diamond size is a critical parameter for the calculation of diamond resource revenue.

CHAPTER 2 – REGIONAL GEOLOGICAL FRAMEWORK

2.1 MAJOR REGIONAL GEOMORPHIC UNITS

The study region is characterised by three distinct geomorphic units :

a) The Namib Sand Sea (Figure 2.1), which represents a depositional basin for the accumulation of aeolian sand that has been transported northwards by the dominant southerly winds (Corbett, 1989).

b) A deflation basin, encompassing the study area, which is situated on the southern, upwind side of the Namib Sand Sea (Kaiser, 1926). The deflation basin is characterised by north-south trending ridge-and-valley topography, which bears a strong relation to the underlying basement geology (Corbett, 1989). Chlorite schists, easily eroded and deflated by salt weathering and wind corrasion, form the valley floors, while more resistant psammitic lithologies constitute the valley walls (Figure 2.2). The study area of Sites 2 and 3 is located in the proximal reach of the deflation basin unit (ie. upwind, updrift and closer to the Orange River mouth). The deflation basin coastline consists of alternating sandy bays and rocky headlands, reflecting the alternating valleys and ridges respectively. This is in contrast to the MA1 stretch of coastline to the south, which is relatively devoid of embayments.

c) A flat, gently undulating plain is situated to the east of the deflation basin. This plain extends as far eastwards as the Great Escarpment and encompasses two distinct duricrusts. The older of these duricrusts is a silcrete, which caps a kaolinitic deep weathering profile. The younger duricrust is a mature calcrete, which is sometimes developed at the level of the older silcrete or within the deeply weathered profile where the silcrete has been eroded away (Stocken, 1978; Corbett, 1989).

2.2 PROTEROZOIC TO PALAEOZOIC FRAMEWORK

The oldest rocks in the broader region are those of the Middle-to-Late Proterozoic Namaqua Metamorphic Complex (NMC) (Tankard, *et al.*, 1982). The NMC forms the basement into which a large portion of the Orange River is incised (Figure 2.3).

The Pan-African Gariep Belt unconformably overlies the NMC and constitutes the basement in the study area (Figure 2.3). The dominant structural trend in the Gariep Belt is north-south (Tankard *et al.*, 1982; Frimmel, 1995). The aforementioned chlorite schists and psammites (Figure 2.2), which occur in the study area, form part of the Chameis Complex of the Gariep Belt. The age of the oldest unit in the Gariep Belt is estimated at around 780 Ma (Frimmel *et al.*, 1996).

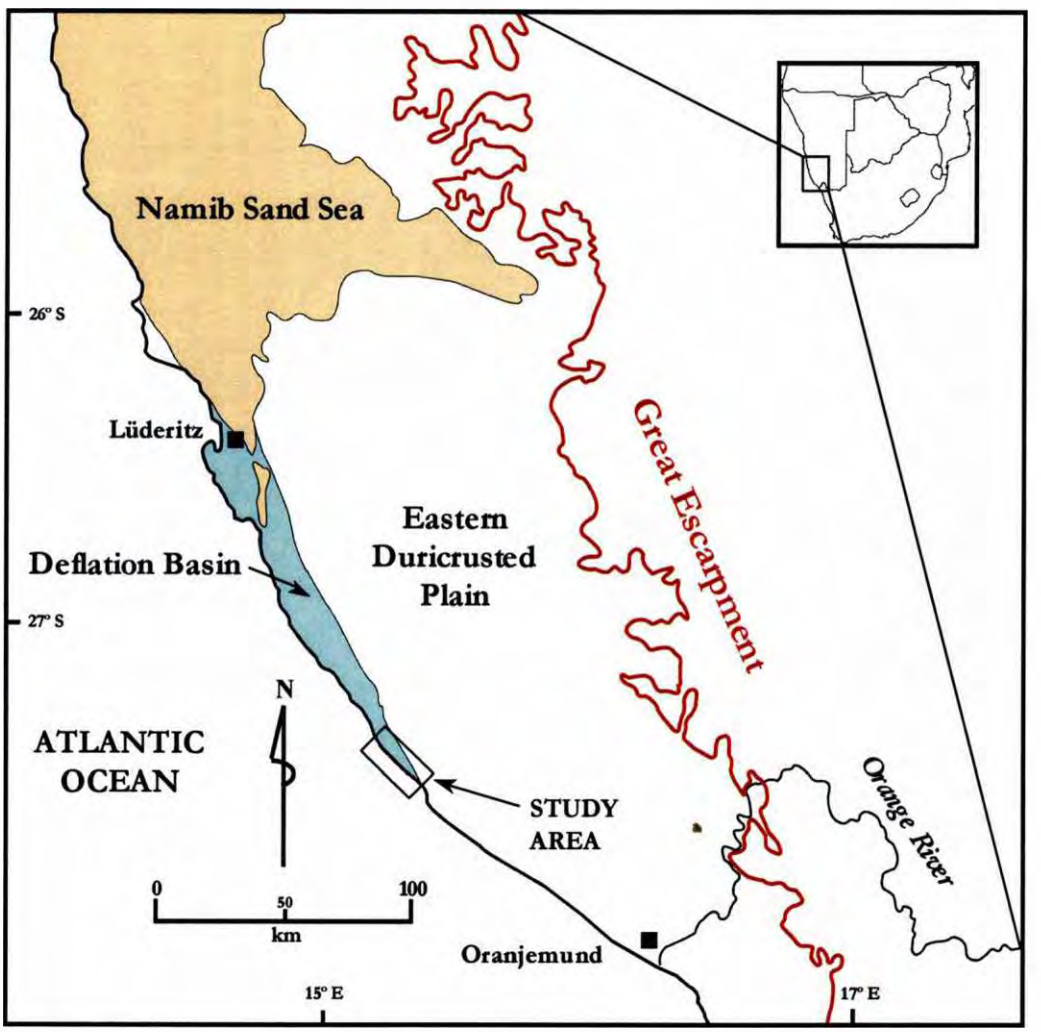

Figure 2.1. The major regional geomorphic elements of the study region (modified after Corbett, 1989).

The Latest Proterozoic to Early Cambrian Nama Group, consisting largely of undeformed platform-type sediments, variously overlies the eastern margin of the Gariep Belt and large parts of the NMC in southern Namibia (SACS, 1980; Tankard *et al.*, 1982; Figure 2.3). Deposition of the Nama Group was succeeded by deposition of the Palaeozoic Cape Supergroup in the south

(Tankard *et al.*, 1982; Frimmel, 1995). The Nama rocks were also extensively covered by sediments of the Permian-to-Jurassic Karoo Supergroup in the north and east. Deposition of the Karoo Supergroup embraces the Palaeozoic-Mesozoic boundary.

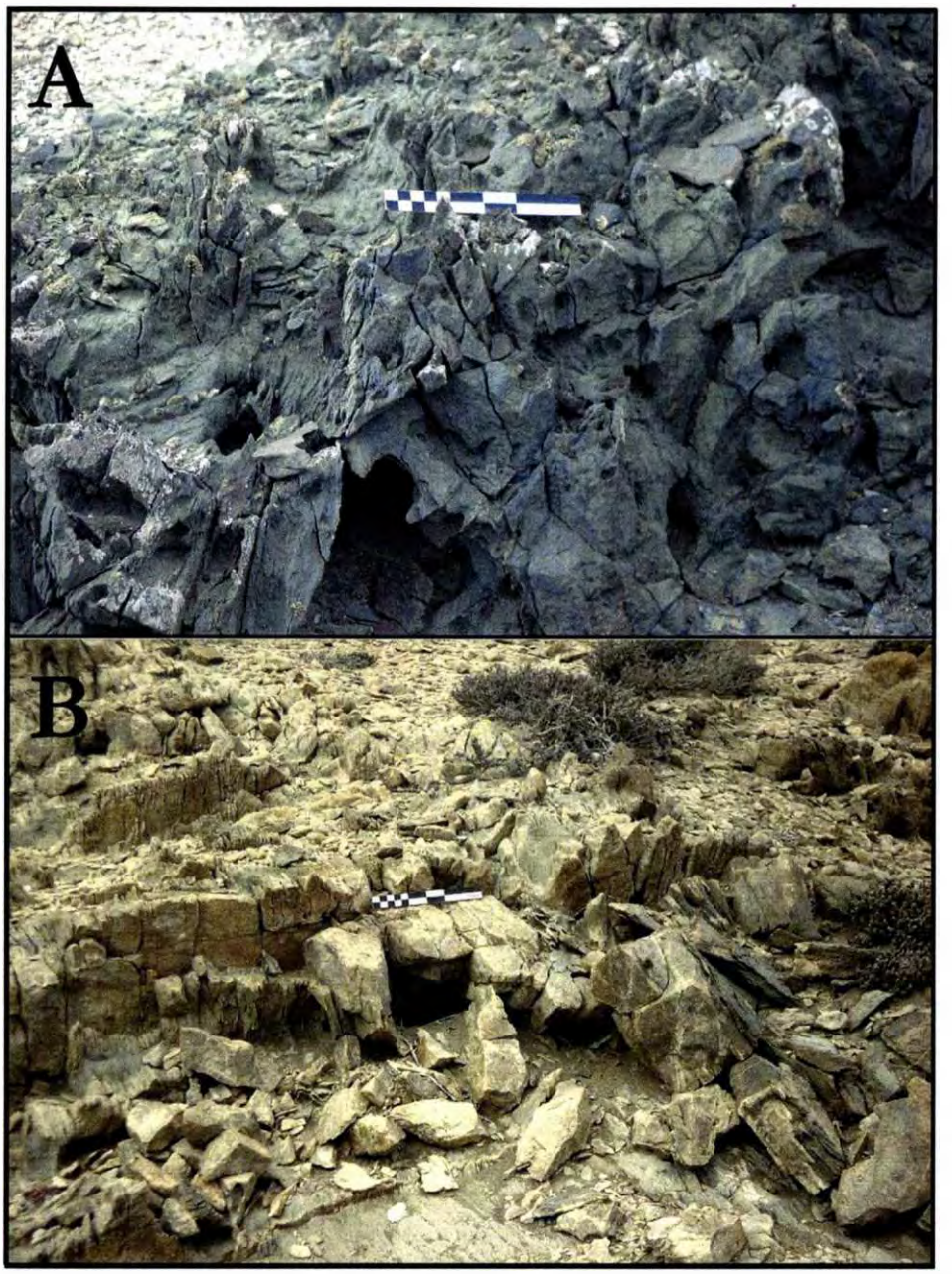

Figure 2.2. The two main rock types of the Gariep Belt basement in the study area. A – chlorite schist, easily broken down by salt weathering and readily eroded by wind corrasion or fluvial action. B – psammite, which is relatively resistant to the erosional processes operating in the deflation basin. The psammites form the north-south trending ridges of the deflation valleys, defining rocky headlands at the coast, while the chlorite schists form the floors of the valleys. Pocket beach sediments fill the valleys. Scale is 150 mm.

2.3 MESOZOIC FRAMEWORK

Karoo sedimentation was halted by huge basaltic outpourings over much of southern Africa between 200 and 180 Ma (Tankard *et al.*, 1982). This volcanic episode was the precursor to the rifting and break-up of Gondwana. Rifting along the western margin of southern Africa, and the consequent formation of the proto-Atlantic Ocean, commenced at around 130 Ma (Tankard *et al.*, 1982; Partridge, 1998; de Wit *et al.*, 2000).

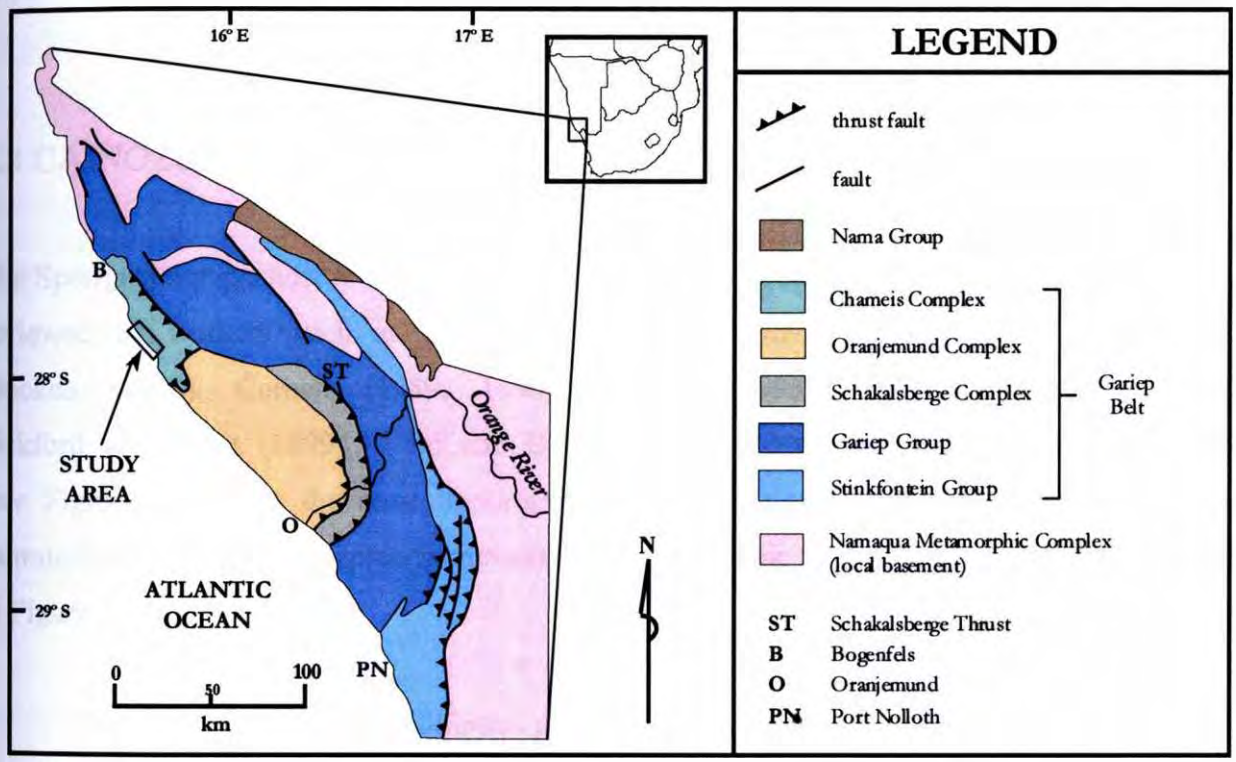

Figure 2.3. The Proterozoic to Palaeozoic rock units of the study region. Note that the study area falls wholly within the Chameis Complex of the Gariep Belt (modified after Frimmel and Hartnady, 1992).

The Mesozoic also saw the development of a dominant westward-flowing southern African drainage network which still persists in the modern situation (de Wit 1993; de Wit *et al.*, 2000; Partridge and Maud, 1987; Partridge, 1998). The emplacement of numerous diamondiferous kimberlites in the interior of southern Africa was accompanied by rapid denudation of the land surface during the Cretaceous, (Brown *et al.*, 1990; Dingle and Hendey, 1984;

Smith, 1988). This resulted in the erosion of many diamondiferous kimberlite pipes (Hawthorne, 1975; de Wit, 1993). Numerous diamonds were released into the Cretaceous drainage systems, and some are believed to have found their way to the west coast of southern Africa at this time (de Wit, 1993, 1996; de Wit *et al.*, 2000).

The only equivocally Mesozoic deposit preserved onshore on the Sperrgebiet coastline is the Wanderveld IV occurrence (SACS, 1980; Figure 2.4). The Wanderveld IV deposit consists primarily of a calcified shell bed, indicating a marine origin. Klinger (1977) assigned a Cenomanian (90 to 100 Ma) or Middle Cretaceous age to Wanderveld IV on the basis of dateable fossil shells.

2.4 CAINOZOIC FRAMEWORK

The Sperrgebiet plays host to a number of deposits of Cainozoic age which have been described or reviewed by workers such as Kaiser (1926), C.D. Hallam, (1964), Fowler (1976; 1982), Stocken (1978), Corbett (1989; 1996), Apollus (1995), R.J. Jacob, *et al.* (1999), Pickford and Senut (1999), Ward and Bluck (1997), Ward (2000) and Bluck *et al.* (2001) (see Figure 2.4). Only the most important deposits and those of relevance to this study are summarised here. A stratigraphic framework for the Cainozoic Sperrgebiet occurrences is provided in Figure 2.5.

The oldest known diamondiferous deposits in the Sperrgebiet are onshore marine gravels dated to the Late Eocene (ca. 42 Ma) (Kaiser, 1926; Siesser and Salmon, 1979; SACS, 1980). They contain exotic clasts derived from the interior of southern Africa and are situated between Buntfeldschuh and Granitberg (Figure 2.4). Although largely eroded away, some isolated occurrences remain at elevations of up to approximately 170 mamsl. Importantly, these deposits exhibit a highly distinctive exotic clast assemblage typified by the presence of yellow chalcedony associated with agate, banded ironstone, well rounded vein quartz, red jasper and rare chrysoprase, and which are sourced from the Vaal-Orange River catchment (C.D. Hallam, 1964; Stocken, 1978; Corbett, 1989; Ward, 2000; Figure 2.6). The Buntfeldschuh marine sediments are capped by a conformable aeolian sequence, which records a dominant southerly wind regime (Corbett, 1989). The Late Eocene marine sediments between Bogenfels and Granitberg are important for the following reasons :

Smith, 1988). This resulted in the erosion of many diamondiferous kimberlite pipes (Hawthorne, 1975; de Wit, 1993). Numerous diamonds were released into the Cretaceous drainage systems, and some are believed to have found their way to the west coast of southern Africa at this time (de Wit, 1993, 1996; de Wit *et al.*, 2000).

The only equivocally Mesozoic deposit preserved onshore on the Sperrgebiet coastline is the Wanderveld IV occurrence (SACS, 1980; Figure 2.4). The Wanderveld IV deposit consists primarily of a calcified shell bed, indicating a marine origin. Klinger (1977) assigned a Cenomanian (90 to 100 Ma) or Middle Cretaceous age to Wanderveld IV on the basis of dateable fossil shells.

2.4 CAINOZOIC FRAMEWORK

The Sperrgebiet plays host to a number of deposits of Cainozoic age which have been described or reviewed by workers such as Kaiser (1926), C.D. Hallam, (1964), Fowler (1976; 1982), Stocken (1978), Corbett (1989; 1996), Apollus (1995), R.J. Jacob, *et al.* (1999), Pickford and Senut (1999), Ward and Bluck (1997), Ward (2000) and Bluck *et al.* (2001) (see Figure 2.4). Only the most important deposits and those of relevance to this study are summarised here. A stratigraphic framework for the Cainozoic Sperrgebiet occurrences is provided in Figure 2.5.

The oldest known diamondiferous deposits in the Sperrgebiet are onshore marine gravels dated to the Late Eocene (ca. 42 Ma) (Kaiser, 1926; Siesser and Salmon, 1979; SACS, 1980). They contain exotic clasts derived from the interior of southern Africa and are situated between Buntfeldschuh and Granitberg (Figure 2.4). Although largely eroded away, some isolated occurrences remain at elevations of up to approximately 170 mamsl. Importantly, these deposits exhibit a highly distinctive exotic clast assemblage typified by the presence of yellow chalcedony associated with agate, banded ironstone, well rounded vein quartz, red jasper and rare chrysoprase, and which are sourced from the Vaal-Orange River catchment (C.D. Hallam, 1964; Stocken, 1978; Corbett, 1989; Ward, 2000; Figure 2.6). The Buntfeldschuh marine sediments are capped by a conformable aeolian sequence, which records a dominant southerly wind regime (Corbett, 1989). The Late Eocene marine sediments between Bogenfels and Granitberg are important for the following reasons :

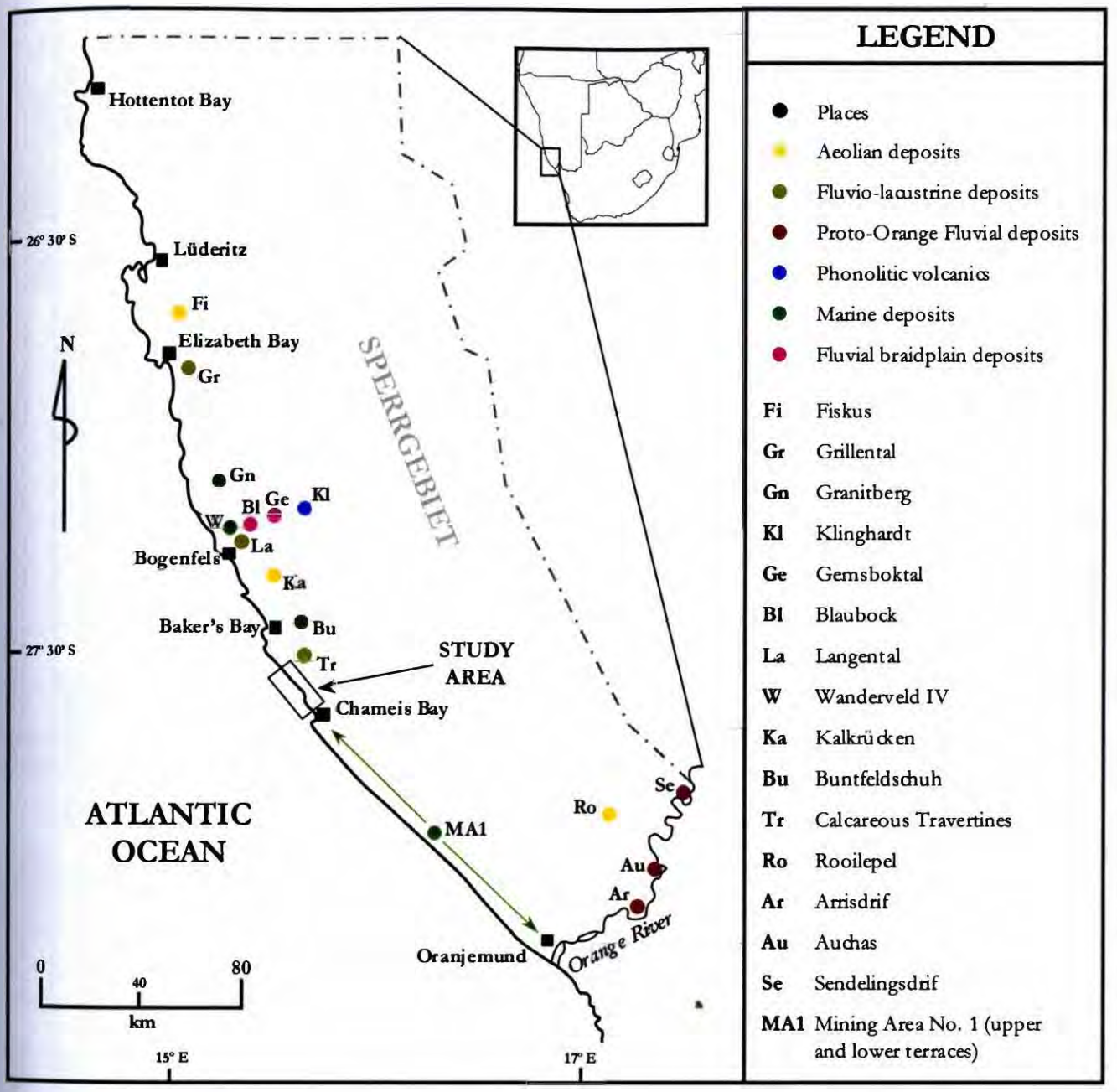

Figure 2.4. Important Cretaceous to Quaternary occurrences in the Sperrgebiet (modified after Ward, 2000).

a) Their distinctive exotic clast assemblage, together with the presence of diamonds, proves that diamondiferous material from the interior of southern Africa was being tapped and transported to the Sperrgebiet coastline by the Late Eocene. The principal conduit for this sediment and diamond transport to the Atlantic Ocean was the long-lived Vaal-Orange River drainage system (Ward and Bluck, 1997).

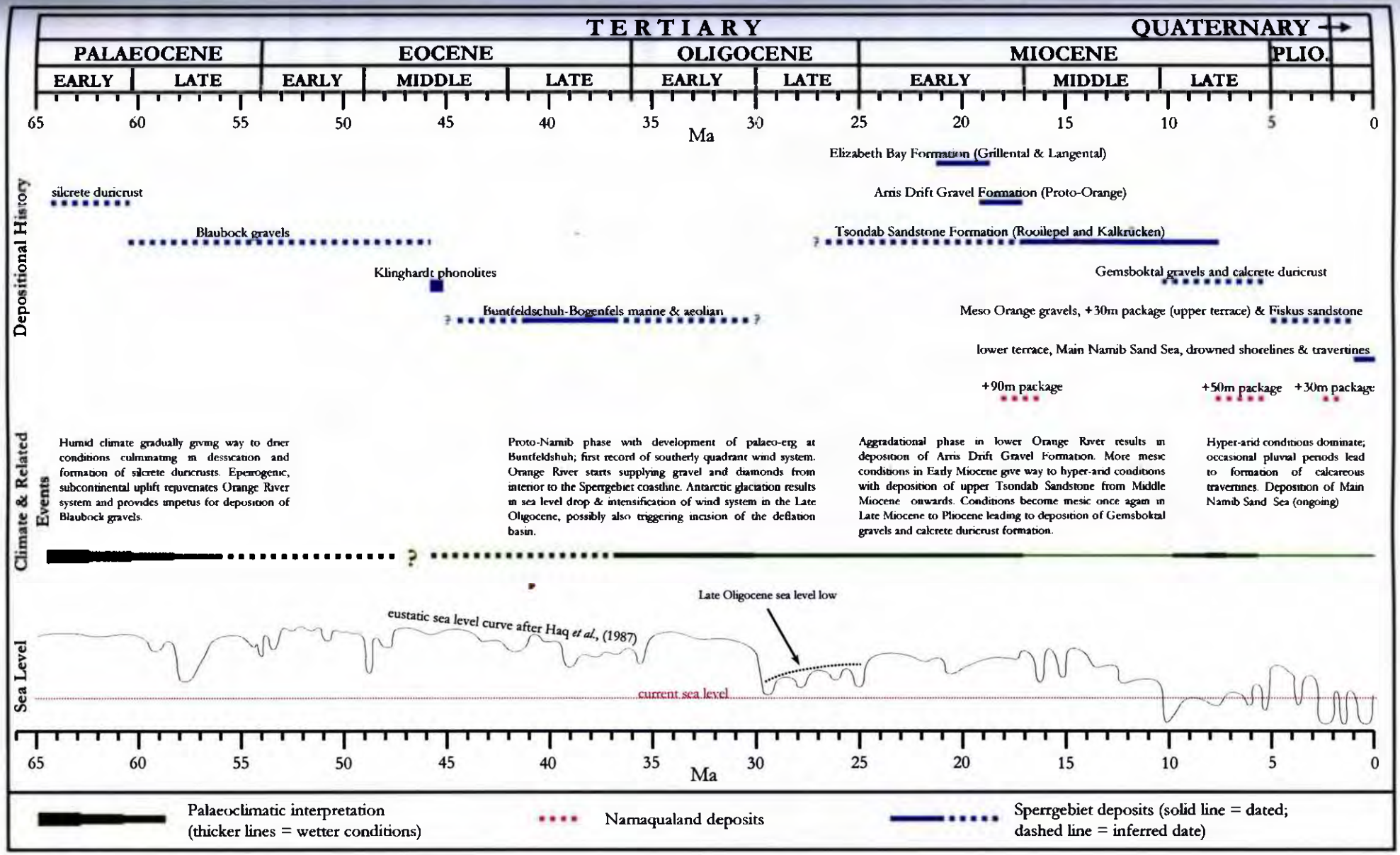

Figure 2.5. The stratigraphic framework for important Tertiary and Quaternary deposits of the Sperrgebiet and the coast of Namaqualand. Sources are C.D. Hallam (1964), Stocken (1978), Siesser and Salmon, (1979), Haq *et al.*, (1987), Corbett (1989; 1996), Pickford and Senut (1999), Ward and Bluck (1997), Ward (2000), Pether, (2000) and J.S. Marsh (pers. comm., 2002).

b) They demonstrate that the dominant southerly wind regime, which reigns in the present situation, was already established by the Late Eocene, and that the northerly littoral drift was already operating at this time.

Figure 2.6. A marine gravel layer at Buntfeldschuh, showing the clast assemblage that typifies the Eocene succession in the Sperrgebiet. Clast Types: yc=yellow chalcedony, rj=red jasper, bi=banded ironstone, ag=agate and rvq=well rounded vein quartz. Scale is 150 mm long.

The incision of the deflation basin may have been initiated by a protracted, well known Oligocene sea level lowstand (Tankard, 1975; Siesser and Dingle, 1981; Haq *et al.*, 1987; A. Hallam, 1992; Ward, 2000). The deflation basin is famous for its rich, thin, valley-floor diamond deposits. Significantly, the deflation basin diamonds are almost invariably associated with an exotic clast assemblage, which is typical of the Late Eocene marine sediments mentioned above. This has led most workers to conclude that the deflation basin diamonds accumulated by long-lived erosion and deflation of the Late Eocene marine sediments (Kaiser, 1926; C.D. Hallam, 1964; Stocken, 1978).

b) They demonstrate that the dominant southerly wind regime, which reigns in the present situation, was already established by the Late Eocene, and that the northerly littoral drift was already operating at this time.

Figure 2.6. A marine gravel layer at Buntfeldschuh, showing the clast assemblage that typifies the Eocene succession in the Sperrgebiet. Clast Types: yc=yellow chalcedony, rj=red jasper, bi=banded ironstone, ag=agate and rvq=well rounded vein quartz. Scale is 150 mm long.

The incision of the deflation basin may have been initiated by a protracted, well known Oligocene sea level lowstand (Tankard, 1975; Siesser and Dingle, 1981; Haq *et al.*, 1987; A. Hallam, 1992; Ward, 2000). The deflation basin is famous for its rich, thin, valley-floor diamond deposits. Significantly, the deflation basin diamonds are almost invariably associated with an exotic clast assemblage, which is typical of the Late Eocene marine sediments mentioned above. This has led most workers to conclude that the deflation basin diamonds accumulated by long-lived erosion and deflation of the Late Eocene marine sediments (Kaiser, 1926; C.D. Hallam, 1964; Stocken, 1978).

Diamondiferous gravel deposits comprising the Arrisdrift Gravel Formation (SACS, 1980), which are currently mined along the lower Orange River, have been dated to the Early Middle Miocene (ca. 17.5 Ma) (Corvinus and Hendey, 1978; Pickford and Senut, 1999). They are proof of the fixing of the course of the lower Orange near its current position by the Middle Miocene and underline the longevity of this important diamond conveyor.

C.D. Hallam, (1964) provided a good description of the Late Cainozoic, diamondiferous linear gravel beach deposits of MA1. He divided them into an upper and lower set of terraces (Figure 2.7). Upper terrace gravels, which are now largely mined out, have been completely reworked by the lower terrace in the north of MA1. C.D. Hallam, (1964) divided the lower terrace into three beaches. The first and oldest of these is known as the main terrace or 'C' beach, which reaches a maximum elevation of +10 mamsl. The main terrace is not preserved in the Sperrgebiet to the north of MA1. The intermediate terrace or 'B' beach reaches an elevation of +4 mamsl and is younger than the main terrace while the advanced terrace or 'A' beach represents the most recent sea level highstand at about +2 mamsl (Apollus, 1995; Ward, 2000). The gravel beaches of the lower terrace maintain a constant elevation along the Sperrgebiet coastline (C.D. Hallam, 1964). Along the seaward edge of the deflation basin, to the north of MA1, down-wasting processes have lowered some exoreic valley floors down to –25 mamsl. These valleys have been infilled with Late Quaternary pocket beach sediments, some of which form the subject of this study. The equivalents of the intermediate and advanced terraces are preserved within the pocket beach sequences at Sites 2 and 3 (this study). A number of drowned shoreline deposits of Late Quaternary age also occur on the inner continental shelf, offshore of the Sperrgebiet (Murray *et al.*, 1970; Joynt and Foster, 1976; Rogers, 1977).

The modern beaches of the Sperrgebiet comprise grit and sand, reflecting the current paucity of gravel supply to the coast by the Orange River (C.D. Hallam, 1964). The sediment load of the Orange River is sorted rapidly when it enters the Atlantic Ocean, with the suspended mud load being deposited out to sea and the sand/grit bedload being moved northward under the influence of the northerly littoral drift (Rogers, 1977; Mabote *et al.*, 1997). The sand by-passes the MA1 stretch of coastline and is moved onshore in log-spiral bays along the seaward edge of the deflation basin. The strong southerly winds then pick the sand up and move it through several aeolian transport corridors where it is ultimately deposited in the Namib Sand Sea (Corbett, 1989; Figure 2.8). The inner shelf is thus relatively deficient in finer sediment and the remaining gravels have been subject to continuous reworking by the sea during Tertiary transgressions and regressions (Rogers, 1977;

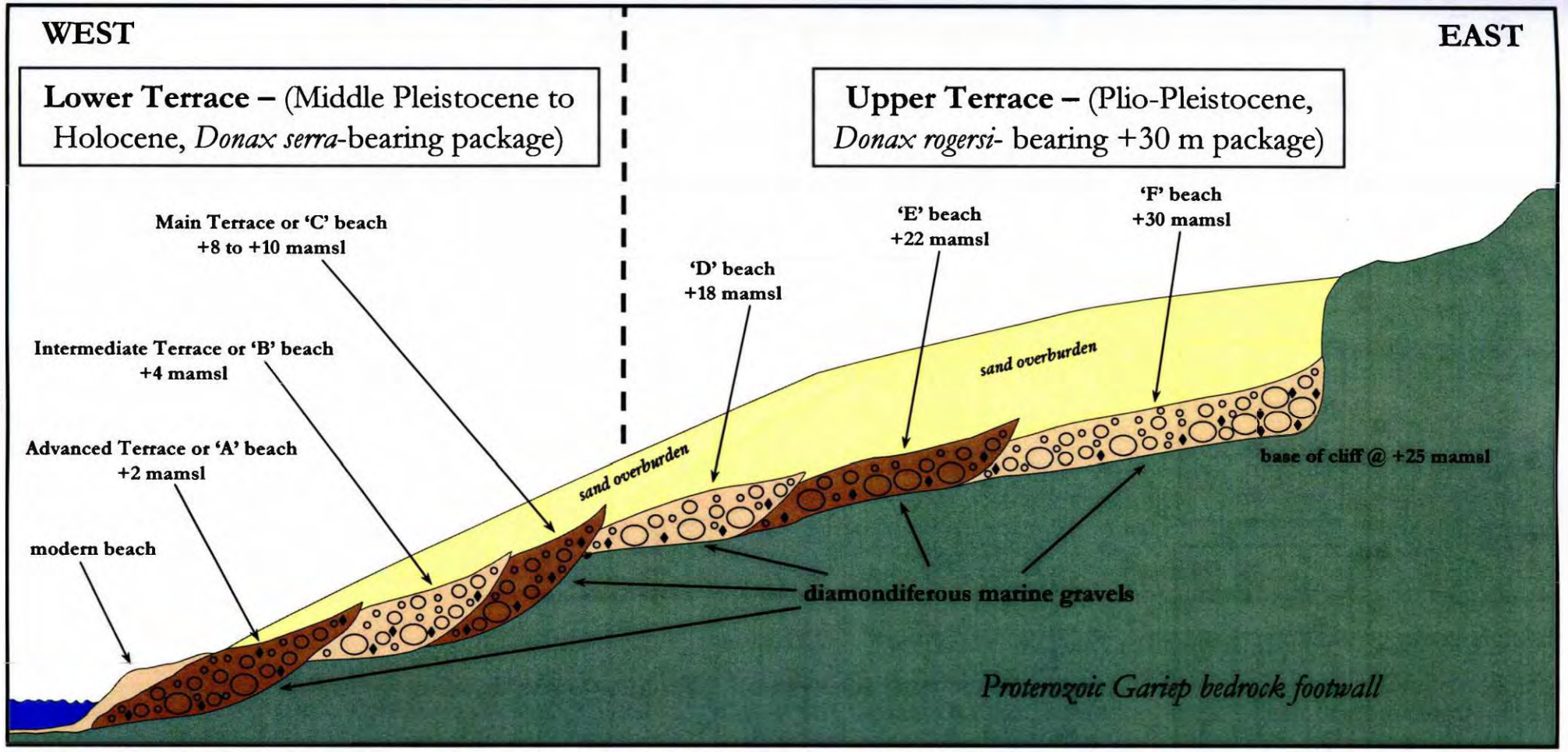

Figure 2.7. A schematic cross-section of the gravel beach deposits on MA1 (modified after C.D. Hallam, 1964 and J. Jacob, 2001).

Corbett, 1989). Downwasting still continues to take place in the deflation basin at the current time (Corbett, 1989; Ward, 2000).

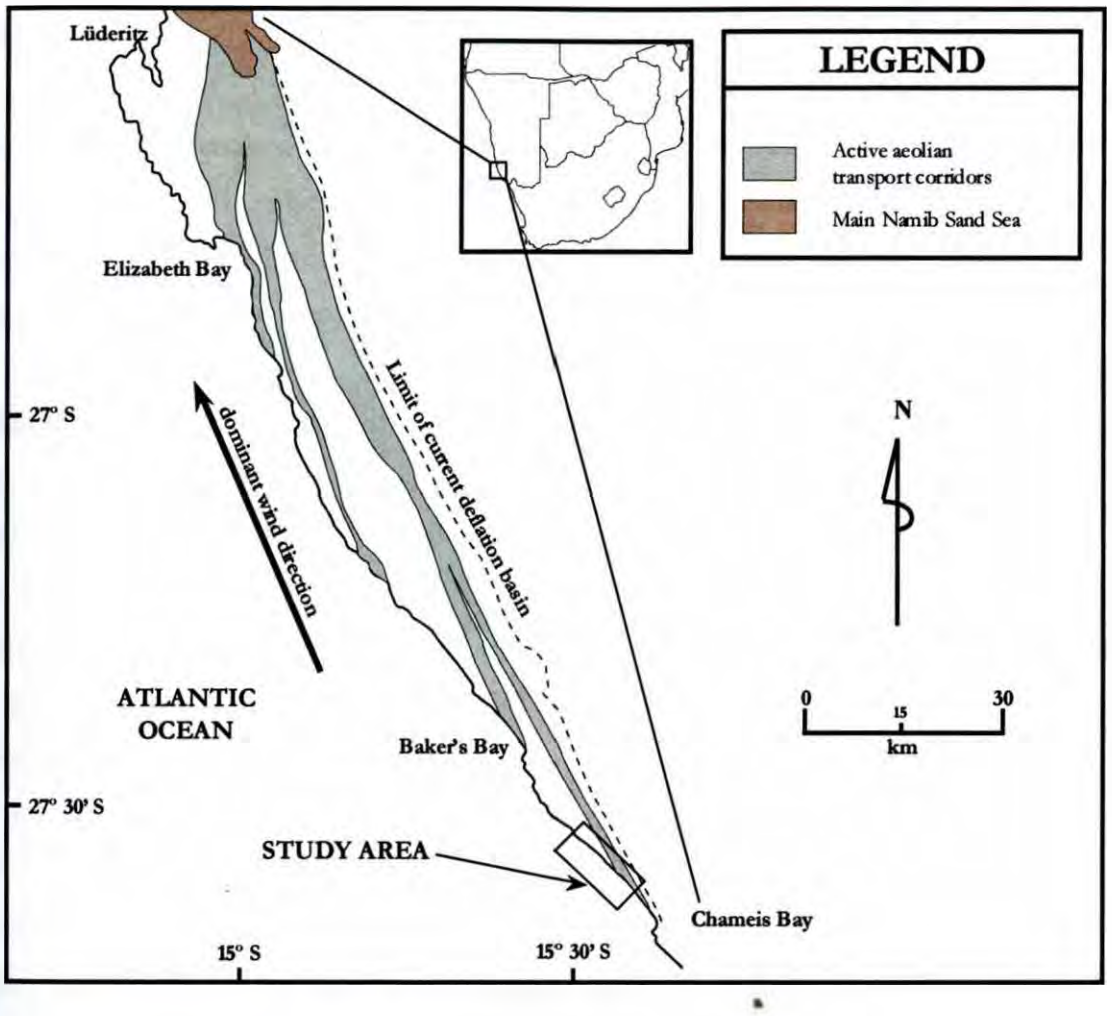

Figure 2.8. The positions of current aeolian transport corridors in the deflation basin (after Corbett, 1989).

CHAPTER 3 – METHODS

3.1 INTRODUCTION

The fourteen pocket beaches, which include Sites 2 and 3, were identified in an earlier prospecting campaign (1979 to 1981). The recent (1997 to 2002) pocket beach evaluation programme, which also included Sites 2 and 3, resulted in improved sedimentary facies identification and evaluation sampling of diamondiferous marine gravels using :

a) Small diameter delineation drilling.
b) Three-dimensional geological modeling, with the Vulcan© software package.
c) Bulk sampling, by means of trenching and also with a hydraulic grab tool called the GB50.
d) A limited number of gravel size distribution analyses of bulk sample tailings.
e) Mapping of the study area, using Airborne Laser Survey (ALS) imagery combined with field-checking.
f) Analysis, interpretation and radiocarbon dating of shell assemblages, collected from delineation drill holes, outcrops and bulk sample sites.

Access to drill and sample sites, handling of sample material, and related logistical activities were undertaken in an environmentally responsible manner, to ISO14001 standards.

3.2 EARLIER PROSPECTING CAMPAIGN (1979 TO 1981)

During the earlier prospecting campaign, a Frankipile-Casagrande casing-oscillator drill rig was used to excavate sample holes with a footprint of between 0.75 m^2 and 0.92 m^2 each. This campaign was conducted by geologists working for Consolidated Diamond Mines (Pty) Ltd. (which changed its name to Namdeb Diamond Corporation (Pty) Ltd. in the 1990's). The author was not involved in this earlier programme. Sediment type, grain size, shell content and the presence or absence of Orange River-derived exotic clasts was recorded. Down-the-hole samples of the sediments were taken in order to determine their diamond content, but these results have been omitted from this

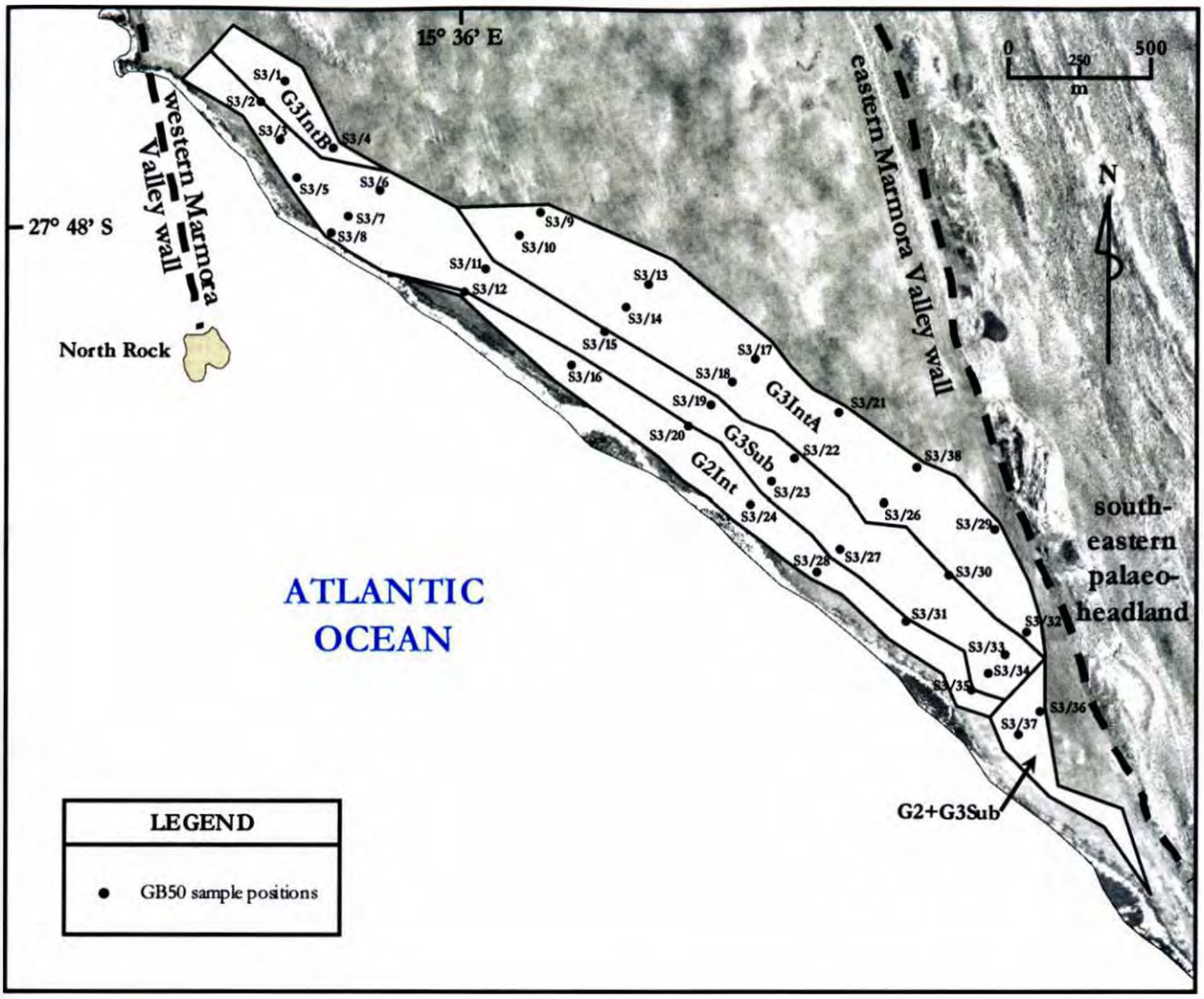

Figure 5.2. The positions of the GB50 samples of the marine gravels at Site 3. The backdrop is an aerial photograph of the area. Geological subdivisions of the marine gravels are as follows : *G3IntA* and *G3IntB* – intertidal gravels of G3; *G2+G3* – intertidal and subtidal gravels of G2 and G3 directly adjacent to each other, compressed into a narrow zone; *G3Sub* – subtidal gravels of G3; *G2Int* – intertidal gravels of G2.

5.2 ASPECTS OF THE POCKET BEACH GRAVELS

5.2.1 Gravel Size Distribution at Sites 2 and 3

Relative gravel size distribution for the marine gravel deposit at Sites 2 and 3 was determined by visual examination of the GB50 sample tailings, supported by a limited number of clast size

distribution analyses. These data are shown in Table 5.1 as well as in Figures 5.3 and 5.4. Three broad gravel coarseness categories were identified :

a)*fine gravel* – consisting mostly of clasts below 64 mm in size (ie. pebbles to small cobbles)

b)*medium gravel* – contain a significant proportion of cobbles greater than 64 mm, but less than 128 mm in size (ie. a significant number of medium cobbles)

c)*coarse gravel* – gravels with a relatively large proportion of clasts greater than 128 mm in size

Table 5.1. Four clast size distributions of GB50 sample tailings from Site 3. See Figure 5.2 for the positions of the GB50 samples.

Size Fraction	S3/7 (wt%)	S3/11 (wt%)	S3/23 (wt%)	S3/32 (wt%)
+4 mm-8 mm	18.0%	17.3%	20.3%	11.7%
+8 mm-16 mm	17.0%	16.6%	18.7%	9.8%
+16 mm-25 mm	16.4%	19.5%	11.9%	9.0%
+25 mm-32 mm	12.7%	17.4%	7.7%	5.6%
+32 mm-60 mm	29.2%	18.0%	36.8%	8.7%
+60 mm-95 mm	6.7%	9.5%	4.7%	22.8%
+95 mm-120 mm	0.0%	1.3%	0.0%	13.7%
+120 mm-150 mm	0.0%	0.4%	0.0%	11.7%
+150 mm	0.0%	0.0%	0.0%	6.8%

Data points are relatively sparse at Site 2, but coarser gravels generally occur on the south-eastern side of the marine gravel body, against the south-eastern palaeo-headland. The central and north-western sections of the Site 2 gravel body encompass fine-to-medium gravels.

At Site 3, coarse gravels are also concentrated in the southeast, against the palaeo-headland. Another small area of coarse gravels is evident at the north-western end of G2Int. The rest of G2Int and the north-western end of G3Sub contain fine gravels. The remainder of the marine gravel body at Site 3 consists of medium gravels.

The gravel coarseness variations are common to most of the beach gravel subdivisions. This indicates that the beach depositional processes responsible for this zonation do not represent the overriding control on gravel size distribution. Increased gravel coarseness is indicative of relatively

study because of the availability of larger, more representative samples from the recent evaluation programme. Figures 3.1 and 3.2 show the positions of the Frankipile holes at Sites 2 and 3.

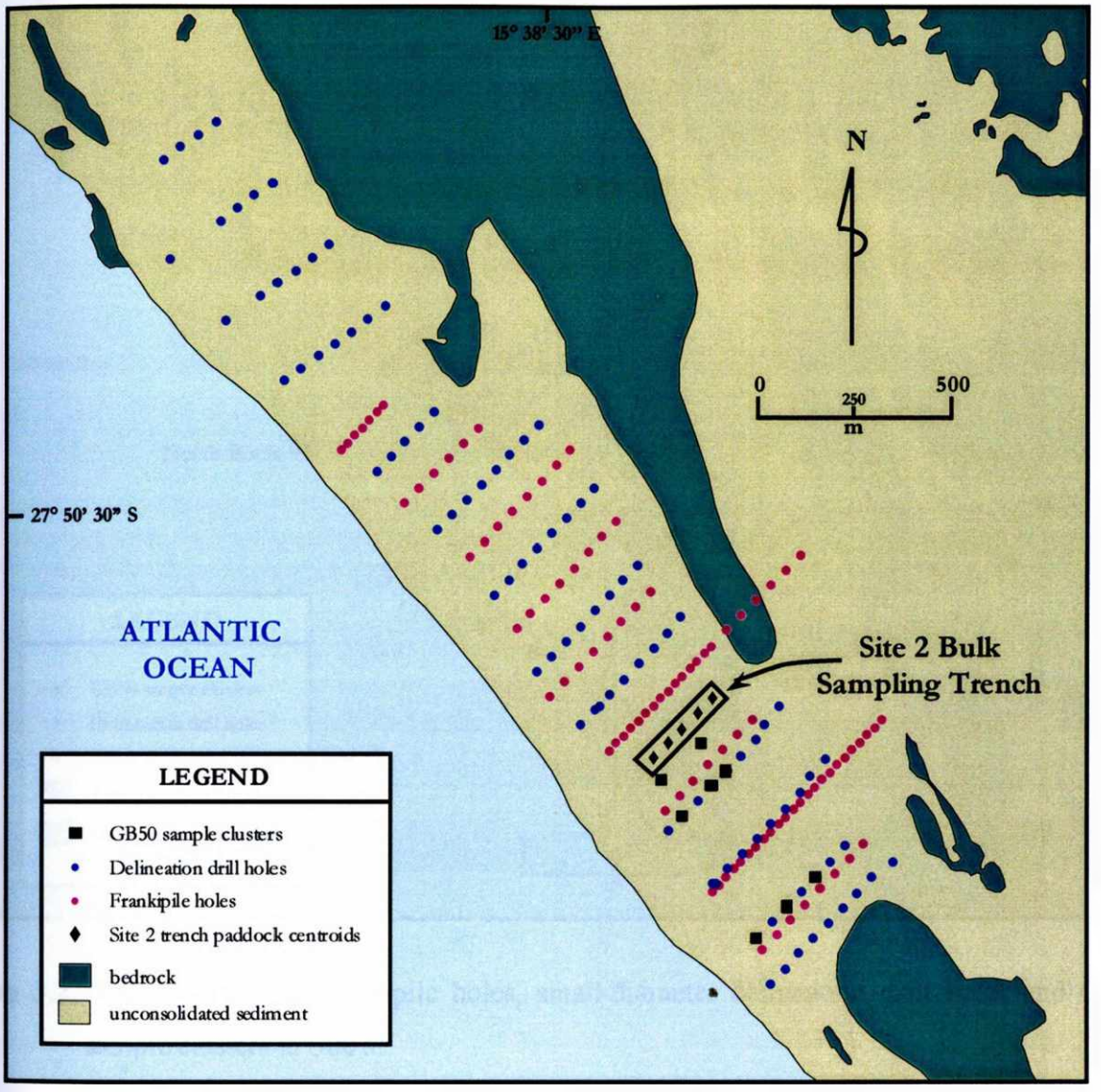

Figure 3.1. The positions of Frankipile holes, small-diameter delineation drill holes, GB50 sample clusters and the bulk sampling trench at Site 2.

3.3 RECENT EVALUATION PROGRAMME (1997 TO 2002)

The author assumed responsibility for the recent evaluation programme in late-1997, and supervised or conducted all of the work described below except where otherwise indicated.

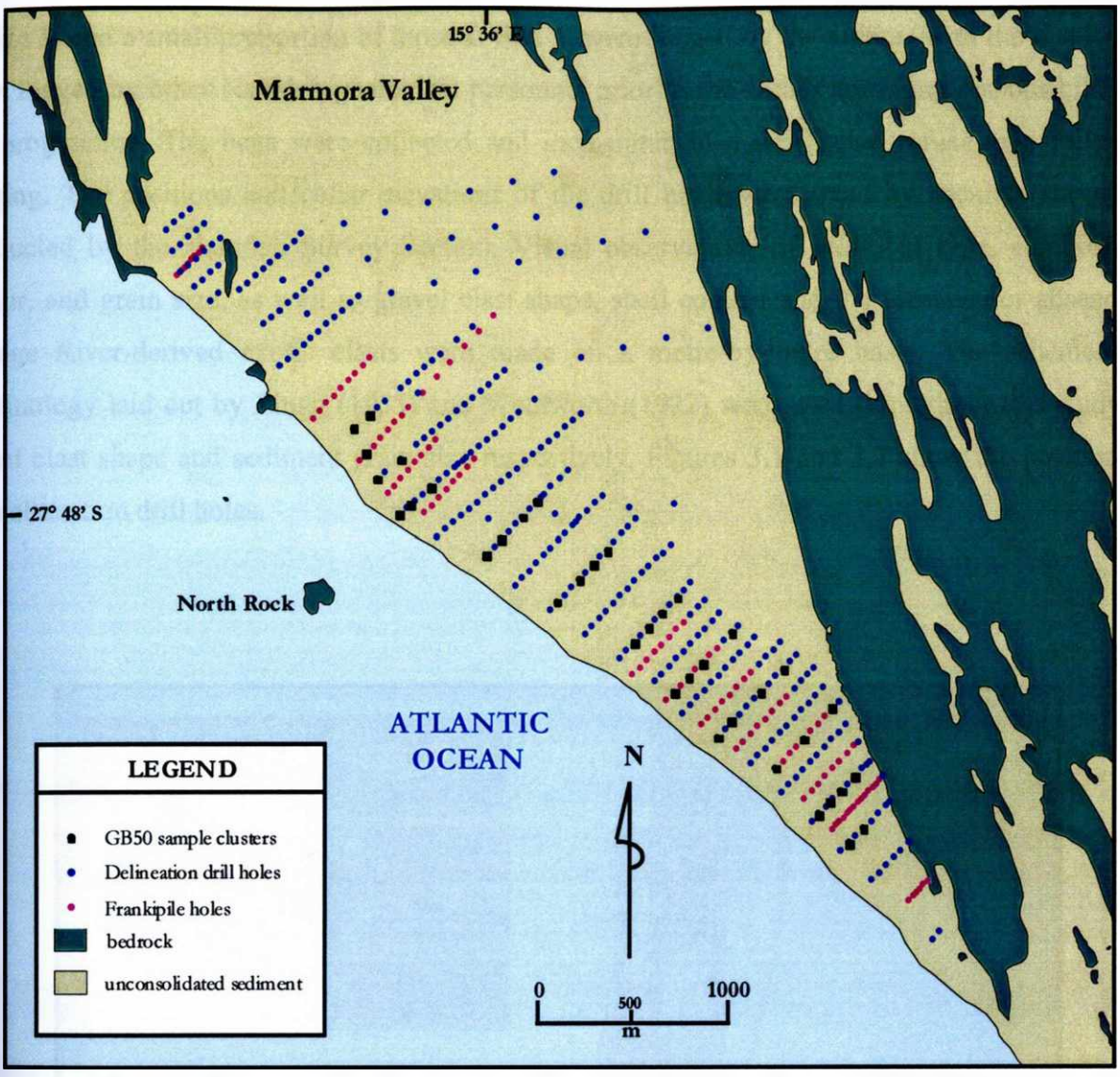

Figure 3.2. The positions of Frankipile holes, small-diameter delineation drill holes and GB50 sample clusters at Site 3.

3.3.1 Small Diameter Delineation Drilling

Small-diameter (6") delineation drilling constituted the first phase of work in the recent evaluation programme at Sites 2 and 3. The object of this drilling was to gather geological data and to determine the extent of the economic horizons, particularly the marine gravels, at these sites. A mud drilling system was used to accomplish this (see Figure 3.3). This system relies on a mixture of sea-water and a bio-degradeable polymer to transport the sediment up the hole. The sediment from each metre of advance was bagged and labelled for sedimentological logging. The majority of the holes

at Site 3, and a small proportion of those at Site 2, were logged by the author, with the rest having been logged by other Namdeb geological personnel prior to the author assuming responsibility for the programme. The bags were collected and incinerated in a designated refuse area following logging. The positions and collar elevations of the drill holes were fixed by accurate surveying, conducted by the Namdeb Survey Section. Visual observations of sediment type, composition, colour, and grain size, as well as gravel clast shape, shell content and the presence or absence of Orange River-derived exotic clasts were made on a metre-by-metre basis. The schemes and terminology laid out by Zingg (1935) and Wentworth (1922) were used throughout this study for visual clast shape and sediment grain size respectively. Figures 3.1 and 3.2 show the positions of the delineation drill holes.

Figure 3.3. The mud drill rig used to conduct small diameter delineation drilling at pocket beach Sites 2 and 3. This drilling constituted the first phase of a recent (1997 to 2002) evaluation programme. The inset shows a hollow-core bit that was used.

3.3.2 Three Dimensional Geological Modeling

The drill hole data gathered during the Frankipile and small diameter delineation drilling programmes was electronically captured and inputted into a three dimensional geological modeling software package called Vulcan©. Three dimensional models of the marine gravels (Figure 3.4) and other geological units in the pocket beach sequences were created. This greatly aided in :

a) The recognition of individual beach packages and beach sub-environments within the marine gravels at Sites 2 and 3.

b) The interpretation of the other units comprising the pocket beach sequences, primarily because of the clear visualisation of their morphology provided by the three dimensional views generated in Vulcan©.

c) The optimal siting of GB50 evaluation samples (see below), which were subsequently used to estimate the diamond content of the marine gravels.

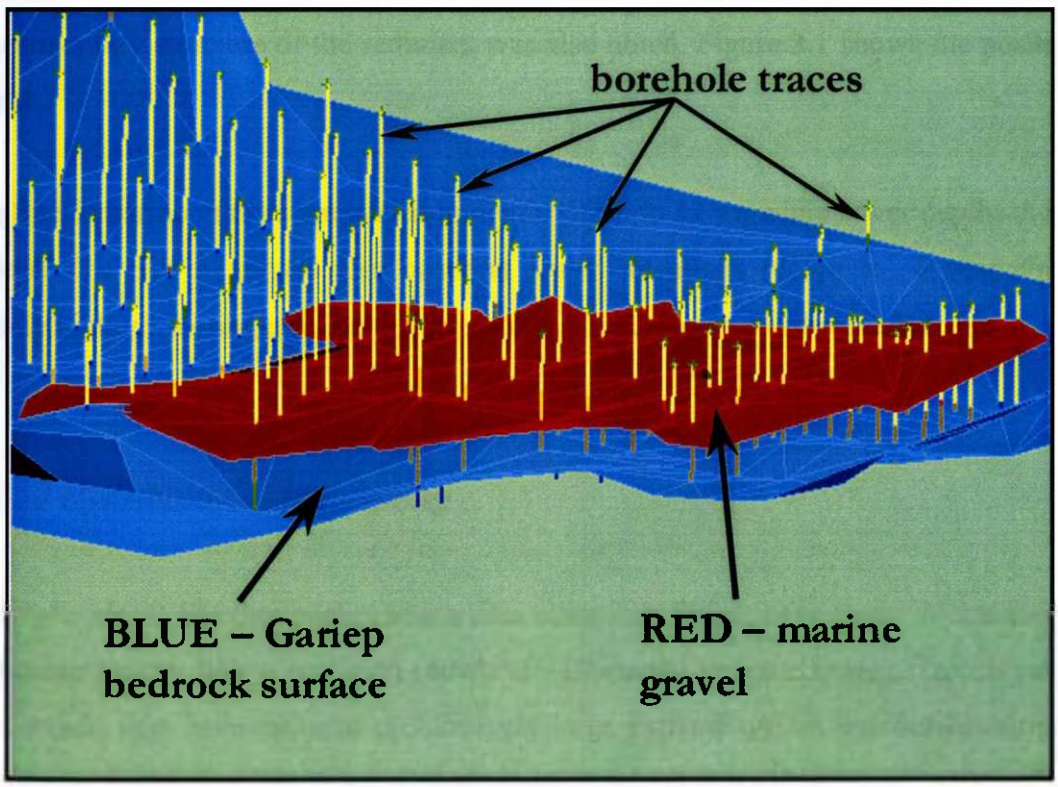

Figure 3.4. A three-dimensional view from the southwest, in Vulcan©, of the bedrock surface and buried marine gravel body at Site 2. The green crosses at the top of the borehole traces are the positions of the hole collars. Vertical exaggeration is 10x. Width of view is approximately 1 km.

3.3.3 Site 2 Bulk Sampling Trench

In 1997 a bulk sampling trench, oriented perpendicular to the coastline in order to cross the strike of the pocket beach sediments, was excavated at Site 2. The primary objective of this was to obtain a representative sample of the marine gravel, in order to evaluate its diamond content. The sand overburden was mechanically stripped away to expose the buried marine gravels over a distance of 250 m. Five paddock samples of the marine gravel, each 50 m in length, were then taken. The stripping and paddock excavation was conducted prior to the author's involvement in the recent evaluation programme.

Diamonds falling within the 2 mm to 16 mm fraction were recovered from the samples using heavy mineral separation and X-Ray treatment plants, followed by hand sorting in a dedicated, high-security prospecting laboratory. The northern wall of the trench was accurately logged by the author, using survey points as reference. The same sedimentological parameters recorded during logging of the delineation drill holes were also recorded in the trench, and in addition to these, the internal sedimentary structure of the sediment was also noted. Figure 3.1 shows the position of the Site 2 trench.

The Site 3 marine gravels are buried to depths of up to 13 m, while cover depths at Site 2 are 7 m or less. The Site 3 gravels also occur at lower elevations (down to –8 mamsl), and are consequently highly waterlogged. For these reasons, a trench was not attempted at Site 3.

3.3.4 GB50 Hydraulic Grab Sampling

The marine gravels, at all other pocket beach sites other than Site 2, have cover thicknesses of up to 20 m and occur mostly below sea level (down to –18 mamsl in some cases). Trench sampling at these sites would thus have required prohibitively large expenditure on overburden stripping and de-watering equipment. For this reason, an alternative sampling method was sought and found in the GB50 hydraulic grab tool. The GB50, manufactured and marketed by Bauer-Germany, is capable of excavating a rectangular hole 1.2 m by 2.8 m in size (hole area = 3.36 m^2) through unconsolidated, waterlogged sediment, to depths of 80 m or more. The GB50 was used to dig through the sand overburden, discarding it, until the marine gravel horizon was reached

(Figure 3.5). The marine gravel was then sampled, and the diamonds in the 2 mm to 16 mm fraction were recovered in a process similar to that outlined for the Site 2 bulk sampling trench (Figure 3.6). A full GB50 sample typically comprised three holes clustered close together; the marine gravel from these three holes was batched during sample treatment. A GB50 sample thus had a total footprint of 10.08 m^2, being an order of magnitude larger than a Frankipile sample. GB50 samples were therefore considered to be far more representative than the earlier Frankipile samples. GB50 sample tailings, consisting of the original sample with the –2 mm fraction removed, served as valuable sources of geological information. Visual observations of sediment type, composition, colour and grain size, as well as gravel clast shape, shell content and the presence or absence of Orange River-derived exotic clasts were recorded from the GB50 tailings. The GB50 programme at Sites 2 and 3 took place during 1999 and was supervised entirely by the author. Figures 3.1 and 3.2 show the positions of the GB50 sample clusters at Sites 2 and 3.

3.3.5 Gravel Size Distribution Analyses

The tailings of four GB50 samples of the marine gravel at Site 3 were sieved in order to determine their clast size distribution. The primary objective of this work was to assist the mining feasibility team in the design of mining tools for Site 3. Each of the four sample tailings was first sieved into five fractions, namely +2 mm –60 mm, +60 mm –95 mm, +95 mm –120 mm, +120 mm –150 mm and +150 mm. The weights of each of the five fractions were recorded; the total weights of the tailings ranged between 1 ton and 6 tons. A well-mixed sub-sample of approximately 5kg was then taken from the +2 mm –60 mm fraction of each of the GB50 sample tailings and sieved into six additional fractions, namely +2 mm –4 mm, +4 mm –8 mm, +8 mm –16 mm, +16 mm – 25 mm, +25 mm –32 mm, and +32 mm –60 mm. The results of the two sieving analyses were then combined to give a comprehensive clast size distribution for each of the four GB50 sample tailings.

3.3.6 Airborne Laser Survey (ALS) Imagery

The entire coastal strip between Oranjemund and Lüderitz, which includes pocket beach Sites 2 and 3, was recently surveyed using an airborne laser device, under the supervision of the Namdeb Survey Section. The survey system incorporates a high-resolution, colour digital

Figure 3.5. Taking a GB50 sample - i) Digging in of the standpipe, pumping a mud medium of attapulgite and sea water into the hole and beginning excavation. ii) Discarding the sand and grit overburden. iii) Careful placing of the marine gravel sample in a 12 ton multibucket. iv) Transport of the gravel to the heavy mineral separation treatment plant.

Figure 3.6. Heavy Mineral (HM) Separation process for the Site 2 Trench and GB50 samples - i) Tipping bin, 90 mm grizzly and 2 mm de-sanding screen (-2 mm and +90 mm material removed). ii) The scrubber and 16 mm trommel (+16 mm material removed). iii) +2-16 mm feed to 200 mm cyclone (HM separator – using ferrosilicon medium). iv) Discharge chute for floats and +16-90 mm material from scrubber. The orange object under the conveyor belt is the HM concentrate cage. The HM concentrate was taken to a secure location for X-Ray treatment and hand sorting.

imaging system. The laser equipment was used to obtain centimetre-accuracy elevation data of the land surface while the digital camera acquired colour images with a ground resolution of 30 cm. The ALS imagery was used, by the author, to map the surface geology and nearshore wave refraction patterns at pocket beach Sites 2 and 3. The maps, and especially the more significant geomorphic features, were carefully field-checked over the course of the recent evaluation programme.

3.3.7 Fossil Shell Studies

A number of fossil shell samples were collected by the author from delineation drill holes, GB50 sample tailings, outcrops and the Site 2 trench at Sites 2 and 3, as well as from the surrounding area. The shell assemblages were identified and interpreted by Pether (2001). Several shells were then selected from these assemblages and submitted to the Quaternary Dating Laboratory in Pretoria for radiocarbon dating. None of the submitted shells showed evidence of recrystallisation or calcite overgrowths. Every effort was made to collect and submit shells that showed the least degree of abrasion, and which could reasonably be assumed to have lived close to the time that their sediment of origin was deposited. Where more than 30 g of shell material was available, the conventional ^{14}C method was employed for analysis; where less than 30 g was available, the Ablation Mass Spectrometry (AMS) method was used. Calibrated ages for the shells were obtained using the CAL4P program (Talma and Vogel, 1993). A reservoir age of 550 years is assumed for South Atlantic waters by this program, which also makes use of the marine data set of Stuiver and Braziunas (1993). Besides analytical errors, there are uncertainties associated with the age of upwelling water in the South Atlantic and the rate of carbon uptake in the different species analysed.

CHAPTER 4 – GEOLOGY AND DEPOSITIONAL HISTORY

The aim of this chapter is to describe the geomorphology and geology of pocket beach Sites 2 and 3 with a view towards deriving a model for their depositional history. Understanding the geology, geomorphology and depositional history of the pocket beaches, and particularly the beach gravels they encompass, is essential to the evaluation of their diamond content.

4.1 GEOMORPHOLOGICAL SETTING

4.1.1 The Central and Southern Sperrgebiet Coastline

The deflation basin coastline, which hosts the pocket beaches, consists of a series of bays and intervening headlands. The bays are formed at exoreic valley mouths or where a ridge has been breached, and the headlands occur where ridges intersect the coastline. This configuration is a consequence of drowning of the north-south, deflation basin valleys by the sea (see Figure 4.1).

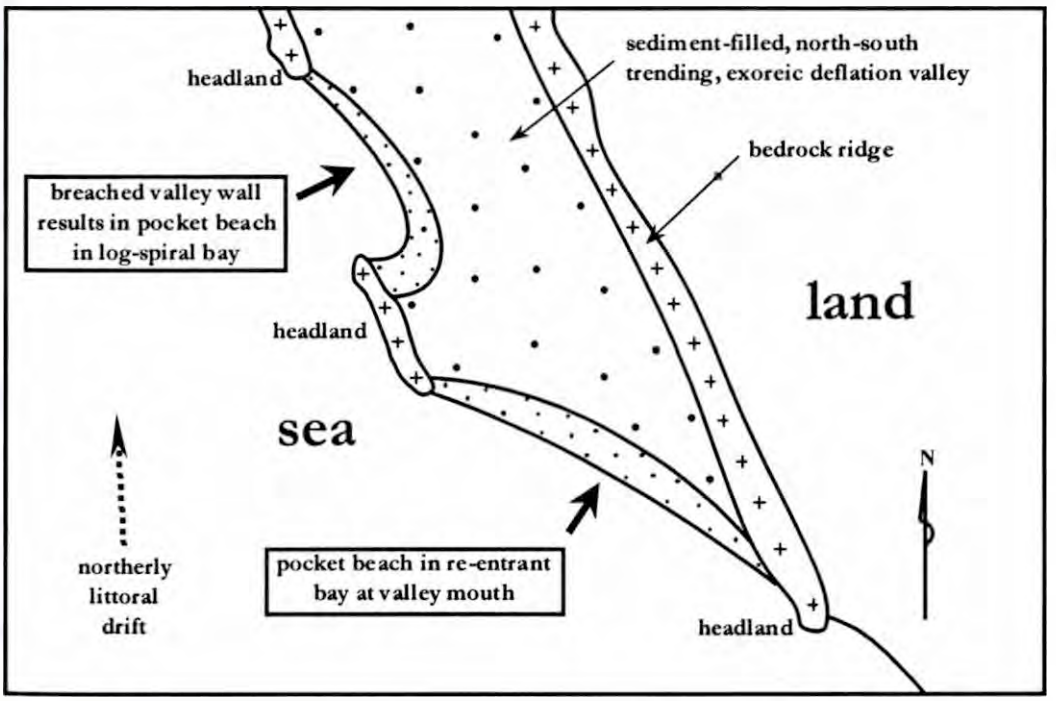

Figure 4.1. A sketch showing the types of pocket beaches that have formed due to drowning of the deflation basin valleys along the Central Sperrgebiet coastline.

The over-deepened valleys of the deflation basin have therefore provided the required accommodation space for the pocket beaches at Sites 2 and 3.

The MA1 stretch of coastline is relatively straight (ie. devoid of embayments) and its associated linear beach deposits are relatively thin and laterally unconfined. This is partly a reflection of the limited relief on the Gariep basement, which places restrictions on the extent to which sediments can vertically accrete; it is also partly a reflection of the higher beach accretion rates closer to the Orange River mouth, which have tended to smooth out the coastline. Vertical accommodation space within the more deeply eroded valleys of the deflation basin is much greater and the pocket beach sedimentary fills are thus relatively thick, although laterally confined (see Figure 4.2).

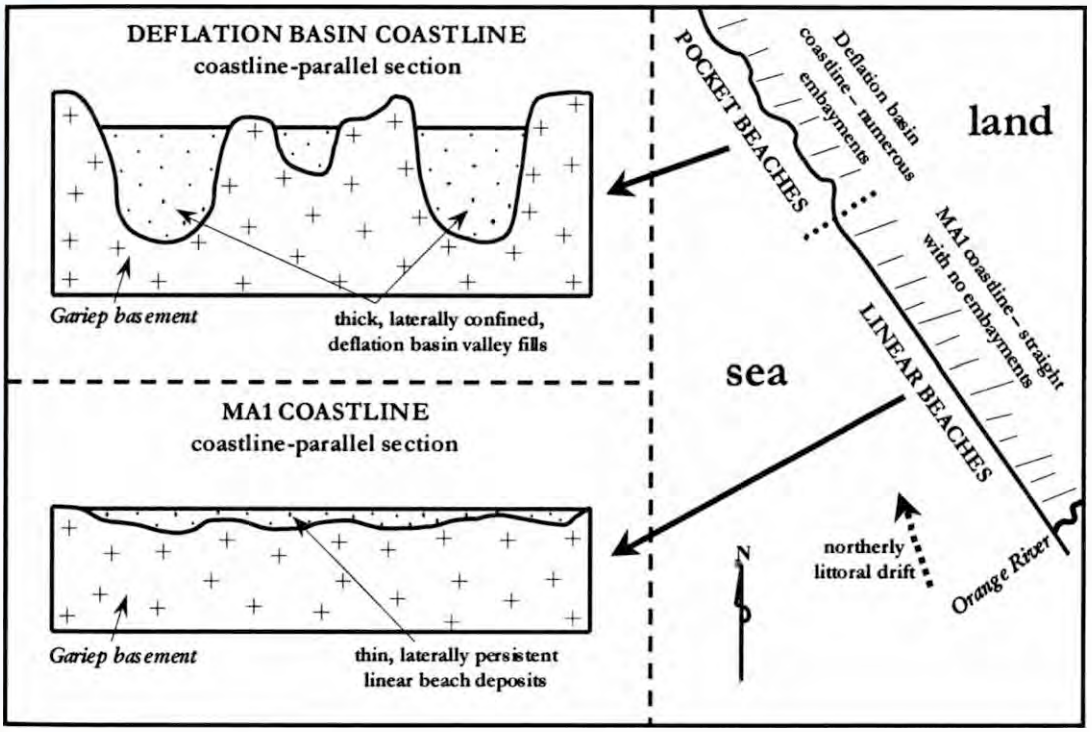

Figure 4.2. A sketch illustrating the difference between pocket beach and linear beach deposits of the Sperrgebiet coastline with respect to accommodation space.

4.1.2 Geomorphology of Site 2

Site 2 lies within a re-entrant bay at the mouth of a small, north-south trending deflation valley called the Site 2 palaeo-drainage (Figure 4.3). The valley walls swing towards the west close to the

coast. Delineation drilling indicates that the bedrock floor of the Site 2 palaeo-drainage has been eroded to an average maximum depth of between –8 mamsl and –10 mamsl. The more prominent eastern bedrock ridge of the Site 2 palaeo-drainage forms a headland at the south-eastern end of the site. The western ridge is poorly developed and is covered by sediment (see Figures 4.3 and 4.4).

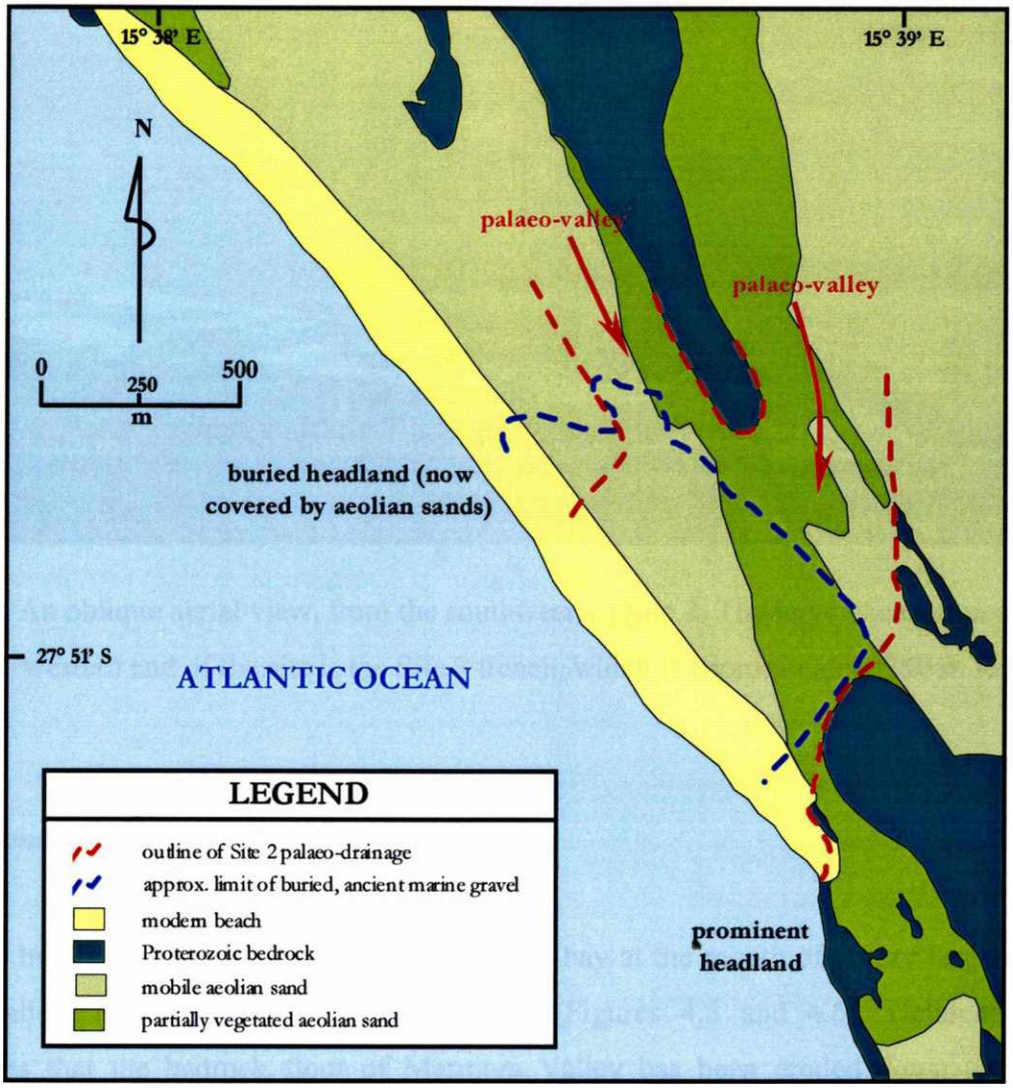

Figure 4.3. Aspects of the surface and sub-surface geomorphology of the pocket beach at Site 2. The western bedrock ridge of the Site 2 palaeo-drainage forms a buried headland at the northern end of the site and is onlapped by buried pocket beach gravels.

The eastern portion of the site is blanketed by northward-migrating aeolian sand dunes and grit sheets, which are derived from the modern beach to the southwest. The dunes increase in height towards the north. The modern beach at Site 2 has a relatively uniform grain size, steepness and width, is slightly arcuate in shape, and has a south-westerly aspect. The buried, ancient marine

gravel deposit at Site 2 is best developed within its palaeo-drainage valley, onlaps the northwest bank, and then becomes patchy further to the north (Figure 4.3).

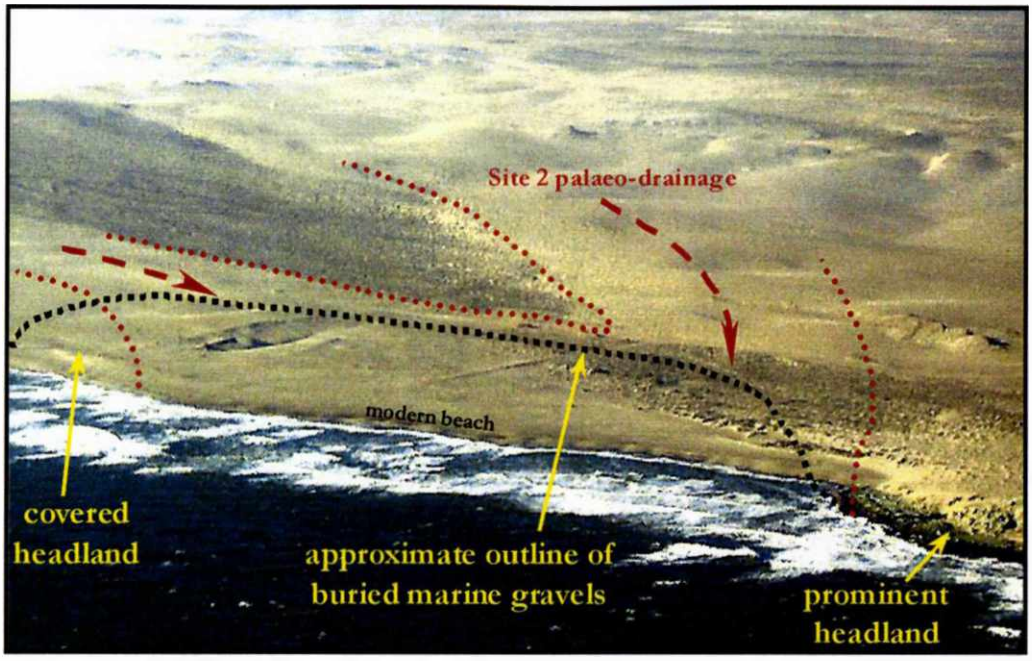

Figure 4.4. An oblique aerial view, from the southwest, of Site 2. The large excavation at the north-western end of the site is the Site 2 trench, which is approximately 250 m long.

4.1.3 Geomorphology of Site 3

The pocket beach at Site 3 is situated in a re-entrant bay at the mouth of a very large north-south trending valley, locally termed Marmora Valley (Figures 4.5 and 4.6). Delineation drilling demonstrates that the bedrock floor of Marmora Valley has been eroded down to an average elevation of –25 mamsl, and that the valley has subsequently been infilled with unconsolidated sediment. Two prominent north-south trending bedrock ridges protrude several tens of metres above the surface of the sediment fill and form the south-eastern and north-western headlands of the pocket beach where they obliquely intersect the coastline. The submarine extension of the western Marmora Valley wall is manifested by North Rock, which protrudes a few metres above sea level in the immediate offshore.

A very large pan, known locally as Marmora Pan, occupies the central and northern portions of Marmora Valley. The surface of Marmora Pan has an elevation close to current sea level and is

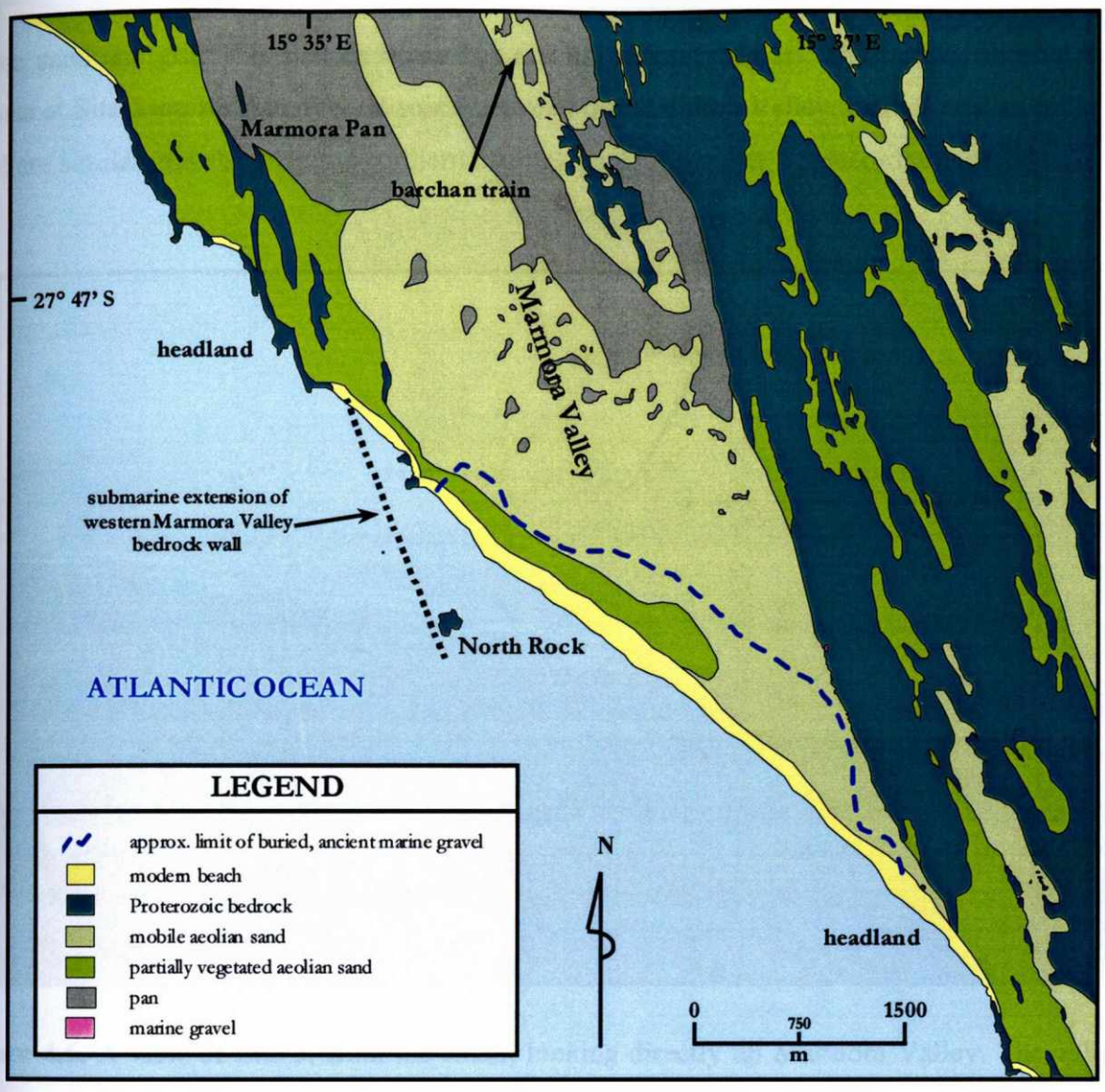

Figure 4.5. Aspects of the surface and sub-surface geomorphology of the pocket beach at Site 3. Note the submarine extension of the western Marmora Valley wall.

damp, coinciding with the water table. Adhesion warts and anhydrite crusts are a common feature on the pan surface (Figure 4.7). These features are typical of sabkhas (Reineck and Singh, 1975; Collinson, 1978a) and Marmora Pan therefore represents a coastal sabkha, cut off from the sea by the modern beach. Aeolian sand sheets and granule mega-ripples as well as transverse and barchan dunes occur on Marmora Pan, especially towards its seaward (southern) end. As with Site 2, the aeolian sediment is being transported northward by the dominant southerly winds and is sourced from the modern beach. A small barchan dune train is currently migrating over the pan surface and exiting at the northern end of Marmora Valley. A series of partially vegetated backshore dunes occur to the west of the mobile aeolian sediments and fringe the modern beach, which consists of

coarse sand and grit. The modern beach has a south-westerly aspect. The buried, ancient marine gravels at Site 3 are restricted to the space between the Marmora Valley bedrock walls (unlike Site 2, where similar gravels onlap the northern bedrock bank of the Site 2 palaeo-drainage).

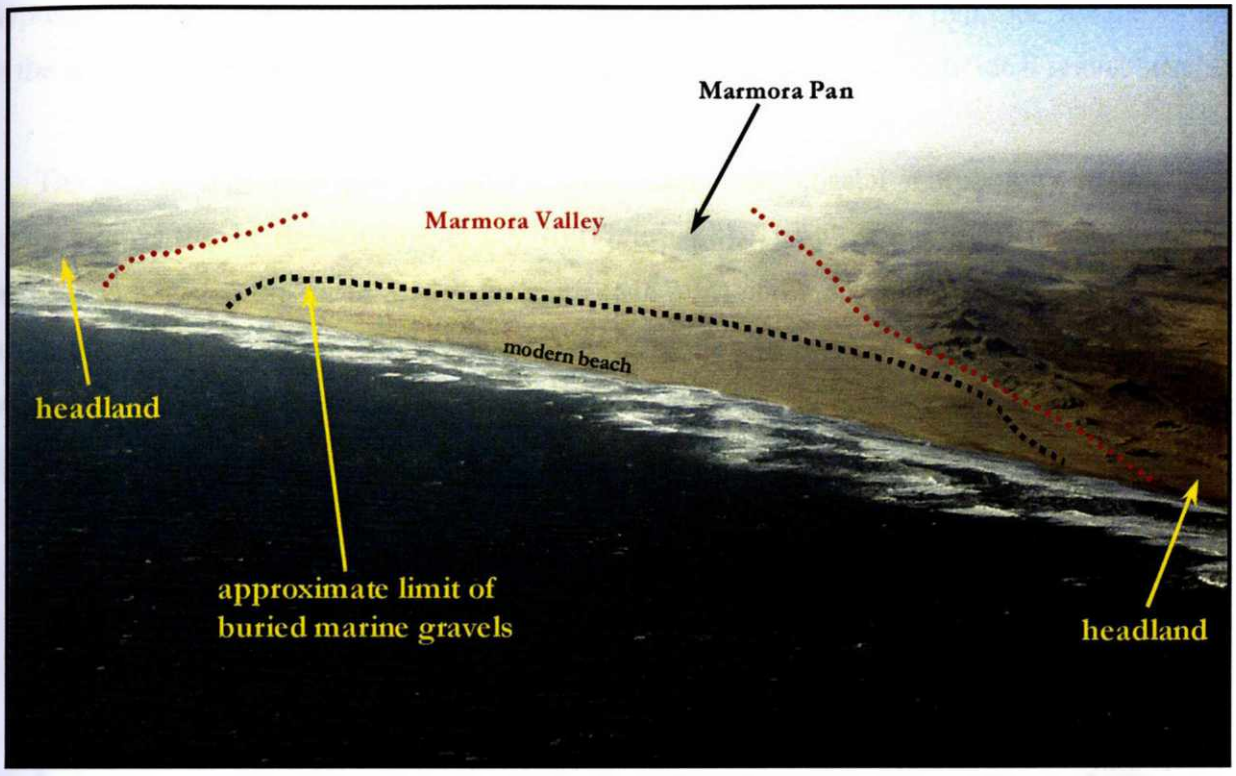

Figure 4.6. A view of Site 3, from the south, looking directly up Marmora Valley. The valley is approximately 3 km wide.

Figure 4.7. Adhesion warts and anhydrite crusts on the surface of Marmora Pan. These features are typical of coastal sabkhas. Scale is 150 mm.

4.2 RELEVANT CHARACTERISTICS OF GRAVEL BEACHES

Buried gravel pocket beaches at Sites 2 and 3 have been identified using morphological and sedimentological criteria. The ability to identify gravel beach environments is vital to the interpretation of the geology and economic geology of the marine gravel deposits. It follows then that the accurate evaluation of them also depends upon the recognition of individual gravel beaches.

The terminology and general classification scheme for coastal morphology in this study broadly follows that of Brenninkmeyer (1976) (Figure 4.8). The most important feature to note is that the area between the mean low water mark (MLWM) and mean high water mark (MHWM), also known as the beachface, is characterised by a prominent break in slope at its seaward end. Similar breaks in slope were identified in the marine gravels at Sites 2 and 3, using coastline-perpendicular cross-sections constructed from the delineation drill and Site 2 trench data.

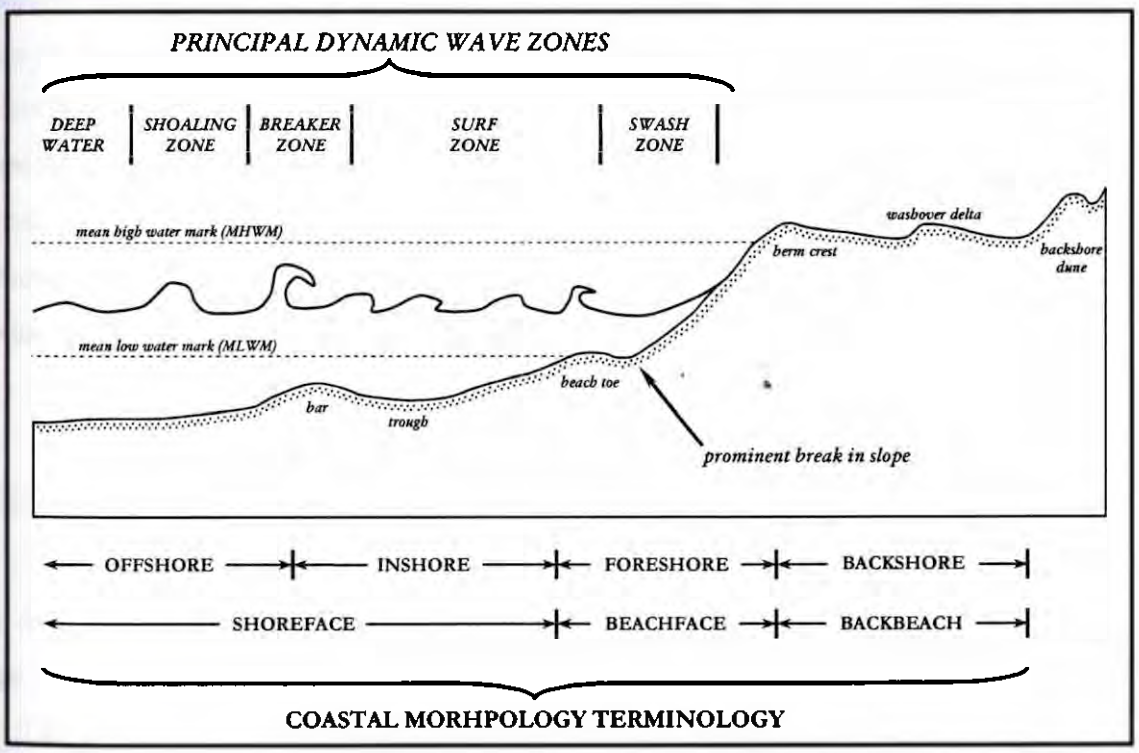

Figure 4.8. The terminology applied in this study for coastal morphological and principal dynamic wave zones. Note the prominent break in slope at the seaward end of the beachface (modified after Brenninkmeyer, 1976).

A benchmark study of gravel beaches by Bluck (1967) showed that they are zoned on the basis of the shape and size of clasts constituting the surface layers. Four zones were identified :

a) A *large disc zone* fringing and to the landward of the MHWM and consisting of cobble sized, disc shaped clasts.
b) An *imbricate zone* to the immediate seaward of the large disc zone, consisting of pebble sized, disc shaped clasts. The small discs in this zone display seaward-dipping imbrication.
c) An *infill zone* to the seaward of the imbricate zone, where spherical and rod shaped pebbles infill a framework of spherical cobbles.
d) An *outer framework*, fringing the seaward beach margin and consisting of spherical cobbles.

This zonal classification scheme has since been confirmed and sometimes modified by workers such as Williams and Caldwell (1988) and Hobday and Banks (1971). The lattermost workers, very significantly, identified Bluck's (1967) zonation in a gravel pocket beach in Tanafjord, Norway. Delineation drilling and logging of the Site 2 trench resulted in the clear identification of Bluck's (1967) zones in the marine gravels at pocket beach Sites 2 and 3, although not all of the zones are preserved in some of the gravels units. Where present, the large disc zone was observed to correspond with the berm crest, the imbricate zone was identified as the upper beachface, the infill zone corresponded with the beach toe, and the outer framework was identified as the upper shoreface (see Figure 4.9). For evaluation purposes (discussed later), only subtidal and intertidal subdivisions were recognised.

4.3 GENERALISED LITHOSTRATIGRAPHY - POCKET BEACH SITES 2 & 3

Using data drawn from logging of the Site 2 trench, delineation drill holes and GB50 sample tailings, several marine and terrestrial packages were identified in the pocket beach Sites 2 and 3 valley fills, and their lithostratigraphic relationships were unravelled (Table 4.1). It was found that some of the marine units could be correlated with packages described by C.D. Hallam (1964) and Apollus (1995). Descriptions, in order of decreasing age, of the various unconsolidated sedimentary units at Sites 2 and 3 (ie. post-Gariep Belt), are presented below. The range of permutations in the contact relationships between lithostratigraphic units is shown in Figure 4.10. The areal distribution of some of the key units is shown in Figures 4.11 and 4.12.

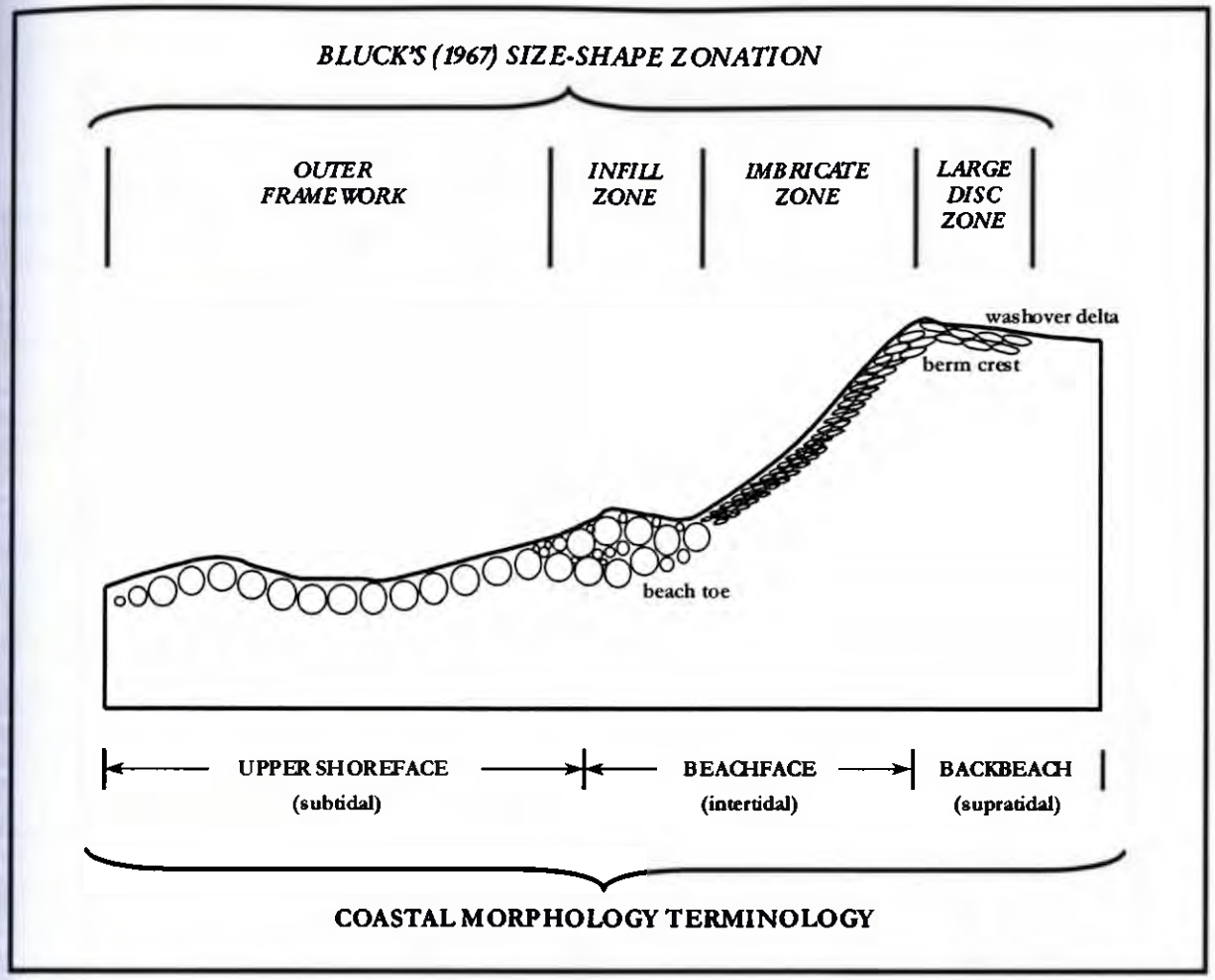

Figure 4.9. Bluck's (1967) gravel beach zones and their relationship to the coastal morphological zones of the marine gravel deposits at pocket beach Sites 2 and 3 (sources are Brenninkmeyer, 1976 and Bluck, 1967).

4.3.1 Unit A

Unit A occurs at Site 2, where it directly overlies the Proterozoic bedrock along a major unconformity (Figure 4.10). Its distribution is mostly limited to the Site 2 palaeo-drainage (Figure 4.11), although some remnants may be present on the bedrock floor of Marmora Valley (Site 3). These possible remnants are, however, difficult to distinguish from elements of Unit B at Site 3. Unit A reaches a maximum thickness of 8 m in the Site 2 palaeo-drainage.

Unit A consists of non-fossiliferous gravel and grit with a framework clast assemblage dominated by angular vein quartz, but also contains minor amounts of angular, locally-derived

Table 4.1. A table showing the lithostratigraphy of pocket beach Sites 2 and 3. Note that the deposition of Units B, C and D covers the timespans indicated by the arrows.

STRATIGRAPHIC UNIT	AGE	BRIEF DESCRIPTION	MAXIMUM THICKNESS
UNIT F	< ca. 5 000 BP (recent)	medium-to-coarse grained sand	15 m
UNIT E	< ca. 5 000 BP (recent)	fossiliferous, coarse grained sand and pebbly grit	7 m
GRAVEL UNIT 3	ca. 5 000 BP	fossiliferous, pebble to cobble gravel	2 m
GRAVEL UNIT 2	ca. 7 600 BP to ca. 5 600 BP	fossiliferous, pebble to cobble gravel	1 m
UNIT D	ca. 9 000 BP to ca. 5 000 BP	non-fossiliferous, fine-to-medium grained sand intercalated with three fossiliferous, variegated sub-units	26 m
UNIT C	ca. 120 000 BP to ca. 5 000 BP	medium-to-coarse grained sand	2 m
UNIT B	ca. 120 000 BP to ca. 9 000 BP	rounded pebble and cobble lag sometimes superseded by angular quartz rubble in clay-rich matrix	0.5 m
GRAVEL UNIT 1	120 000 BP to 130 000 BP	fossiliferous, pebble to cobble gravel	2 m
UNIT A	> ca. 130 000 BP	angular quartz rubble in clay-rich matrix	8 m

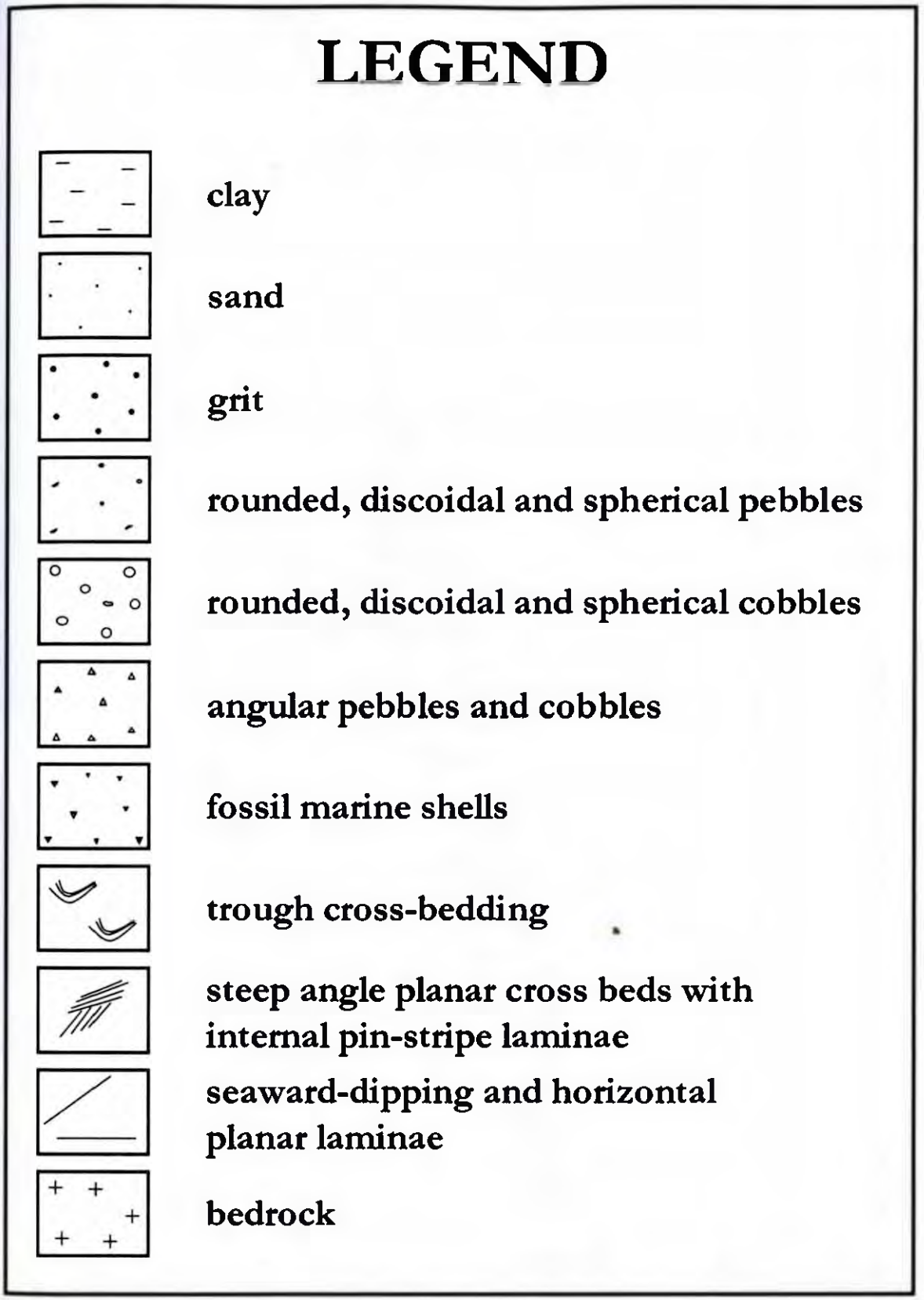

Figure 4.10a. Legend for the schematic cross-sections of the lithostratigraphic units at pocket beach Sites 2 and 3.

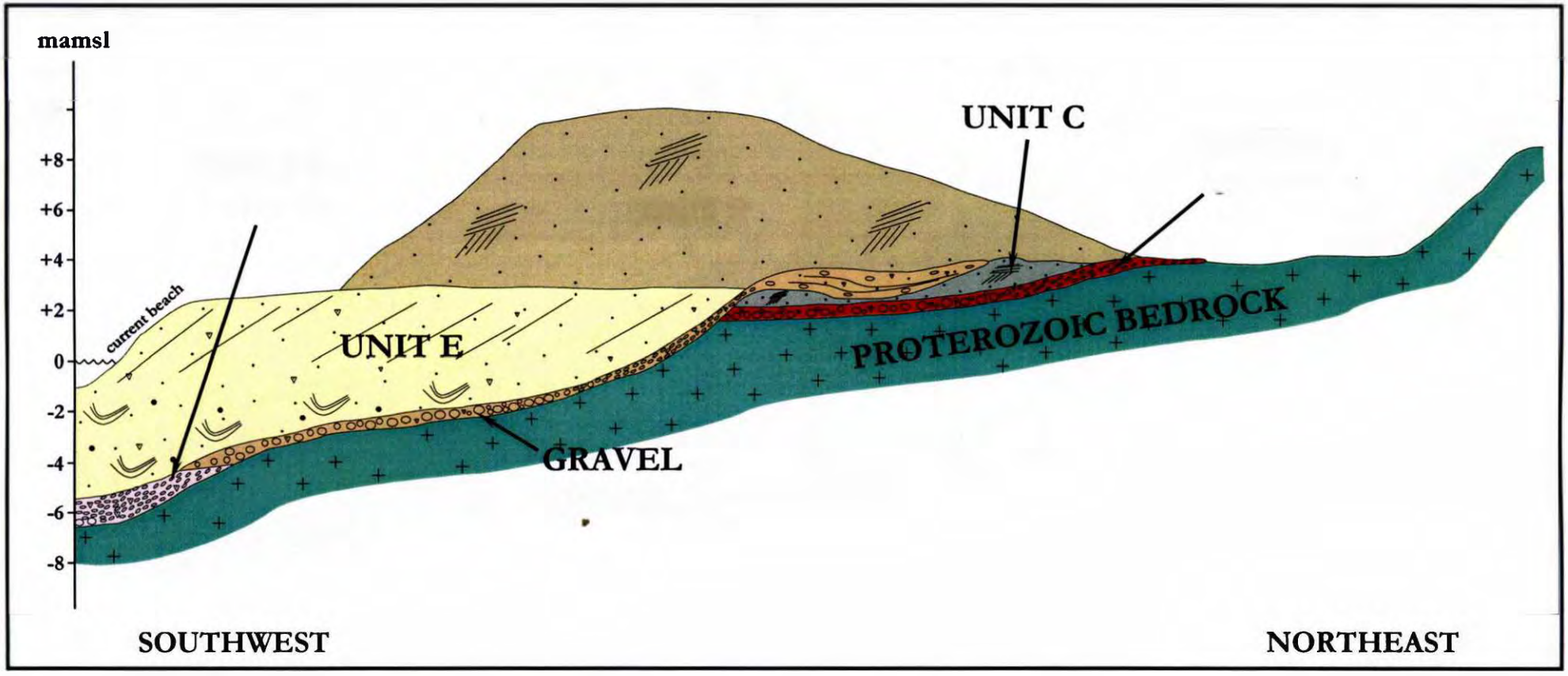

Figure 4.10b. A schematic cross-section of the lithostratigraphic units at pocket beach Site 2. Case 1: outside the boundaries of the Site 2 palaeo-drainage – marine gravels directly overlie Proterozoic bedrock.

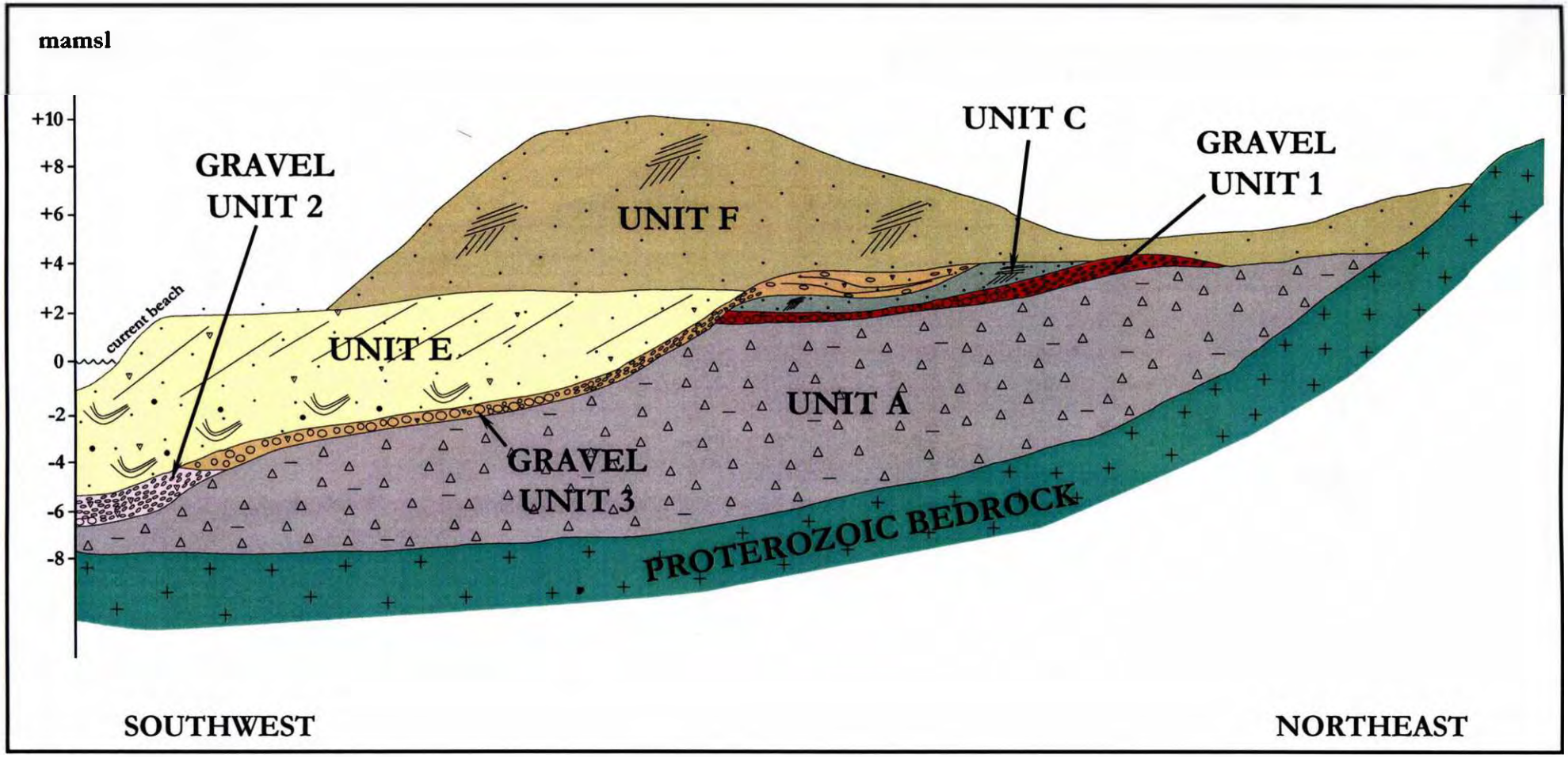

Figure 4.10c. A schematic cross-section of the lithostratigraphic units at pocket beach Site 2. Case 2: inside the boundaries of the Site 2 palaeo-drainage – marine gravels directly overlie Unit A.

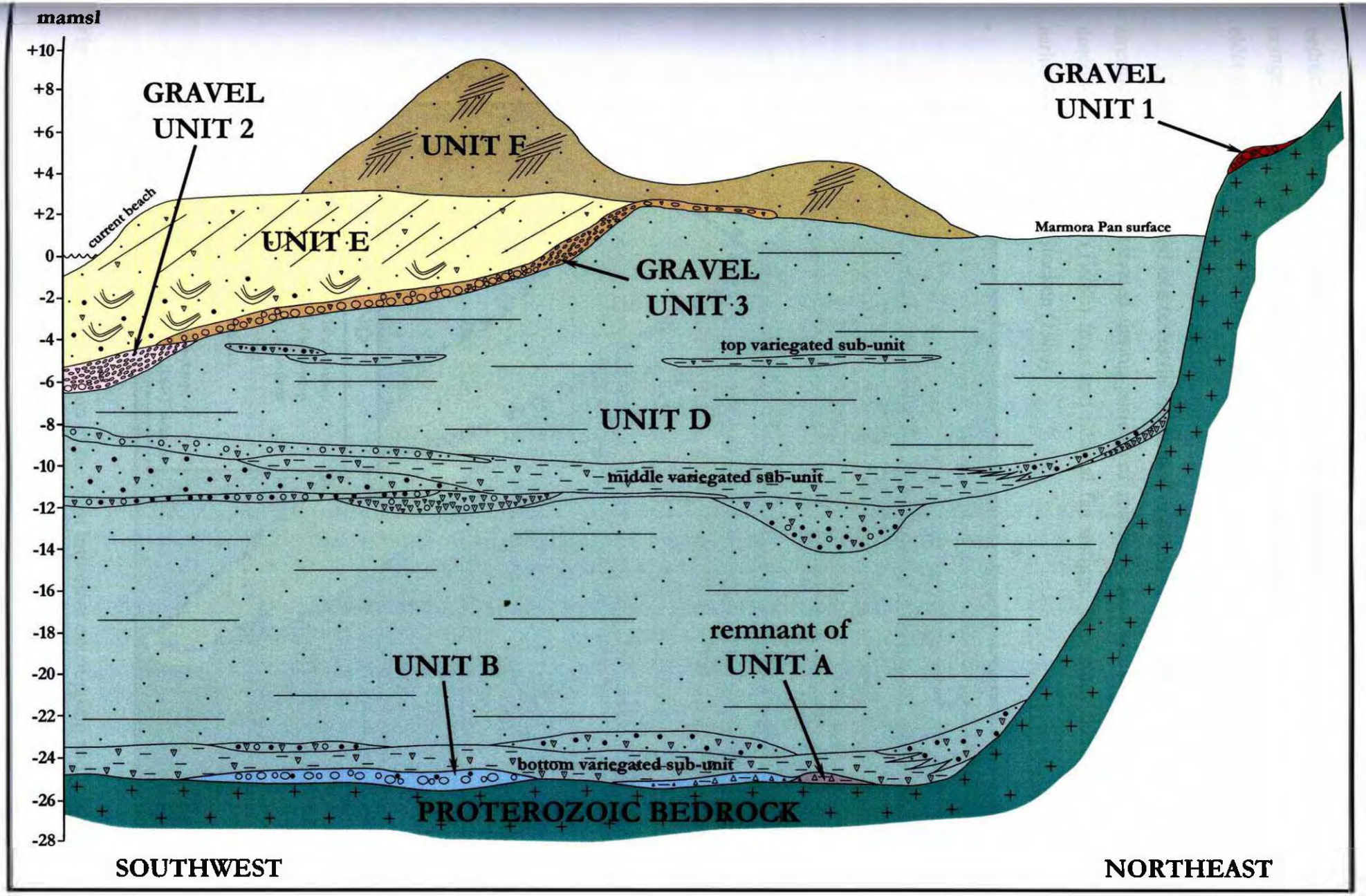

Figure 4.10d. A schematic cross-section of the lithostratigraphic units at pocket beach Site 3.

bedrock fragments. The gravels and grits may be either clast- or matrix-supported. The matrix is orange in colour and consists mostly of clay. Unit A is overlain by Gravel Unit 1 and is therefore older than 120 000 to 130 000 BP.

Unit A is interpreted as a terrestrial sheetflood or debris flow deposit, laid down by ephemeral streams, which were activated during periods of relatively low sea level. Similar deposits are described by Collinson (1978b) from arid alluvial fan settings. This study therefore confirms the earlier interpretation of Stocken (1980).

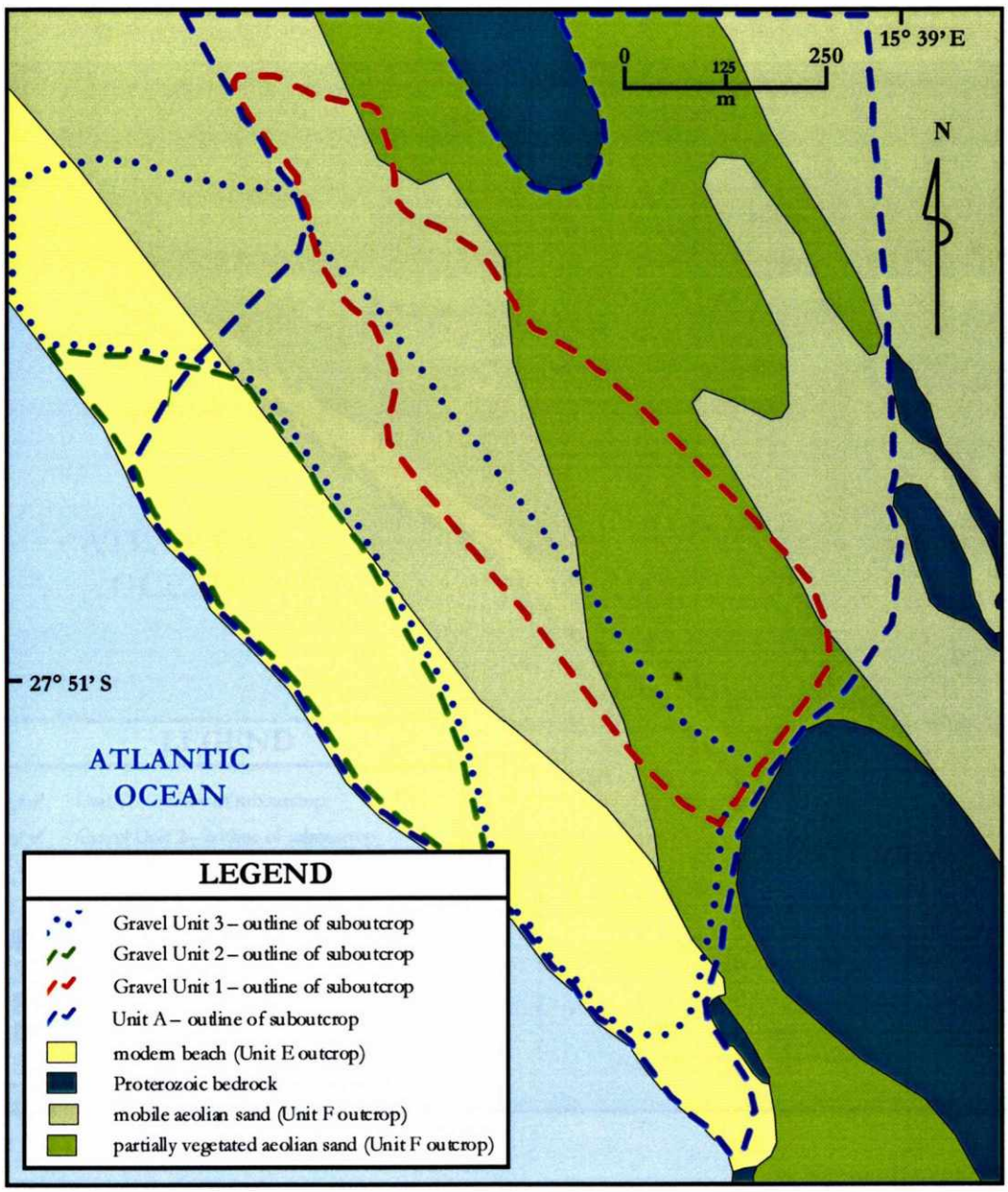

Figure 4.11. The onshore, areal distribution of the most important outcropping and suboutcropping lithostratigraphic units at Site 2.

4.3.2 Gravel Unit 1

Gravel Unit 1 (G1) occurs at Sites 2 and 3. At Site 2, it unconformably overlies Unit A in the south and Late Proterozoic bedrock in the north (Figures 4.10 and 4.11). At Site 3 only a small remnant of this unit is preserved along the eastern ridge of Marmora Valley, where it unconformably overlies the Late Proterozoic bedrock, at a higher elevation than the nearby Unit D (Figures 4.10, 4.12 and 4.13). G1 reaches a maximum elevation of +4 mamsl along its north-eastern (landward) edge.

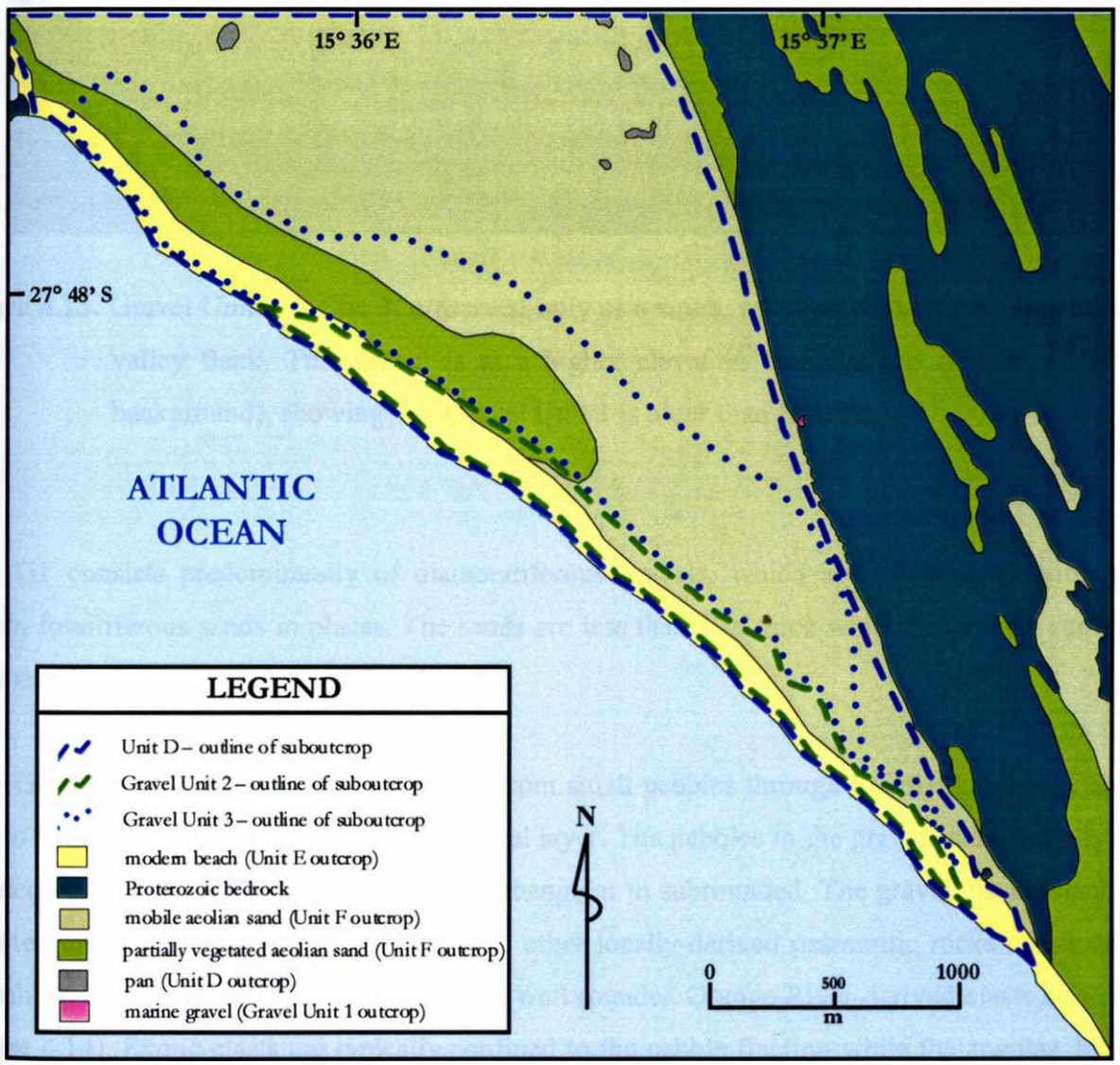

Figure 4.12. The onshore, areal distribution of the most important outcropping and suboutcropping lithostratigraphic units at Site 3.

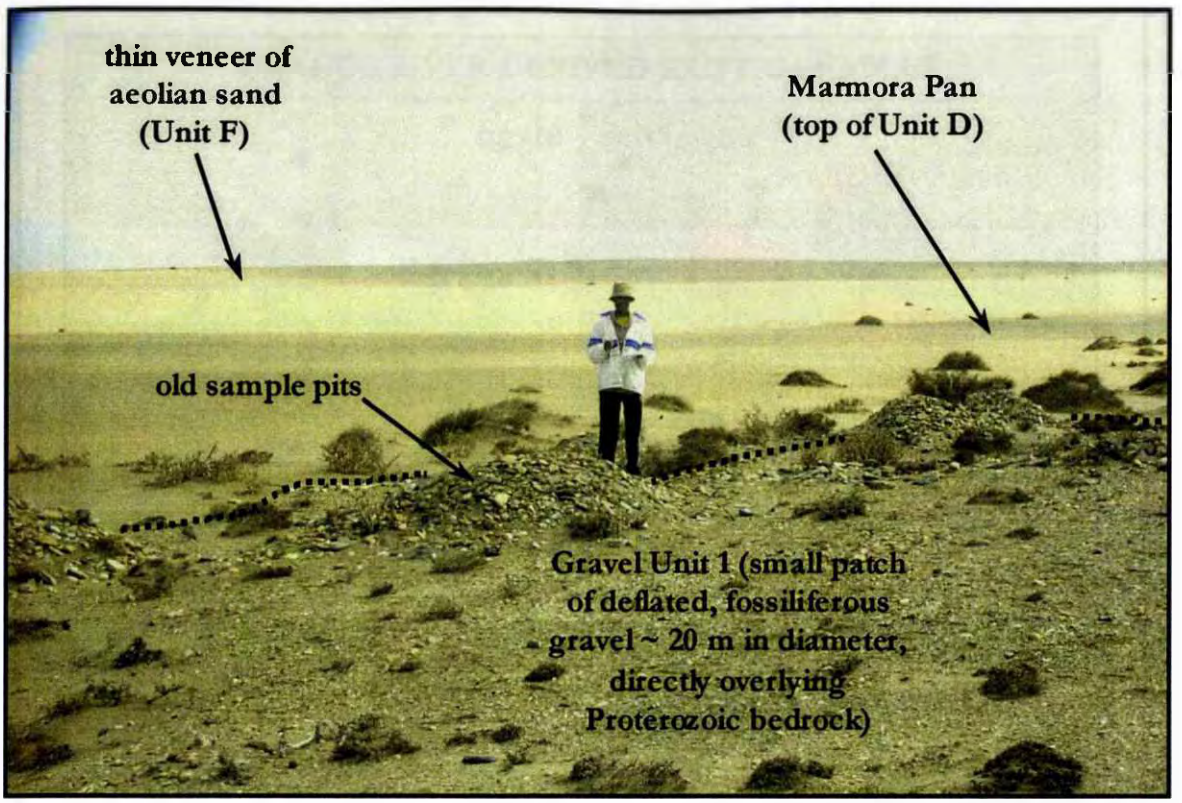

Figure 4.13. Gravel Unit 1 at Site 3, preserved only as a small, relict patch on the eastern bedrock valley flank. This gravel is at a higher elevation than the top of Unit D (in the background), showing that Gravel Unit 1 is older than Unit D.

G1 consists predominantly of diamondiferous gravels, which are intercalated with grey-brown, fossiliferous sands in places. The sands are less than 1 m thick while the gravels can attain thicknesses of up to 2 m.

Gravel framework clasts range in size from small pebbles through to large cobbles. Cobbles tend to be concentrated at the base of the gravel layer. The pebbles in the gravels are generally well rounded while the cobbles vary from being subangular to subrounded. The gravel clast assemblage is varied; quartzite, vein quartz, dolomite and other locally-derived psammitic rocks dominate the assemblage but significant amounts of exotic, well rounded Orange River-derived clasts also occur (Figure 4.14). Exotic clasts are typically confined to the pebble fraction while the angular, locally-derived clasts dominate the cobble fraction. The most distinctive exotics are banded ironstone, red jasper, agate and quartz porphyry. The quartz porphyry clasts appear to be relatively abundant in G1. The framework clasts are set in a coarse sand or grit matrix. The gravels are clast-supported in the east of Site 2, but become increasingly matrix-supported towards the west. A poorly developed,

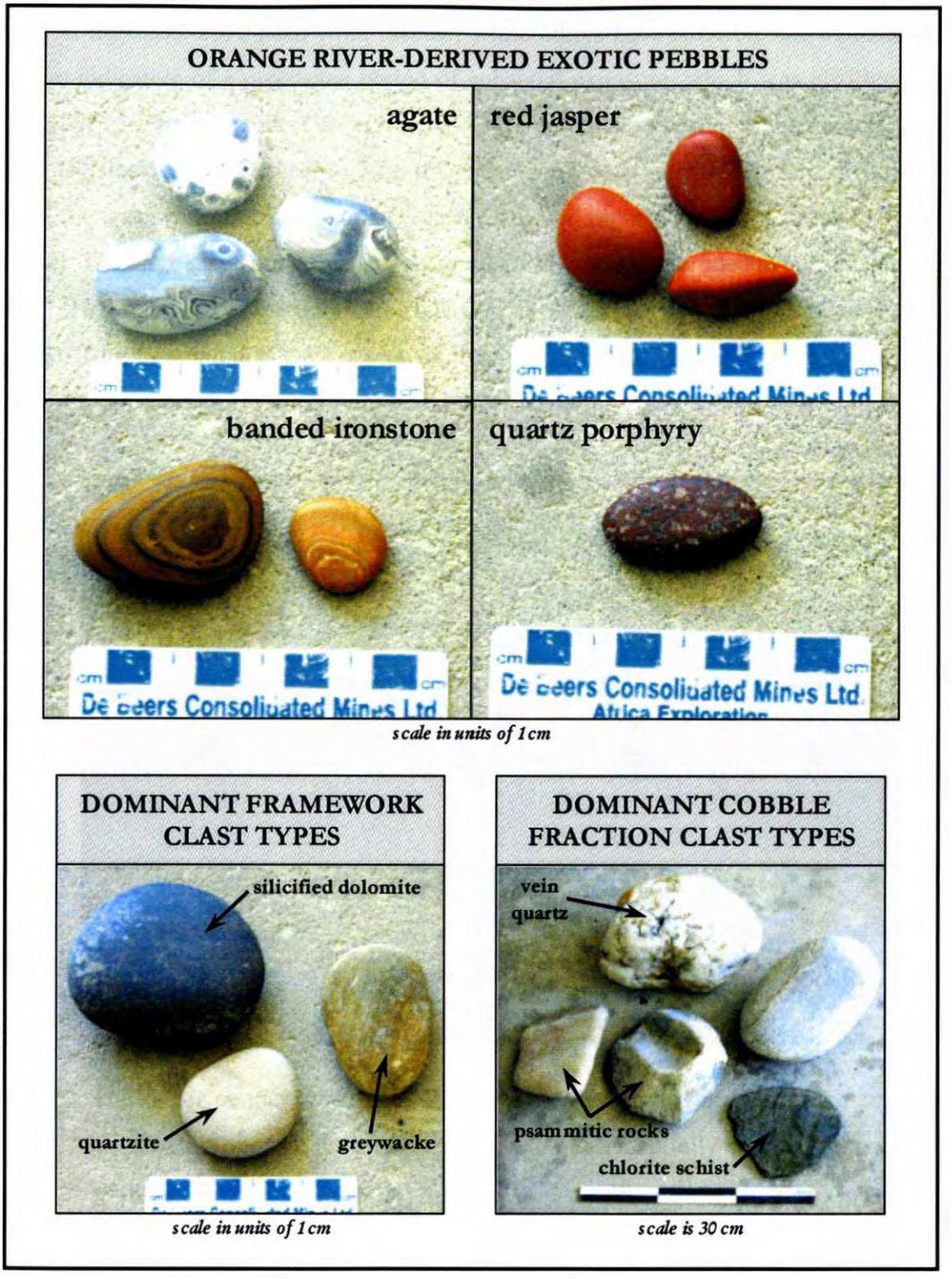

Figure 4.14. Locally-derived clasts and Orange River-derived exotic clasts that make up the framework clast assemblage of Gravel Units 1, 2 and 3 at pocket beach Sites 2 and 3.

impersistent nodular calcrete occurs in the top few centimetres of the gravels, and in places, a dark-brown palaeosol is also evident (Figure 4.15). Another feature of the upper surface of the gravel is

that some of the clasts have been wind-faceted, while others have suffered salt weathering. These features are indicative of a protracted period of subaerial exposure, which was also recognised by Apollus (1995) in his red unit. The gravels of G1 are zoned in terms of their internal structure according to Bluck's (1967) scheme. The imbricate zone occurs in the landward (north-eastern) portion of the unit while the infill zone (Figure 4.16) and outer framework occur to the seaward (southwest). The large disc zone is absent, and appears to have been eroded away. The difference in elevation between the top of the imbricate zone (top of beachface) and the infill zone (beach toe) is around 3 m. This approximates what is seen on the modern beach. The tidal range during deposition of G1 was therefore similar to the current tidal range (ie. micro-tidal).

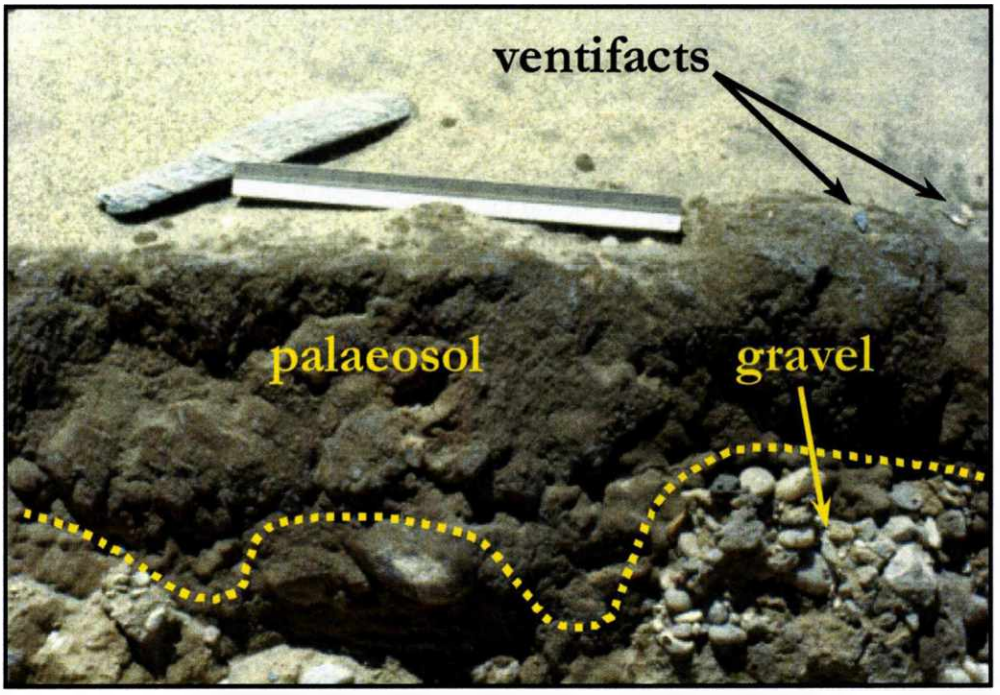

Figure 4.15. The upper contact of Gravel Unit 1. The presence of a dark-brown palaeosol and ventifacts demonstrates that Gravel Unit 1 was subaerially exposed for a considerable period of time. Scale is 30 cm.

The sands in G1 are coarse grained and typically quartzo-feldspathic in composition. Their internal structure is dominated by low-angle, seaward-dipping, parallel laminae, which are typical of beachface deposition (Reineck and Singh, 1975).

Both the sand and gravel in G1 contain abundant fossil marine shells. The most commonly occurring macrofauna are :

BIVALVIA
Choromytilus meriodionalis (black mussel – intertidal)
Aulacomya ater (ribbed mussel – intertidal)

GASTROPODA
various *Patella* species (limpets – intertidal)
Nucella squamosa

Most of the shells are fragmented and abraded, indicating that they have been transported to their current position under high energy conditions, or have suffered a high degree of reworking. Most of the fauna would have lived in the intertidal zone.

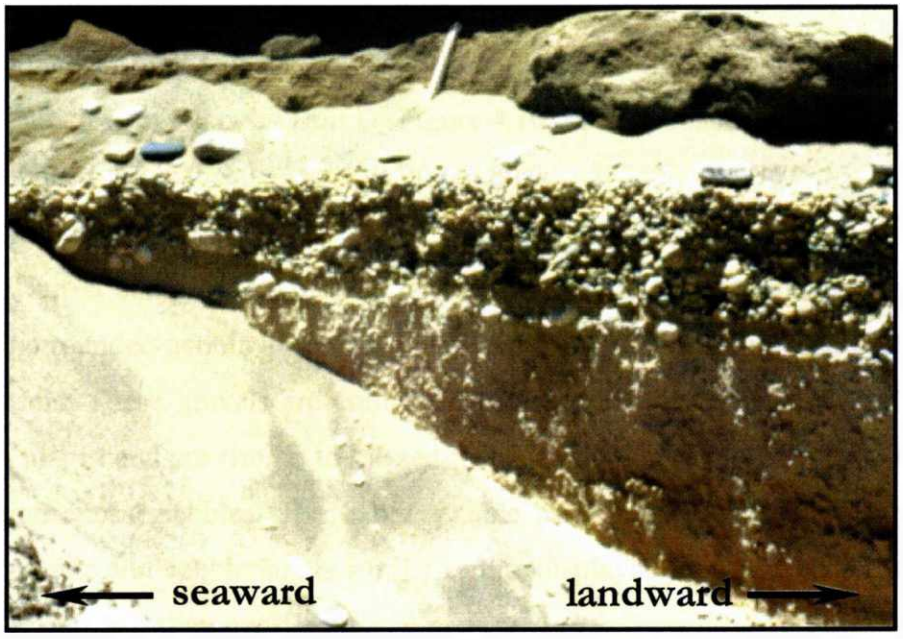

Figure 4.16. The infill zone of Gravel Unit 1. Note the abundant small, spherical clasts infilling a coarser framework of large spheres. View is towards the north. Scale is 30 cm.

G1 is correlated with Apollus's (1995) red unit on the basis of both elevation and clear evidence of subaerial exposure. It is also correlated with C.D. Hallam's (1964) intermediate terrace on the basis of elevation. G1 is clearly older than Unit D, because it is preserved as a higher remnant on the flank of Marmora Valley at Site 3. A tentative age of 120 000 to 130 000 BP is therefore assigned to G1 (Apollus, 1995).

To summarise, the gravels in G1 are interpreted as beachface and upper shoreface deposits, laid down during a sea level highstand some 120 000 to 130 000 BP, which reached a maximum

elevation of ~ +4 mamsl. The sands were deposited in a beachface environment as part of the same event. The evidence of subaerial exposure indicates a subsequent lowering of sea level, which left the package exposed to the elements for a protracted period of time. The occurrence of Orange River-derived exotic pebbles demonstrate that G1 contains sediment which, at some time, moved northward on the longshore drift and would have included diamonds. A more proximal Gariep source is indicated for the larger clasts in the gravel.

4.3.3 Unit B

Unit B is only found at Site 3, where it occurs as occasional thin lenses directly overlying Late Proterozoic bedrock. It is overlain by Unit D (Figure 4.10). Unit B reaches a maximum thickness of 0.5 m in rare instances, but is mostly less than 20 cm thick.

Most of Unit B comprises a rounded pebble and cobble lag that contains rolled ventifacts (Figure 4.17). The rounded pebble and cobble lenses are sometimes superseded by lenticular, non-fossiliferous gravels. These gravels are composed of angular quartz fragments set in an orange-brown, clay-rich matrix and are similar to the sediments comprising Unit A, with the exception that they contain some exotic pebbles. The exotic pebble assemblage, which is also present in the aforementioned pebble and cobble lag, is similar to that displayed by the Eocene marine sediments at Buntfeldschuh. Unit B is diamondiferous.

The rounded pebble/cobble lag is interpreted as the likely result of multicyclic deflation of pre-existing marine gravel deposits, probably including G1, which once occupied a position well above the valley floor and within former valley-fills at Site 3. The presence of rolled ventifacts also indicates that reworking of deflation deposits, of the type described by Corbett (1989), has taken place, probably by fluvial and marine processes. The angular quartz gravels, being almost identical in nature to Unit A, are also interpreted as terrestrial sheetflood deposits resulting from ephemeral stream deposition during a period of low relative sea level. Landward-directed aeolian transport (Corbett, 1989) and seaward-directed ephemeral stream transport are considered most likely to have been responsible for the removal and deflation of pre-existing valley fills. The basal contact of Unit B is significantly more diamondiferous than Unit D, further reflecting the deflationary nature of Unit B. The most recent deflationary episode must have taken place between the deposition of G1

and ca. 9 000 BP, when the sea had not yet transgressed into Marmora Valley (see below). However, some of the sheetflood deposits associated with Unit B may be remnants from older lowstand periods, one of which triggered the deposition of Unit A. Some of the sheetflood deposits associated with Unit B could therefore be older than G1.

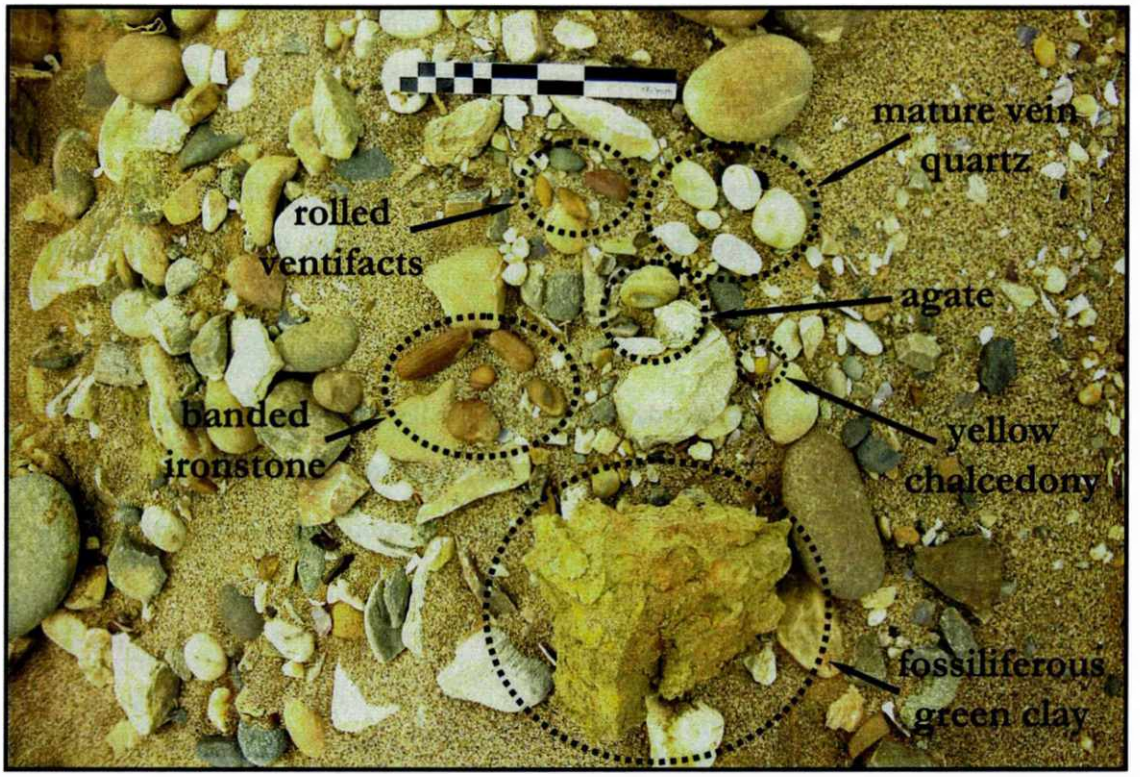

Figure 4.17. The treatment tailings from a GB50 sample of Unit B, Site 3. The mature vein quartz, agate and yellow chalcedony are prominent components of the Eocene marine succession in the Sperrgebiet. A rounded pebble and cobble lag, as well as rolled ventifacts, directly overlie the Proterozoic bedrock. Scale is 150 mm.

4.3.4 Unit C

Unit C occurs only at Site 2, where it attains a maximum thickness of 2 m. It overlies G1 and has been truncated by Gravel Unit 3 (Figure 4.10).

Unit C is composed of grey-brown, quartzo-feldspathic, medium-to-coarse grained sand. Only minor amounts of fossil shell occur within Unit C, which also displays large scale cross-bedding with well defined, internal pin-stripe laminae. There is no evidence of palaeosol development, suggesting limited subaerial exposure prior to burial.

The exact age of Unit C is unknown, except that it post-dates G1 and is therefore probably younger than ca. 120 000. It is also overlain and has been truncated by Gravel Unit 3, and is therefore older than ca. 5 000 BP. Since Unit C contains no evidence of subaerial exposure, it is likely to be part of a transgressive event that followed the subaerial exposure of G1. Unit C is therefore probably relatively young and closer to the age of Gravel Unit 3 (ca. 5 000 BP) than to G1 (ca. 120 000 BP).

The paucity of fossil shells, well developed pin-stripe laminae and large scale cross beds in Unit C are typical of aeolian deposition (Reineck and Singh, 1975; Collinson, 1978a). Unit C is therefore interpreted as a coastal dune deposit.

4.3.5 Unit D

Unit D occurs only at Site 3, where it overlies Late Proterozoic bedrock and Unit B (Figures 4.10 and 4.12). It is not present at Site 2. Unit D reaches a maximum thickness of 26 m.

Unit D is a lithologically composite unit, consisting mostly of grey-brown, fine-to-medium grained sands, which crop out as the surface of Marmora Pan. Interbedded with these fine-to-medium grained sands are three distinctive, sub-horizontal, variegated sub-units at elevations of between –25 mamsl and –21 mamsl (bottom), -12 mamsl and –8 mamsl (middle) as well as between –6 mamsl and –4 mamsl (top). These variegated sub-units are composed of green clays, grits, localised coquinites and coarse grained sands. A detailed description of the sediments comprising Unit D is given in Figure 4.18. The variegated sub-units do not crop out in the study area and so their internal structure could not be discerned.

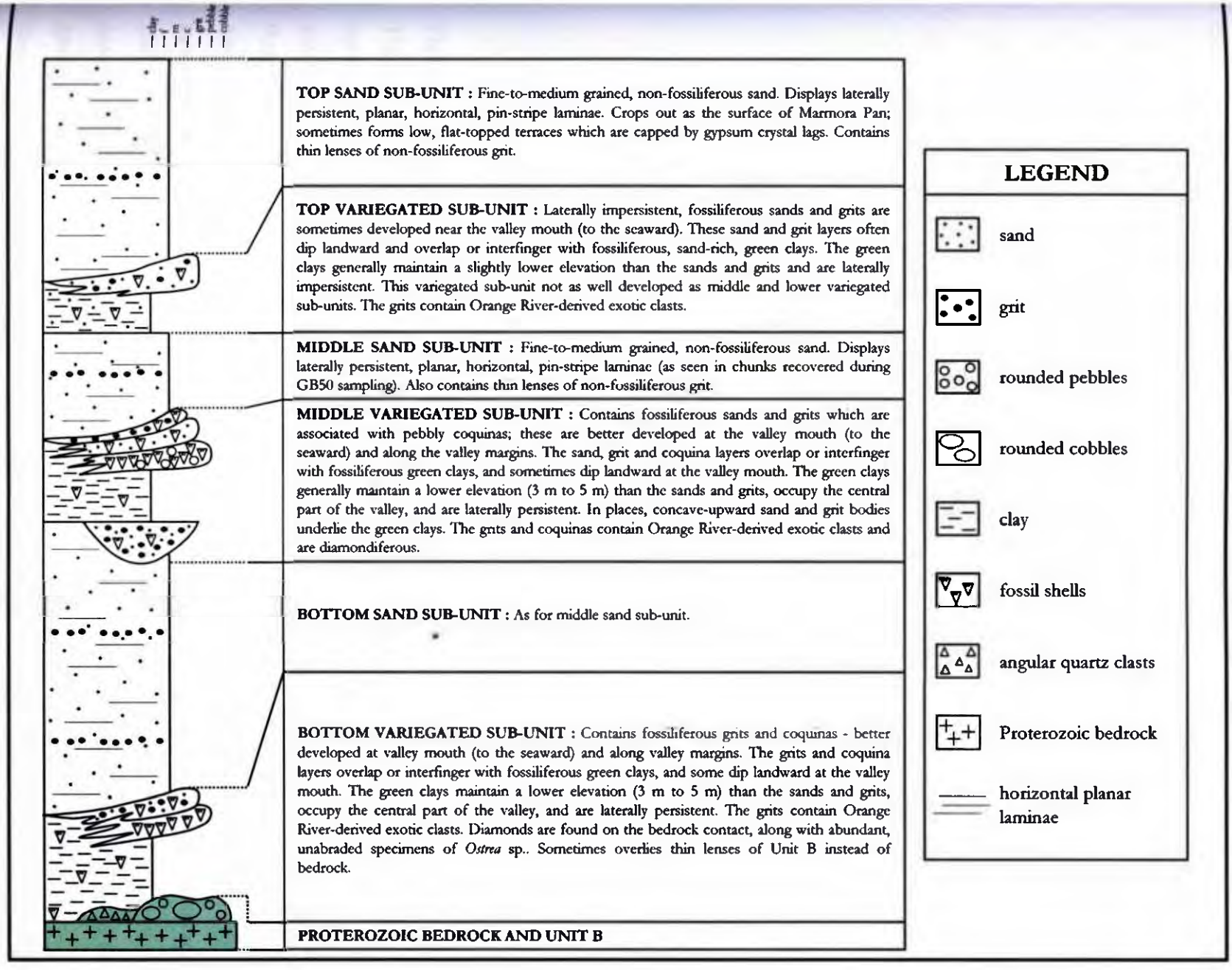

Figure 4.18. A graphic log and sedimentological descriptions for the sub-units comprising Unit D at pocket beach Site 3.

Some of the lithologies comprising the variegated sub-units were sampled for fossil shells. The shell assemblages were identified, described and interpreted by Pether (2001). The most commonly occurring macrofauna are:

BIVALVIA
Venerupis corrugata (infaunal clam – infratidal)
Ostrea sp. (oyster – infratidal)
Aulacomya ater (ribbed mussel – intertidal – usually fragmented and abraded)
Choromytilus meriodionalis (black mussel – intertidal)
Nucula sp. (usually found in fine sediment on open shelf or in sheltered bays - infratidal)
Carditella sp. (same as for *Nucula*)
Tellina analogica (same as for *Nucula*)
Tellimya trigona (infratidal – open, quiet conditions)

GASTROPODA
Assiminea sp. (found on lagoonal flats or rocky shorelines – intertidal)
Protomella capensis (found in lagoons or shallow sheltered bays)
Crepidula porcellana
Nassarius plicatellus
Volvarina capensis
Granula sp.
Fissurella mutabilis (limpet – intertidal – specimens abraded)

CIRRIPEDIA
Austromegabalanus sp.

ECHINOIDEA
Echinoid spines

The most varied assemblage was obtained from a pebbly coquina in sample CNPB/2 (Figure 4.19). The rest of the samples are dominated by unabraded, organically-stained specimens of *Venerupis corrugata* and *Ostrea* sp. as well as a few abraded shells of *Aulacomya ater* and *Fissurella mutabilis*. The intertidal species in all of the samples are generally more fragmented and abraded than the infratidal species. Many articulated specimens of *Tellimya* were recovered from the green clays. The infratidal species can thus be interpreted as having been preserved in-situ or being at most para-autocthonous, while most of the intertidal species have been transported. Unabraded shells of *Ostrea* sp. were recovered exclusively from the Proterozoic bedrock contact (base of the bottom variegated sub-unit), which is in keeping with the required rocky substrate habitat for this species. *Ostrea atherstonei* usually lives in water depths of between 2 m and 5 m (Compton, 2001), demonstrating that shallow water depths existed at this time. Pether (2001) describes the assemblage as being characteristic of "a sheltered habitat into which material from the open coast or

shoreline has been introduced". He goes further to say that the macrofauna indicate several possible depositional scenarios. These are:

a) A lagoonal or estuarine setting, with good connectivity to the open sea via a tidal inlet or channel.
b) A shallow, sheltered bay, with storm currents introducing the rocky shoreline or intertidal macrofauna.
c) Initial open coast conditions introducing the rocky shoreline macrofauna followed by barrier growth to create sheltered conditions and the growth of the infratidal macrofauna.

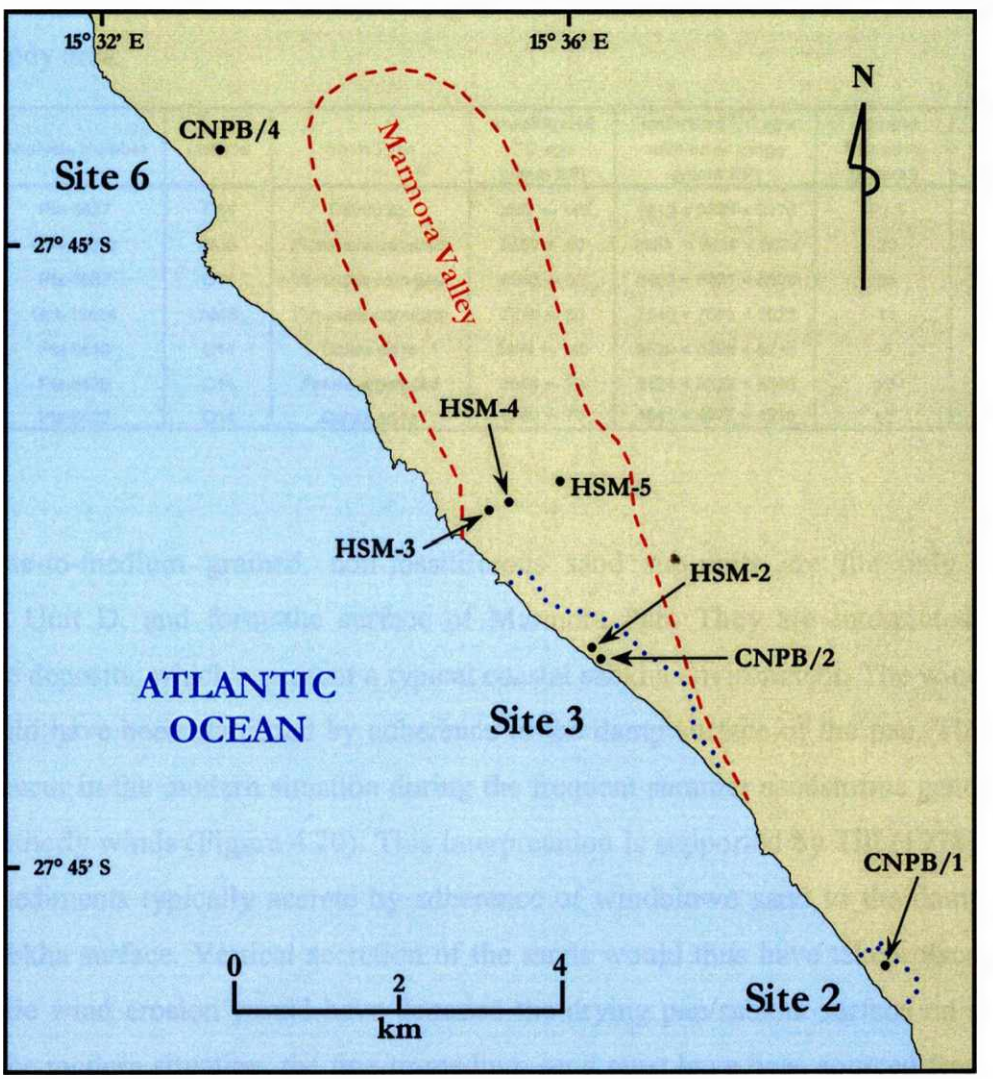

Figure 4.19. The positions of fossil shell samples collected for identification, interpretation and carbon dating.

Several ^{14}C and Ablation Mass Spectrometry (AMS) dates have been obtained from shells in the assemblages described above. Two shells from samples HSM-4 and HSM-5 (Figure 4.19), recovered from the basal contact of Unit D (elevation –24 mamsl), yielded calibrated ^{14}C ages of 8 691 BP (Pta-8637) and 9 034 BP (Pta-8627) respectively. A specimen of *Protomella capensis* from sample CNPB/2 of the bottom variegated sub-unit (elevation –20 mamsl) was dated using the AMS method and yielded a calibrated age of 9 010 BP (GrA-18073). A specimen of *Venerupis corrugata* from sample HSM-3 of the middle variegated sub-unit (elevation –11 mamsl) produced a calibrated age of 7 591 BP (GrA-19664). More details for these dates, including error ranges, are revealed in Table 4.2. The ages demonstrate a maximum age of ca. 9 000 BP for Unit D at Site 3.

Table 4.2. Details and results of ^{14}C and AMS dating of fossil shells recovered in and around the study area.

Sample No.	Analysis Number	Method	Shell Type	uncalibrated ^{14}C age (years BP)	calibrated ^{14}C age with error range (years BP)	Sample Elevation (mamsl)	Recovered from :
HSM-4	Pta-8627	C14	*Ostrea sp.*	**8590** +- 140	8812 < **9034** < 9178	-23.5	Unit D
CNPB/2	GrA-18073	AMS	*Protomella capensis*	**8550** +- 80	8951 < **9010** < 9073	-20	Unit D
HSM-5	Pta-8637	C14	*Venerupis corrugata*	**8360** +- 90	8492 < **8691** < 8806	-24	Unit D
HSM-3	GrA-19664	AMS	*Venerupis corrugata*	**7270** +- 60	7540 < **7591** < 7622	-11	Unit D
HSM-2	Pta-8640	C14	*Donax serra*	**5310** +- 100	5539 < **5598** < 5715	-5	Gravel Unit 2
CNPB/1	Pta-8426	C14	*Patella argenvillei*	**5010** +- 70	5124 < **5222** < 5366	+2	Gravel Unit 3
CNPB/4	Pta-8422	C14	*Donax serra*	**4790** +- 70	4841 < **4887** < 4918	+2	Gravel Unit 3

The fine-to-medium grained, non-fossiliferous sand sub-units are the only outcropping sediments in Unit D, and form the surface of Marmora Pan. They are interpreted as aeolian, adhesion-type deposits, which represent a typical coastal sabkha environment. The windblown sand particles would have been stabilised by adherence to the damp surface of the pan. This process is still seen to occur in the modern situation during the frequent summer sandstorms generated by the dominant southerly winds (Figure 4.20). This interpretation is supported by Till (1978), who states that sabkha sediments typically accrete by adherence of windblown sand to the damp, sea level-controlled sabkha surface. Vertical accretion of the sands would thus have taken place on a rising sea level while wind erosion would have denuded the drying pan/sabkha surface on a falling sea level. As in the modern situation, the fine-to-medium sand must have been sourced from a beach to the south, meaning that the mouth of Marmora Valley would have been cut off from the sea by a barrier beach during periods of sabkha accretion. The raised, flat-topped terraces (see Figure 4.21), with their gypsum crystal lags, are interpreted as remnants of an ancient pan/sabkha surface, which

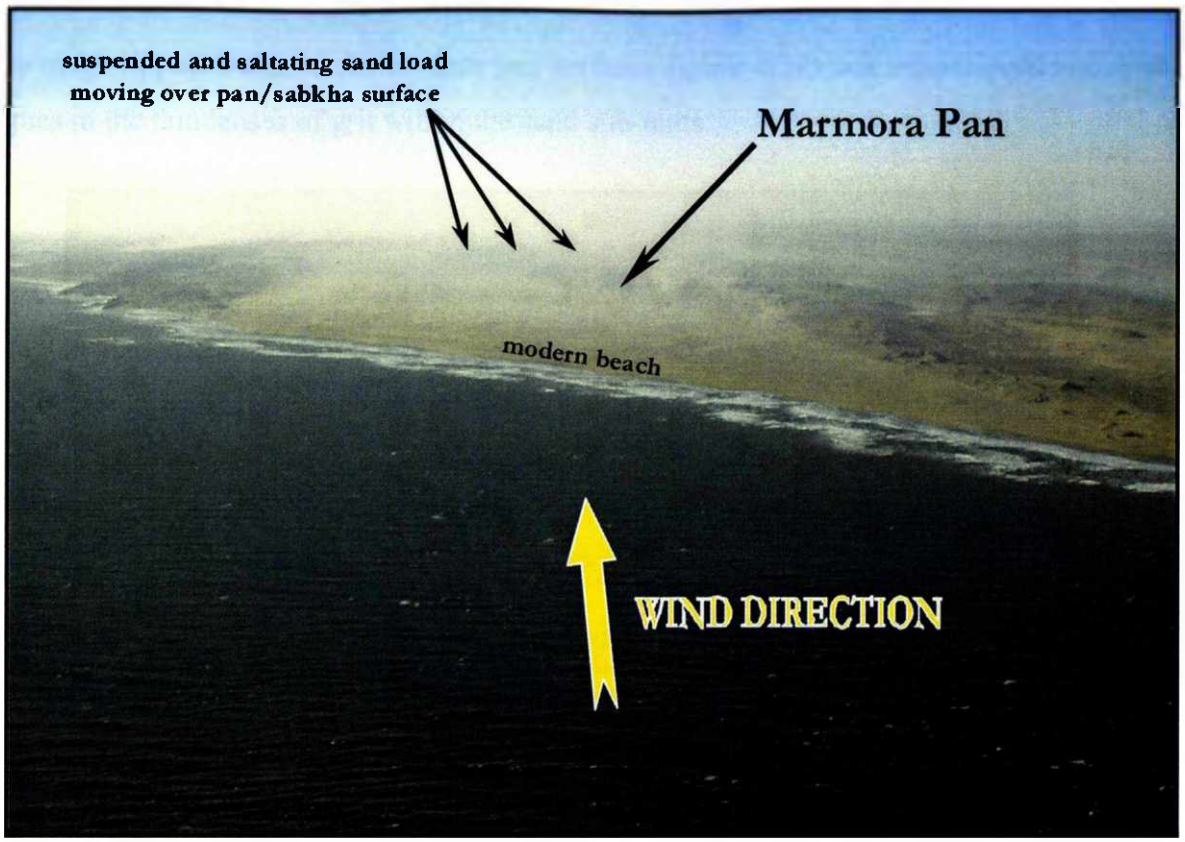

Figure 4.20. A view, from the south, of a summer sandstorm at Site 3. The dominant southerly winds mobilise sand from the modern beach and transport it over the surface of Marmora Pan, where it has the opportunity to adhere to the moist sabkha surface.

formed when sea level was slightly higher than at present. This view is supported by the fact that crystals of discoidal gypsum, which are found on the terraces, are known to grow in sabkha environments (Till, 1978). Reineck and Singh (1975) and Collinson (1978a) describe aeolian adhesion ripples from sabkha environments. These were not observed in the sand sub-units of Unit D, although this may be a function of the limited number of exposures of their internal structure. The few known exposures display uniform planar horizontal laminae, which are more characteristic of sand sheets deposited under high wind velocity conditions (Reineck and Singh, 1975). Large sand sheets do occur on the modern pan surface, which is swept by high velocity winds in the summer months. It is thus very likely that sand sheet deposition also contributed to the accretion of the fine-to-medium grained sand sub-units. Alternatively, the extraordinarily high wind velocities may have precluded the widespread formation of adhesion ripples. The thin lenses of non-fossiliferous grit, found within the sand sub-units, are interpreted as granule mega-ripple deposits of the type described by Reineck and Singh (1975). Thin patches of

granule mega-ripples occur on the modern pan surface (Figure 4.22) and are believed to be modern analogues to the thin lenses of grit within the sand sub-units.

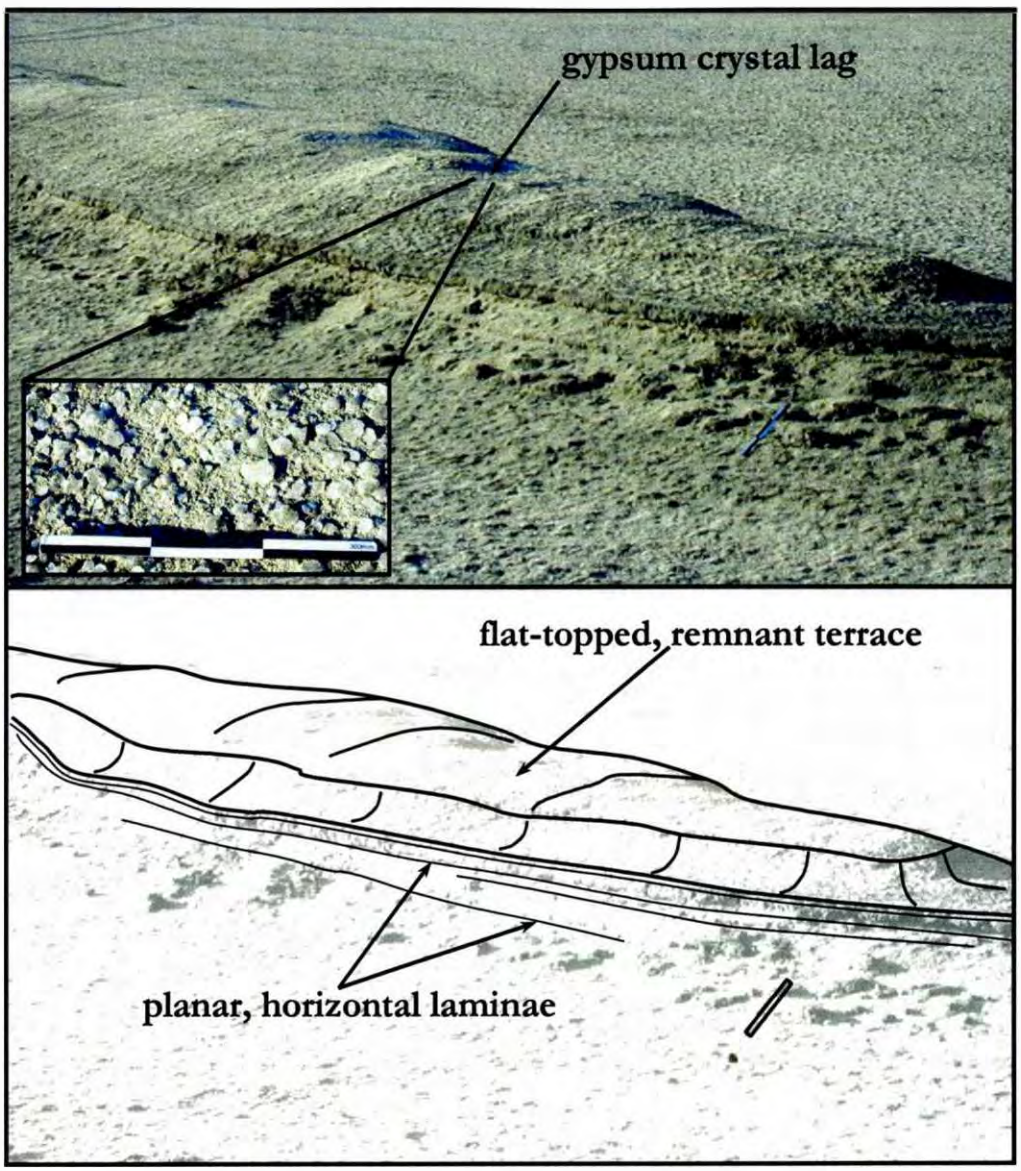

Figure 4.21. One of the flat-topped, remnant terraces on the surface of Marmora Pan. These terraces are believed to represent a former pan level, which existed when sea level was slightly higher than at present. Note the lag of discoidal gypsum crystals on the terrace surface. Scale is 30 cm.

At the time of deposition of the variegated sub-units at Site 3, Marmora Valley had been flooded by seawater. The macrofaunal assemblages indicate deposition in a shallow, sheltered subtidal setting with good connection to the open sea (Pether, 2001). The coquinites, sands and grits along the valley walls probably represent low energy shorelines on a sheltered bay or lagoon margin

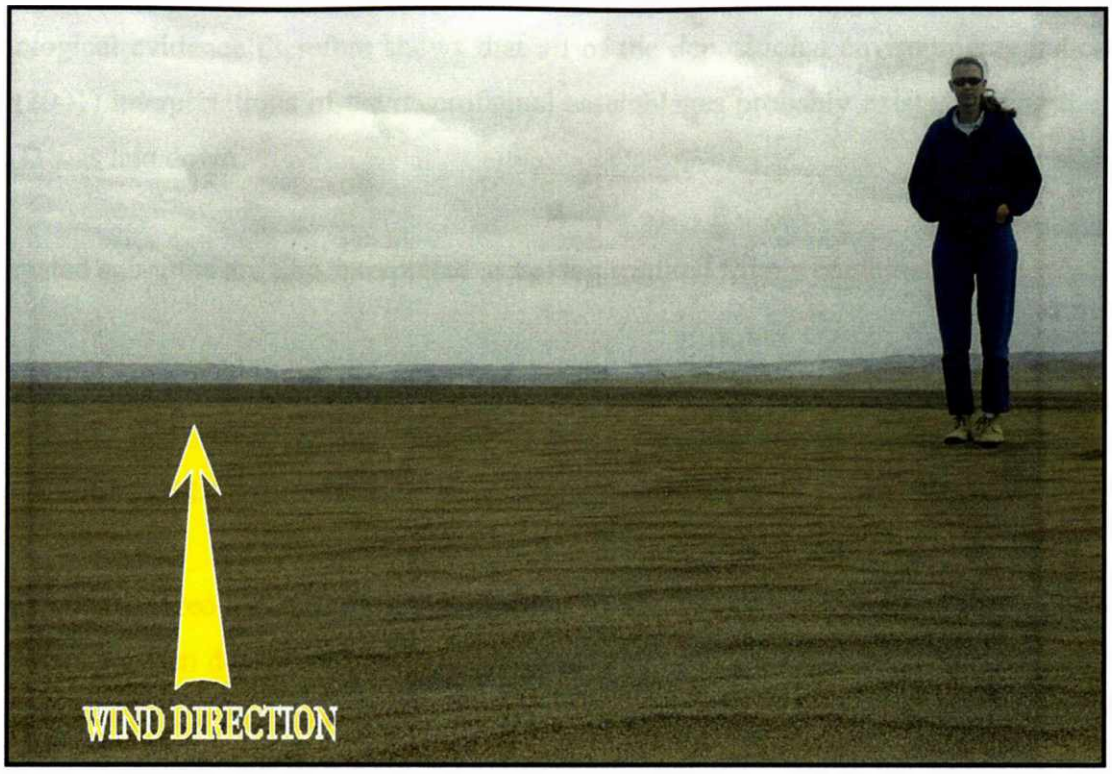

Figure 4.22. A view, from the south, of a granule mega-ripple sheet migrating northward over the surface of Marmora Pan.

while the green clays in the centre of the valley would have been deposited concurrently in the bay or lagoon bottom. The maximum elevation difference between the clays and their probable shoreline equivalents is 5 m. This fact, along with the maximum depth of habitat for *Ostrea* sp. of around 5 m, points to a probable maximum water depth of 5 m in the ancient Marmora Valley in times of flooding. Pebbly coquinites, sands and grits at the valley mouth probably reflect storm-induced transport of material from the open sea into the seaward end of the bay or lagoon. The concave-upward bodies directly underlying the middle variegated sub-unit are interpreted as tidal channel fills and show that the bay was periodically cut off from the open sea by a barrier or spit, creating true lagoonal conditions. The channels may also reflect the transition from open bay through to lagoonal conditions and finally to barrier beach formation, with the consequent onset of adhesion-type aeolian deposition on the pan surface. It is also probable that some of the fossiliferous sands and grits in the variegated sub-units at the seaward end of the valley represent flood tidal deltas and/or washover deltas. This view is based on the presence of the lithologies that dip landward. The interpretations of the various elements of the variegated sub-units, as outlined above, are consistent with descriptions of modern and ancient coastal lagoonal deposits and associated environments from elsewhere in the world (Reineck and Singh, 1975; Elliott, 1978). The

sedimentological evidence therefore shows that all of the depositional environments indicated by Pether's (2001) interpretations of the macrofaunal assemblages probably existed during the period that Unit D was laid down.

The variegated sub-units are thus interpreted as having resulted from a combination of :

a) Deposition in a shallow, sheltered bay.
b) Deposition under true lagoonal conditions, with good open sea connectivity.
c) Deposition in tidal channel, washover delta and flood tidal delta settings.

In summary, three distinct cycles of flooding of Marmora Valley, barrier beach cut-off and subsequent aeolian/pan deposition can be recognised. The three cycles are represented by the three variegated sub-units and their associated fine-to-medium grained sand cappings. These events took place within the context of a rising sea level, which first transgressed the Marmora Valley at ca. 9 000 BP and had passed –11 mamsl by ca. 7 600 BP (Figure 4.23). It is speculated that periods of valley flooding relate to rapid sea level rises that outstripped the rate of sediment supply, while barrier beach cut-off and sabkha accretion occurred during periods of relatively slow sea level rise. Orange River-derived gravels and diamonds were available in the sediment supply during deposition of Unit D.

4.3.6 Gravel Unit 2

Gravel Unit 2 (G2) occurs at both Sites 2 and 3. At Site 2, it unconformably overlies Unit A in the south and Late Proterozoic bedrock in the north. At Site 3, G2 overlies Unit D (Figures 4.10, 4.11 and 4.12). G2 reaches a maximum elevation of -5 mamsl along its north-eastern (landward) edge.

G2 consists of diamondiferous, fossiliferous gravels, which are sometimes intercalated with thin, grey-brown, fossiliferous, coarse-grained sands. The sands are typically less than 0.5 m thick while the gravels reach thicknesses of up to 1 m. Although G2 is similar compositionally to G1, the following differences were noted :

a) The gravels of G2 are generally clast-supported.

b) Quartz porphyry clasts are not as abundant in the G2 gravels.

c) G2 displays no evidence of protracted subaerial exposure.

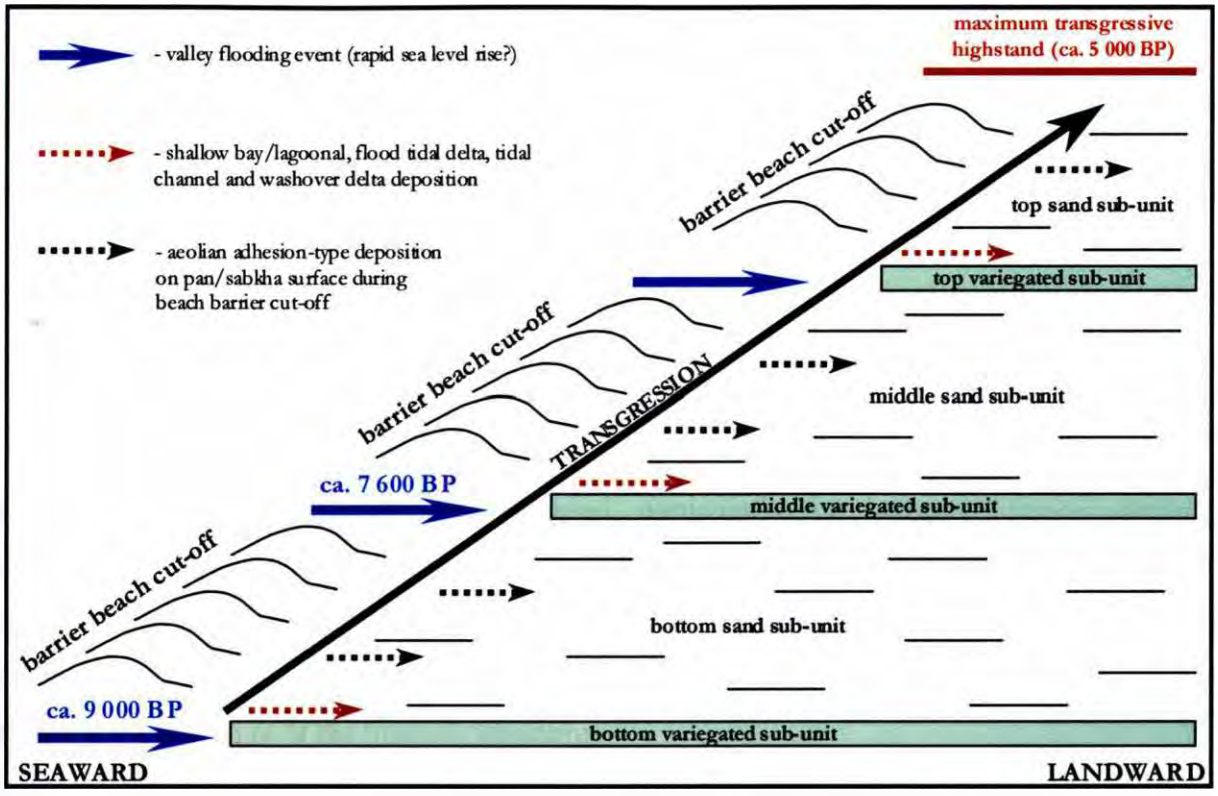

Figure 4.23. A depositional model for Unit D, whereby three cycles of valley flooding, barrier cut-off and aeolian pan/sabkha deposition have built up the deposit. These depositional cycles took place within the context of a sea level transgression.

GB50 sampling and delineation drilling of G2 has resulted in the recognition of the imbricate zone, which is preserved onshore. Delineation drilling also reveals that the berm crest of G2 is not preserved, and has probably been truncated by upper shoreface sediments from Gravel Unit 3. The berm crest of the ancient G2 beach was probably about 1 m higher than the maximum elevation of the preserved beachface. The infill zone and outer framework are also not preserved onshore. Since G2 occurs at the westernmost edge of each of the pocket beach sites, the infill zone and outer framework are probably situated under the modern surf zone. G2 has a 2 m elevation difference between the top of the truncated imbricate zone and the infill zone (beach toe). The tidal range at the time of deposition of G2 thus fell into the micro-tidal range. Since G2 does not crop out in the study area, no observations could be made of the internal structure of the coarse grained sands.

The gravel in G2 contains abundant fossil marine shells. The assemblages were identified, described and interpreted by Pether (2001). The most commonly occurring macrofauna are:

BIVALVIA
Choromytilus meriodionalis (black mussel – intertidal)
Aulacomya ater (ribbed mussel – intertidal)
Donax serra (white mussel – intertidal – sandy beaches)
Lutraria lutraria (infaunal clam – infralittoral)

GASTROPODA
Argobuccinum pustulosum (rock and gravel predator – intertidal)
Bullia digitalis (scavenger – intertidal – sandy beaches)

The shells are mostly fragmented and abraded, particularly the *Lutraria lutraria* specimens. Similarly to G1, this indicates transport to their final positions under highly energetic conditions or a high degree of reworking. Pether (2001) states that the assemblage is typical of a beach or shoreface setting. The *Donax serra* and *Bullia digitalis* shell fragments indicate that a sandy beach existed nearby, before or at the time of deposition.

A single ^{14}C date has been obtained from shells in the assemblages described above. A specimen of *Donax serra* from HSM-2 (Figure 4.19), recovered from a GB50 sample at Site 3 (elevation –5 mamsl), yielded a calibrated ^{14}C age of 5 598 BP (Pta-8640; Table 4.2). The current estimate of the age of G2 must currently be held at ca. 5 600 BP, although, as will be explained later, there is reason to believe that this represents a minimum age.

To summarise, the gravels and sands of G2 are interpreted as having being deposited in a beachface environment during a sea level stillstand at ~ –5 mamsl. The upper shoreface equivalents of this beachface are probably preserved under the current surf zone, beyond the limits of the onshore delineation techniques used. As for G1, the presence of Orange River-derived exotic clasts shows that G2 contains a component of sediment that has been transported northward by the longshore drift and which could have included diamonds. Again, the subangular clasts in the cobble grade have a local provenance.

4.3.7 Gravel Unit 3

Gravel Unit 3 (G3) occurs at Sites 2 and 3. At Site 2, it unconformably overlies Unit A, G1 and Unit C in the south. In the north of Site 2, it unconformably overlies Late Proterozoic bedrock and G1. At Site 3, G3 overlies Unit D (Figures 4.10, 4.11 and 4.12). G3 reaches a maximum elevation of +2 to +3 mamsl along its north-eastern (landward) edge.

G3 is compositionally indistinguishable from G2 and is also diamondiferous. It attains thicknesses of up to 2 m. Bluck's (1967) large disc, imbricate (Figure 4.24), infill and outer framework zones were recognised in the gravels. A washover delta deposit is also associated with G3. This washover deposit consists mostly of sand, which contains scattered discoidal cobbles and unbroken, unabraded fossil shells (Figure 4.25). At Site 3 this washover zone crops out and has been deflated by the wind. Importantly, the almost complete preservation of all of Bluck's (1967) zones shows that G3 represents a recent sea level highstand. Similarly to G1, G3 displays a 3 m elevation difference between the top of the imbricate zone (berm crest) and the infill zone (beach toe). The tidal range at the time of deposition of G3 thus also fell into the micro-tidal range.

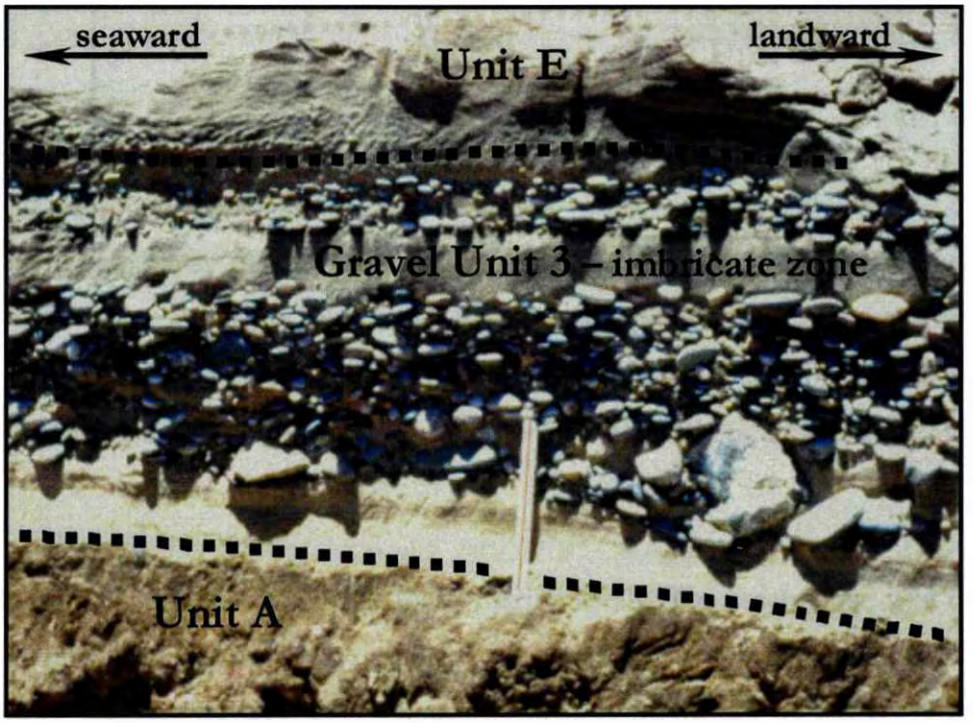

Figure 4.24. The imbricate zone of Gravel Unit 3, as seen in the Site 2 trench. Note the abundance of small, tightly-packed discoidal clasts which define the imbrication. View is towards the north. Scale is 30 cm.

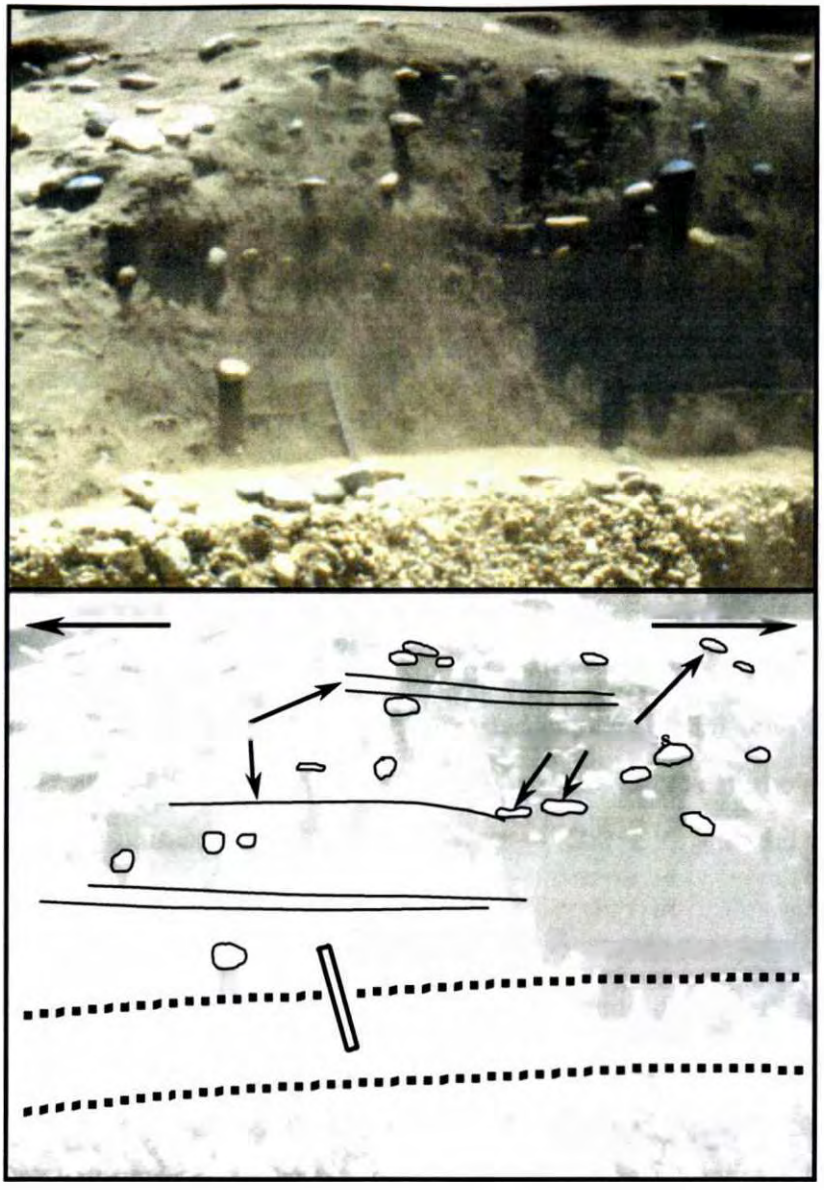

Figure 4.25. The washover deposit associated with Gravel Unit 3. The washover zone thins seaward towards the berm crest, where it is superseded by the large disc zone. Note the landward-dipping laminae and discoidal cobbles, with long and intermediate axes in the plane of the laminae. View is towards the north. Scale is 30 cm.

The gravel in G3 contains abundant fossil marine shells. The assemblage was described and interpreted by Pether (2001) and is very similar to that recovered from G2. As for G1 and G2, the shells are mostly fragmented and abraded, indicating a high degree of transport or reworking. Pether (2001) once again states that the assemblage is typical of a beach or shoreface setting.

Two ^{14}C dates have been obtained from shells recovered directly from exposures of G3. A specimen of *Patella argenvillei* from CNPB/1 (Figure 4.19), recovered from the in-situ gravel in

the Site 2 trench (elevation +2 mamsl), yielded a calibrated ^{14}C age of 5 222 BP (Pta-8426; Table 4.2). A specimen of *Donax serra* was also collected in sample CNPB/4 from an outcrop of the large disc zone of G3 at pocket beach Site 6, situated just outside the study area, some 8 km north of Site 3 (Figure 4.19). This shell yielded a calibrated ^{14}C age of 4 887 BP (Pta-8422). The average of the two ^{14}C dates is 5 055 BP. The two dated indicators are considered reliable, since the origins of the shells are well constrained to G3. G3 is correlated with the grey unit of Apollus (1995), dated at ca. 5 000 BP, and therefore to C.D. Hallam's (1964) advanced terrace on MA1.

It is highly likely that shoreface sands associated with G3 partly overlie the beachface gravels of G2 at the pocket beaches. This has implications for the ^{14}C date obtained for G2, since the dated shell may in fact represent contamination by inclusion of shell material from the overlying G3. The ca. 5 600 BP age obtained for G2 should therefore be treated with suspicion and probably represents a minimum age for this unit. The age of G2 can thus be bracketed between the age obtained from the middle variegated sub-unit of Unit D, which is ca. 7 600 BP, and the minimum age of ca. 5 600 BP.

In summary, the gravels of G3 are interpreted as having being deposited in beachface, upper shoreface and backbeach environments during a ~ +2 to +3 mamsl sea level highstand at ca. 5 000 BP. The presence of Orange River-derived exotic clasts in G3 once again points to northward transport of sediment and diamonds by the longshore drift. Similarly to G1 and G2, the subangular clasts in the cobble grade have a local, Gariep Belt source.

4.3.8 Unit E

Unit E occurs at Sites 2 and 3, where it overlies G2 and G3. (Figures 4.10, 4.11 and 4.12). The south-western portion of this unit crops out as the modern beach at all of the sites. Unit E reaches a maximum elevation of +2 mamsl to +3 mamsl in the northeast.

Unit E consists entirely of fossiliferous, coarse grained sands and pebbly grits, and contains Orange River-derived exotic pebbles. The unit fines upward and coarsens seaward, while also thickening seaward, attaining a maximum thickness of 7 m. The internal structure of Unit E has

been observed in the Site 2 trench. Near the interface with the beachface portion of G3, Unit E displays parallel, planar laminae, which dip gently seaward. These parallel laminae are typical of beachface deposition (Elliott, 1978) and can be traced seaward towards the current beach, where they are underlain by grit trough cross-beds with pebbly foresets (Figure 4.26). The grit trough cross-beds are probably the result of lunate mega-ripple bedforms, which occur on the upper shoreface (Elliott, 1978).

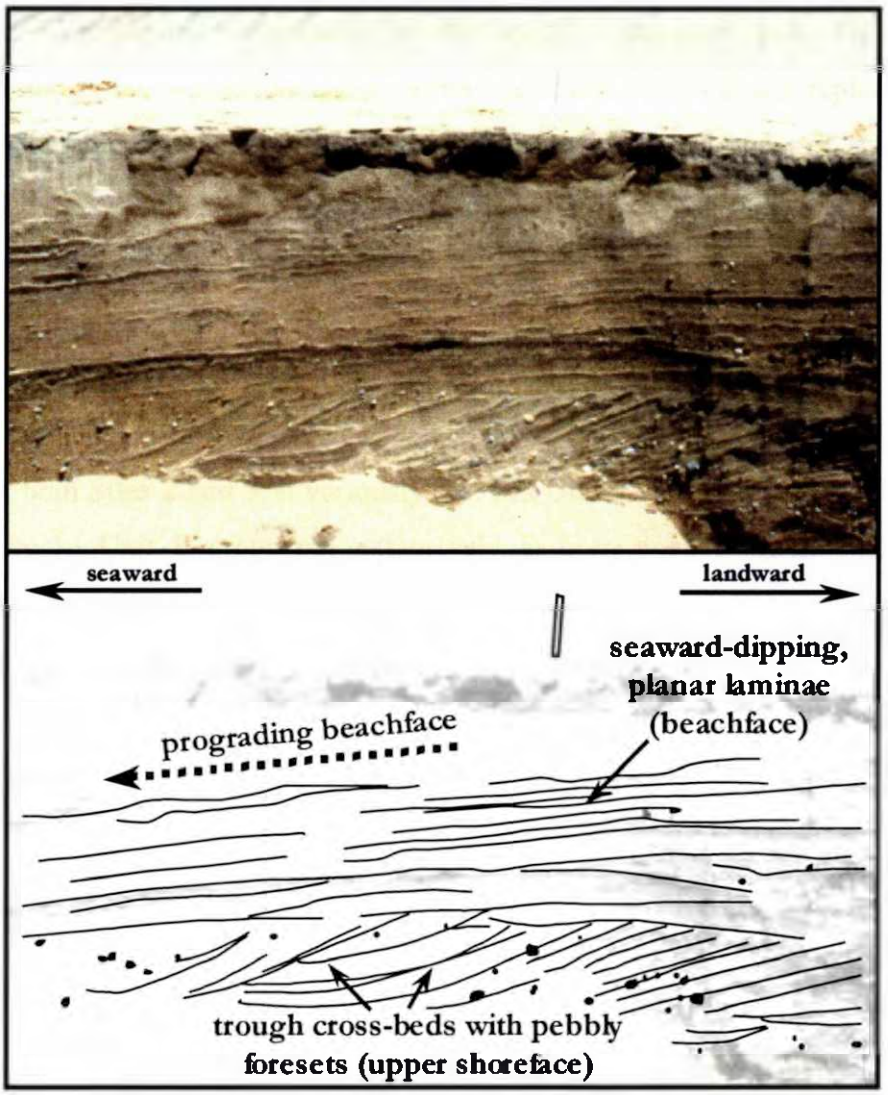

Figure 4.26. Unit E, as exposed in the Site 2 trench. The planar, parallel, seaward-dipping laminae represent a sandy beachface which has prograded seaward over trough cross-bedded sediments of the upper shoreface. View is towards the north. Scale is 30 cm.

The sands and grits of Unit E contain abundant, abraded, comminuted fossil marine shells. Identification of shells proved difficult because of the small size of the fragments, but *Choromytilus*

meriodionalis and *Aulacomya ater* appeared to dominate the assemblage. The macrofaunal assemblage is indicative of deposition under conditions of high energy or a high degree of reworking in a beach or shoreface environment. No ^{14}C dating was attempted on the shell.

The sands and grits of Unit E record the progradation of the shoreline, from the highstand represented by G3, as a result of a minor regression to the current sea level. The seaward-dipping parallel beds represent this prograding shoreline. The shoreline prograded back over its subtidal, upper shoreface equivalents, represented by the trough cross-beds (see Figure 4.26). It is noteworthy that during the regression to the current sea level, sand and grit replaced gravel as the dominant sediment type supplied to this part of the coastline. Sand and grit still dominates the sediment supply to the modern day beaches along the Sperrgebiet coastline.

4.3.9 Unit F

Unit F occurs at both Sites 2 and 3. It variously overlies Unit A, Unit D, Unit E, G3, G1, and Late Proterozoic bedrock. Unit F crops out extensively at both pocket beach sites as backshore, transverse and barchanoid dunes.

Unit F is composed of medium-to-coarse grained sands and can attain thicknesses of up to 15 m. The sands are relatively enriched in dark, dense mineral grains. Unit F displays internal pin-stripe laminae and steep, planar cross-bedding. Fossil shells are rarely found.

The composition and internal structure of Unit F are typical of aeolian deposition (Reineck and Singh, 1975; Collinson, 1978a). Unit F is therefore interpreted as a Late Holocene to modern coastal dune deposit. Aeolian processes are still actively modifying the surface of this unit in the modern setting.

4.4 LATE QUATERNARY SEA LEVEL CHANGES

This section considers some of the current evidence relating to sea level change in the Late Quaternary. The pocket beach sequences described at Sites 2 and 3 are interpreted in the context of

these Late Quaternary sea level changes. Evidence relating specifically to Late Quaternary sea level fluctuation along the Sperrgebiet coastline has not been well documented, and it is hoped that this section will provide a basis for further work in this area.

The subject of relative sea level change is, at best, a complicated one, and involves many variables. Relative sea level change along any given stretch of coastline is dependent upon a number of factors such as glacio-eustasy, tectono-eustasy, local tectonic activity, shelf sedimentation rate and glacio-isostasy (Clark and Lingle, 1979; Plint, *et al.*, 1992). The effect of each of these factors need to be considered before the relative sea level changes along a given stretch of coastline can be unravelled. Tectono-eustasy operates on a time scale far exceeding the period represented by the pocket beaches in this study and can be discounted. The Late Quaternary beach terraces of the Sperrgebiet coastline maintain a constant elevation (C.D. Hallam, 1964) and it is therefore highly unlikely that local tectonics have played a role. As previously mentioned, most of the sediment load of the Orange River is ultimately deposited in the Namib Sand Sea (Rogers, 1977; Corbett, 1989; Mabote *et al.*, 1997) resulting in very low net shelf sedimentation rate. This means that shelf sedimentation can be discounted as a significant sea level control along the Sperrgebiet coastline. With respect to glacio-eustasy and glacio isostasy, the work of Clark and Lingle (1979) and Tankard (1975) show that meaningful Late Quaternary sea level comparisons can be drawn between the pocket beaches at Sites 2 and 3 and the rest of the southern African coastline, and probably also with the East Australian and Pacific island coastlines.

The best records of glacio-eustatic sea level changes for the Late Pleistocene have been derived using oxygen isotope measurements from deep-sea cores (Shackleton and Opdyke, 1973; Shackleton, 1987; Williams *et al.*, 1981). These clearly show that the last time glacio-eustatic sea level was higher than in the Middle Holocene was at 120 000 to 130 000 BP (Eemian) (Figure 4.27). Through an independent line of reasoning, mostly Uranium series dating, a prominent sea level highstand of Eemian age has been recognised both worldwide (Veeh, 1966; Broecker *et al.*, 1968; Veeh and Chappell, 1970; Vézina *et al.*, 1999) and in southern Africa (Tankard, 1975; Roberts and Berger, 1997; Ramsay and Cooper, 2001). Tankard (1975) stated that this highstand usually occurs at elevations between +2 mamsl and +7 mamsl on tectonically stable coastlines. Studies by Shackleton and Opdyke (1973), Williams *et al.* (1981), Shackleton (1987), Fairbanks, (1989), Miller (1990) and Yokoyama *et al.*, (2001) reveal that relative sea level withdrew to a lowstand of around –120 mamsl to –130 mamsl at 18 000 BP, during the Last Glacial Maximum (LGM). A period of about 100 000 years thus exists in which deposits associated with

the Eemian highstand would have been subaerially exposed. This ties in very well with the evidence of protracted subaerial exposure in both G1 and Apollus's (1995) red unit. The field relationships also demonstrate that G1 is older than Unit D (maximum age ca. 9 000 BP - this study) and therefore cannot be of Holocene age. The facts strongly support the conclusion that G1 represents the widely recognised Eemian highstand at 120 000 to 130 000 BP.

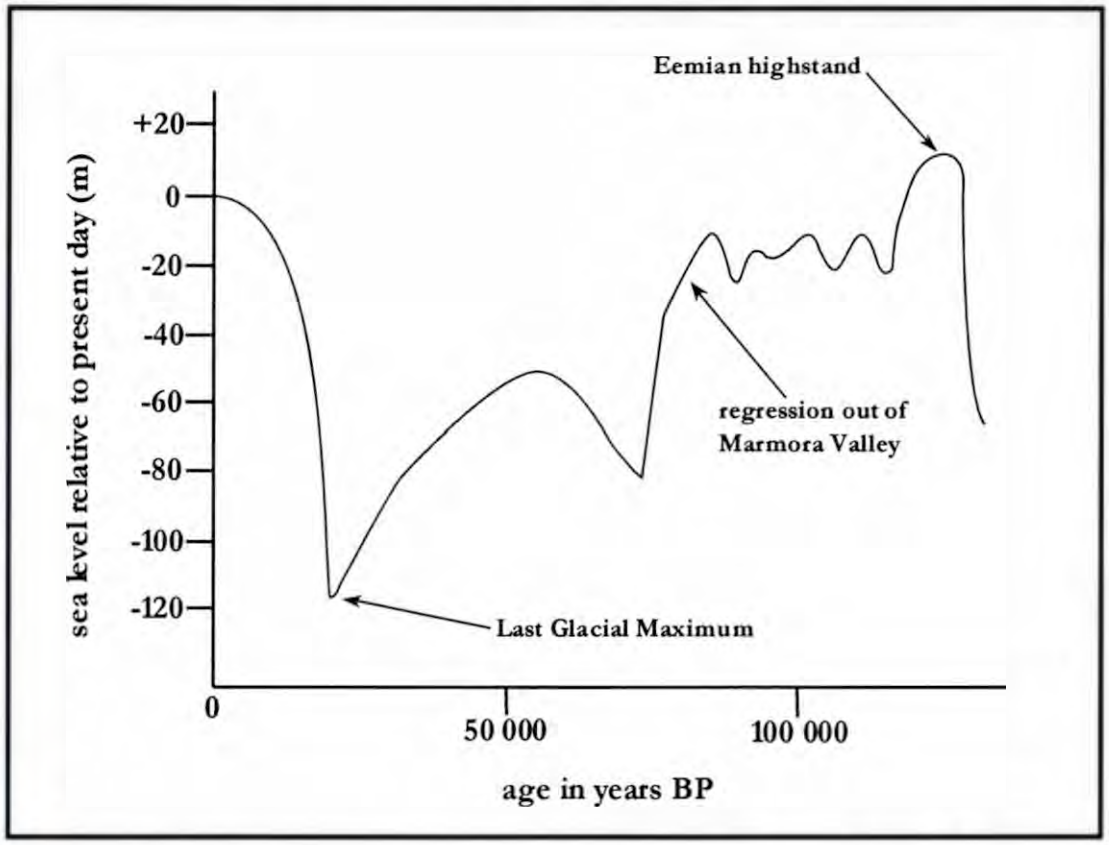

Figure 4.27. A glacio-eustatic sea level curve, derived using oxygen isotope measurements from deep-sea cores, for the last 130 000 years. Note the sea level highstand at around 120 000 to 130 000 BP, which is believed to be represented at pocket beach Sites 2 and 3 by Gravel Unit 1. The curve also shows that Gravel Unit 1 would have been subaerially exposed for at least 100 000 years (after Shackleton and Opdyke, 1973).

The most widely accepted record of glacio-eustatic sea level changes since the LGM is probably that of Fairbanks (1989), who dated coral reefs off Barbados. Fairbanks' (1989) sea level curve was compared to the sea level indicators from G3 and Unit D (Figure 4.28; data from Table 4.2). The ages of subtidal indicators (maximum 5 m water depth) from Unit D agree well with the Barbados curve, and record the sea level transgression into Marmora Valley, starting at ca. 9 000 BP. The intertidal indicators from G3 fall several metres above the corrected Barbados

curve, which does not resolve a Holocene highstand. However, studies in Australia (Larcombe and Carter, 1998) and from the coast of South Africa (Miller, 1990; Miller *et al.*, 1993; Compton, 2001; Ramsay and Cooper, 2001) have clearly demonstrated the existence of a Middle Holocene highstand at an elevation of ~ +2 to + 3 mamsl (Figure 4.29; data from Table 4.2). It is concluded that G3 represents this Middle Holocene highstand.

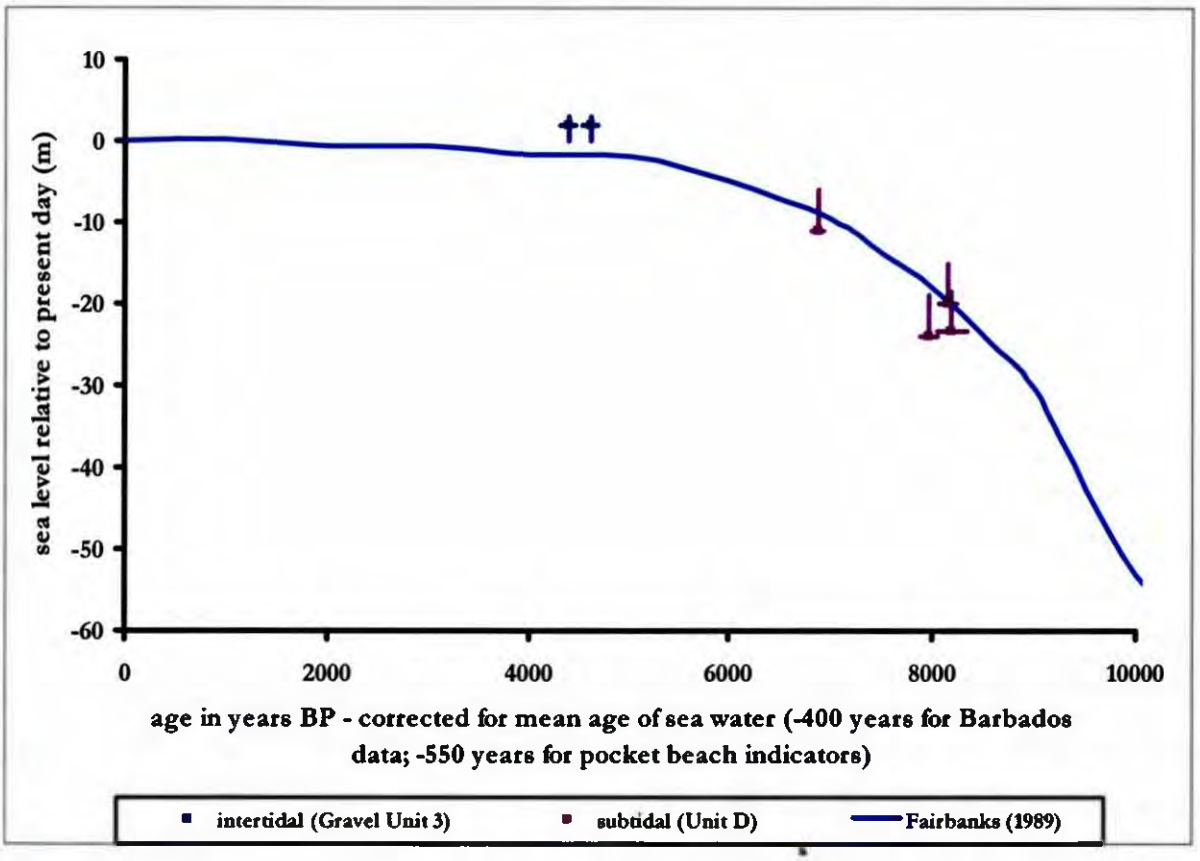

Figure 4.28. The Barbados glacio-eustatic sea level curve, as compared to the dated indicators from Gravel Unit 3 and Unit D. Error bars for age and sea level are shown for the pocket beach indicators. The uncalibrated ^{14}C ages of the indicators have been corrected for the mean age of sea water by subtracting 550 years, so that they are compatible with the data used to define the curve. Agreement between the two data sets is good, although the Barbados curve does not resolve a Middle Holocene highstand (after Fairbanks, 1989).

Larcombe and Carter (1998) also detected a stillstand at –5 mamsl, dated at ca. 6 800 BP, on the Queensland coast. The –5 mamsl stillstand from Queensland may be represented at pocket beach Sites 2 and 3 by G2, for which sea level has also been estimated at ~ –5 mamsl. Although

such a correlation is speculative, it is supported by the recognition of the Middle Holocene highstand at the same approximate elevation and age at both localities, thus providing a point of reference. The Queensland age of ca. 6 800 BP also falls well within the age range defined for G2 in this study, which is 7 600 to 5 600 BP.

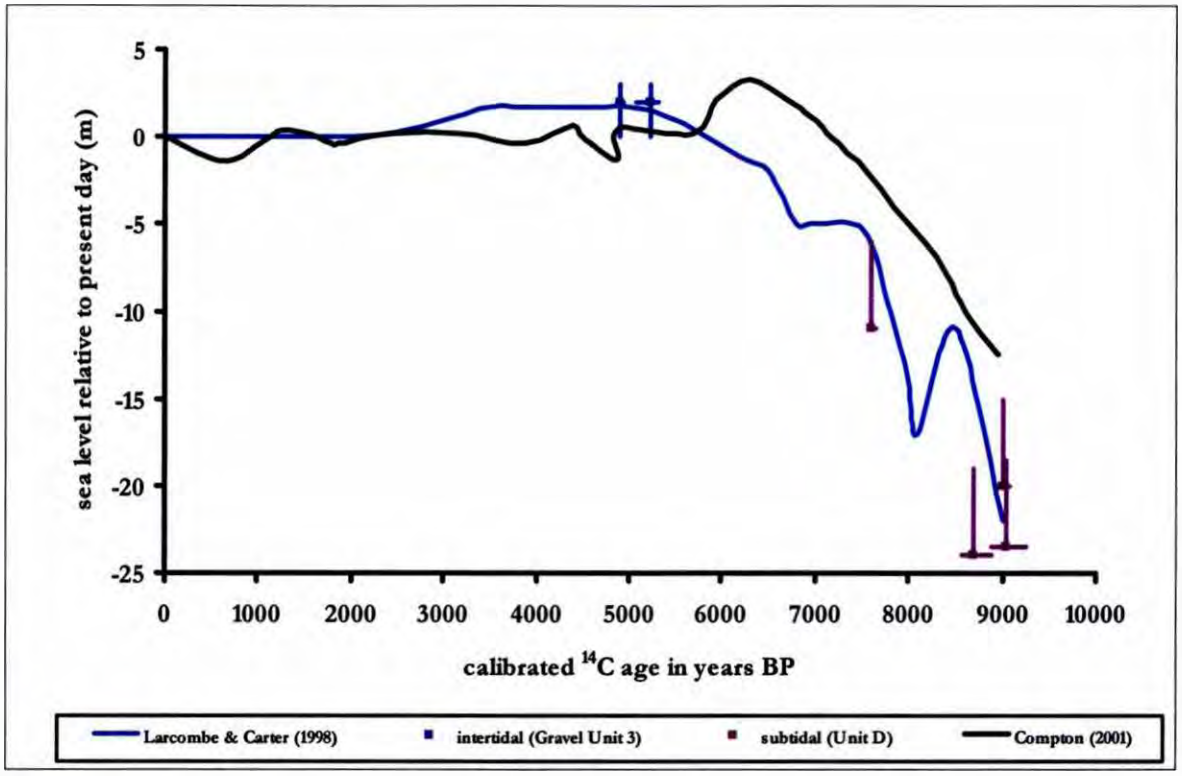

Figure 4.29. Sea level curves from the Queensland coast in Australia and the southwest coast of South Africa as compared to the dated indicators from Gravel Unit 3 and Unit D. Both curves define a Middle Holocene highstand, which is represented by Gravel Unit 3 at pocket beach Sites 2 and 3. Compton's (2001) curve is slightly displaced towards older ages, a fact which he attributes to neotectonic activity. Agreement between the data sets is, nevertheless, reasonably good if one considers the error ranges associated with these measurements (after Larcombe and Carter, 1998 and Compton, 2001).

4.5 DEPOSITIONAL HISTORY OF POCKET BEACH SITES 2 AND 3

A model for the depositional history of the valley fills at pocket beach Sites 2 and 3 is presented below. This model is illustrated in Figure 4.30.

a) The oldest known valley fill unit at the pocket beach sites is Unit A, which is interpreted as a sheetflood deposit. This unit pre-dates G1, which makes it older than 120 000 to 130 000 BP. Unit A was deposited by ephemeral streams activated in times of low relative sea level. At Site 3 some elements of Unit B are indistinguishable from the sediments comprising Unit A.

b) An Eemian marine trangression truncated Unit A, and terminated in a sea level highstand at an elevation of ~ +4 mamsl between 120 000 BP and 130 000 BP. The beachface and shoreface gravels of G1 were deposited at the time of this highstand. G1 was deposited on a bedrock footwall along the margins of the Sites 2 and 3 palaeo-valleys, and on pre-existing sedimentary fills in the central portions of the palaeo-valleys. At Site 2, this pre-existing sedimentary fill is represented by Unit A; at Site 3 it has been eroded and deflated to the bedrock valley floor. G1 has therefore only been preserved where it rests on more resistant footwall types. A supply of Orange River-derived gravel and diamonds was available at the time that G1 was deposited.

c) Unit B consists predominantly of a deflated pebble and cobble lag, which is sometimes superseded by sheetflood deposits. This unit is evidence of the deflation of Marmora Valley sediment fills to the valley floor during lowstand periods. This probably took place by a combination of aeolian and fluvial processes. Some of the sheetflood deposits at the valley floor may be remnants from previous periods of lowstand ephemeral stream activity, for instance the period that resulted in the deposition of Unit A (older than 120 000 to 130 000 BP). The most recent deflationary episode, which resulted in the deposition of Unit B, must have occurred between 120 000 and 9 000 BP.

d) Unit C is preserved only at Site 2 and occupies an uncertain position in the stratigraphy. The field evidence demonstrates that it is older than G3 (ca. 5 000 BP) and younger than G1 (120 000 to 130 000 BP), but is likely to be closer in age to G3. Unit C is interpreted as a coastal dune deposit.

e) Deposition of Unit D commenced at ca. 9 000 BP at Site 3, when the bedrock floor of Marmora Valley (~ –25 mamsl) was flooded by the most recent sea level transgression. Radiocarbon dating shows that sea level had passed –11 mamsl by ca. 7 600 BP. Unit D reflects cyclical marine flooding and barrier cut-off of Marmora Valley. The deposition of Unit D would have been terminated when the Middle Holocene highstand, represented by G3, was attained at ca. 5 000 BP. The palaeo-surface of Marmora Pan at ca. 5 000 BP would therefore have been

slightly higher than at present. Remnants of a higher pan level, in the form of flat-topped terraces, probably represent this palaeo-surface. Orange River-derived gravel and diamonds were available in the sediment supply during deposition of Unit D.

f) G2 was deposited sometime between 7 600 BP and 5 600 BP. The beachface and shoreface gravels of G2 represent a sea level stillstand at ~ –5 mamsl. This unit is developed all the way across the mouths of the Sites 2 and 3 palaeo-valleys, and therefore represents a time of barrier beach cut-off of Marmora Valley. G2 has incised into the sediments comprising Unit D, but contemporaneous accretion of the palaeo-Marmora Pan surface would have been ongoing to the landward of the G2 beach. G2 has an elevation close to that of the top variegated sub-unit of Unit D, meaning that they are of similar age. Orange River-derived gravels and diamonds were available in the sediment supply during deposition of G2.

g) Immediately following the deposition of G2, relative sea level rose to a transgressive highstand of ~ +2 to +3 mamsl at ca. 5 000 BP. A final set of beachface and shoreface gravels, which comprise G3, were deposited at this stage. As for G2, G3 is developed all the way across the mouths of the Sites 1 to 3 valleys, meaning that Marmora Valley was cut off from the sea at ca. 5 000 BP. G3 has truncated and reworked the top portion of the G2 beachface gravels, hence G2 is overlain by sandy shoreface sediments of G3. The sediment supply to pocket beach Sites 2 and 3 included Orange River-derived gravel and diamonds at this time.

h) Deposition of Unit E occurred during the minor regression of the last 5 000 years. The supply of gravel and diamonds greatly diminished during this time, and is reflected in the composition of Unit E, which is composed entirely of sand and grit. Net erosion of the palaeo-Marmora Pan surface would also have taken place between ca. 5 000 BP and the present day, as the sea level-controlled water table fell to its current levels, resulting in the formation of the aforementioned remnant, flat-topped terraces.

i) Unit F represents Late Holocene to modern, backbeach aeolian deposition at Sites 2 and 3.

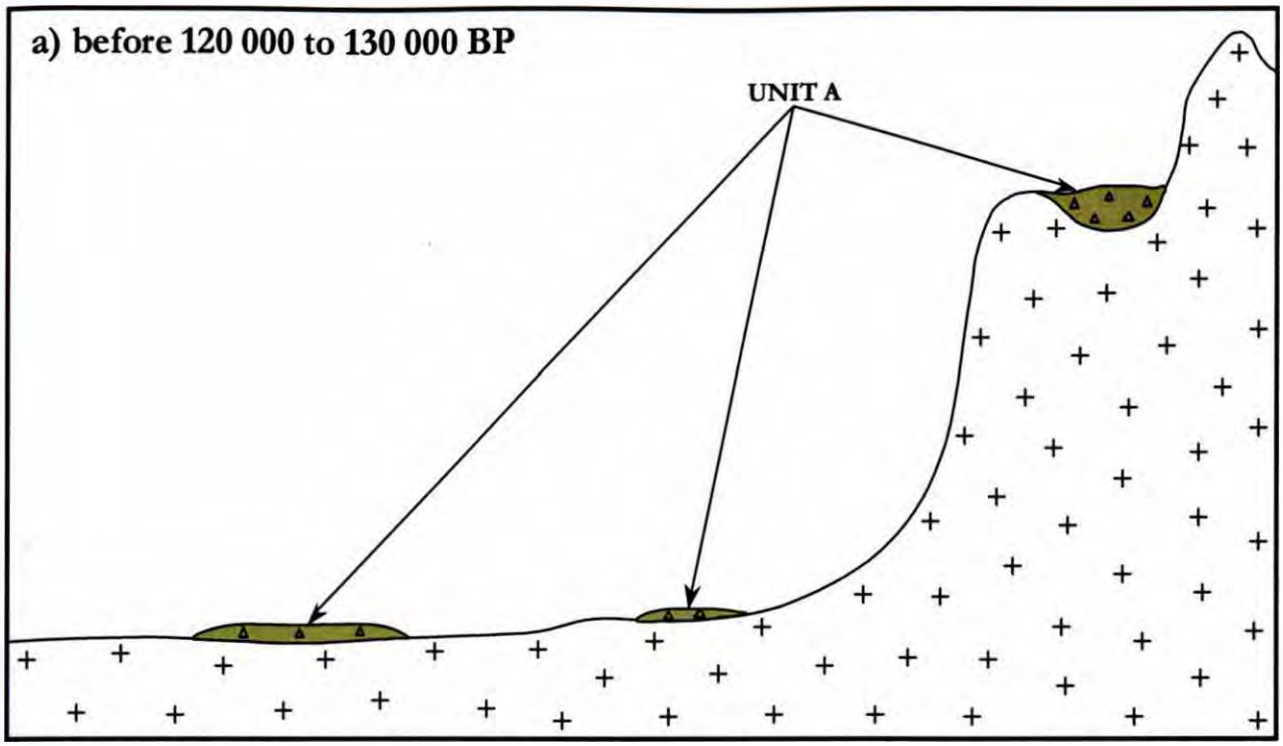

Figure 4.30a. Deposition of Unit A by ephemeral streams, activated by a sea level lowstand.

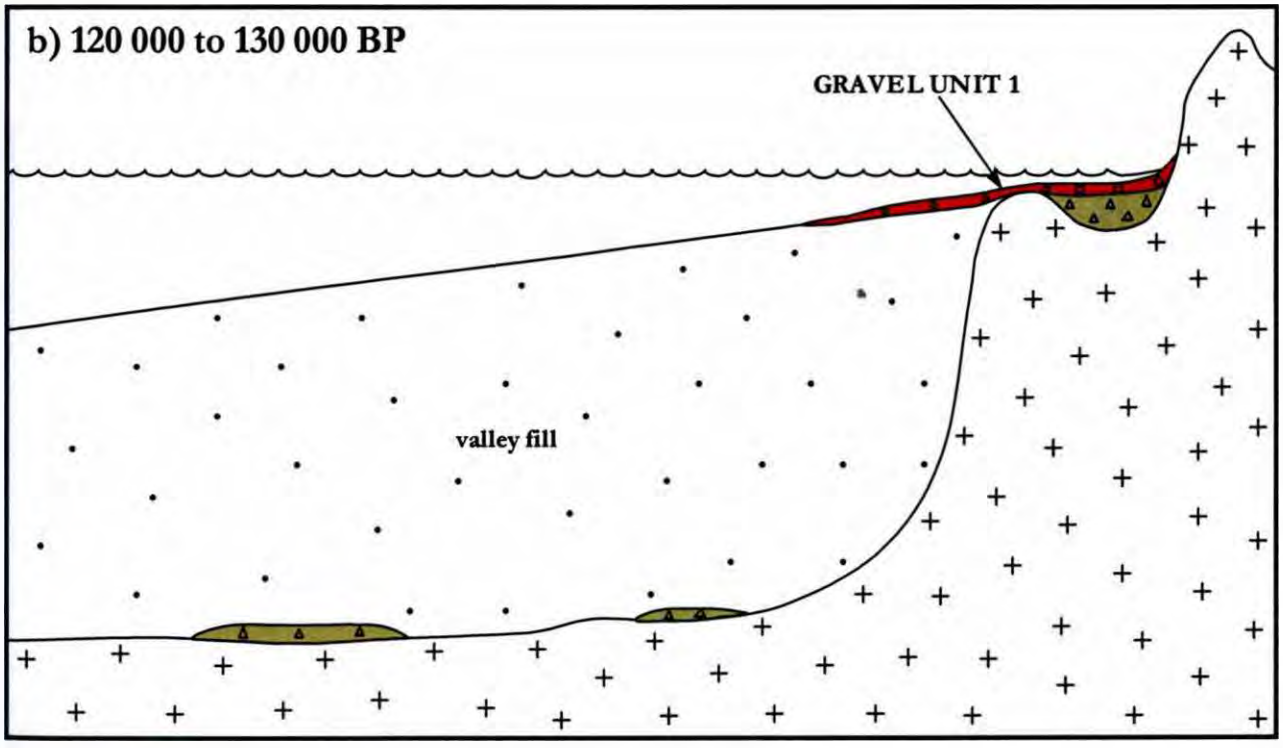

Figure 4.30b. Deposition of Gravel Unit 1 (Eemian highstand) during a +4 mamsl highstand between 120 000 and 130 000 BP.

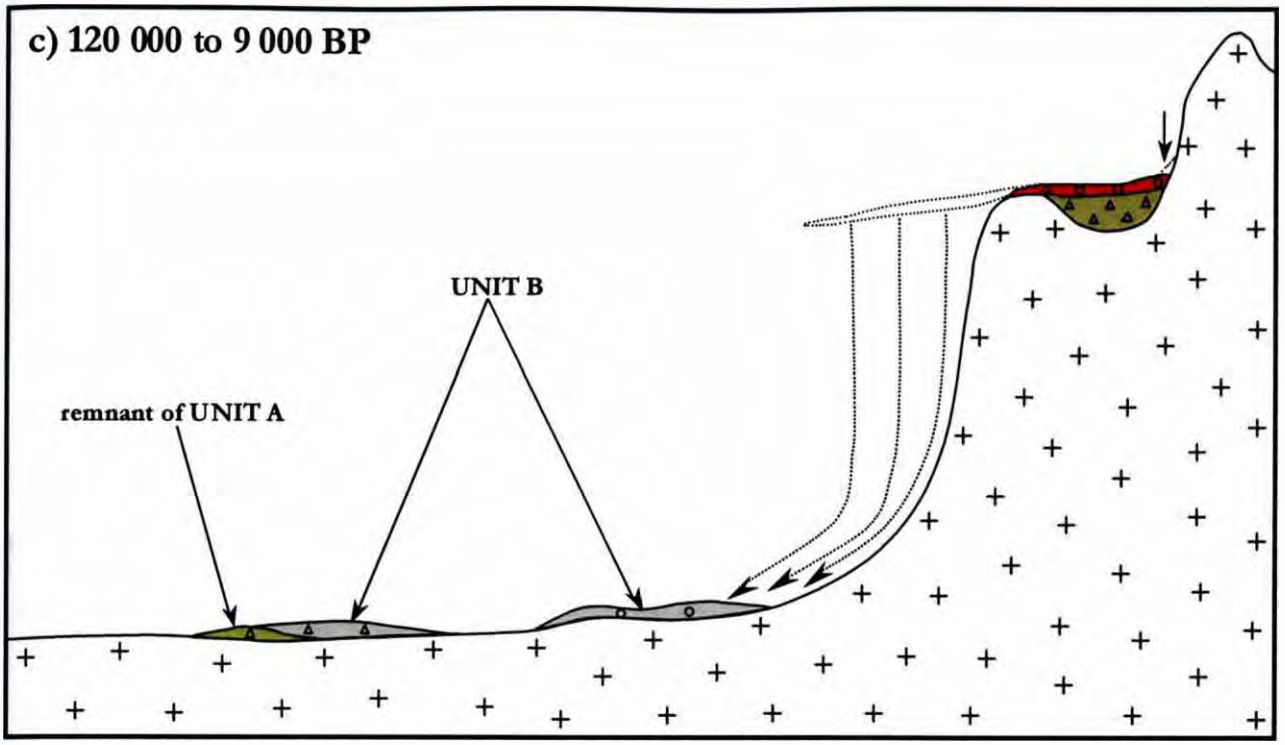

Figure 4.30c. Ephemeral stream action and deflation of the pre-existing valley fill results in the deposition of Unit B between 120 000 and 9 000 BP, which was a period of relatively low sea level. Gravel Unit 1 is subaerially exposed, resulting in incipient pedogenesis and calcretisation of its upper surface.

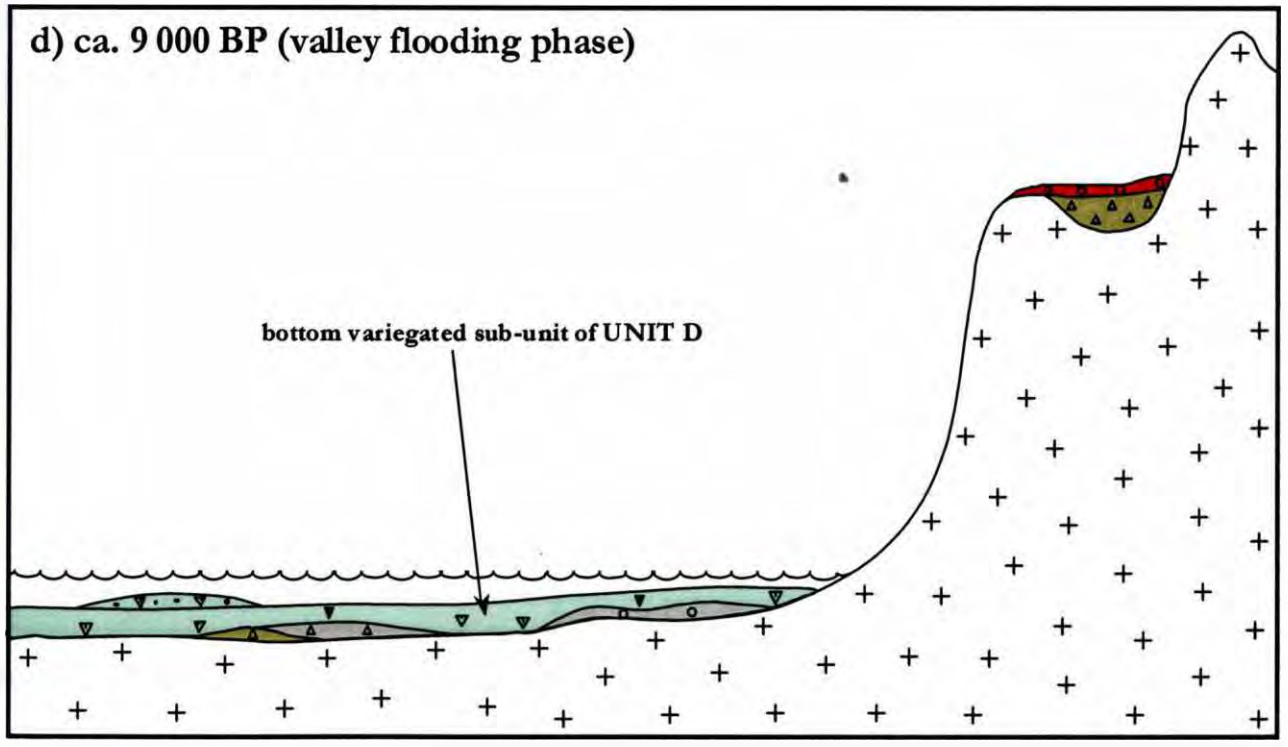

Figure 4.30d. Deposition of the bottom variegated sub-unit of Unit D at Site 3 during the initial stage of flooding of Marmora Valley at ca. 9 000 BP.

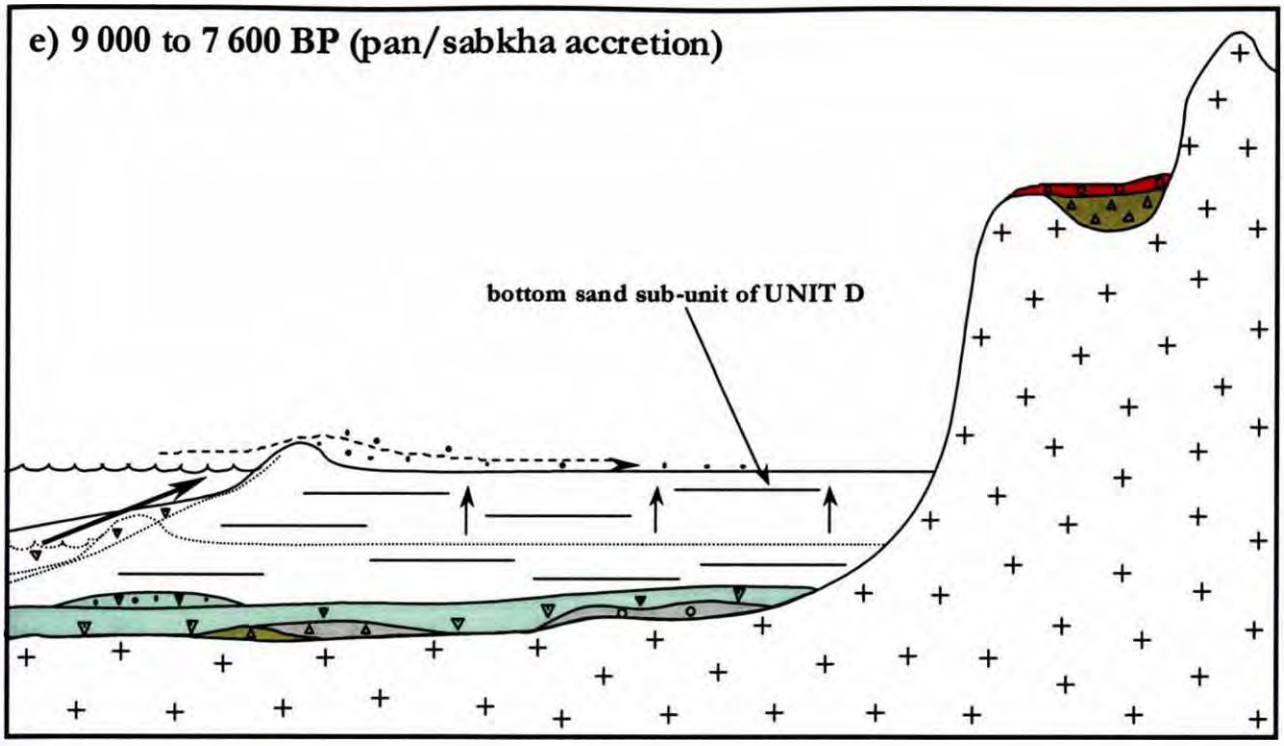

Figure 4.30e. Pan/sabkha accretion by adherence of windblown particles to the moist pan surface during barrier beach cut-off of Marmora Valley. Aggradation of the valley fill is being driven by the ongoing transgression.

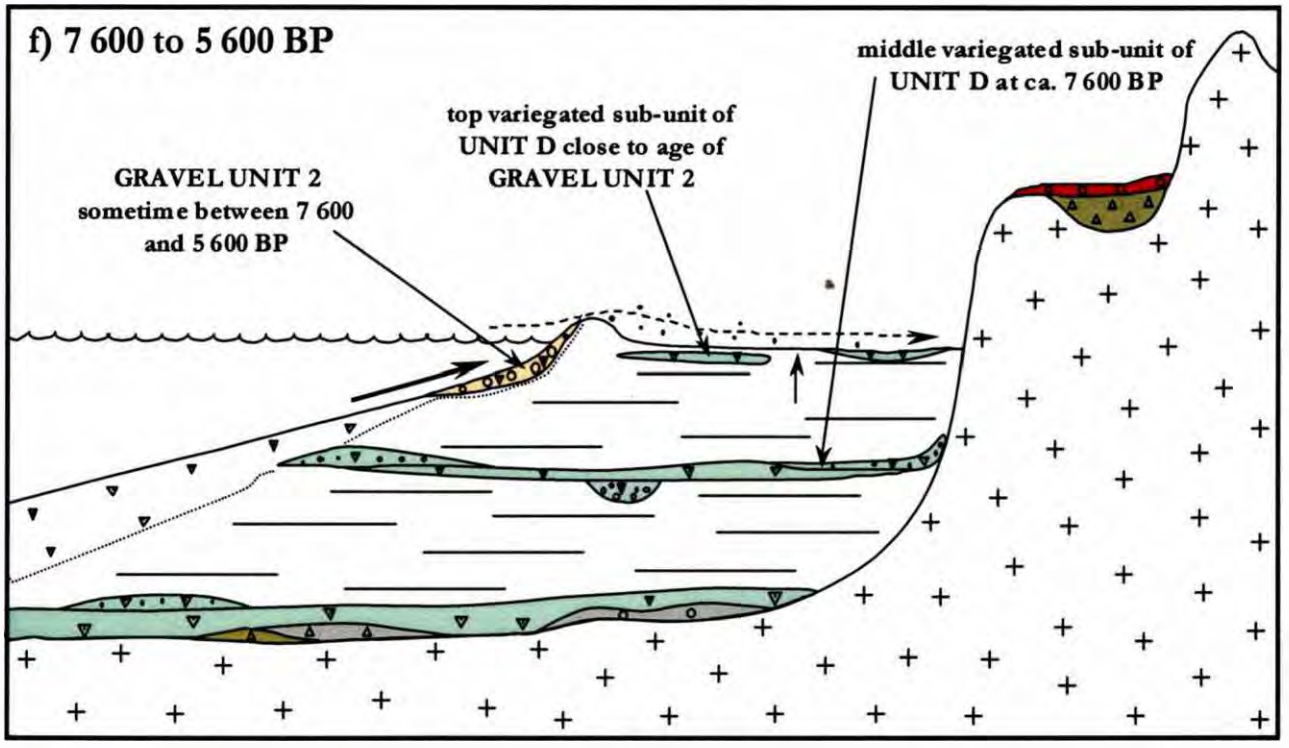

Figure 4.30f. Valley flooding and deposition of middle variegated sub-unit at ca. 7 600 BP, followed by barrier cut-off and renewed pan accretion. This phase culminates in more flooding to produce the top variegated sub-unit with the almost contemporaneous deposition of Gravel Unit 2.

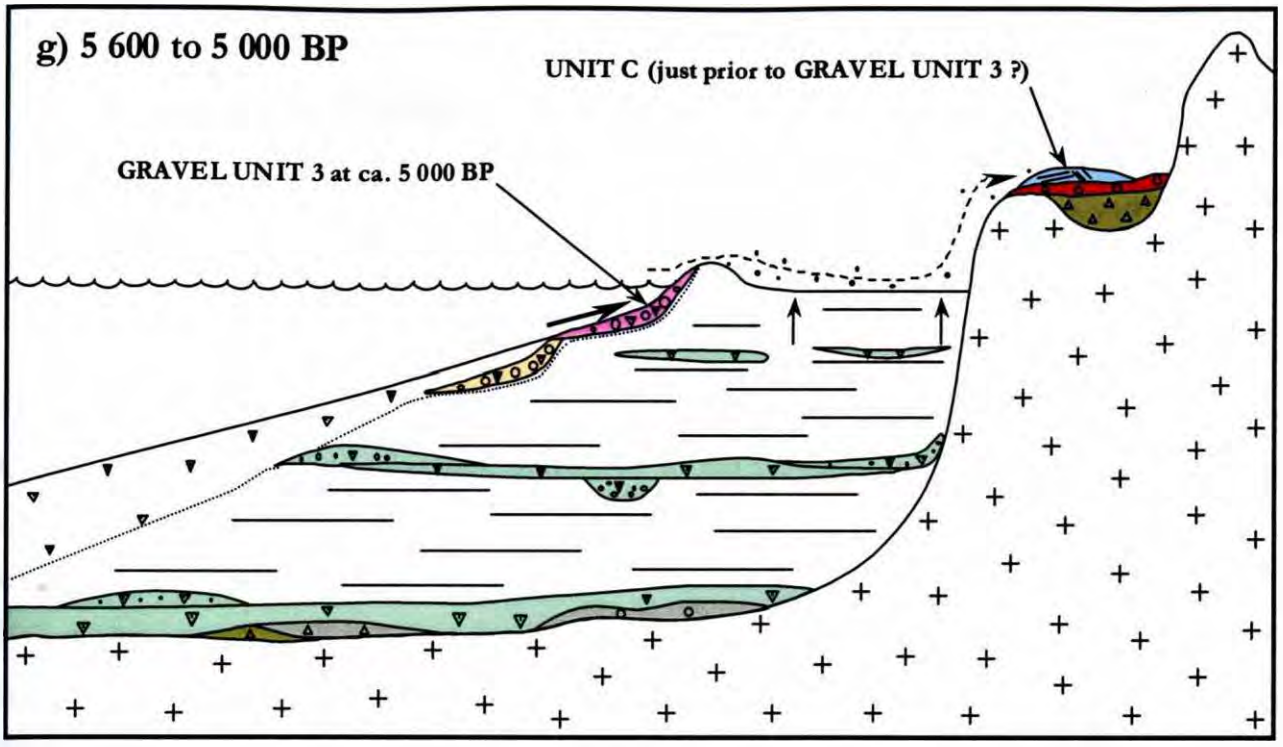

Figure 4.30g. Continued aggradation by pan/sabkha accretion following the deposition of Gravel Unit 2. This is the most likely time for the deposition of Unit C, with the transgression bringing the shoreline ever landward. This phase culminates in the deposition of Gravel Unit 3 (Middle Holocene highstand) at ca. 5 000 BP.

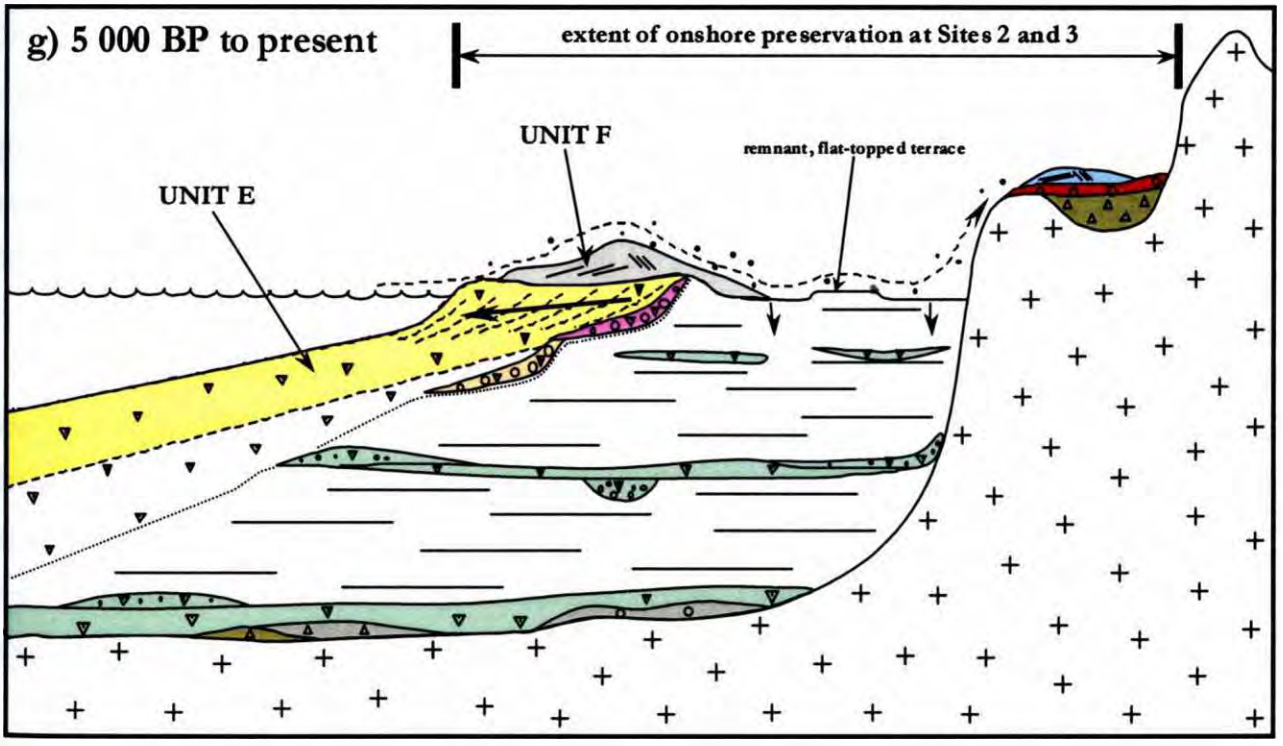

Figure 4.30h. A slight regression to the current sea level leads to progradation of the shoreline and deposition of Unit E, followed by establishment of the modern coastal dune system (Unit F). Slight erosion of drying pan/sabkha surface (because of lowered water table) forms remnant, flat-topped terraces on Marmora Pan.

CHAPTER 5 – POCKET BEACH GRAVELS AND DIAMONDS

5.1 INTRODUCTION

This chapter narrows the focus to the pocket beach gravel units (G1 - +4 m highstand, G2 - -5 m stillstand and G3 - +2 m highstand), introduced in the previous chapter, and especially to the diamonds contained within them. Aspects of the three gravel beach units as a whole, which have a specific bearing on the diamonds within them, are also examined. During the course of the 1979 to 1981 evaluation programme at Sites 2 and 3, it was found that G1, G2, and G3 host economically-promising concentrations of diamonds. The other geological units described in the previous chapter were deemed to hold little potential for economic mineralisation. This part of the study therefore considers only those diamonds that are contained within G1, G2 and G3, which were the primary focus of the recent evaluation programme.

The proportion of gem-quality diamonds in the Sperrgebiet placers consistently exceeds 95 % (Schneider and Miller, 1992). Therefore, the two most important remaining parameters requiring understanding and quantification are the concentration of stones in the deposit (ie. the diamond grade or diamond density distribution) and the size of the stones in that deposit. This chapter attempts to identify the controls on the density distribution and size distribution of the diamonds in the three pocket beach gravel units at Sites 2 and 3.

Samples taken as part of the recent evaluation programme at Sites 2 and 3 were targeted at specific beach gravel subdivisions within G1, G2 and G3, which were defined using delineation drill hole data. This practice is in accordance with the observations of Oosterveld *et al.* (1987) and Sichel (1972), who pointed out that the diamond density and diamond size distribution should remain constant within geologically homogeneous zones. Only intertidal (imbricate and infill zones combined) and subtidal (outer framework) subdivisions were considered because :

a) The large disc and washover zones do not contain economic concentrations of diamonds at Sites 2 and 3.
b) The infill zone is typically very narrow and combining it with the imbricate zone was considered to be more practical. This also resulted in less "clutter" in illustrations of the

density and size distributions of the stones, without compromising the identification of factors controlling mineralisation.

Although diamonds were recovered in the previous (1979-1981) prospecting campaign using the Frankipile tool, these samples were not considered to be representative, being less than 1 m^2 in size. Many years of prospecting experience by Namdeb along the Central Sperrgebiet coastline, as well as proprietary deposit simulation techniques, show that an individual sample size of at least 10 m^2 is required for the confident estimation of economically promising, marine gravel-hosted diamond resources in this area. This study therefore considers only the results of the GB50 (10.08 m^2 each) and Site 2 trench (>> 10 m^2 each) samples. The positions of these samples, relative to the aforementioned geological subdivisions, are shown in Figures 5.1 and 5.2.

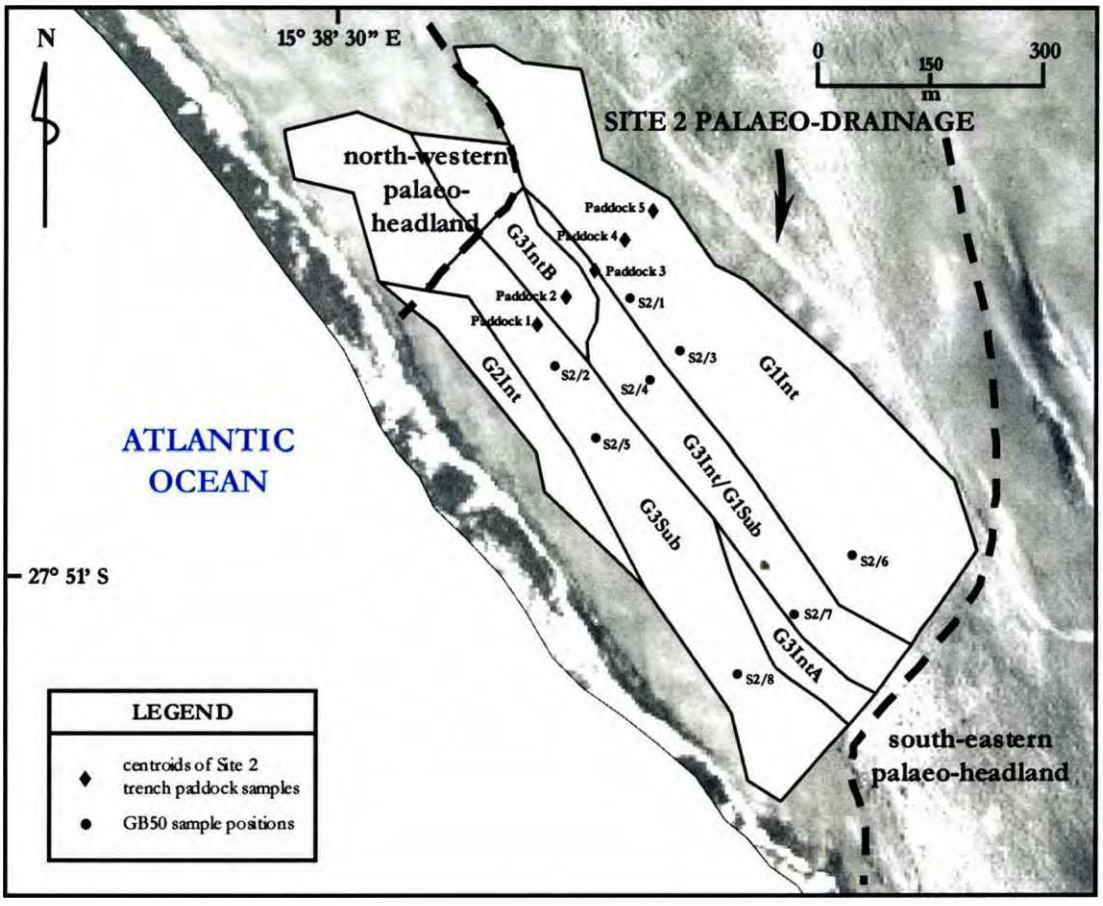

Figure 5.1. The positions of the GB50 and Site 2 trench paddock samples of the marine gravels at Site 2. The backdrop is an aerial photograph of the area. Geological subdivisions of the marine gravels are as follows : *G1Int* – intertidal gravels of G1; *G3Int/G1Sub* – intertidal gravels of G3 overlapping subtidal gravels of G1; *G3IntA* and *G3IntB* – intertidal gravels of G3; *G3Sub* – subtidal gravels of G3; *G2Int* – intertidal gravels of G2.

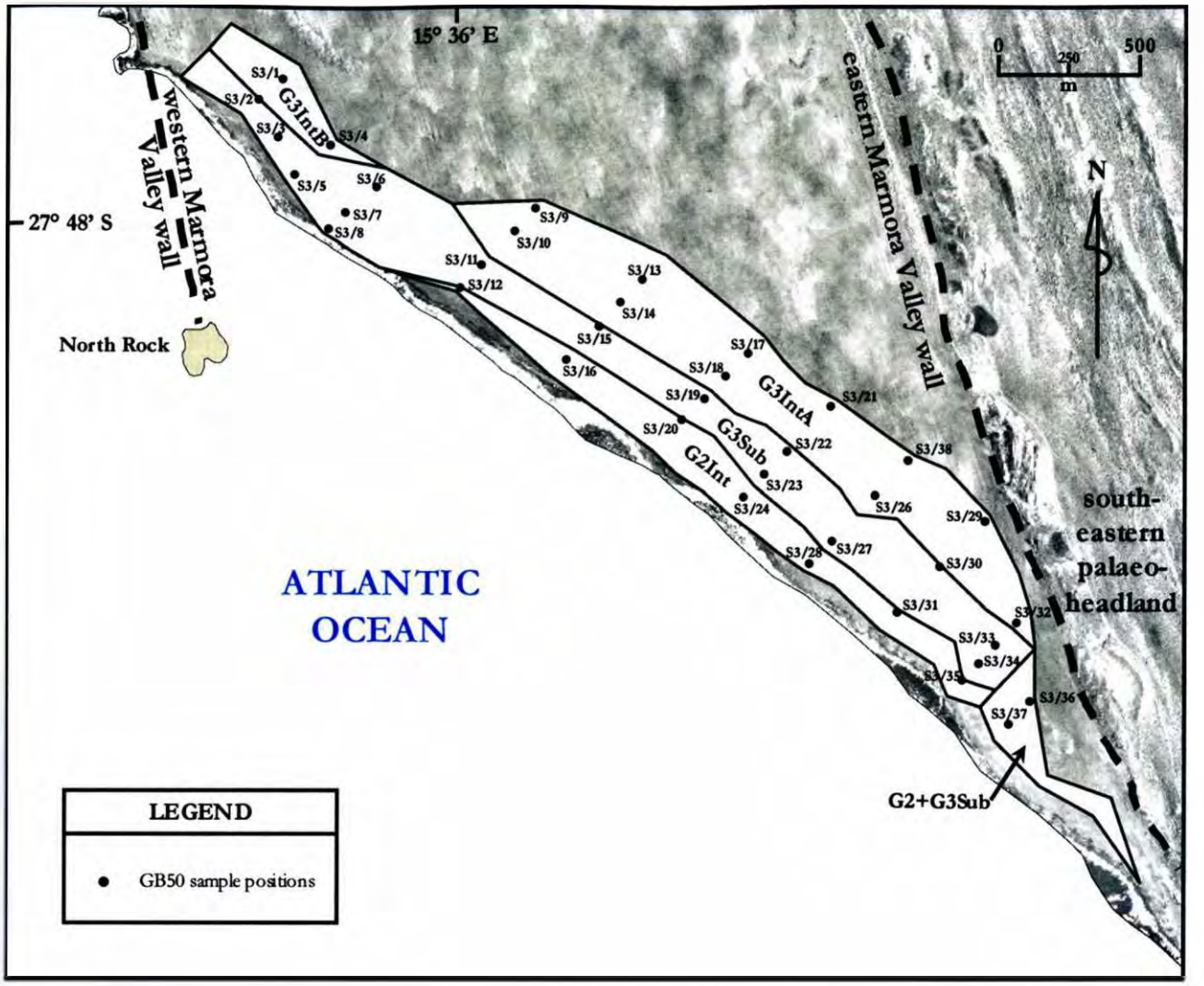

Figure 5.2. The positions of the GB50 samples of the marine gravels at Site 3. The backdrop is an aerial photograph of the area. Geological subdivisions of the marine gravels are as follows : *G3IntA* and *G3IntB* – intertidal gravels of G3; *G2+G3* – intertidal and subtidal gravels of G2 and G3 directly adjacent to each other, compressed into a narrow zone; *G3Sub* – subtidal gravels of G3; *G2Int* – intertidal gravels of G2.

5.2 ASPECTS OF THE POCKET BEACH GRAVELS

5.2.1 Gravel Size Distribution at Sites 2 and 3

Relative gravel size distribution for the marine gravel deposit at Sites 2 and 3 was determined by visual examination of the GB50 sample tailings, supported by a limited number of clast size

distribution analyses. These data are shown in Table 5.1 as well as in Figures 5.3 and 5.4. Three broad gravel coarseness categories were identified :

a)*fine gravel* – consisting mostly of clasts below 64 mm in size (ie. pebbles to small cobbles)

b)*medium gravel* – contain a significant proportion of cobbles greater than 64 mm, but less than 128 mm in size (ie. a significant number of medium cobbles)

c)*coarse gravel* – gravels with a relatively large proportion of clasts greater than 128 mm in size

Table 5.1. Four clast size distributions of GB50 sample tailings from Site 3. See Figure 5.2 for the positions of the GB50 samples.

Size Fraction	S3/7 (wt%)	S3/11 (wt%)	S3/23 (wt%)	S3/32 (wt%)
+4 mm-8 mm	18.0%	17.3%	20.3%	11.7%
+8 mm-16 mm	17.0%	16.6%	18.7%	9.8%
+16 mm-25 mm	16.4%	19.5%	11.9%	9.0%
+25 mm-32 mm	12.7%	17.4%	7.7%	5.6%
+32 mm-60 mm	29.2%	18.0%	36.8%	8.7%
+60 mm-95 mm	6.7%	9.5%	4.7%	22.8%
+95 mm-120 mm	0.0%	1.3%	0.0%	13.7%
+120 mm-150 mm	0.0%	0.4%	0.0%	11.7%
+150 mm	0.0%	0.0%	0.0%	6.8%

Data points are relatively sparse at Site 2, but coarser gravels generally occur on the south-eastern side of the marine gravel body, against the south-eastern palaeo-headland. The central and north-western sections of the Site 2 gravel body encompass fine-to-medium gravels.

At Site 3, coarse gravels are also concentrated in the southeast, against the palaeo-headland. Another small area of coarse gravels is evident at the north-western end of G2Int. The rest of G2Int and the north-western end of G3Sub contain fine gravels. The remainder of the marine gravel body at Site 3 consists of medium gravels.

The gravel coarseness variations are common to most of the beach gravel subdivisions. This indicates that the beach depositional processes responsible for this zonation do not represent the overriding control on gravel size distribution. Increased gravel coarseness is indicative of relatively

high hydraulic energy (equivalent to wave energy in the littoral environment) (Selley, 1982). The coarsest gravels at Sites 2 and 3 generally occur where the gravel beaches abut headlands, reflecting increased wave energy in this area at the time of deposition. The reasons for this higher wave energy are considered below.

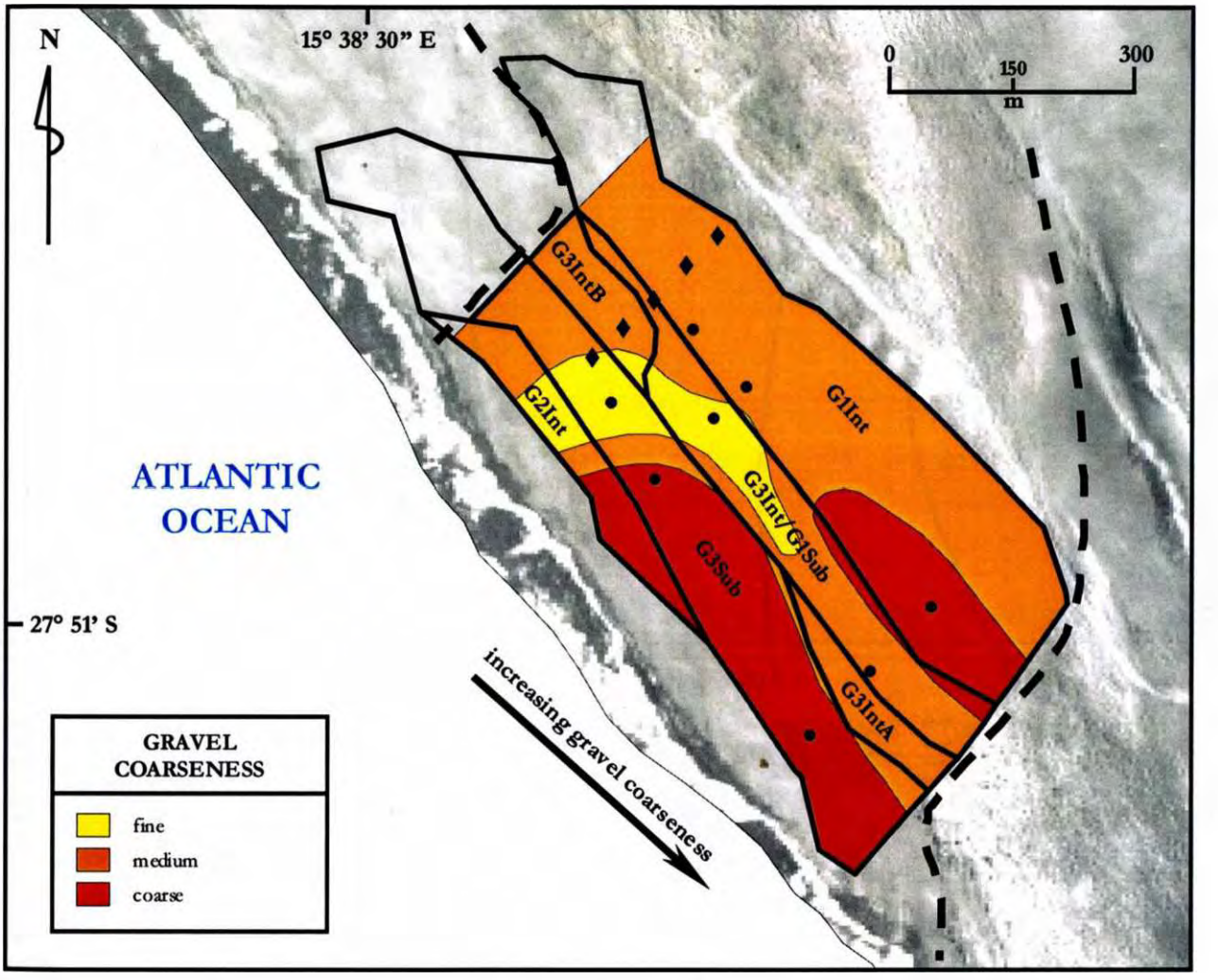

Figure 5.3. Relative gravel coarseness at Site 2, derived from visual observations of GB50 sample tailings. Subdivisions of the marine gravels are as follows : *G1Int* – intertidal gravels of G1; *G3Int/G1Sub* – intertidal gravels of G3 overlapping subtidal gravels of G1; *G3IntA* and *G3IntB* – intertidal gravels of G3; *G3Sub* – subtidal gravels of G3; *G2Int* – intertidal gravels of G2.

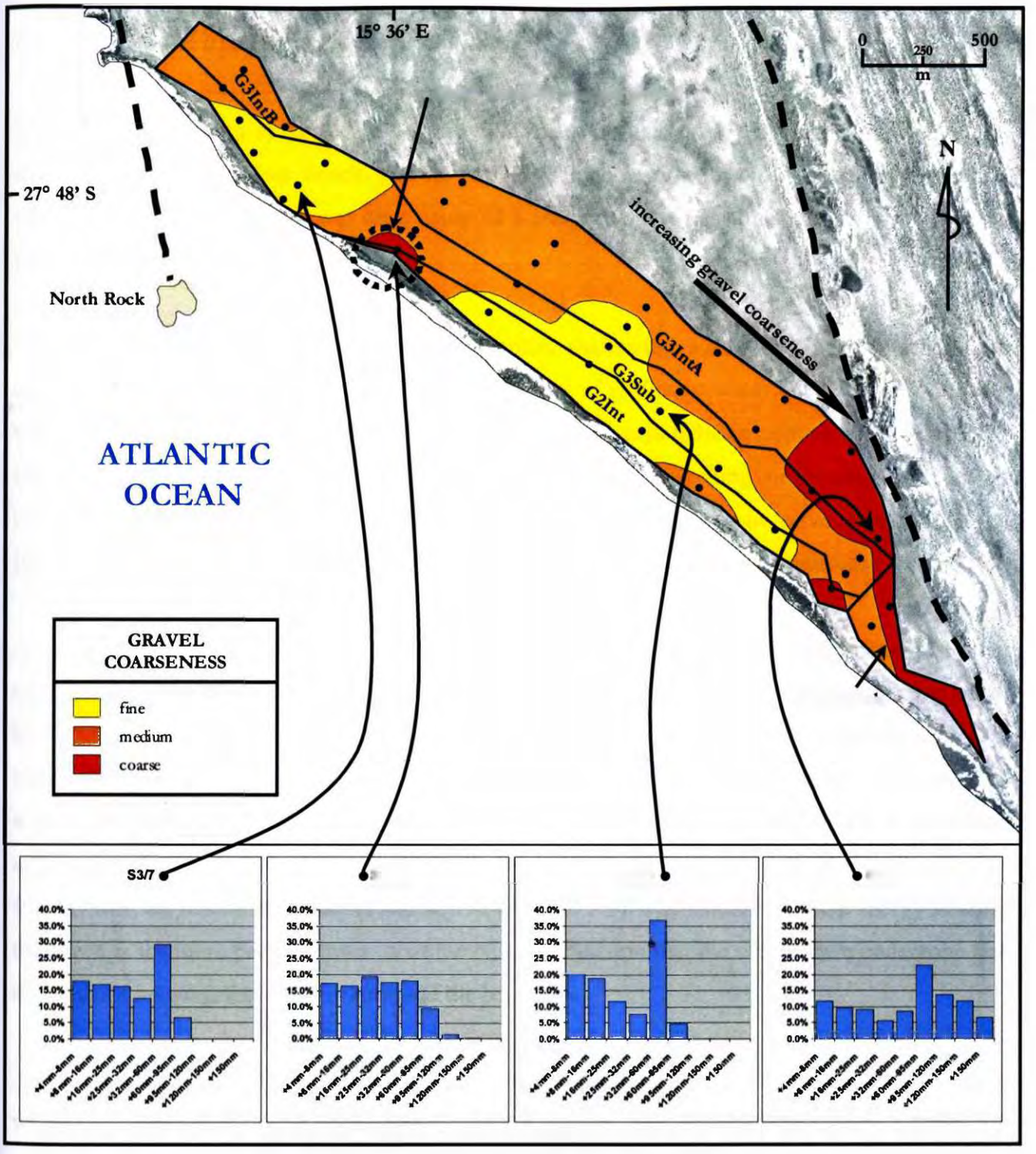

Figure 5.4. Relative gravel coarseness at Site 3, derived by visual examination of GB50 sample tailings, and supported by four clast size distribution analyses. Subdivisions of the marine gravels are as follows : *G3IntA* and *G3IntB* – intertidal gravels of G3; *G2+G3* – intertidal and subtidal gravels of G2 and G3 directly adjacent to each other, compressed into a narrow zone; *G3Sub* – subtidal gravels of G3; *G2Int* – intertidal gravels of G2.

5.2.2 Modern Wave Patterns at Sites 2 and 3

Modern wave patterns at Sites 2 and 3 provide valuable clues that shed light on the clast size distribution of the ancient beach gravels and their associated, ancient wave energy regimes. Analysis of the wave patterns was done using ALS imagery of the coastline, and was backed up by field observations.

A wave will refract when part of it encounters shallowing water. That portion which is in deeper water continues to move faster than the portion in shallower water with the result that the wave crest becomes curved (Pethick, 1984). Diverging wave rays indicate refraction of a wave such that its energy per unit length is being decreased; this is due to 'stretching' of the deep water length of the wave as it is refracted (see Figure 5.5). Conversely, convergent wave rays indicate an increase in the amount of energy per unit length as the deep water length is compressed.

As a wave approaches the coastline over a shallowing shoreface, it begins to 'feel' the sediment surface; this area is known as the shoaling zone. Eventually, it will oversteepen and break in a landward direction (Elliott, 1978), thus initiating the breaker zone. A gentler shoreface slope is indicated by waves that begin to shoal further out to sea. A steeper shoreface slope is indicated by waves that shoal closer to the beach. Wider shoaling and breaker zones result in increased attenuation of wave energy because of the greater amount of time that the wave will spend in friction with the sediment surface (Pethick, 1984; Figure 5.5). The amount of wave energy striking the beach is therefore partly a function of the type of refraction that the waves have undergone and the distance between the shoaling zone and the beachface.

Slight refraction of waves is taking place at the south-eastern headlands of Sites 2 and 3, where their respective eastern valley walls obliquely intersect the coastline (see Figures 5.6, 5.7, 5.8 and 5.9). The oblique angle of intersection means that wave refraction is limited, and wave energy is not significantly attenuated. In addition to this, the shoaling and breaker zones decrease markedly in width at the south-eastern headlands, with the result that wave energy striking the beach is relatively high. These areas of increased wave energy are modern equivalents for the south-eastern portions of the ancient pocket beach gravels at Sites 2 and 3. The coarser gravels abutting the headlands at Sites 2 and 3 are therefore a response to increased wave energy at the time of deposition, which resulted from reduced attenuation in narrower shoaling and breaker zones.

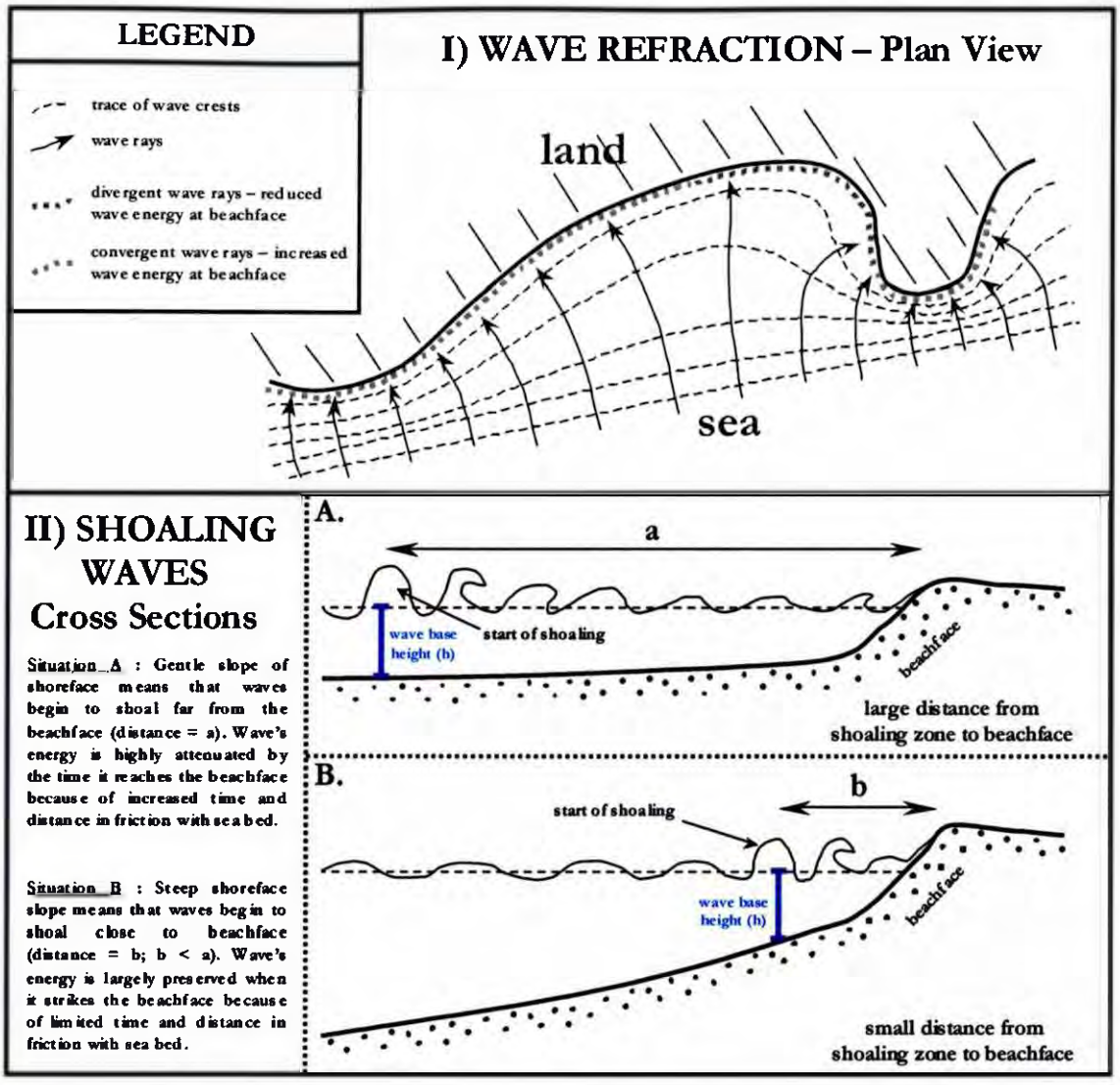

Figure 5.5. Sketches showing the effect that wave refraction and shoreface steepness have on the wave energy striking the beachface. Sources are Pethick (1984) and Elliot (1978).

Modern wave patterns at Site 3 point to a probable reason for the area of coarser gravels at the north-western end of G2Int. This is the northernmost section of the beach gravel at Site 3 that is not sheltered behind the offshore extension of the western Marmora Valley wall. Another feature of this area is that the ancient and modern gravel beaches appear to be curving back towards the western Marmora Valley wall, and are facing directly southward. The distance between the shoaling zone and modern beach also decreases slightly at this point, indicating reduced attenuation of wave energy in the modern situation. It is suggested that the increased wave energy, indicated by the coarser gravel in the pocket beach gravels in the north of G2Int, resulted primarily from the change in angle of the ancient beaches, such that they were directly facing the oncoming swell. Another contributing factor may have been that wave energy rapidly dropped off to the north of this point, as

the beaches went into the lee of the western Marmora Valley wall; this could have resulted in the immediate settling out of the coarser bedload fraction.

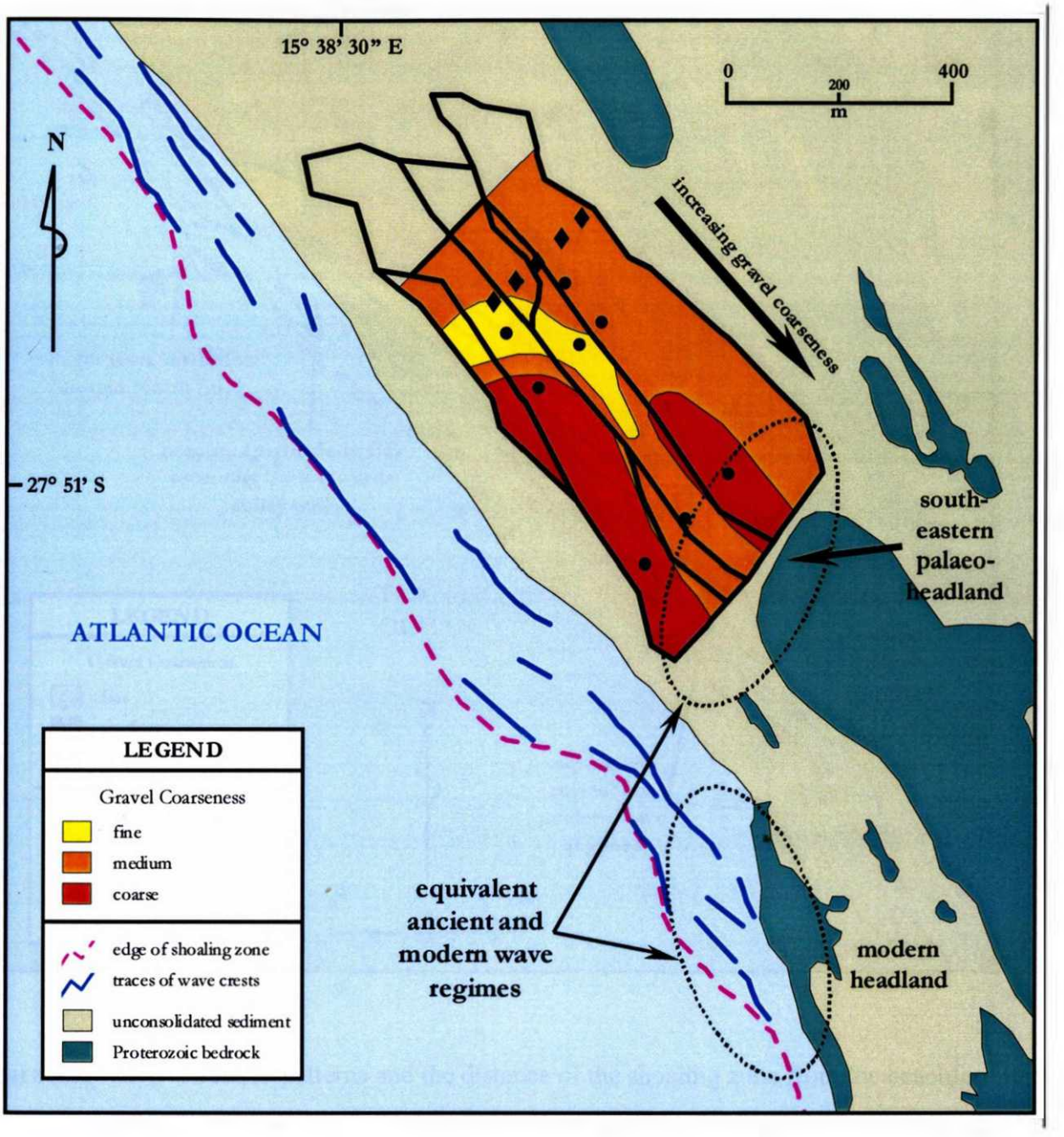

Figure 5.6. Wave refraction patterns and the distance of the shoaling zone from the beachface in the modern setting at Site 2. Note that while wave refraction is limited against the south-eastern headland, the distance between the shoaling zone and shoreline narrows considerably, resulting in relatively high wave energy at the beachface. The wave regime at the south-eastern palaeo-headland would have been similar to that seen at the modern headland, giving rise to coarser gravels.

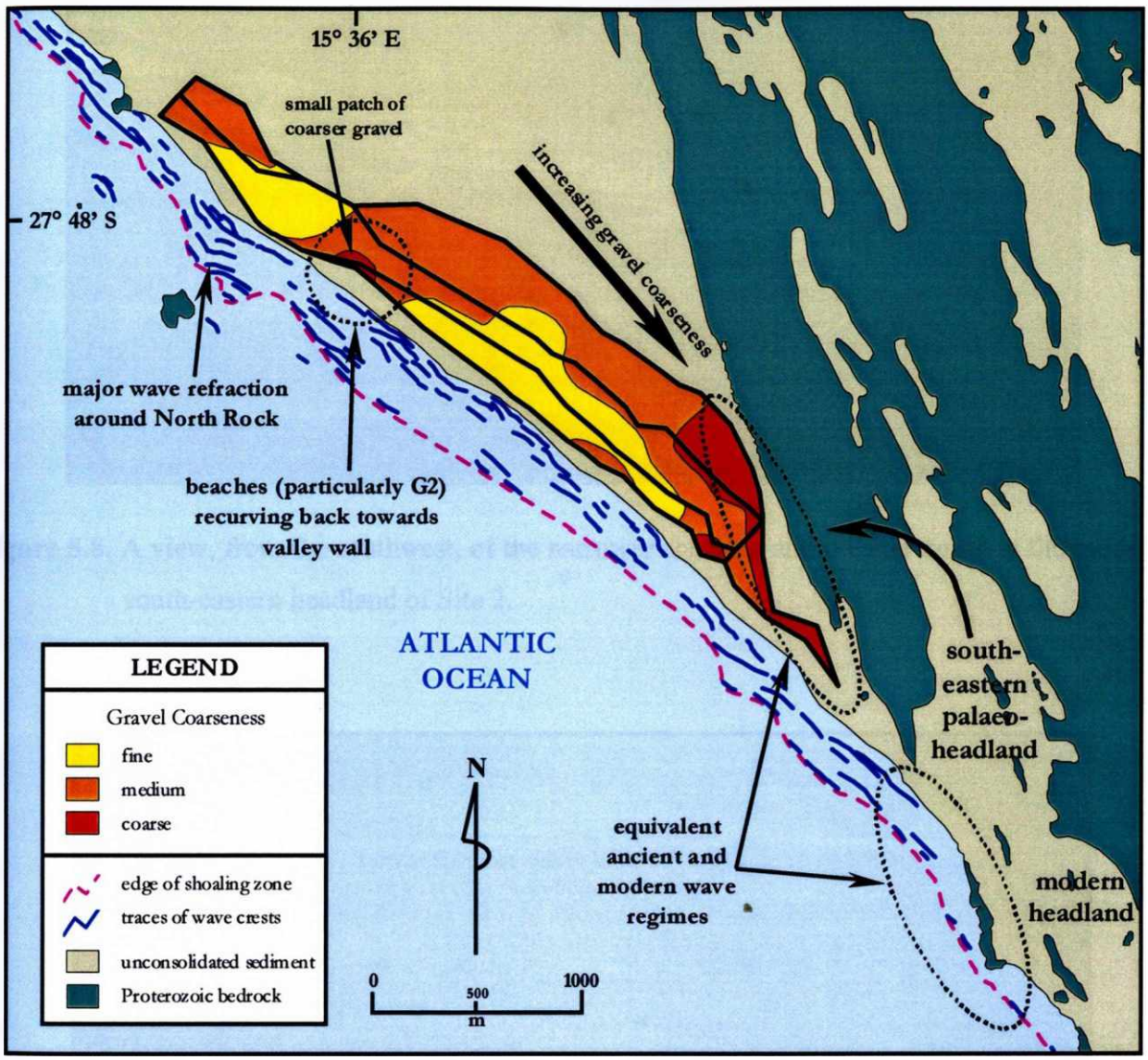

Figure 5.7. Wave refraction patterns and the distance of the shoaling zone from the beachface in the modern setting at Site 3. The modern wave regime at the south-eastern headland echoes what is seen at Site 2. As at Site 2, the wave regime at the south-eastern palaeo-headland of Site 3 would have been similar to that seen at the modern headland, resulting in coarser beach gravels.

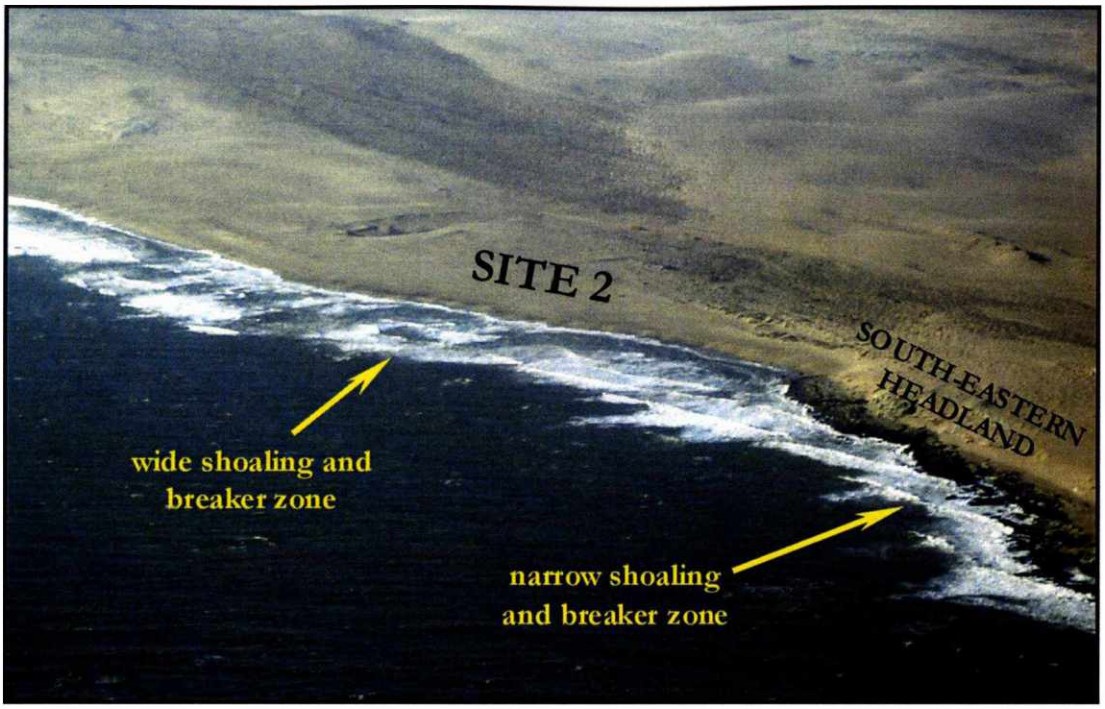

Figure 5.8. A view, from the southwest, of the narrower shoaling and breaker zones at the modern, south-eastern headland of Site 2.

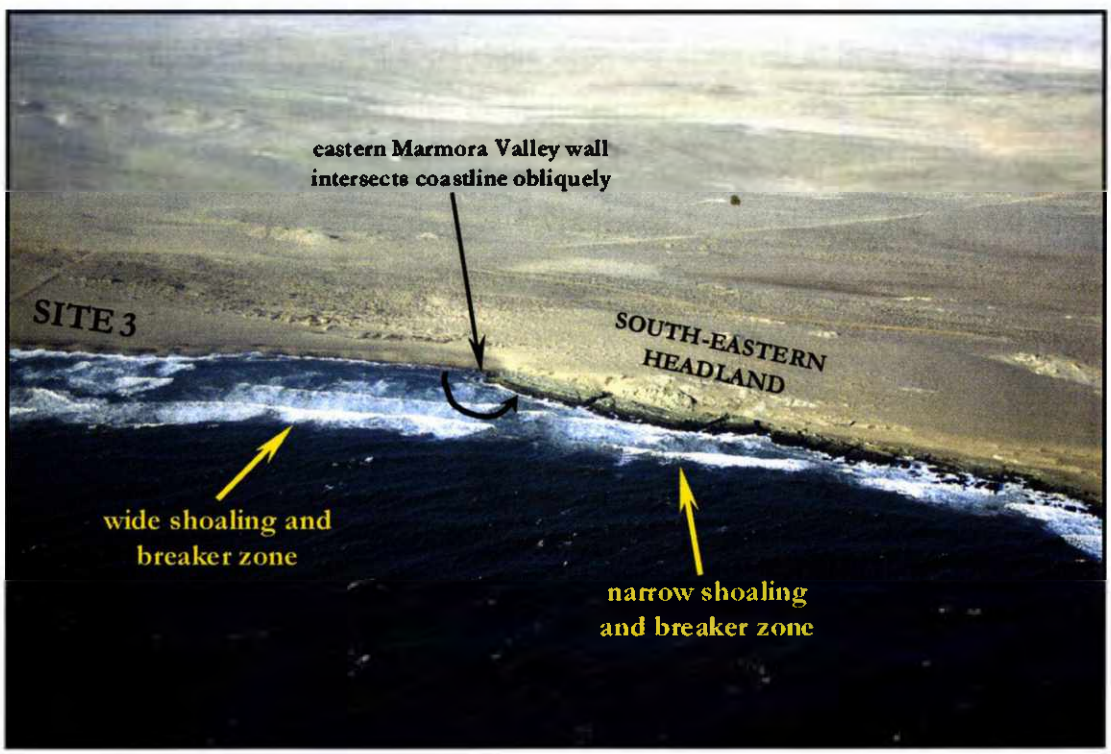

Figure 5.9. A view, from the west, of the narrowing of the shoaling and breaker zones at the modern, south-eastern headland of Site 3.

5.3 EVALUATION SAMPLING RESULTS

5.3.1 Units of Measurement

The marine gravels of G1, G2 and G3 are thin, tabular bodies and approximate a two-dimensional surface. There was also greater certainty in the measurement of sample areas than in the measurement of sample volumes during the recent evaluation programme. Under these conditions, the stone density distribution is best measured in units of stones per m^2 (stns/m^2), and is correctly referred to as the areal stone density (Oosterveld, 2003). For reasons of confidentiality, a scale of relative areal stone density with five subdivisions has been used :

1)barren – sample recovered no diamonds (ie. negative samples)
2)low
3)moderate
4)high
5)very high

This scale is specific to the range of areal stone densities observed at Sites 2 and 3 and does not relate in any way to stone densities in other diamondiferous deposits.

The size distribution of diamonds was investigated by looking at the spatial variation of average stone size, as evident in the evaluation samples. The average stone size for a sample was calculated as the *arithmetic mean of the carat weights of the diamonds recovered in the sample* (ie. units of carats/stone – abbreviated cts/stn).

5.3.2 Results

The results of the GB50 and Site 2 trench evaluation samples are shown in Tables 5.2, 5.3 and 5.4 and contoured in Figures 5.10, 5.11, 5.12 and 5.13. Sample results from the Site 2 trench are shown in Figure 5.14. Measures of dispersion are not given for average stone size, since individual stone

weights were not recorded during the sampling programmes. However, as will become apparent in the following chapter, the variance for diamond size at Site 3 is relatively low.

Table 5.2. Results of Site 2 trench paddock evaluation samples of the marine gravels at Site 2.

Paddock Sample Number	Sample Area (m^2)	Relative Areal Stone Density (stns/m^2)	Average Stone Size (cts/stn)
Paddock 1	807.00	low	0.33
Paddock 2	819.00	high	0.39
Paddock 3	675.00	very high	0.33
Paddock 4	623.00	moderate	0.38
Paddock 5	635.00	moderate	0.40

Table 5.3. Results of GB50 evaluation samples of the marine gravels at Site 2.

GB50 Sample Number	Sample Area (m^2)	Relative Areal Stone Density (stns/m^2)	Average Stone Size (cts/stn)
S2/1	10.08	high	0.44
S2/2	10.08	low	0.40
S2/3	10.08	high	0.27
S2/4	10.08	very high	0.31
S2/5	10.08	moderate	0.27
S2/6	10.08	moderate	0.48
S2/7	10.08	very high	0.46
S2/8	10.08	moderate	0.62

It is noteworthy that the paddock samples taken in the Site 2 trench were orders of magnitude larger than the samples excavated by the GB50 hydraulic grab. The paddock sample results are therefore highly representative of the actual areal stone density and average stone size values. The extent to which the average stone size of a particular GB50 sample represents reality at the sample locality will depend largely upon the number of stones recovered in that sample. GB50 samples that delivered higher areal stone densities are more representative of actual average stone size. Overall, the GB50 samples proved to be of sufficient size to detect mineralisation patterns and to conduct confident resource estimates. Regarding the interpretation of GB50 sample data, and to take account of instances where a single sample may not be representative, a distribution pattern was only

accepted as being significant where two or more GB50 sample results were observed to define a clear, spatial trend in the density or size distribution of diamonds.

Table 5.4. Results of GB50 evaluation samples of the marine gravels at Site 3.

GB50 Sample Number	Sample Area (m^2)	Relative Areal Stone Density (stns/m^2)	Average Stone Size (cts/stn)
S3/1	10.08	low	0.25
S3/2	10.08	high	0.33
S3/3	13.44	barren	no stones recovered
S3/4	10.08	moderate	0.23
S3/5	10.08	barren	no stones recovered
S3/6	10.08	moderate	0.22
S3/7	10.08	barren	no stones recovered
S3/8	10.08	barren	no stones recovered
S3/9	10.08	barren	no stones recovered
S3/10	10.08	barren	no stones recovered
S3/11	10.08	low	0.48
S3/12	10.08	moderate	0.36
S3/13	10.08	barren	no stones recovered
S3/14	10.08	barren	no stones recovered
S3/15	10.08	low	0.19
S3/16	10.08	very high	0.25
S3/17	10.08	barren	no stones recovered
S3/18	10.08	low	0.08
S3/19	10.08	low	0.24
S3/20	10.08	very high	0.29
S3/21	10.08	low	0.52
S3/22	10.08	high	0.32
S3/23	10.08	low	0.21
S3/24	10.08	moderate	0.23
S3/26	10.08	moderate	0.26
S3/27	10.08	barren	no stones recovered
S3/28	10.08	very high	0.25
S3/29	10.08	moderate	0.31
S3/30	10.08	low	0.21
S3/31	10.08	high	0.23
S3/32	10.08	high	0.37
S3/33	10.08	low	0.34
S3/34	10.08	low	0.23
S3/35	10.08	moderate	0.29
S3/36	10.08	high	0.49
S3/37	10.08	high	0.32
S3/38	10.08	barren	no stones recovered

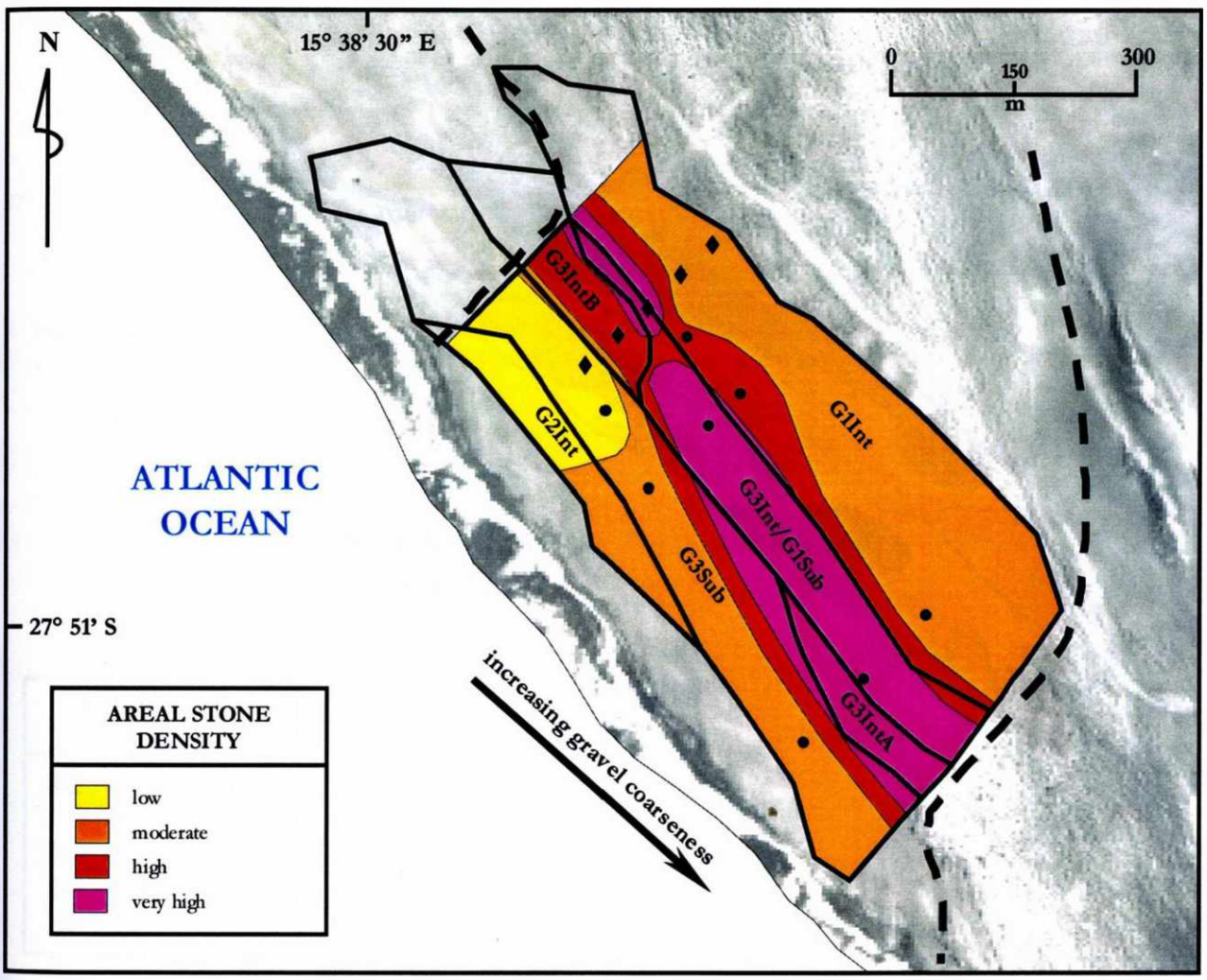

Figure 5.10. The variation in areal stone density at Site 2, as measured by GB50 and Site 2 trench paddock evaluation samples. Subdivisions of the marine gravels are as follows : *G1Int* – intertidal gravels of G1; *G3Int/G1Sub* – intertidal gravels of G3 overlapping subtidal gravels of G1; *G3IntA* and *G3IntB* – intertidal gravels of G3; *G3Sub* – subtidal gravels of G3; *G2Int* – intertidal gravels of G2.

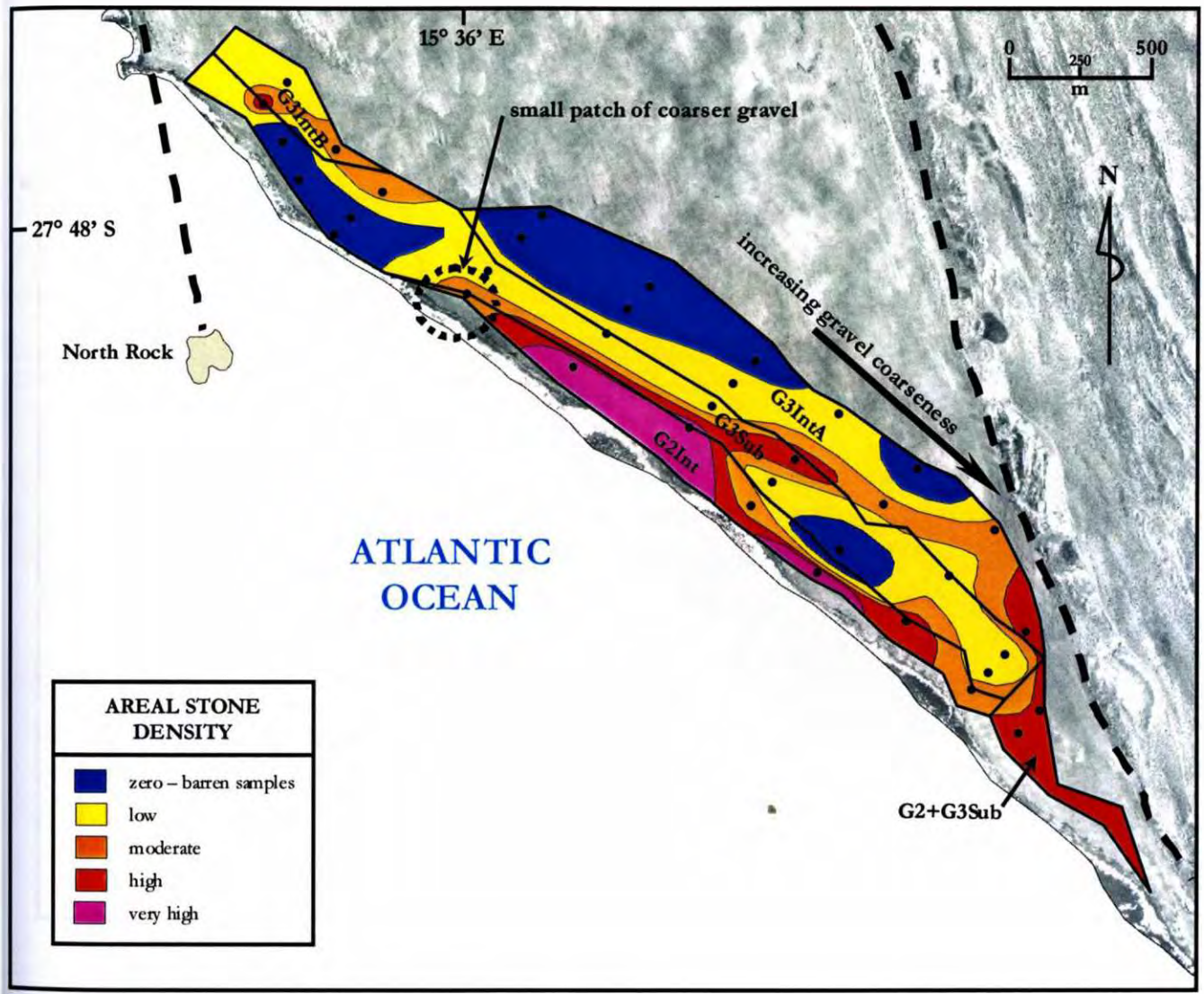

Figure 5.11. The variation in areal stone density at Site 3, as measured by GB50 evaluation samples. Subdivisions of the marine gravels are as follows : *G3IntA* and *G3IntB* – intertidal gravels of G3; *G2+G3* – intertidal and subtidal gravels of G2 and G3 directly adjacent to each other, compressed into a narrow zone; *G3Sub* – subtidal gravels of G3; *G2Int* – intertidal gravels of G2.

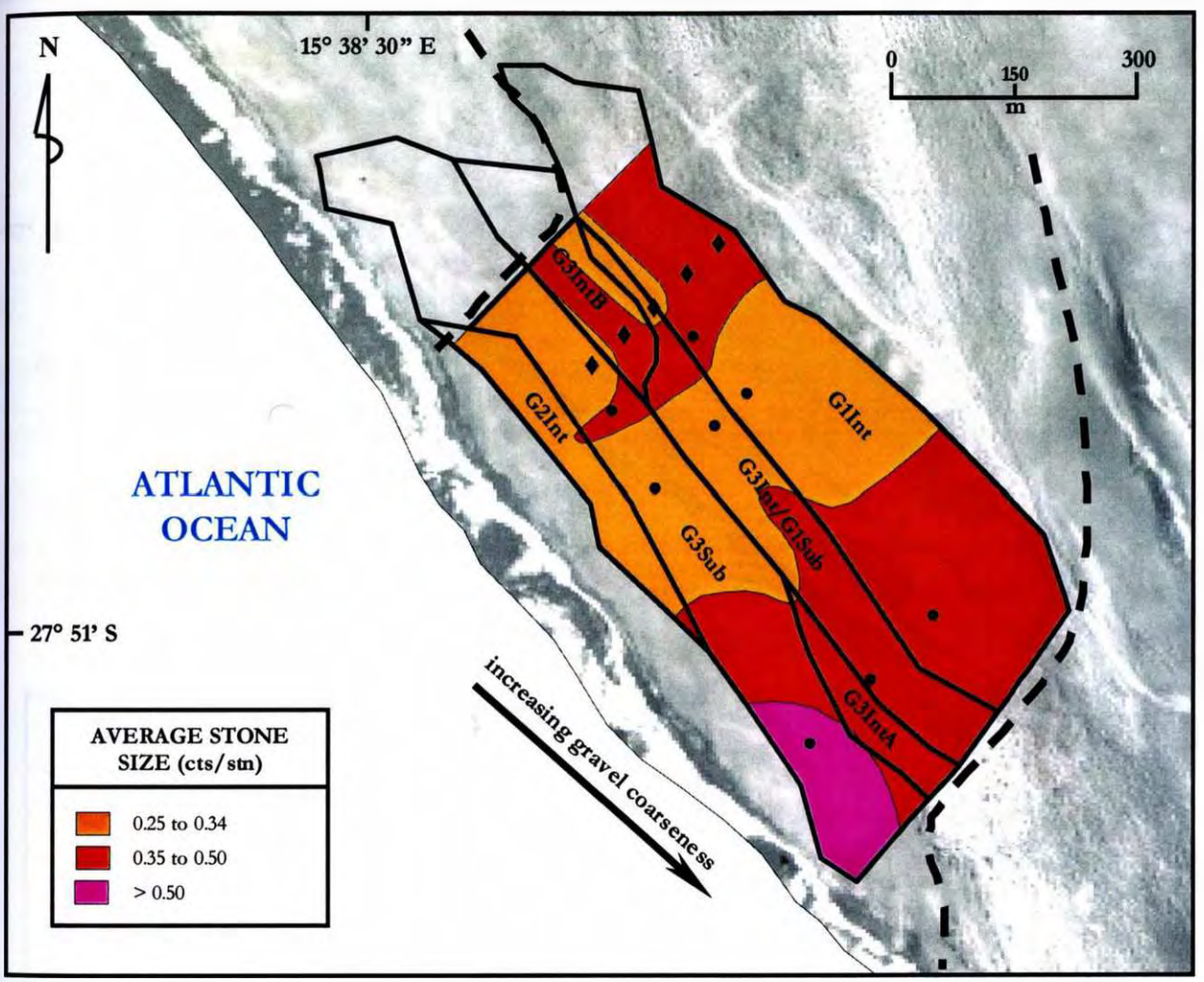

Figure 5.12. The variation in average stone size at Site 2, as measured by GB50 and Site 2 trench paddock evaluation samples. Subdivisions of the marine gravels are as follows : *G1Int* – intertidal gravels of G1; *G3Int/G1Sub* – intertidal gravels of G3 overlapping subtidal gravels of G1; *G3IntA* and *G3IntB* – intertidal gravels of G3; *G3Sub* – subtidal gravels of G3; *G2Int* – intertidal gravels of G2.

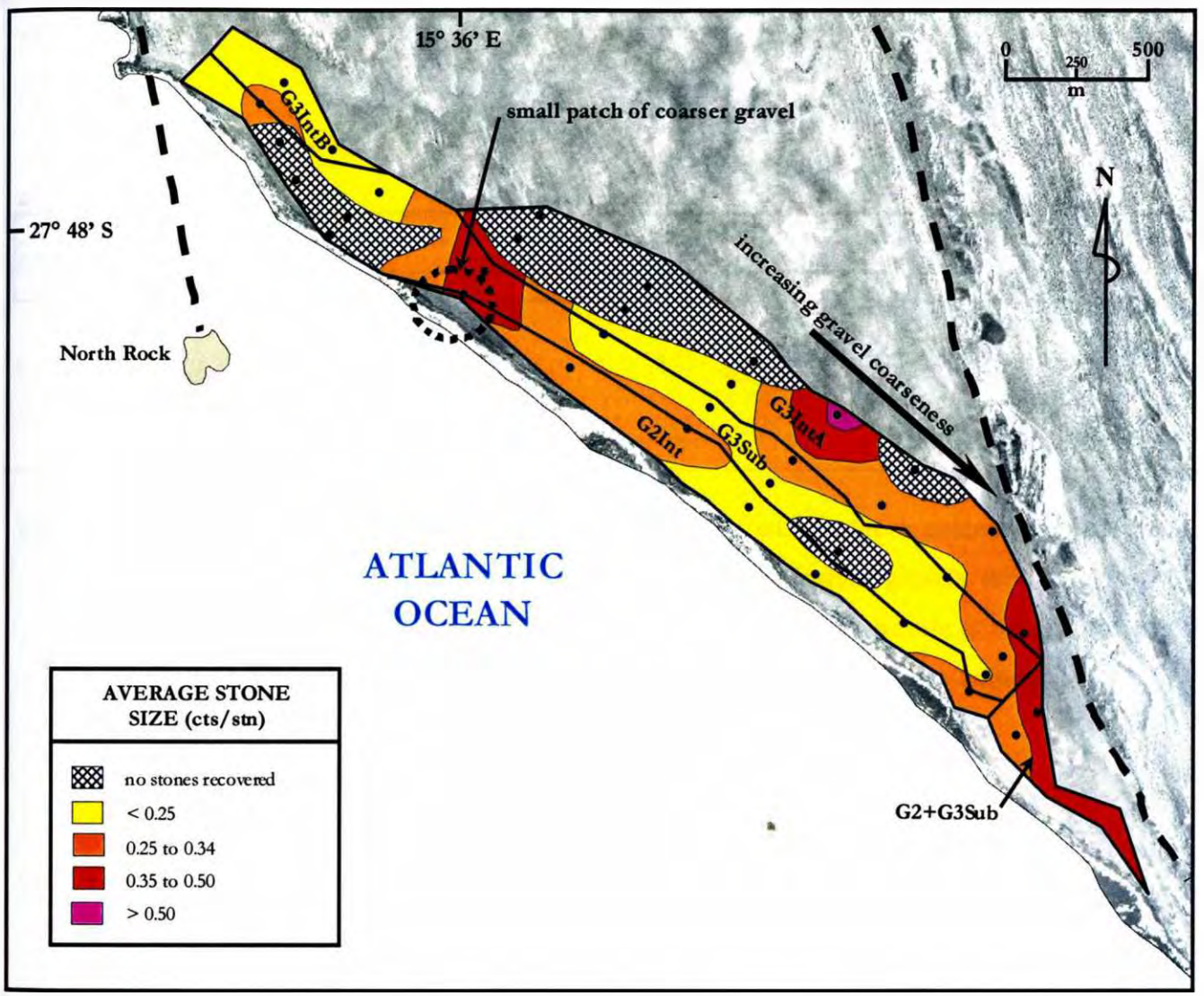

Figure 5.13. The variation in average stone size at Site 3, as measured by GB50 evaluation samples. Geological subdivisions of the marine gravels are as follows : *G3IntA* and *G3IntB* – intertidal gravels of G3; *G2+G3* – intertidal and subtidal gravels of G2 and G3 directly adjacent to each other, compressed into a narrow zone; *G3Sub* – subtidal gravels of G3; *G2Int* – intertidal gravels of G2.

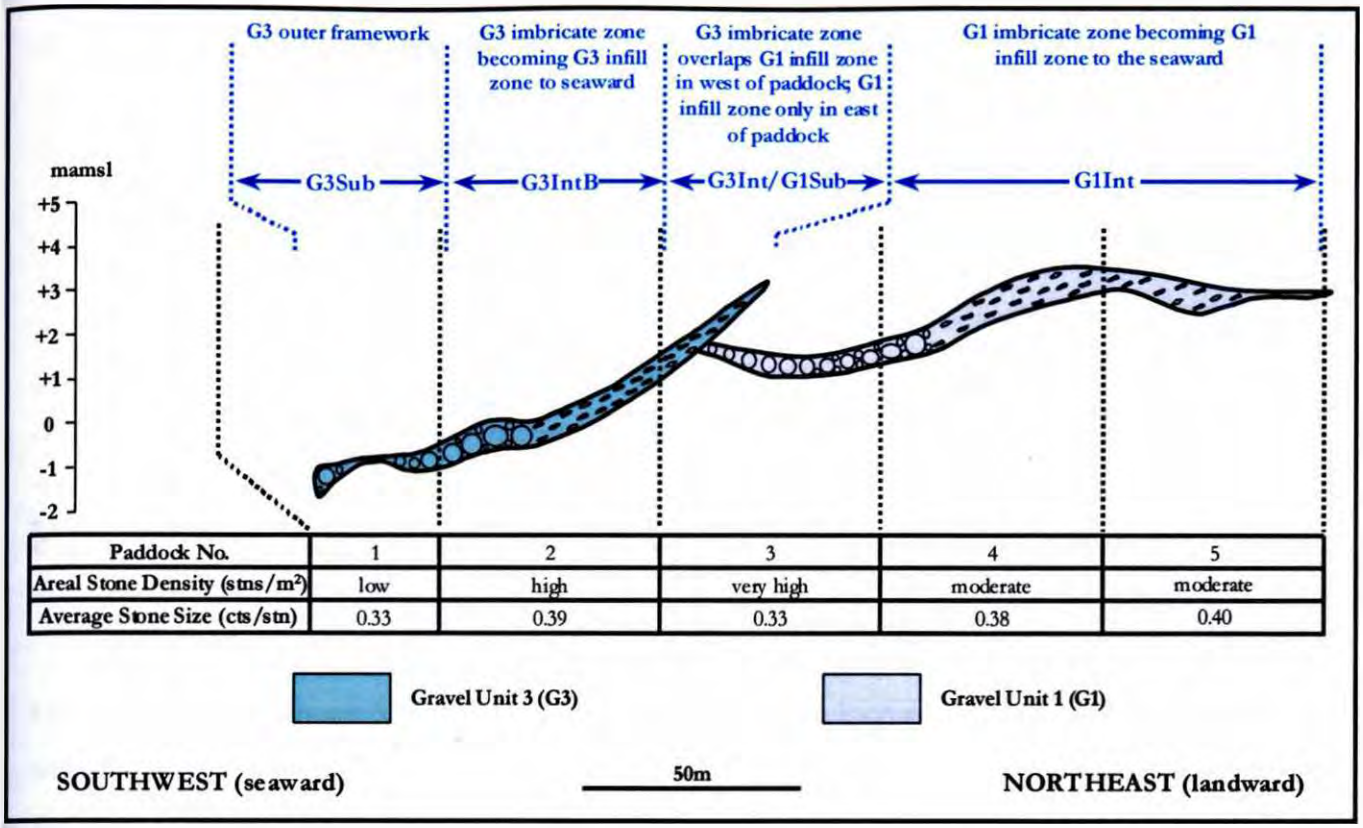

Paddock No.	1	2	3	4	5
Areal Stone Density (stns/m²)	low	high	very high	moderate	moderate
Average Stone Size (cts/stn)	0.33	0.39	0.33	0.38	0.40

Figure 5.14. A cross-section showing the results of the Site 2 trench paddock evaluation samples of the marine gravels at Site 2. Subdivisions of the marine gravels are as follows : *G1Int* – intertidal gravels of G1; *G3Int/G1Sub* – intertidal gravels of G3 overlapping subtidal gravels of G1; *G3IntB* – intertidal gravels of G3; *G3Sub* – subtidal gravels of G3.

5.4 CONTROLS ON STONE DENSITY AND SIZE DISTRIBUTION

5.4.1 Stone Density Distribution at Site 2

Only the south-western two-thirds of the Site 2 marine gravel deposit has been sampled. All of the sampled gravels are underlain by Unit A, which represents an unconsolidated sediment footwall. The marine gravel at Site 2 has high overall areal stone densities (Figure 5.10).

The Site 2 trench data (Figure 5.14) revealed moderate areal stone densities in the imbricate zone of G1 (G1Int - Paddocks 4 and 5). Paddock 3 partly encompasses the infill zone of G1 (G1Int)

and the zone of overlap between G3 and G1 (G3Int/G1Sub); paddock 3 delivered a very high areal stone density. Paddock 2, which encompasses both the imbricate and infill zones of G3 (G3Int), delivered a high areal stone density. Paddock 1, which sampled the outer framework sediments of G3 (G3Sub), delivered a low areal diamond density.

The Site 2 trench sample data demonstrate that areal stone densities vary with a change in geological sub-environment within a single sea level stillstand. This implies that gravel beach depositional processes, which are responsible for the gravel size and shape sorting that defines the various sub-environments (Bluck, 1967; 1999), are also exercising control over the density distribution of diamonds. The highest stone densities are in the infill zone of G1.

The GB50 data at Site 2 are sparse, but nevertheless reveal very high areal stone densities in G3Int/G1Sub (see Figure 5.10). There is also evidence of an increase in stone density towards the seaward edge of G1Int. The very high areal stone densities in G3Int/G1Sub are readily explained by the stacked nature of the gravel units, which result in an addition of the areal stone densities (see geological zones in Figure 5.10). This highlights the important role that spatial relationships between separate beach placers can play in areal stone density distribution. The seaward increase in areal stone density in G1Int indicates higher concentrations of diamonds in the infill zone, a trend that was also noted in the Site 2 trench. The Site 2 trench data and GB50 data collectively demonstrate that the infill zone of G1 has the highest diamond concentrations. Therefore, the beach depositional processes responsible for the accretion of the infill zone appear to be most favourable for the concentration of diamonds. C.D. Hallam (1964) also noted that higher concentrations of diamonds in the gravel beach deposits of MA1 were associated with the beach toe (ie. infill zone).

5.4.2 Stone Density Distribution at Site 3

Site 3 has an overall areal stone density that is lower than Site 2. Individual GB50 samples varied between being barren in certain areas and having returned very high areal stone densities in others (Figure 5.11).

The highest stone densities at Site 3 occur in G2Int, which is composed of relatively fine-grained gravels. There is a clear trend of decreasing stone density in G3IntA from the southeast,

where it abuts the eastern Marmora Valley wall and consists of coarser gravels, towards the northwest (see Figure 5.10). The central, unconfined portion of G3IntA is characterised by very low areal stone densities, with many GB50 samples being barren. By contrast, G3Sub yielded slightly higher stone densities than G3Int through the central portion of Site 3. The northernmost portion of G3Sub, which is sheltered behind the western Marmora Valley wall, displays anomalously low areal stone densities. G2Int+G3Sub represents an area where the +2m subtidal gravels and –5m intertidal gravels are compressed against the south-eastern palaeo-headland, and where gravel coarseness is high; higher areal stone densities were recorded in this zone.

The GB50 sample results from Site 3 demonstrate a link between a change in sea level stillstand and a change in areal stone density. This shows that there is a strong temporal control on stone density distribution and points to a greater availability of diamonds during the deposition of G2 relative to G3. The GB50 results at Site 3 also support the conclusion that stone density varies with a change in the geological sub-environment within each stillstand, as illustrated by the generally higher grades in G3Sub relative to G3Int. This further highlights the control that beach depositional processes can exert over diamond concentration. Coarser gravel beach deposits, which occur directly adjacent to the south-eastern headland, correlate with higher areal stone densities at Site 3, and therefore reflect enhanced concentration of diamonds by increased wave energy. Increased wave energy, however, does not appear to have as strong an influence over stone density distribution as does a change in stillstand. This is borne out by the highest stone densities in G2Int, despite the fact that it is composed of fine-grained gravels.

5.4.3 Size Distribution of Diamonds at Site 2

The average stone size for both the Site 2 trench and Site 2 GB50 samples is 0.36 carats/stone; this is based on 4 814 recovered stones, which is considered representative. The vast majority of the GB50 samples at Site 2 yielded relatively large numbers of stones (often more than 10 stones/sample), making the average stone size calculations representative.

The Site 2 trench reveals higher average stone size in the G1Int subdivision, with decreasing stone size from the imbricate zone towards the infill zone (from 0.40 to 0.33 cts/stn;

see Figure 5.14). Average stone size in G3Int is also higher (0.39 cts/stn), decreasing slightly in G3Sub (0.33 cts/stn).

The GB50 results at Site 2 reveal highest average stone sizes (exceeding 0.50 cts/stn) in the southeast, where the gravel abuts the south-eastern palaeo-headland (see Figure 5.12), and where gravel coarseness is high. The central portion of the marine gravel body is characterised by smaller stones (between 0.25 and 0.35 cts/stn). Towards the north-western end of the sampled area, average stone size increases once more to above 0.35 cts/stn in the proximity of the north-western palaeo-headland. These northwest-to-southeast diamond size variations are common to all of the sea level stillstands/highstands.

The Site 2 trench data demonstrate that there are definite, albeit subtle, variations in stone size with changes in beach subdivision. Intertidal beach gravels host larger stones (0.38 to 0.40 cts/stn) than their subtidal equivalents (0.33 cts/stn; see Figure 5.14). G1Int also displays a trend of diminishing average stone size from the imbricate zone towards the infill zone (0.40 to 0.38 to 0.33 cts/stn for Paddocks 5, 4 and 3 respectively; see Figure 5.14). Beach depositional processes have therefore exerted some control over the size distribution of diamonds. It is noteworthy that the areal stone densities in G1Int, as seen in the Site 2 trench, increase from the imbricate zone towards the infill zone. The evidence therefore shows that the beach depositional processes responsible for increasing stone density in the infill zone of G1Int have also resulted in a diminution of stone size. The GB50 data at Site 2 reveal a strong correlation between increased average stone size and location of the gravel body against the north-western and south-eastern headlands. This is particularly evident at the south-eastern headland, where increased average stone size correlates with increased gravel coarseness, which is, in turn, equated to increased wave energy. It is concluded that wave energy has exercised strong control over diamond size distribution at Site 2, and that the influence of these wave energy variations has been greater than changes in beach depositional process.

5.4.4 Size Distribution of Diamonds at Site 3

The average size of all stones recovered from GB50 samples of marine gravel at Site 3 is 0.29 carats/stone. This figure is based on 210 recovered stones, which is considered representative,

and reflects a significant reduction (~ 20 %) in average stone size relative to Site 2. The reason for this anomalous reduction in overall average stone size is discussed in an upcoming section.

Average stone sizes are relatively low throughout most of G3Sub and G2Int, and in the extreme northwest of the Site 3 gravel body (typically < 0.35 cts/stn; refer to Figure 5.13). There is a strong correlation between increased average stone size (> 0.35 cts/stn) and increased gravel coarseness at the south-eastern headland (in the southeast of G3Int and in G2+G3Int). A second, smaller area of larger-than-average stones exists at the northern end of G2Int and crosses the boundary into G3Sub, also correlating well with increased gravel coarseness.

The GB50 sample data at Site 3 reinforce the conclusion that higher wave energy at the time of deposition, reflected in increased gravel coarseness, results in increased average stone size. It is worth noting that the extreme north-western portion of the Site 3 marine gravel body is not compressed against the north-western headland, but is in fact sheltered behind the offshore extension of the western Marmora Valley wall, where wave energy would have been relatively low at the time of deposition.

5.5 THE LARGE REDUCTION IN AVERAGE STONE SIZE AT SITE 3

5.5.1 Longshore Sorting of Diamonds

It has long been recognised that average diamond size in the marine gravel deposits of the Sperrgebiet gradually decreases northward from the Orange River mouth point source (C.D. Hallam, 1964; Schneider and Miller, 1992; Figure 5.15). This echoes a similar diminution in overall gravel coarseness. This fact is attributed to long term longshore sorting of the diamonds in response to the dominant northerly littoral drift (C.D. Hallam, 1964; Stocken, 1978). Average stone size at Oranjemund is approximately 1.0 carat/stone, dropping to ~0.70 carats/stone at Kerbehuk, ~0.60 carats/stone at Affenrücken and eventually 0.36 carats/stone at Site 2 (C.D. Hallam, 1964; Site 2 – this study). The average stone size of sample diamonds drops from 0.36 cts/stn at Site 2 to 0.29 cts/stn at Site 3, a large reduction of ~ 20 % over just 6 km. While it is certain that longshore

and reflects a significant reduction (~ 20 %) in average stone size relative to Site 2. The reason for this anomalous reduction in overall average stone size is discussed in an upcoming section.

Average stone sizes are relatively low throughout most of G3Sub and G2Int, and in the extreme northwest of the Site 3 gravel body (typically < 0.35 cts/stn; refer to Figure 5.13). There is a strong correlation between increased average stone size (> 0.35 cts/stn) and increased gravel coarseness at the south-eastern headland (in the southeast of G3Int and in G2+G3Int). A second, smaller area of larger-than-average stones exists at the northern end of G2Int and crosses the boundary into G3Sub, also correlating well with increased gravel coarseness.

The GB50 sample data at Site 3 reinforce the conclusion that higher wave energy at the time of deposition, reflected in increased gravel coarseness, results in increased average stone size. It is worth noting that the extreme north-western portion of the Site 3 marine gravel body is not compressed against the north-western headland, but is in fact sheltered behind the offshore extension of the western Marmora Valley wall, where wave energy would have been relatively low at the time of deposition.

5.5 THE LARGE REDUCTION IN AVERAGE STONE SIZE AT SITE 3

5.5.1 Longshore Sorting of Diamonds

It has long been recognised that average diamond size in the marine gravel deposits of the Sperrgebiet gradually decreases northward from the Orange River mouth point source (C.D. Hallam, 1964; Schneider and Miller, 1992; Figure 5.15). This echoes a similar diminution in overall gravel coarseness. This fact is attributed to long term longshore sorting of the diamonds in response to the dominant northerly littoral drift (C.D. Hallam, 1964; Stocken, 1978). Average stone size at Oranjemund is approximately 1.0 carat/stone, dropping to ~0.70 carats/stone at Kerbehuk, ~0.60 carats/stone at Affenrücken and eventually 0.36 carats/stone at Site 2 (C.D. Hallam, 1964; Site 2 – this study). The average stone size of sample diamonds drops from 0.36 cts/stn at Site 2 to 0.29 cts/stn at Site 3, a large reduction of ~ 20 % over just 6 km. While it is certain that longshore

sorting must be partly responsible for this sudden reduction, the unusually large drop in stone size over such a short distance requires further explanation.

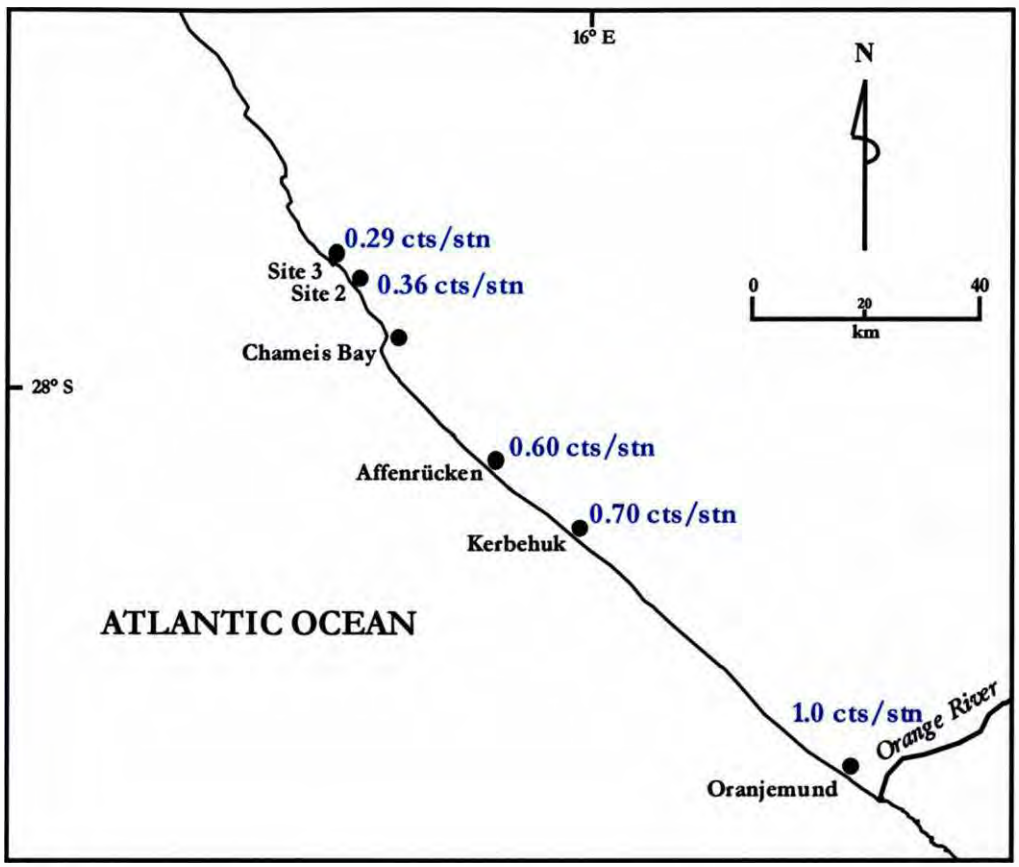

Figure 5.15. The diminution in average stone size northward from the Orange River mouth. The sudden drop in stone size from Site 2 to Site 3, over only 6 km, is, however, difficult to account for by longshore sorting alone. Sources are C.D. Hallam (1964) and stone size data from this study.

5.5.2 Input of Reworked Sediment from the Eocene Marine Succession at Site 3 and Other Possibilities

A remnant gravel terrace, situated at the northern end of Marmora Pan at an elevation of 20 m to 30m above the modern streams, has been identified. This terrace consists of a thin layer of gravel resting on a planed bedrock surface (Figure 5.16). The terrace is currently being reworked into the modern streams, which flow down Marmora Valley and towards the sea. The gravel clast

assemblage of the terrace comprises angular vein quartz, rounded vein quartz, yellow chalcedony, agate and red jasper (see Figure 5.17). The exotic clast assemblage has a signature similar to remnants of the Eocene shoreline (see Chapter 2). The mixture of mature and immature clasts points to a sheetflood origin for the terrace, which is probably a reflection of ephemeral stream activity.

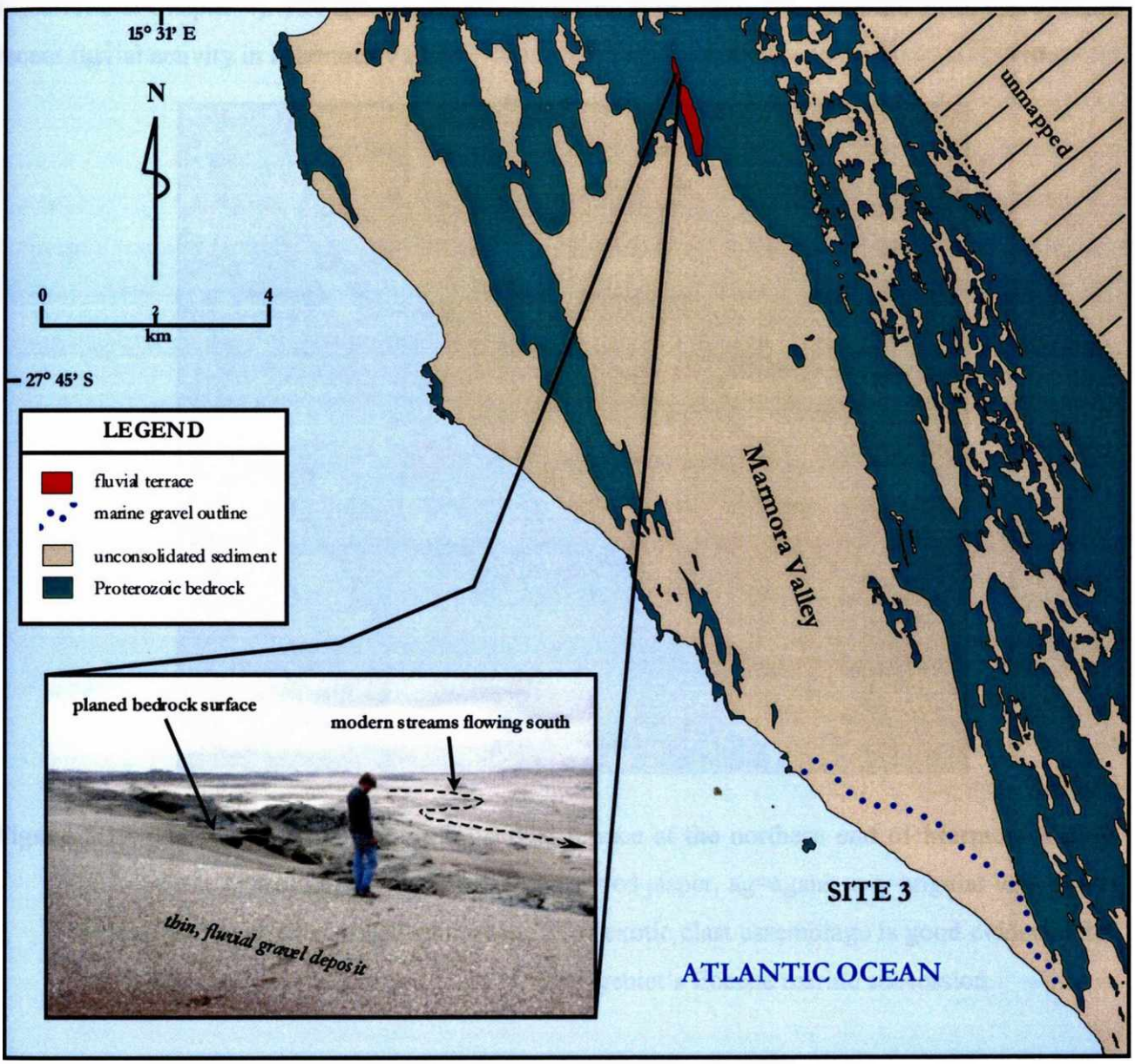

Figure 5.16. The fluvial terrace at the northern end of Marmora Valley. The terrace is raised some 20m above the level of the modern streams. The view in the inset photograph is towards the north.

These streams must have incorporated significant amounts of sediment from the pre-existing, Eocene marine succession. The elevated terrace therefore records an intermediate level of incision for the Marmora Valley, at an earlier time when the Marmora drainage systems had access to Late Eocene marine sediments in the hinterland. Unit B contains similar, diamondiferous sheetflood gravels, which also display an exotic clast assemblage typical of the Eocene marine succession (described in Chapter 4). The sheetflood gravels of Unit B probably represent the distal end of more recent fluvial activity in Marmora Valley.

Figure 5.17. The clast assemblage in the fluvial terrace at the northern end of Marmora Valley. Clast Types: yc=yellow chalcedony, rj=red jasper, ag=agate, avq=angular vein quartz and rvq=well rounded vein quartz. The exotic clast assemblage is good evidence that the exotics were derived from the Sperrgebiet's Eocene marine succession.

There is an association of reworked Eocene sediment and the occurrence of diamonds (Kaiser, 1926; Stocken, 1978; J. Jacob, pers. comm.; see Chapter 2). It is thus reasonable to assume that a certain number of diamonds, derived from the Eocene succession, have entered Marmora Valley. The aforementioned terrace represents the southernmost known occurrence of reworked Eocene marine sediment in the Sperrgebiet. The closest, large-scale historical mining of deflated Eocene sediment was conducted by the Deutsche Diamanten Gesellschaft mbH at Fröhe Hoffnung,

situated some 20 km to the north of the terrace. Oppenheimer and Williams (1914) reported that from 1910 to 1912, diamond production totalled just under 50 000 carats at an average stone size of 0.17 carats/stone. Generally speaking, the average stone size in the deflation deposits decreases northwards from Fröhe Hoffnung (C.D. Hallam, 1964) to an average of less than 0.10 carats/stone at Meob Bay, which is situated 500 km to the north. It is concluded that the diamonds derived from the Eocene succession, which most likely have entered Marmora Valley, had an average size well below that of the marine gravel deposits at Sites 2 and 3. There is no evidence for the similar introduction of reworked Eocene sediment and diamonds at Site 2.

The large drop in stone size at Site 3 could partially be attributed to the introduction of smaller diamonds, which were reworked out of the Eocene succession into Marmora Valley by multi-cyclic fluvial action. These smaller stones might have mixed with a population of larger diamonds, introduced at a later time by the longshore drift, at the seaward end of the valley, thereby producing a reservoir of diamonds with reduced average size. This reservoir of diamonds might then have been reworked from the offshore extension of the Marmora Valley by marine processes, to be incorporated into the marine gravels at Site 3 during the most recent transgression.

While the theory that the Eocene "stepmother" source has contaminated the Site 3 system with smaller diamonds has some supporting evidence, it is not entirely robust for the following reasons :

a) The aforementioned fluvial terrace, with an Eocene exotic signature, has not been proven to contain diamonds, although it is highly likely that it does.
b) It is not certain that the proposed reservoir of diamonds of reduced average size, at the seaward end of Marmora Valley, has in fact remained within the confines of the valley. It might have been mostly flushed out of the seaward end of the valley prior to deposition of the Site 3 gravels, leaving behind a thin lag as evidence of its passing.
c) The size-frequency distributions of diamonds recovered from Sites 2 and 3 during the recent evaluation programme (Table 5.5 and Figure 5.18) indicate that the lower average stone size at Site 3 may be due either to i) a lesser number of large stones, or ii) a greater number of small stones, in the Site 3 sample population, relative to Site 2. It is thus not certain that a population of smaller stones has contaminated the marine gravel deposit at Site 3.

Other possible reasons (these being largely speculative) for the large reduction in average stone size at Site 3 are :

a) The evaluation samples at Site 3 may not be large enough to have recovered a representative amount of the larger, typically more rare, diamonds. However, this seems unlikely, since experience has shown that the total number of stones recovered at Site 3 (210) is representative for the purpose of obtaining an accurate average stone size estimate for most of the Sperrgebiet's diamond placers (personal experience). The size-frequency distributions from Sites 2 and 3 also show a remarkable similarity in shape around the +12 and +13 sieve classes, with both curves revealing a rather unusual inflection point. This suggests that the Site 3 sample population is representative enough to detect trends in the occurrence of the larger stones in the deposit.

b) The fact that the Site 3 pocket beach is much larger than at Site 2 means that there is a smaller proportion of the Site 3 marine gravel body that abuts the headlands. This may mean that, on average, wave energy at Site 3 was lower than for Site 2. Diminished overall wave energy at Site 3, relative to Site 2, may therefore partly account for the observed reduction in average stone size at Site 3.

Table 5.5. Stone size-frequency data from the GB50 and Site 2 trench samples at Sites 2 and 3. The sieve numbers refer to standard round-aperture sieves used in the sorting of diamonds. Higher sieve numbers correspond to larger apertures and therefore larger diamonds.

sieve number	Site 2		Site 3	
	stones	freq %	stones	freq %
+3	0	0.0%	2	1.0%
+5	38	0.8%	5	2.4%
+6	346	7.2%	19	9.0%
+7	690	14.3%	45	21.4%
+9	1,550	32.2%	66	31.4%
+11	1,169	24.3%	51	24.3%
+12	521	10.8%	9	4.3%
+13	356	7.4%	9	4.3%
+15	72	1.5%	1	0.5%
+17	39	0.8%	2	1.0%
+19	25	0.5%	1	0.5%
+21	6	0.1%	0	0.0%
+23	2	0.0%	0	0.0%
Totals :	**4,814**	**100.0%**	**210**	**100.0%**

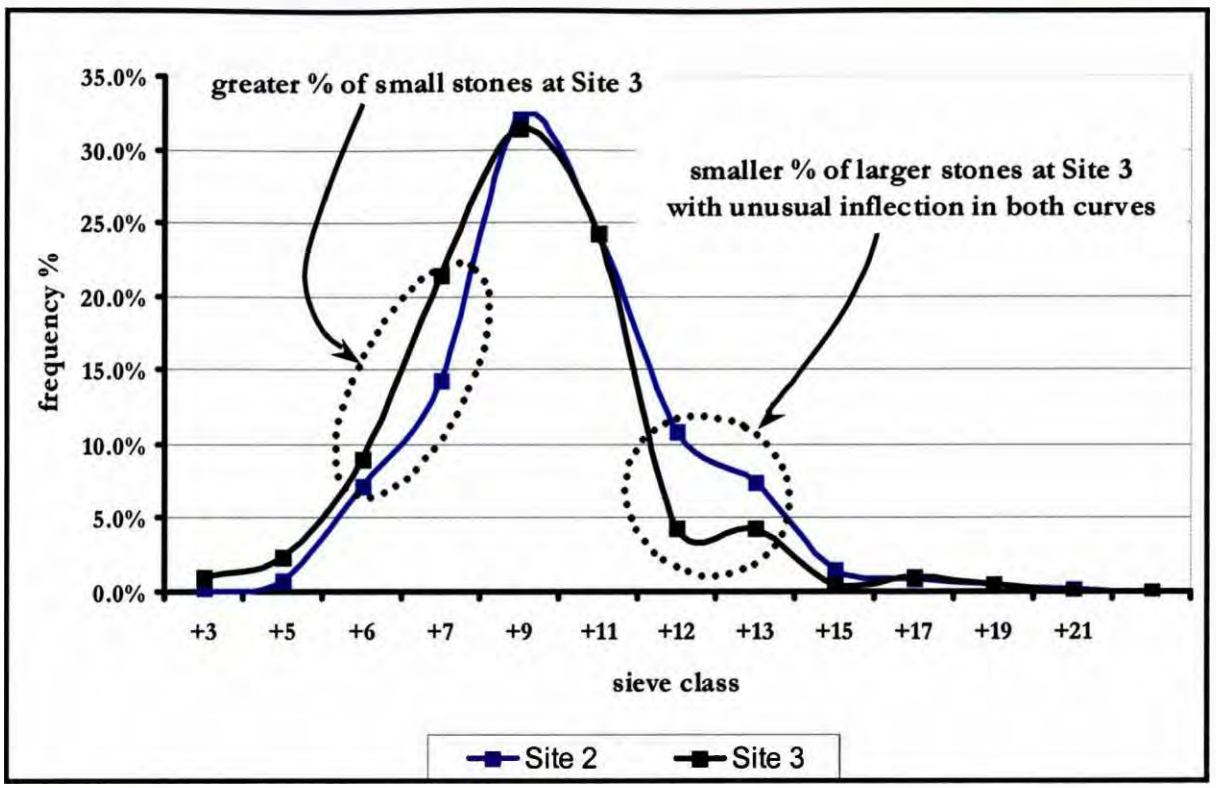

Figure 5.18. Stone size-frequency distribution curves from the GB50 and Site 2 trench samples at Sites 2 and 3. Note that while the modes of the two distributions are similar, the Site 3 population has a greater proportion of small diamonds and smaller proportion of large diamonds than Site 2.

5.6 SUMMARY AND DISCUSSION

The following have been identified as factors which have exercised control over the stone density distribution in the marine gravel deposits at Sites 2 and 3 :

a) *Gravel beach depositional processes*, which are responsible for gravel size and shape sorting, have influenced the stone density distribution. The processes responsible for the formation of the infill zone also favour maximum diamond concentration.

b) The *time of deposition* of a particular gravel beach deposit, indicated by the stillstand/highstand with which it is associated, has been identified as a very strong controlling factor with respect to the density distribution of diamonds. This points to

significant temporal variation in the availability of diamonds in the littoral environment. At Site 3, more diamonds were available when G2 was deposited than when G3 was laid down.

c) *Wave energy at the time of deposition* has played a significant, but subordinate role in determining the stone density distribution. The effect of factors a) and b) above appears to have exerted a stronger influence over the concentration of diamonds.

The following have been identified as controlling factors with respect to the size distribution of diamonds in the marine gravels at Sites 2 and 3 :

a) *Wave energy at the time of deposition* has exerted the strongest influence on the size distribution of stones. Coarser gravels, which are intimately associated with higher average stone sizes, resulted from relatively high wave energy conditions. This greater wave energy was primarily a result of reduced attenuation of waves in narrower shoaling and breaker zones at the palaeo-headlands.

b) *Gravel beach depositional processes* have had some influence on the size distribution of diamonds at Sites 2 and 3. Larger stones have been concentrated in the imbricate zone, while smaller stones are found in the infill zone and subtidal gravels. This is particularly evident in the Site 2 trench, where average stone size gradually diminishes from the imbricate zone towards the infill zone in G1Int and from the intertidal to subtidal subdivisions in G3.

c) The ~ 20% drop in average stone size from Site 2 to Site 3, over only 6 km, is attributed in part to *longshore sorting processes*. Another possible factor has been the *introduction of smaller stones from the Eocene marine succession*, the deflated remains of which are known to host small diamonds. It is also speculated that the *large extent of the Site 3 pocket beach, relative to Site 2,* meant that Site 3 experienced lower average wave energy conditions, resulting in a reduced average stone size.

The observed stone density and size distributions of diamonds in the marine gravel units of Sites 2 and 3 were determined by a multiplicity of factors. These factors have operated at different times and on different scales, superimposing themselves one upon the other to produce the observed mineralisation patterns. From the regional-scale longshore sorting processes, to deposit-scale beach depositional processes, each factor has made its contribution.

CHAPTER 6 – AVERAGE STONE SIZE ESTIMATORS

This chapter narrows the focus still further by considering the estimation of average stone size, using data from Site 3 and a single example from the linear beaches in the south of MA1. Diamond revenue estimates, which are key to the financial evaluation of diamond mining projects, are sensitive to average stone size. As previously mentioned, exact areal stone density measurements cannot be revealed for reasons of confidentiality, and areal stone density estimation is therefore not examined in detail. In order to set the scene, the current estimation method at Site 3, which employed the arithmetic mean estimator for average stone size, is reviewed. This method is typical of the current practice for average stone size estimation in onshore marine deposits of the Sperrgebiet. GB50 sample results from Site 3 and a trench paddock result from the south of MA1 are then used to compare the effectiveness of the arithmetic mean estimator versus lognormal mean estimators for average stone size.

6.1 FROM GEOLOGICAL MODEL TO RESOURCE MODEL AT SITE 3

The pocket beach gravel subdivisions introduced in the previous chapter were used to model the geology of the marine gravels at Sites 2 and 3 prior to knowledge of the mineralisation patterns having been gained through evaluation sampling. Accurate estimation of a diamond resource logically requires the existence of a resource model (otherwise known as a mineralisation model), which faithfully reflects mineralisation patterns. Following identification of the controls on diamond density and size distribution at Site 3, supported by the recognition of similar controls at Site 2, it became obvious that further subdivision of the gravel body was necessary in order to produce an accurate resource model for Site 3. Resource blocks, which reflect zones of homogeneous geology and mineralisation at Site 3, along with explanations as to what they represent, are shown in Figure 6.1. The Site 3 resource blocks are a function of the pre-sampling geological model in conjunction with the additional geological controls on the density and size distributions of the stones (identified post-sampling). The reliable definition of the Site 3 resource blocks would not have been possible without first unravelling the depositional history of the pocket beach gravels, followed by identification of the controls on diamond mineralisation. This highlights the pivotal role that geological understanding plays in alluvial diamond evaluation projects.

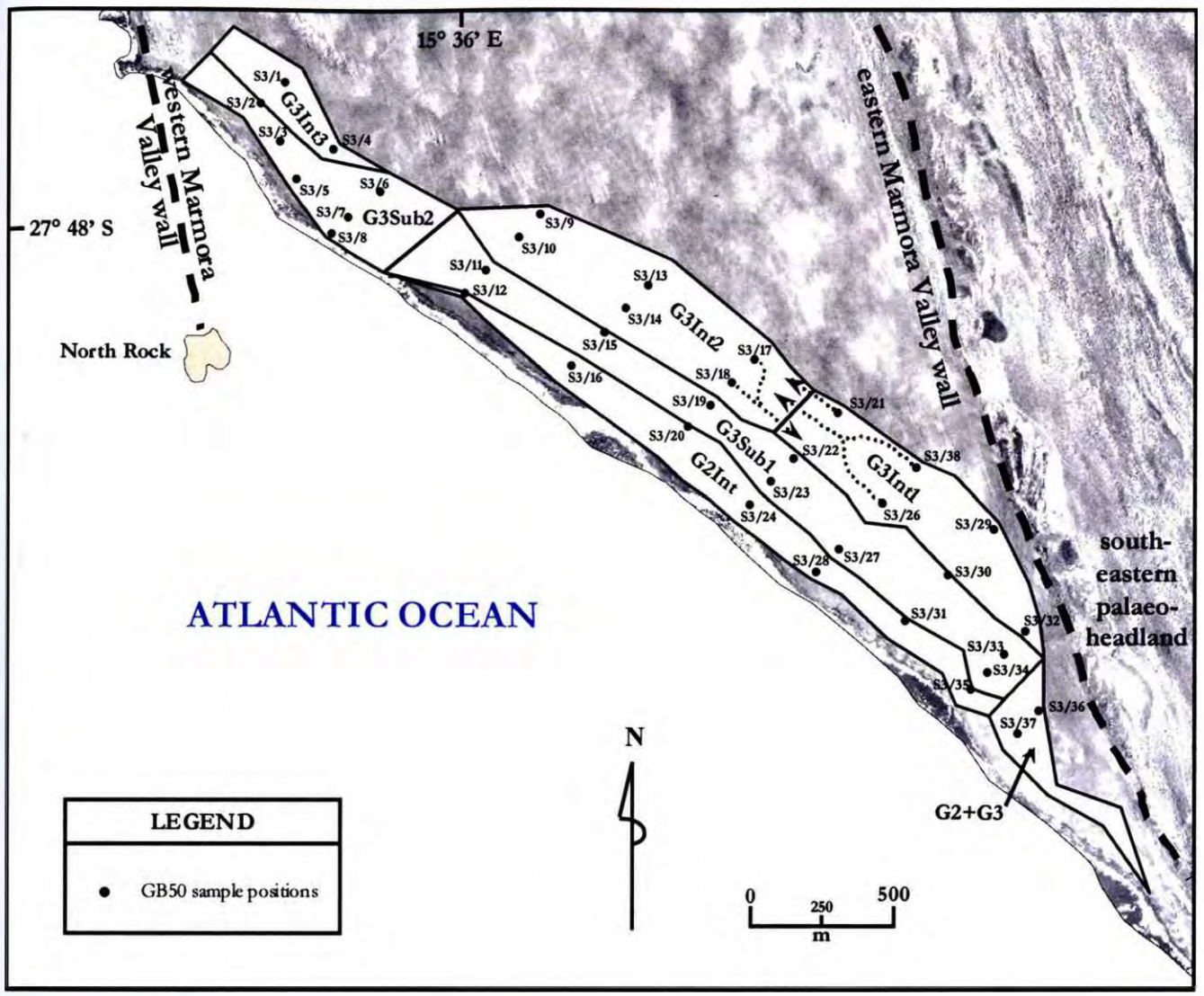

Figure 6.1. The marine gravel resource blocks and positions of GB50 samples at Site 3. Note the overlap of sample sets for G3Int1 and G3Int2 near their common boundary. Explanation of resource blocks : *G2+G3* – zone of high stone density and size at south-eastern headland, with G2 and subtidal gravels of G3 adjacent to each other, compressed into a narrow zone. *G3Int1* – zone of high stone density and size, decreasing towards the north, intertidal gravels of G3. *G3Int2* – zone of low stone density and size, increasing towards boundary with G3Int1, intertidal gravels of G3. *G3Int3* – zone of low-to-moderate stone density and size, intertidal gravels of G3. *G3Sub1* – zone of low-to-moderate stone density and size, subtidal gravels of G3. *G3Sub2* – zone of very low stone density and moderate stone size, subtidal gravels of G3. *G2Int* – zone of very high stone density and low-to-moderate stone size, intertidal gravels of G2.

6.2 CURRENT ESTIMATION METHOD AT SITE 3

The method for average stone size and areal stone density estimation at Site 3 typifies current practice for the gravel beach deposits of the Sperrgebiet. Estimates were made per resource block. GB50 sample results from Site 3 were used to calculate average stone size and average areal stone density. Only GB50 samples falling within a block, or in some instances close to it, were used in the estimation of that block. Selection of the GB50 sample sets to be applied to each resource block was done according to the following rules :

a) The GB50 samples falling within the boundaries of a resource block were included in the sample set for that block.
b) In the case of resource block G3Int1, the first few GB50 samples *to the northwest of its common boundary with* G3Int2 were added to its sample set, and vice-versa for block G3Int2 (see Table 6.1 and Figure 6.1). The common boundary between G3Int1 and G3Int2 is considered to be a gradational or "soft" one, since areal diamond grade and average diamond size gradually diminish towards the north in this part of the marine gravel deposit (see Chapter 5). The overlap of sample sets for these two resource blocks was intended to reflect this gradational change.

Table 6.1. Average stone size estimates for the resource blocks at Site 3, calculated as the arithmetic mean of the weights of the stones recovered in applicable GB50 sample sets.

Resource Block	Applicable GB50 Sample Set	Sum of Stone Weights (cts)	Total Number of Stones (*n*)	Arithmetic Mean Stone Size (cts/stn)
G3Int1	S3/17, S3/18, S3/21, S3/26, S3/29, S3/32, S3/38	8.96	27	0.33
G3Int2	S3/9, S3/10, S3/13, S3/14, S3/17, S3/18, S3/21, S3/26, S3/38	2.68	9	0.30
G3Int3	S3/1, S3/2, S3/4	7.72	27	0.29
G2+G3	S3/36, S3/37	10.05	25	0.40
G3Sub1	S3/11, S3/15, S3/19, S3/22, S3/23, S3/27, S3/30, S3/33, S3/34	10.32	36	0.29
G3Sub2	S3/3, S3/5, S3/6, S3/7, S3/8	1.30	6	0.22
G2Int	S3/12, S3/16, S3/20, S3/24, S3/28, S3/31, S3/35	24.63	93	0.26

An average stone size, measured in cts/stn, for each resource block, was calculated as the arithmetic mean of the weights of the diamonds recovered in its applicable GB50 sample set. The arithmetic mean ($\bar{a}$) is defined as follows :

$$\bar{a} = (\sum_{i=1}^{n} x_i) / n \qquad [1]$$

Where x_i is the i^{th} sample value, or in this case the weight of the i^{th} diamond in the sample set; n is the number of sample values, or in this case the number of diamonds in the sample set. The results of these calculations are summarised in Table 6.1.

Average areal stone density for each resource block, measured in stns/m^2, was calculated as the *sum of recovered stones in the applicable GB50 sample set / sum of the areas of the GB50 samples in that sample set.* By multiplying the average areal stone density for a resource block by the total area of that block, an estimate of the total number of stones in the block was calculated. Since areal stone density measurements are confidential, the results of stone density estimates cannot be considered in this study, and further discussion is limited to methods of estimating average stone size.

6.3 STATEMENT OF THE PROBLEM

As previously discussed, Oosterveld *et al.* (1987) tested Sichel's (1972) method for estimating average stone density in the gravel beaches of MA1 (Chapter 1). They did not, however, present the results of their average stone size estimates. As previously mentioned, the revenue generated by mining a diamondiferous deposit is sensitive to the average stone size of the recovered diamonds. Therefore, in order to assess accurately the financial viability of a diamond-mining project, the best possible estimate of average stone size needs to be obtained. The advantage of the arithmetic mean estimator (AME) is that it is quick and easy to apply. Disadvantages include :

a) The lack of a method to calculate confidence limits for the estimated mean.
b) A tendency to overestimate the mean of the true population in the instance where the sample frequency distribution curve has a long "tail", or, in other words, where the sample population contains large outlier values (David, 1977; Storrar, 1987; see Figure 6.2). This is

particularly true when there are few sample values available (ie. when there are few stones recovered), and the arithmetic mean lends too much weight to the possible occurrence of a single, large sample value.

Krige (1962), Sichel (1947, 1952; 1966) and others noted that sample values from ore deposits often follow the lognormal distribution, which is typified by a long tail resulting from the presence of large outliers. Sichel (1972), by studying sample results from the marine gravel deposit on MA1, concluded that the sample diamond size-frequency distribution within geologically homogeneous

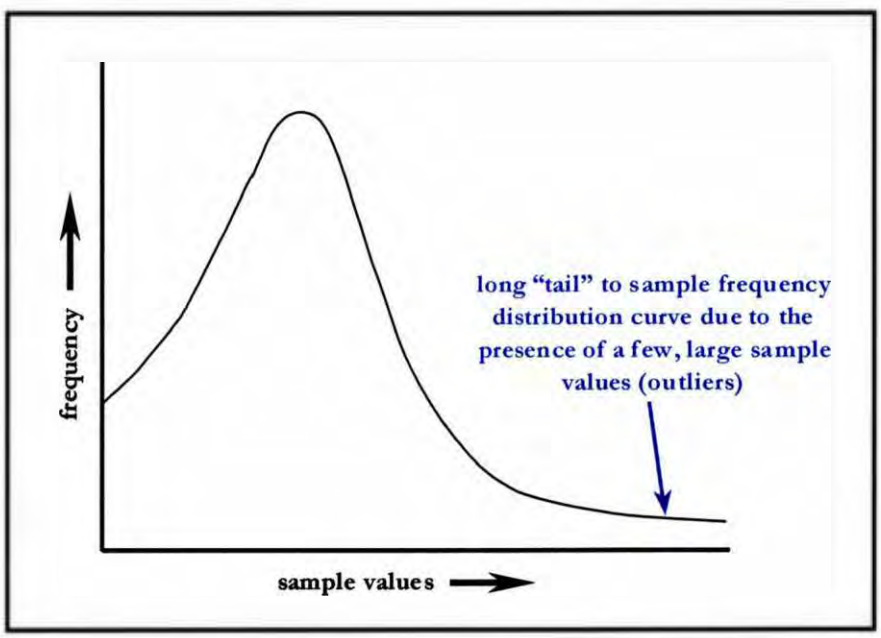

Figure 6.2. A sketch showing the shape of a sample frequency distribution curve in the case where there are a few, large sample values. The arithmetic mean estimator sometimes tends to overestimate the mean of the true population in such instances.

zones is also best modeled by a two-parameter lognormal distribution. Lognormal mean estimators (LME's) for a two-parameter lognormal distribution, which differ from the AME, do exist, and these, at least theoretically, are better equipped to deal with large outlier values in the sample population (Sichel, 1972; David, 1977). Sichel's T estimator, a LME that caters particularly for lognormally distributed sample populations with less than 50 values, also provides for the calculation of confidence limits (Sichel, 1966; Clark, 1987; Table 6.2). This study sets out to answer the following questions with regard to average stone size estimation :

a) Does diamond size follow a two-parameter lognormal distribution within geologically homogeneous zones (equivalent to resource blocks) of the marine gravel deposit at pocket beach Site 3, thus validating the use of LME's?

b) If the answer to a) is yes, what are the practical implications of using LME's instead of the AME for the kinds of two-parameter lognormal distributions which typify sample diamond size-frequency distributions at Site 3?

c) Under what conditions would one or the other type of estimator be more effective, both at Site 3 and in other gravel beach deposits of the Sperrgebiet?

c) What recommendations, if any, could one make regarding estimation of average stone size for the marine gravel deposits of the Sperrgebiet in the future?

Table 6.2. An example of two slightly different sample sets (n = 10), with sample values lognormally-distributed, drawn from the same theoretical lognormal distribution, having a true mean of 1.70. The sample values fall within the range one would expect for stones from a gravel beach deposit in the Sperrgebiet. Sample population 1 contains an extreme outlier, while Population 2 does not (blue numbers). Note that the arithmetic mean estimate for the sample set on the left is far too high.

	Population 1	Population 2
individual stone weights	0.317	0.317
	0.320	0.320
	0.400	0.400
	1.498	1.498
	0.895	0.895
	1.846	1.846
	0.163	0.163
	1.059	1.059
	1.603	1.603
	17.835	4.013
Sichel T mean estimate	**1.954**	**1.237**
Arithmetic mean estimate	**2.594**	**1.211**

6.4 TEST OF LOGNORMALITY AND LOGNORMAL MEAN ESTIMATORS

A quick and simple test of lognormality is to plot the cumulative frequency distribution of a sample population on log-probability graph paper. Sample populations, which follow a two-parameter lognormal distribution, will plot as a straight line (David, 1977; Storrar, 1987). The cumulative frequency distributions for diamond size in each of the Site 3 resource blocks, using the same applicable sample sets outlined in Chapter 6.2, were plotted on log-probability graph paper (see Appendix I and Table 6.3). It was found that the cumulative frequency distribution plots approximated straight lines, and that the sample populations within each resource block were therefore lognormally distributed with respect to diamond size. This validated the use of LME's for average diamond size at Site 3, and confirmed the soundness of the resource block definition.

The parameters that describe a lognormal distribution are the median, denoted here by m_e, and the logarithmic standard deviation, denoted here by σ (Evans *et al.*, 2000). Greater values of σ mean that the distribution has a longer "tail" and therefore has a greater chance of containing extreme outlier values. Theoretically, the mean of a lognormal population, denoted by μ, is best calculated using the following equation (Sichel, 1952; David, 1977) :

$$\mu = m_e \cdot e^{\sigma^2/2} \qquad [2]$$

if we rearrange, then :

$$m_e = \mu / e^{\sigma^2/2} \qquad [3]$$

also,

$$m_e = e^{\xi} \qquad [4]$$

Where ξ = arithmetic mean of the natural logarithms of the sample values

so, by substituting,

$$\mu = e^{\xi} \cdot e^{\sigma^2/2} = e^{\xi+\sigma^2/2} \qquad [5]$$

Table 6.3. Size-frequency distribution data for diamonds recovered in the GB50 sample sets, per resource block, at Site 3. The upper critical size for each sieve class is the average weight of a diamond which will just pass through the sieve defining the next class up. For example, the upper critical size of the +6 sieve class is 0.13 cts/stn; a diamond of 0.13 cts/stn will, on average, just pass through the +7 sieve. These critical sizes have been determined experimentally (Robinson, 1979), using many stones from different sources, and are necessary for plotting cumulative frequency distributions on log-probability graph paper. The critical sizes are largely dependent upon diamond shape, which may vary slightly from area to area, therefore adding a degree of uncertainty to the class interval boundaries of the cumulative frequency distributions.

standard sieve	upper critical size (cts/stn)	G3Int1		G3Int2		G3Int3		G2+G3		G3Sub1		G3Sub2		G2Int	
		freq.	cum. freq. %	freq.	cum. freq. %	freq.	cum. freq. %	freq.	cum. freq. %	freq.	cum. freq. %	freq.	cum. freq. %	freq.	cum. freq. %
+3	0.05													2	2.2%
+5	0.08	1	3.7%											4	6.5%
+6	0.12	2	11.1%	1	11.1%	1	3.7%			2	5.6%	1	16.7%	15	22.6%
+7	0.17	3	22.2%	2	33.3%	9	37.0%	4	16.0%	7	25.0%	4	83.3%	19	43.0%
+9	0.32	8	51.9%	3	66.7%	7	63.0%	9	52.0%	17	72.2%	0	83.3%	25	69.9%
+11	0.50	9	85.2%	2	88.9%	8	92.6%	8	84.0%	7	91.7%	0	83.3%	20	91.4%
+12	0.70	1	88.9%	1	100.0%	1	96.3%	2	92.0%	0	91.7%	1	100.0%	4	95.7%
+13	1.20	2	96.3%			1	100.0%	1	96.0%	3	100.0%			2	97.8%
+15	1.50	0	96.3%					0	96.0%					1	98.9%
+17	1.90	1	100.0%					1	100.0%					0	98.9%
+19	3.90													1	100.0%
	Totals :	27		9		27		25		36		6		93	

Since m_e can be derived from μ and σ, a lognormal distribution can also be described by the parameters μ and σ. The logarithmic variance, σ^2, is often used to describe the distribution instead of σ. Clark (1987) defines σ with the following equation :

$$\sigma = [(\sum_{i=1}^{n} (\ln(x_i))^2) / n] - [(\sum_{i=1}^{n} \ln(x_i)) / n]^2 \qquad [6]$$

The relationships in equations [2], [3] and [5] are best applied to sample populations where $n > 50$ in order to derive an estimate for the mean (Clark, 1987). When $n \leq 50$, the Sichel T mean estimator, as outlined by Sichel (1952; 1966) and Clark (1987), should be applied. The Sichel T estimator requires, as input, the values of m_e and σ^2. A graphical method (David, 1977), which uses the log-probability plots of the distributions, also exists for the estimation of m_e and σ; this method is detailed in Appendix II. The graphical calculation of m_e, σ and μ or Sichel T, for the diamond size distributions from the Site 3 resource subdivisions, are shown on the log-probability plots in Appendix I and summarised in Table 6.4.

Table 6.4. The values of μ ($n > 50$) , Sichel T ($n \leq 50$) and σ^2, as determined by the graphical method. The values of ā are the same as those in Table 6.1.

Resource Block	*n*	μ or Sichel T	ā	σ^2
G3Int1	27	0.26	0.33	0.36
G3Int2	9	0.22	0.30	0.37
G3Int3	27	0.21	0.29	0.32
G2+G3	25	0.27	0.40	0.39
G3Sub1	36	0.23	0.29	0.26
G3Sub2	6	0.12	0.22	0.04
G2Int	93	0.21	0.26	0.42

A significant problem arose in that *individual stone weights were not routinely recorded during the sorting of prospecting samples at Site 3*, mainly because of time constraints. The stones recovered in a sample were instead sized using a set of standard sieves. The total number of stones,

as well as their total weight, were reported per sieve class (see Table 6.3). This, therefore, made it impossible to numerically calculate lognormal mean estimates, since m_e and σ had to be determined graphically. The graphical method introduces bias, mainly because of the subjectivity of fitting a line to the data, and uncertainties associated with the critical sizes of the class intervals. However, this reporting practice does not affect the precision of arithmetic mean estimates, which rely only on knowing the total weight of the stones, in carats, and the total number of stones recovered (n).

6.5 A SIMULATION-BASED COMPARISON: ARITHMETIC MEAN ESTIMATORS VS LOGNORMAL MEAN ESTIMATORS

6.5.1 Selection of Lognormal Parameters for Simulation

Comparing the results of the arithmetic mean estimates to the lognormal mean estimates (Table 6.4) at Site 3 presented problems, because of the inherent imprecision of the graphical method. The data sets were also not considered to be large enough to draw meaningful conclusions. It was therefore decided to take a theoretical approach, based on realistic data, to comparing the AME to the LME's for this site and elsewhere. This approach involved the use of simulated sample campaigns, where individual stones were randomly drawn from lognormal diamond populations. In order to mirror reality as closely as possible, it was first necessary to determine *which sorts of lognormal parameter values best described the range of diamond size-frequency distributions found at Site 3*. A plot of μ and Sichel T vs σ^2 values, as well as $\bar{a}$ vs σ^2, calculated for the Site 3 resource blocks by the graphical method and equation [1], is shown in Figure 6.3; data are drawn from Table 6.4. The vast majority of values for Sichel T, μ and $\bar{a}$ fall between 0.20 cts/stn and 0.40 cts/stn. The majority of values for σ^2 fall between, or close to, the range of 0.15 to 0.45. It was therefore decided to simulate sample campaigns on two-parameter, lognormal, diamond size-frequency distributions having μ = 0.20 cts/stn, 0.30 cts/stn and 0.40 cts/stn; σ^2 would similarly be varied between the values 0.15, 0.30 and 0.45. In order to gain some perspective on the overall effectiveness of the two types of estimators, it was decided to include an extreme case from another geologically homogeneous zone of a Sperrgebiet marine gravel placer. A lognormally distributed diamond population was thus drawn from a sample paddock in the linear beach deposits from the south of MA1, having μ = 1.70 cts/stn and σ^2 = 1.00. This made for a total of ten different lognormal diamond size-

frequency distributions, nine of which typify the kinds of size-frequency distributions found at Site 3, and one that represents an extreme case for the Sperrgebiet coastline. Ten suitably constructed sample campaign simulations would thus be required.

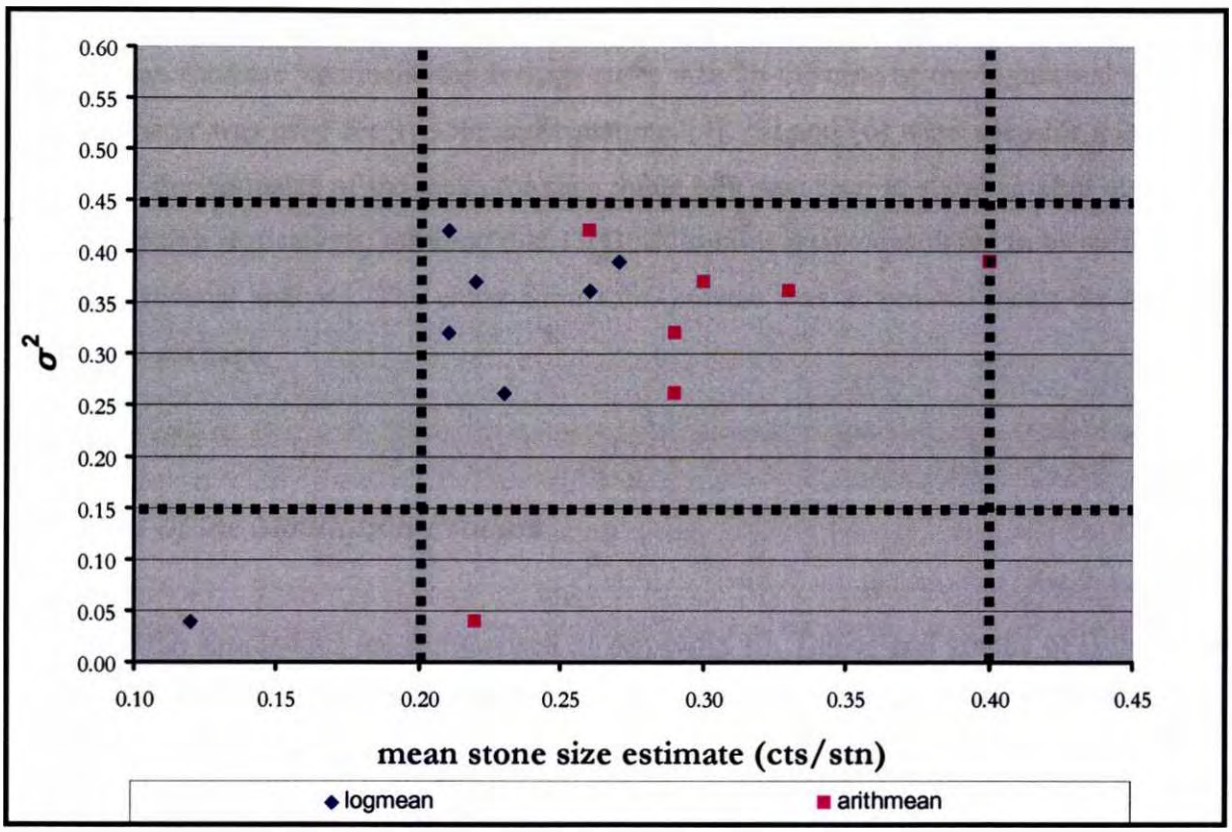

Figure 6.3. A plot of the data from Table 6.4, showing the spread of distribution parameters and mean estimates for the GB50 sample sets at Site 3.

6.5.2 The Simulation Method

The equation for extracting a random sample value (x_r) from a theoretical, two-parameter lognormal distribution is as follows (Evans *et al.*, 2000) :

$$x_r = e^{[\sigma \cdot \sqrt{-2 \cdot \ln(r_1)} \cdot \sin(2 \cdot \pi \cdot r_2) + \ln(m_e)]} \qquad [7]$$

Where r_1 and r_2 are two random numbers with values between 0 and 1.

With the values of μ and σ^2 now set for each of the ten simulations, m_e and σ were easily derived, enabling the use of equation [7] to randomly sample the ten theoretical diamond size distributions. The number of stones recovered (ie. number of sample values generated) in the sampling campaigns, for each of the ten distributions, was varied between $n = 5$ and $n = 500$. The sampling campaigns were realised 1500 times for each value of n in order to produce a significant data set of possible outcomes (see Figure 6.4). For each sample campaign realisation, an arithmetic mean and lognormal mean estimate was made for average stone size. In the case of the lognormal mean, the Sichel T estimator was used for $n \leq 50$, and equations [4], [5] and [6] were used for $n > 50$. The distribution of the estimates of the mean for each value of n was seen to stabilise after about 1000 sampling campaign realisations, meaning that 1500 realisations were considered to be sufficient for meaningful statistical analysis. The entire simulation process was automated using the Microsoft Excel software package.

6.5.3 Results of the Simulation Process

The results of the simulations are summarised in Appendix III. Tables and graphs of i) the 5^{th} and 95^{th} percentile values (ie. 90% central tendency limits) and ii) the median, or 50^{th} percentile values, of the distributions of the mean estimates are shown.

6.6 DISCUSSION OF THE SIMULATION RESULTS

The distributions of the mean estimates display the following general characteristics :

a) The medians of the distributions fall below the actual mean of the population at lower values of n and stabilise close to the actual mean at higher values of n.
b) As σ^2 increases, the medians of the distributions are further removed from the actual mean, and require higher values of n to stabilise close to the actual mean.
c) The 90% central tendency limits and median are insensitive to changes in μ.

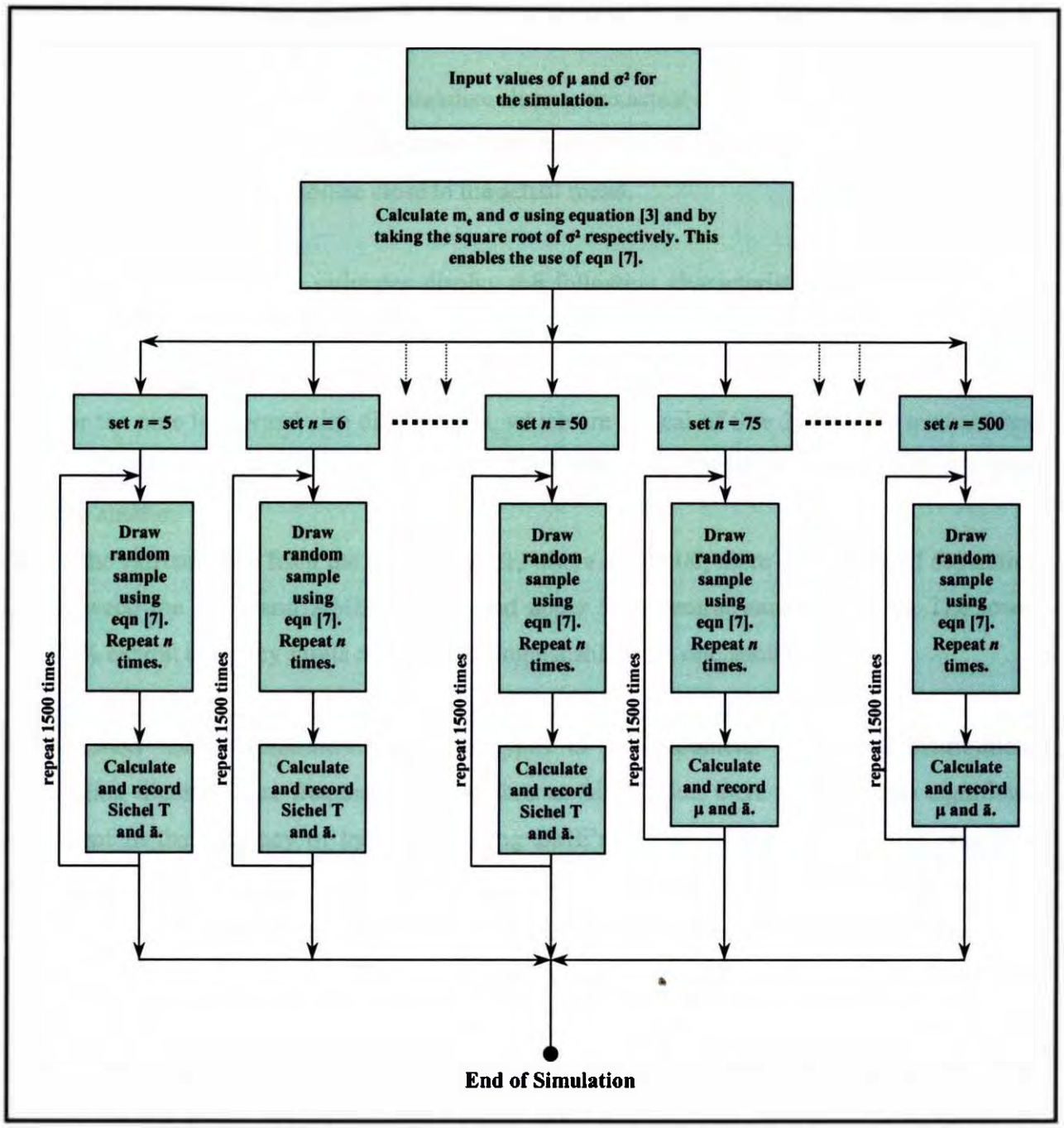

Figure 6.4. A simple flow diagram showing the simulation method employed in this study.

d) The 90% central tendency limits of the distributions are asymmetrical about the actual mean, defining trumpet-shaped curves, and become increasingly more asymmetrical as σ^2 increases. The asymmetry decreases with increasing n, but takes longer to do so as σ^2 increases. The upper 90% central tendency limit is always further away from the actual mean than the lower 90% central tendency limit. This means, that in the case where the

mean is overestimated, the degree of error is likely to be greater than in the case where the mean is underestimated.

e) The 90% central tendency limits stabilise close to the actual mean at higher values of n.

f) As σ^2 increases, the 90% central tendency limits of the distributions widen and require higher values of n to stabilise close to the actual mean.

The distributions of the mean estimates display the following characteristics with respect to the LME's and AME :

a) For the nine lognormal size distributions, which are typical of Site 3, both the medians and 90% central tendency limits of the LME's and AME are practically indistinguishable from one another.

b) In the extreme case from the south of MA1, where $\sigma^2 = 1.00$, there is a degree of separation between the LME and AME medians and upper 90% central tendency limits. The lower 90% central tendency limits remain indistinguishable from one another.

The simulation results demonstrate, for the types of two-parameter lognormal distributions approximating diamond size-frequency distributions at Site 3, that there would be no significant improvement in the accuracy of the results using LME's instead of the AME at this site. It is evident that the key parameter to consider is the variance of the sample population (σ^2), since the results are insensitive to μ. The value of σ^2 is not large enough at Site 3, even when n is small, to create a significant degree of separation between the 90% central tendency limits of the AME and LME's. However, when one encounters an extreme case, like the one from the south of MA1 ($\sigma^2 = 1.00$), the accuracy of mean estimates can be improved significantly by using LME's. In the instance where n is small, and a large outlier stone exists in the sample population (ie. σ^2 is large), LME's should always take preference over the AME, even if individual weights were not recorded for each of the stones. Such a case is unlikely at Site 3, because of the low value of σ^2 at this locality, but may occur elsewhere (eg. the extreme case from MA1).

Considering the additional uncertainty involved in using LME's to estimate average stone size at Site 3, mainly because of the need to use the graphical method, it would be more practical to stay with the AME in this particular case. However, if individual stone weights were to be recorded during prospecting, making possible the numerical solution methods for LME's, then LME's become the method of choice, because this allows for the calculation of confidence limits. The

calculation of confidence limits for resource estimates is becoming increasingly more important as financial institutions are insisting on better quantification of the risks involved in mineral projects. It is therefore recommended that, in future, individual stone weights be recorded as a matter of routine and that LME's be employed for lognormally-distributed stone populations.

CHAPTER 7 – CONCLUSIONS

7.1 DEPOSITIONAL HISTORY

a) The pocket beach sediments at Sites 2 and 3 record a period of ephemeral stream deposition prior to ca. 130 000 BP, during a time of relatively low sea level.

b) The ephemeral stream deposition was succeeded by a transgressive phase, which culminated in the deposition of a gravel beach sequence, representing a sea level highstand of +4 mamsl, between 120 000 to 130 000 BP.

c) The ensuing sea level drop to the Last Glacial Maximum resulted in the subaerial exposure of the +4 mamsl gravel beach sequence and triggered the deflation of pre-existing pocket beach valley fills, both by aeolian and fluvial processes, to the bedrock valley floors. The aforementioned +4m gravel beach was only preserved where it rested on a resistant footwall.

d) The bedrock floor of Marmora Valley was flooded at ca. 9 000 BP, during the latter stages of the transgression that followed the Last Glacial Maximum. A variegated sequence was deposited in the Marmora Valley between ca. 9 000 BP and ca. 5 000 BP and consists of :

i) pan/coastal sabkha sediments,
ii) shallow, sheltered bay sediments, and
iii) sediments typical of back-barrier lagoonal settings.

e) Two gravel beach sequences were deposited contemporaneously with this variegated sequence, and form part of the most recent transgressive wedge. The older of these gravel beaches records a sea level stillstand at –5 mamsl, which occurred between 7 600 BP and 5 600 BP. The younger gravel beach represents a sea level highstand, which reached an elevation of +2 to +3 mamsl at ca. 5 000 BP, coinciding with the well known Middle Holocene high recorded from around the southern African coastline and elsewhere.

f) The +2 to +3 mamsl highstand was followed by a minor regression to the current sea level, which was embodied by progradation of the beach to its current position. This progradational beach sequence is composed mainly of sand and grit, reflecting the paucity of gravel supply to this part of the coastline in the most recent past.

g) The modern coastal dunes cap the pocket beach sequence and form the youngest sediments in the study area.

7.2 CONTROLS ON THE DENSITY AND SIZE DISTRIBUTION OF DIAMONDS

The following were identified as factors controlling the density distribution of diamonds in the marine gravel deposits of pocket beach Sites 2 and 3 :

a) Gravel beach depositional processes, which sort clasts by size and shape on a gravel beach, have also exercised control over the stone density distribution. The processes that formed the infill zone favour maximum diamond concentration.
b) The time of deposition of the host gravel beach has strongly controlled the density distribution of diamonds. A significant temporal variation in the availability of diamonds in the littoral environment is therefore evident.
c) Wave energy has played a limited role in determining the stone density distribution. Gravel beach depositional processes and the time of deposition have had greater influence over the concentration of diamonds.

The following have been identified as controlling factors with respect to the size distribution of diamonds in the marine gravels at Sites 2 and 3 :

a) Wave energy has exerted the strongest influence over the size distribution of diamonds. Larger diamonds are intimately associated with coarser gravels, which are a reflection of relatively high wave energy conditions. Greater wave energy at the palaeo-headlands of the pocket beaches was a consequence of reduced attenuation of waves in narrower shoaling and breaker zones.
b) Gravel beach depositional processes have exercised some control over the size distribution of diamonds in the pocket beach gravels. The largest stones occur in the imbricate zone, with the size decreasing seaward to the subtidal gravels, where the smallest stones were recovered.

c) Longshore sorting processes, which are known to have played a role in the diminution of average stones size northwards from the Orange River mouth, have had an effect on the size distribution of diamonds, partly accounting for the drop in stone size from Site 2 to Site 3.

d) Input of reworked sediment and diamonds from the Eocene marine succession, the deflated remains of which host small diamonds, has possibly played a role in reducing the average stone size at pocket beach Site 3. Another possibility is that the greater extent of Site 3, relative to Site 2, resulted in lower average wave energy conditions at Site 3, with the consequence that average stone size was reduced.

7.3 AVERAGE STONE SIZE ESTIMATORS

a) There would be no significant improvement in the accuracy of average stone size estimates using lognormal mean estimators instead of the arithmetic mean estimator for the kinds of diamond size-frequency distributions that typify the marine gravels at Site 3. The logarithmic variance (σ^2) is small at Site 3, meaning that the two kinds of estimators produce similar results. The lognormal mean estimator also suffers from the need to use the graphical solution method, this being a consequence of the fact that individual stone weights were not recorded during the evaluation sampling of the marine gravels at Site 3. It is therefore considered more practical to use the arithmetic mean estimator in the instance of Site 3.

b) Lognormal mean estimators will produce more accurate average stone size estimates than the arithmetic mean estimator in the case where the logarithmic variance (σ^2) of a lognormal diamond size-frequency distribution is high, or where n is small and a large outlier is present. Use of the lognormal mean estimator is recommended in this instance, even if it means using the graphical solution method. Such cases are unlikely to occur at Site 3, but can occur elsewhere, as illustrated by an example from the south of MA1.

c) It is recommended that individual stone weights be recorded as a matter of routine in the future, in order to allow for the numerical solution of lognormal mean estimates for average stone size in all cases. This would enable quantification of confidence limits for the stone size estimates. Quantification of the risk associated with a resource estimate is becoming increasingly more important in the context of the tighter preconditions being imposed by financial lending institutions on new mineral projects.

REFERENCES

Apollus, L., 1995. The distribution of diamonds on a late Cainozoic gravel beach, southwestern Namibia. *Unpublished M.Sc. thesis, University of Glasgow, Scotland*, 170 pp.

Bluck, B.J., 1967. Sedimentation of gravel beaches: examples from south Wales. *Journal of Sedimentary Petrology*, **37**, p. 128-156.

Bluck, B.J., 1999. Clast assembling, bed-forms and structure in gravel beaches. *Transactions of the Royal Society of Edinburgh: Earth Sciences*, **89**, p. 291-323.

Bluck, B.J., Ward, J.D. and Spaggiari, R.I., 2001. Gravel Beaches of Southern Namibia *in* Ecology and Geomorphology of Coastal Shingle (J.R. Packham, R.E. Randall, R.S.K. Barnes and A. Neal, eds), Westbury Academic and Scientific Publishing, p. 56-76.

Brenninkmeyer, B.M., 1976. Sand fountains in the surf zone *in* Beach and Nearshore Sedimentation (R.A Davis Jr. and R.L. Ethington, eds), A publication of *The Society of Economic Paleontologists and Mineralogists*, p. 69-91.

Broecker, W.S., Thurbler, D.L., Goddard, J., Ku, T-L., Matthews, R.K. and Mesolella, K.J., 1968. Milankovitch hypothesis supported by precise dating of coral reefs and deep sea sediments. *Science*, **159**, p. 297-300.

Brown, R.W., Rust, D.J., Summerfield, M.A., Gleadow, A.J.W. and de Wit, M.C.J., 1990. An Early Cretaceous phase of accelerated erosion on the south-western margin of Africa: Evidence from apatite fission track analysis and the offshore sedimentary record. *Nuclear Tracks and Radiation Measurements* (Int. J. Radiation and Applied Instrumentation Part D), **17**, p. 339-350.

Clark, J.A. and Lingle, C.S., 1979. Predicted relative sea-level changes (18,000 Years B.P. to Present) caused by Late-Glacial retreat of the Antarctic Ice Sheet. *Quaternary Research*, **11**, pp. 279-298.

Clark, I, 1987. Statistical Tables for Mineral Reserve Evaluation. Geostokos Limited, London, ISBN 0 9513084 0 8, 31 pp.

Collinson, J.D., 1978a. Deserts *in* Sedimentary Environments and Facies (H.G. Reading, ed.), Blackwell Scientific Publications, Oxford, ISBN 0-632-00435-5, 557 pp.

Collinson, J.D., 1978b. Alluvial Sediments *in* Sedimentary Environments and Facies (H.G. Reading, ed.), Blackwell Scientific Publications, Oxford, ISBN 0-632-00435-5, 557 pp.

Compton, J.S., 2001. Holocene sea-level fluctuations inferred from the evolution of depositional environments of the southern Langebaan Lagoon salt marsh, South Africa. *The Holocene*, **11**, p. 395-405.

Corbett, I.B., 1989. The sedimentology of the diamondiferous deflation deposits within the Sperrgebiet, Namibia. *Unpublished Ph.D. thesis, University of Cape Town, Cape Town*, 430 pp.

Corbett, I.B., 1996. A review of diamondiferous marine deposits of western southern Africa. *African Science Review*, **3**, p. 157-174.

Corbett, I.B and Burrell, B., 2001. The earliest Pleistocene(?) Orange River fan-delta: an example of successful exploration delivery aided by applied Quaternary research in diamond placer sedimentology and palaeontology. *Quaternary International*, **82**, p. 63-73.

Corvinus, G. and Hendey, Q.B., 1978. A new Miocene vertebrate locality at Arrisdrift in South West Africa (Namibia). *Neue Jaarbuch Geologie Paläontologie Mb. Stuttgart*, **4**, p. 193-205.

David, M., 1977. Geostatistical Ore Reserve Estimation. Elsevier Scientific Publishing Company, Amsterdam, ISBN 0-444-41532-7, 364 pp.

De Decker, R.H., 1988. The wave regime on the inner shelf south of the Orange River and its implications for sediment transport. *South African Journal of Geology*, **91 (3)**, p. 358-371.

De Wit, M.C.J., 1993. Cainozoic evolution of drainage systems in the North-Western Cape. *Unpublished Ph.D. thesis, University of Cape Town, Cape Town*, 371 pp.

De Wit, M.C.J., 1996. The distribution and stratigraphy of inland alluvial diamond deposits in South Africa. *Special edition of Africa Geoscience Review*, p. 19-33.

De Wit, M.C.J., Marshall, T.R. and Partridge, T.C., 2000. Fluvial Deposits and Drainage Evolution *in* The Cenozoic of Southern Africa (T.C. Partridge and R.R. Maud, eds.), *Oxford Monographs on Geology and Geophysics*, **40**, ISBN 0195125304, p. 55-72.

Dingle, R.V. and Hendey, Q.B., 1984. Late Mesozoic and Tertiary sediment supply to the Eastern Cape Basin (SE Atlantic) and palaeo-drainage systems in Southwestern Africa. *Marine Geology*, **56**, p. 13-26.

Elford, K., 1980a. Results from Site 3, Marmora. Consolidated Diamond Mines (Pty) Ltd., unpublished internal report, 6 pp.

Elford, K., 1980b, Results from Site 4, North Rock. Consolidated Diamond Mines (Pty) Ltd., unpublished internal report, 6 pp.

Elliott, T., 1978. Siliciclastic Shorelines *in* Sedimentary Environments and Facies (H.G. Reading, ed.), Blackwell Scientific Publications, Oxford, ISBN 0-632-00435-5, 557 pp.

Evans, M., Hastings, N. and Peacock, B., 2000. Statistical Distributions. 3rd edition, John Wiley and Sons Inc., New York, 221 pp.

Fairbanks, R.G., 1989. A 17,000-year glacio-eustatic sea level record: influence of glacial melting rates on the Younger Dryas event and deep-ocean circulation. *Nature*, **342**, p. 637-642.

Fowler, J.A., 1976. The alluvial geology of the lower Orange River and adjacent deposits, South West Africa, *Unpublished M.Phil thesis, University of London, London*, 285 pp.

Fowler, J.A., 1982. Sedimentology and distribution of heavy minerals in the Lower Orange River Valley, *Unpublished Ph.D. thesis, University of London, London*, 317 pp.

Frimmel, H.E. and Hartnady, C.J.H., 1992. Blue amphiboles and their significance for the metamorphic history of the Pan-African Gariep Belt, Namibia. *Journal of Metamorphic Petrology*, **10**, p. 651-669.

Frimmel, H.E., 1995. Metamorphic evolution of the Gariep Belt. *South African Journal of Geology*, **98 (2)**, p. 176-190.

Frimmel, H.E., Klötzli, U.S. and Siegfried, P.R., 1996. New Pb-Pb Single zircon age constraints on the timing of Neoproterozoic glaciation and continental break-up in Namibia. *The Journal of Geology*, **104**, p. 459-469.

Hallam, C.D., 1964. The geology of the coastal diamond deposits of southern Africa. *The Geology of some Ore Deposits of Southern Africa*, **2**, p. 671-728.

Hallam, A., 1992. Phanerozoic Sea-Level Changes. Columbia University Press, New York, ISBN 0-231-07424-7, 255 pp.

Haq, B.U., Hardenbol, J. and Vail, P.R., 1987. Chronology of fluctuating sea levels since the Triassic. *Science*, **235**, p. 1156-1167.

Hawthorne, J.B., 1975. Model of a kimberlite pipe *in* Physics and Chemistry of the Earth, **9**, (L.H. Ahrens, J.B. Dawson, A.R. Duncan and A.J. Erlank, eds.), Pergamon, Oxford, p.1-15.

Hobday, D.K. and Banks, N.L., 1971. A coarse-grained pocket beach complex, Tanafjord (Norway). *Sedimentology*, **16**, p. 129-134.

Jacob, R.J., Bluck, B.J. and Ward, J.D., 1999. Tertiary-age diamondiferous fluvial deposits of the Lower Orange River Valley, southwestern Africa. *Economic Geology*, **94**, p. 749-758.

Jacob, J., 2001. Late Proterozoic bedrock geology and its influence on Neogene littoral marine diamondiferous trapsites, MA1 – Sperrgebiet, Namibia. *Unpublished M.Sc. thesis, University of Cape Town, Cape Town*, 140 pp.

Joynt, R.H. and Foster, R.W., 1976. Notes on submerged beaches off the Namaqualand and southern South West Africa coasts. Marine Diamond Corporation (Pty) Ltd., unpublished internal report, 2 pp.

Kaiser, E., 1926. Die Diamantenwüste Süd West-Afrikas, Dietrich Reimer, Berlin, Vols 1 & 2, 241 pp.

Klinger, H.C., 1977. Cretaceous deposits near Bogenfels, South West Africa. *Annals of the South African Museum*, **73 (3)**, p. 81-92.

Krige, D.G., 1962. Statistical applications in mine valuation. *Journal of the Institute of Mining Surveyors of South Africa*, **12**, p. 45-84 and p. 95-136.

Larcombe, P. and Carter, R.M., 1998. Sequence architecture during the Holocene transgression: an example from the Great Barrier Reef shelf, Australia. *Sedimentary Geology*, **117**, p. 97-121.

Mabote, M.E., Rogers, J. and Meadows, M.E., 1997. Sedimentology of terrigenous mud from the Orange River delta and the inner shelf off Namaqualand, South Africa. *Special Edition of the South African Geographical Journal*, p. 108-114.

Merensky, H., 1909. The diamond deposits of Lüderitzland, German South West Africa. *Transactions of the Geological Society of South Africa*, **12**, p. 13-23.

Miller, D.E., Yates, R.J., Parkington, J.E. and Vogel, J.C., 1993. Radiocarbon-dated evidence relating to a mid-Holocene relative high sea-level on the south-western Cape coast, South Africa. *South African Journal of Science*, **89**, p. 35-44.

Miller, D.E., 1990. A southern African Late Quaternary sea-level curve. *South African Journal of Science*, **86**, p. 456-458.

Murray, L.G., Joynt, R.H., O'Shea, D.O.C., Foster, R.W. and Kleinjan, L., 1970. The geological environment of some diamond deposits off the coast of South West Africa. ICSU/SCOR Working Party 31 Symposium, Cambridge 1970: The Geology of the East Atlantic Continental Margin (F.M. Delaney, ed). *Institute of Geological Sciences Report*, **70/13**, p. 119-141.

Oosterveld, M.M., Campbell, D. and Hazell, K.R., 1987. Geology related to statistical evaluation parameters for a diamondiferous beach deposit. *Proceedings of the Twentieth International Symposium on the Application of Computers and Mathematics in the Mineral Industries*, South African Institute of Mining and Metallurgy, *Geostatistics*, **3**, Johannesburg, p.129-136.

Oosterveld, M.M., 2003. Evaluation of alluvial diamond deposits. Alluvial Diamonds in South Africa Workshop, Directorate of Professional Programmes of the Geological Society of South Africa, Glenhove Conference Centre, Johannesburg, 17 pp.

Oppenheimer, E. and Williams, A.F., 1914. Diamond deposits of German South West Africa. De Beers Consolidated Mines Ltd., unpublished internal report, 58 pp.

Partridge, T.C. and Maud, R.R., 1987. Geomorphic evolution of southern Africa since the Mesozoic. *South African Journal of Geology*, **90**, p. 179-208.

Partridge, T.C., 1998. Of diamonds, dinosaurs and diastrophism: 150 million years of landscape evolution in southern Africa, *South African Journal of Geology*, **101 (3)**, p. 167-184.

Pether, J., 2000. *In* The Cenozoic of Southern Africa (T.C. Partridge and R.R. Maud, eds.), *Oxford Monographs on Geology and Geophysics*, **40**, ISBN 0195125304, p. 33-54.

Pether, J., 2001. Macrofauna from embayment infill sequences, the Marmora area, southern Namibia. De Beers Marine, in-house report, 21 pp.

Pethick, J., 1984. An Introduction to Coastal Geomorphology. Edward Arnold, London, ISBN 0 7131 6391 7, p. 9-19.

Pickford, M. and Senut, B., 1999. Geology and Palaeobiology of the central and southern Namib Desert, Southwestern Africa. Memoir 18 of the Geological Survey of Namibia, Volume 1 : Geology and History of Study, 155 pp.

Plint, A.G., Eyles, N., Eyles, C.H. and Walker, R.G., 1992. Control of sea level change *in* Facies Models – Response to sea level change (R.G. Walker and N.P. James, eds.), Geological Association of Canada, p. 15-25.

Ramsay, P.J. and Cooper, J.A.G., 2001. Late Quaternary sea-level change in South Africa. *Quaternary Research*, **57**, p. 1-9.

Reineck, H.E. and Singh, I.B., 1975. Depositional Sedimentary Environments. 1st edition, Springer-Verlag, New York, ISBN 3-540-06115-0, 439 pp.

Roberts, D. and Berger, L.R., 1997. Last Interglacial (c. 117kyr) human footprints from South Africa. *South African Journal of Science*, **93**, p. 349-350.

Robinson, D.N., 1979. Surface textures and other features of diamonds. *Unpublished Ph.D. thesis, University of Cape Town, Cape Town*, 382 pp.

Rogers, J., 1977. Sedimentation on the continental margin off the Orange River and the Namib Desert. Department of Geology, University of Cape Town, *Marine Geoscience Group Bulletin*, **7**, 162 pp.

Schneider, G.I. and Miller, R. McG., 1992. Diamonds *in* The Mineral Resources of Namibia, 1st Edition, p. 5.1-1 to 5.1-31.

Selley, R.C., 1982. An Introduction to Sedimentology. 4th edition, Academic Press, New York, ISBN 0-12-636362-5, 417 pp.

Shackleton, N.J., 1987. Oxygen isotopes, ice volume and sea level. *Quaternary Science Reviews*, **6**, p. 183-190.

Shackleton, N.J. and Opdyke, N.D., 1973. Oxygen isotope and palaeomagnetic stratigraphy of Equatorial Pacific Core V28-238: Oxygen isotope temperatures and ice volumes on a 10^5 year and 10^6 year scale. *Quaternary Research*, **3**, p. 39-55.

Sichel, H.S., 1947. An experimental and theoretical investigation of bias error in mine sampling with special reference to narrow gold reefs. *Transactions of the Institution of Mining and Metallurgy*, **56**, p. 403-473.

Sichel, H.S., 1952. New methods in the statistical evaluation of mine sampling data. *Transactions of the Institution of Mining and Metallurgy*, **61 (6)**, p. 261-288.

Sichel, H.S., 1966. The estimation of means and associated confidence limits for small samples from lognormal populations *in* Symposium on mathematical statistics and computer applications in ore valuation, *Journal of the South African Institute of Mining and Metallurgy*, **0**, p. 106-122.

Sichel, H.S., 1972. Statistical valuation of diamondiferous deposits. *Proceedings of the International Symposium on the Application of Computers in the Mineral Industry*, South African Institute of Mining and Metallurgy, Johannesburg, p. 17-25.

Siesser, W.G. and Salmon, D., 1979. Eocene marine sediments in the Sperrgebiet, South West Africa. *Annals of the South African Museum*, **79 (2)**, p. 9-34.

Siesser, W.G. and Dingle, R.V., 1981. Tertiary sea-level movements around southern Africa. *Journal of Geology*, **89**, p. 83-96.

Smith, C.B., 1988. Chronology of kimberlite emplacement in the Northern Cape Province: A complex record. *Bulletin of the Geological Society of South Africa*, **31 (1)**, p. 31-32.

South African Committee for Stratigraphy (SACS), 1980. Stratigraphy of South Africa, Kent, L.E. (comp.); Part 1. Lithostratigraphy of the Republic of South Africa, South West Africa/Namibia, and the Republics of Bophuthatswana, Transkei and Venda. Handbook of the Geological Survey of South Africa, **8**, 690 pp.

Stocken, C.G., 1978. A review of Cenozoic climatic and geological events in the Sperrgebiet. Consolidated Diamond Mines (Pty) Ltd., unpublished internal report, 38 pp.

Stocken, C.G., 1980. Results from Site 2, South Rock. Consolidated Diamond Mines (Pty) Ltd., unpublished internal report, 6 pp.

Storrar, C.D., 1987. South African Mine Valuation. Revised Edition, Chamber of Mines of South Africa, ISBN 0620 02155 1, 470 pp.

Stuiver, M. and Braziunas, T.F., 1993. Modeling atomospheric ^{14}C influences and ^{14}C ages of marine samples to 10,000 BC, *Radiocarbon*, **35**, p. 137-189.

Talma, S. and Vogel, J.C., 1993. A simplified approach to calibrating ^{14}C dates. *Radiocarbon*, **35**, p. 317-322.

Tankard, A.J., 1975. Cenozoic sea-level changes: a discussion. *Proceedings of the South African Society for Quaternary Research*, p. 1-17.

Tankard, A.J., Jackson, M.P.A., Eriksson, K.A., Hobday, D.K., Hunter, D.R. and Minter, W.E.L., 1982. Crustal evolution of Southern Africa 3.8 Billion Years of Earth History, Springer-Verlag, New York, ISBN 0-387-90608-8, 523 pp.

Till, R., 1978. Arid shorelines and evaporites *in* Sedimentary Environments and Facies (H.G. Reading, ed.), Blackwell Scientific Publications, Oxford, ISBN 0-632-00435-5, 557 pp.

Veeh, H.H., 1966. Th^{230}/U^{238} and U^{234}/U^{238} ages of Pleistocene high sea level stand. *Journal of Geophysical Research*, **71**, p. 3379-3386.

Veeh, H.H. and Chappell, J., 1970. Astronomical theory of climatic change: support from New Guinea. *Science*, **167**, p. 862-865.

Vézina, J., Jones, B. and Ford, D., 1999. Sea-level highstands over the last 500,000 years: evidence from the Ironshore Formation on Grand Cayman, British West Indies. *Journal of Sedimentary Research*, **69 (2)**, p. 317-327.

Ward, J.D. and Bluck, B.J., 1997. The Orange River – 100 million years of fluvial evolution in southern Africa. *Abstracts volume of the 6th International Fluvial Conference*, Cape Town: International Association of Sedimentologists.

Ward, J.D., 2000. *In* The Cenozoic of Southern Africa (T.C. Partridge and R.R. Maud, eds.), *Oxford Monographs on Geology and Geophysics*, **40**, ISBN 0195125304, p. 33-54.

Wentworth, C.K., 1922. A scale of grade and class terms for clastic sediments. *Journal of Geology*, **30**, p. 377-392.

Williams, A.T. and Caldwell, N.E., 1988. Particle size and shape in pebble-beach sedimentation. *Marine Geology*, **82**, p. 199-215.

Williams, D.F., Moore, W.S. and Fillon, R.H., 1981. Role of Arctic Ocean ice sheets in Pleistocene oxygen isotope and sea level records. *Earth and Planetary Science Letters*, **56**, p. 157-166.

Yokoyama, Y., De Deckker, P., Lambeck, K., Johnston, P. and Fifield, L.K., 2001. Sea-level at the Last Glacial Maximum: evidence from northwestern Australia to constrain ice volumes for oxygen isotope stage 2. *Palaeogeography, Palaeoclimatology, Palaeoecology*, **165**, p. 281-297.

Zingg, T., 1935. Beitrage zur Schotteranalyse. *Schweizerische Mineralogisch Petrographische Mitteilungen.*, **15**, p. 39-140.

APPENDIX I – CUMULATIVE FREQUENCY DISTRIBUTION PLOTS FOR DIAMOND SIZE

RESOURCE SUBDIVISION: G3Int1 $n = 27$ $\bar{a} = 0.33$ cts/stn

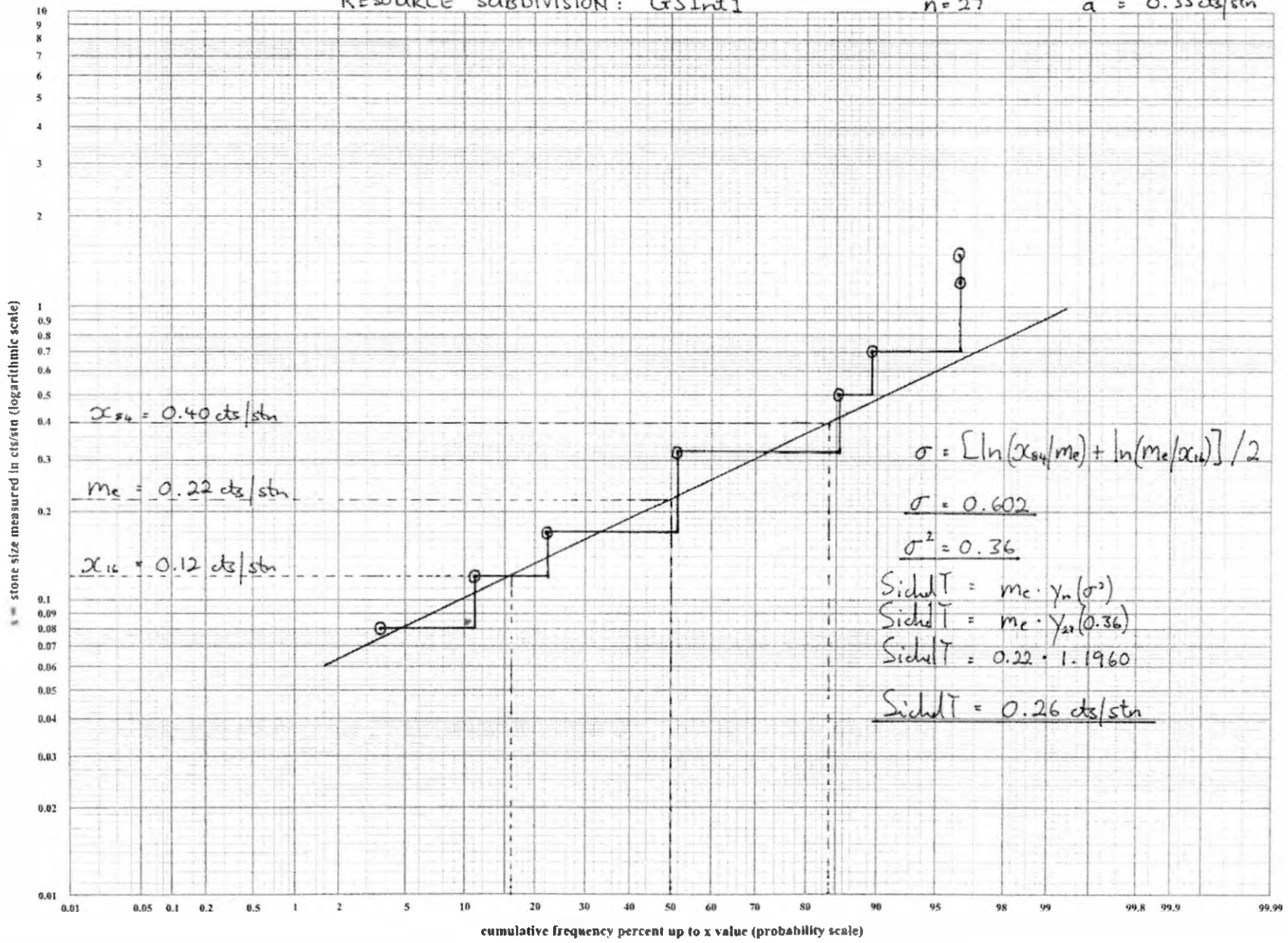

$x_{84} = 0.40$ cts/stn

$m_e = 0.22$ cts/stn

$x_{16} = 0.12$ cts/stn

$$\sigma = [\ln(x_{84}/m_e) + \ln(m_e/x_{16})]/2$$

$\sigma = 0.602$

$\sigma^2 = 0.36$

$\text{SichdT} = m_e \cdot \gamma_n(\sigma^2)$

$\text{SichdT} = m_e \cdot \gamma_{25}(0.36)$

$\text{SichdT} = 0.22 \cdot 1.1960$

$\text{SichdT} = 0.26$ cts/stn

RESOURCE SUBDIVISION : G3Int2 $n = 9$ $\bar{a} = 0.30$ cts/stn

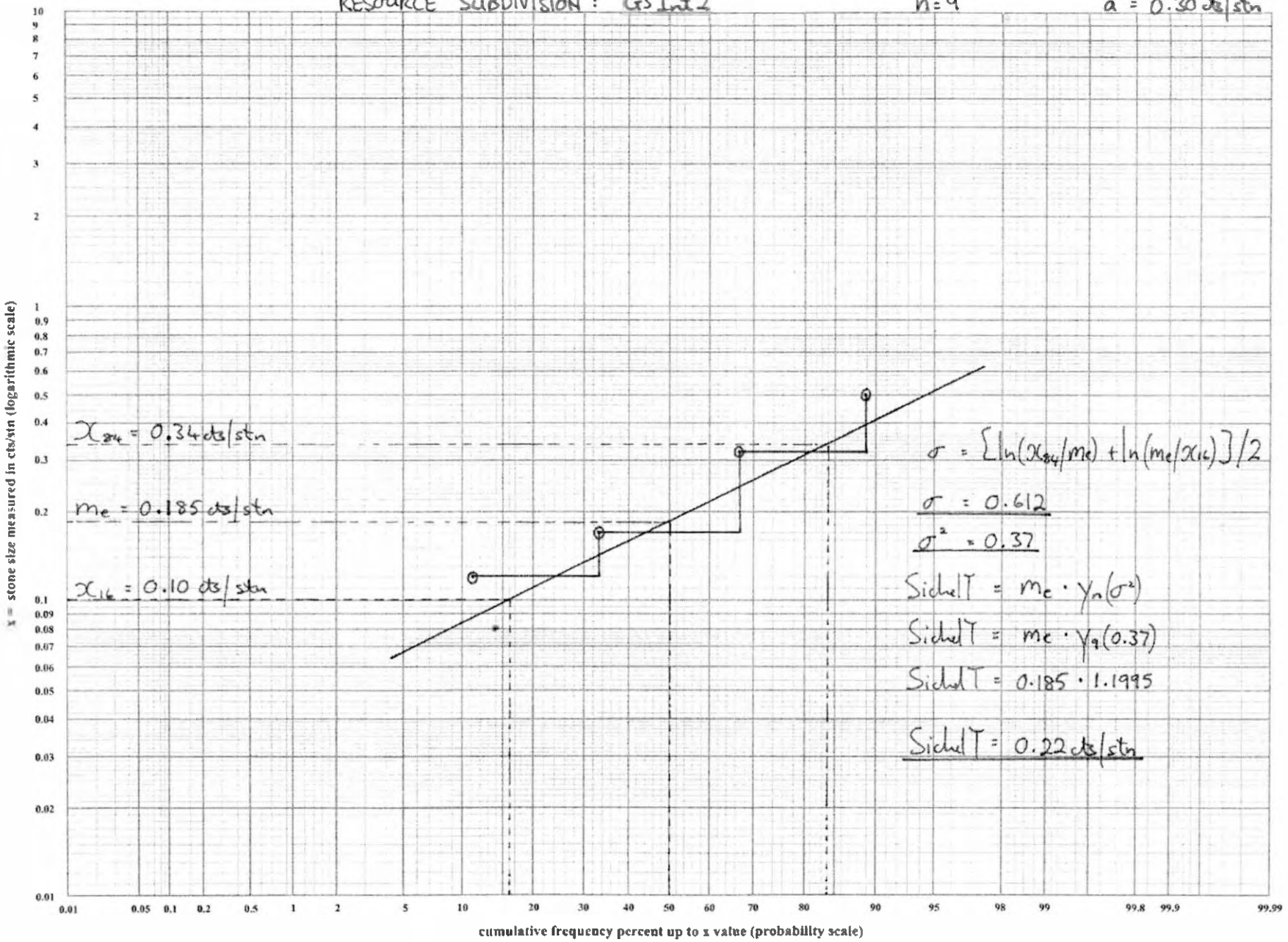

RESOURCE SUBDIVISION: G3Int3 $n = 27$ $\bar{a} = 0.29$ cts/stn

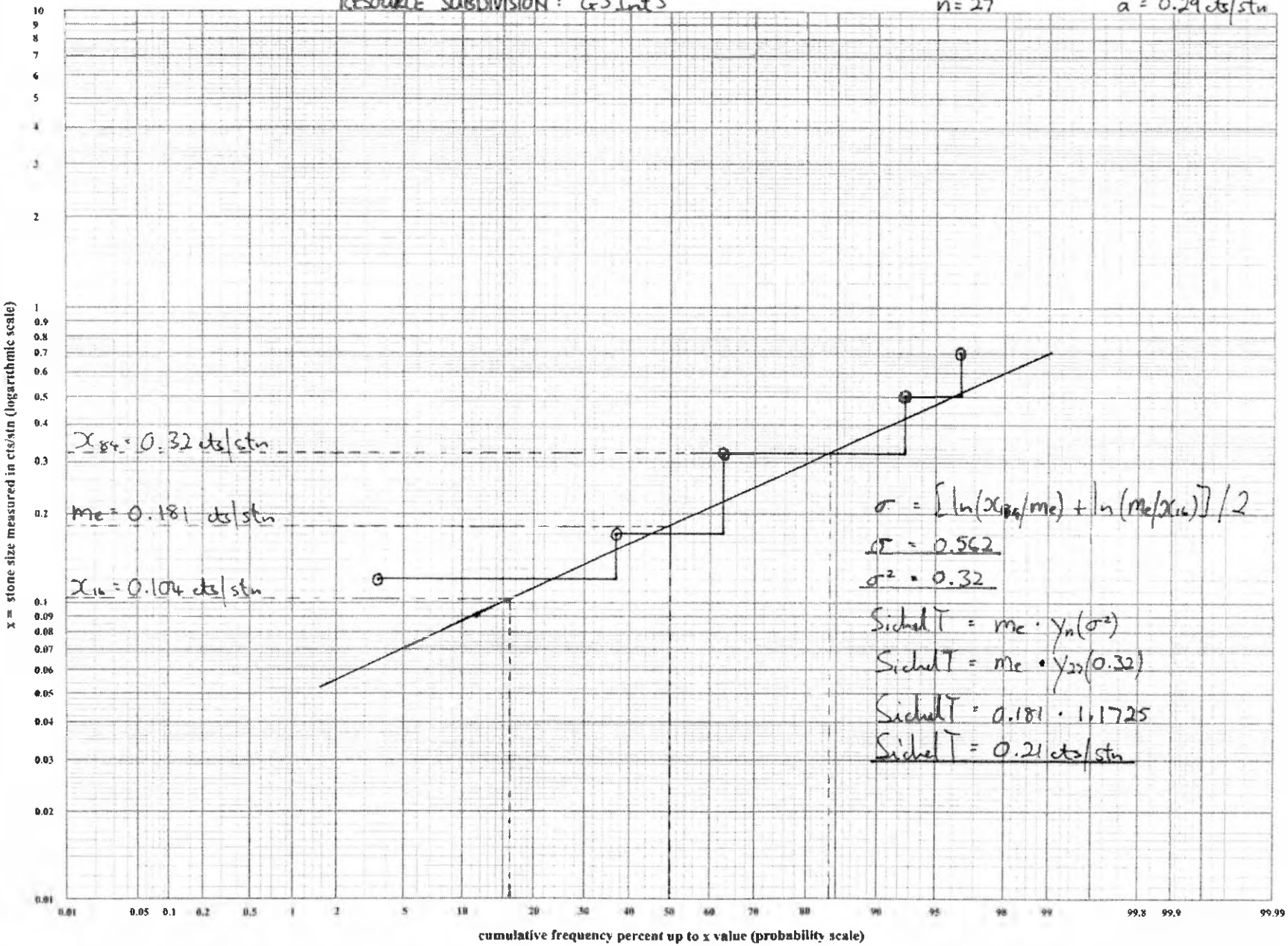

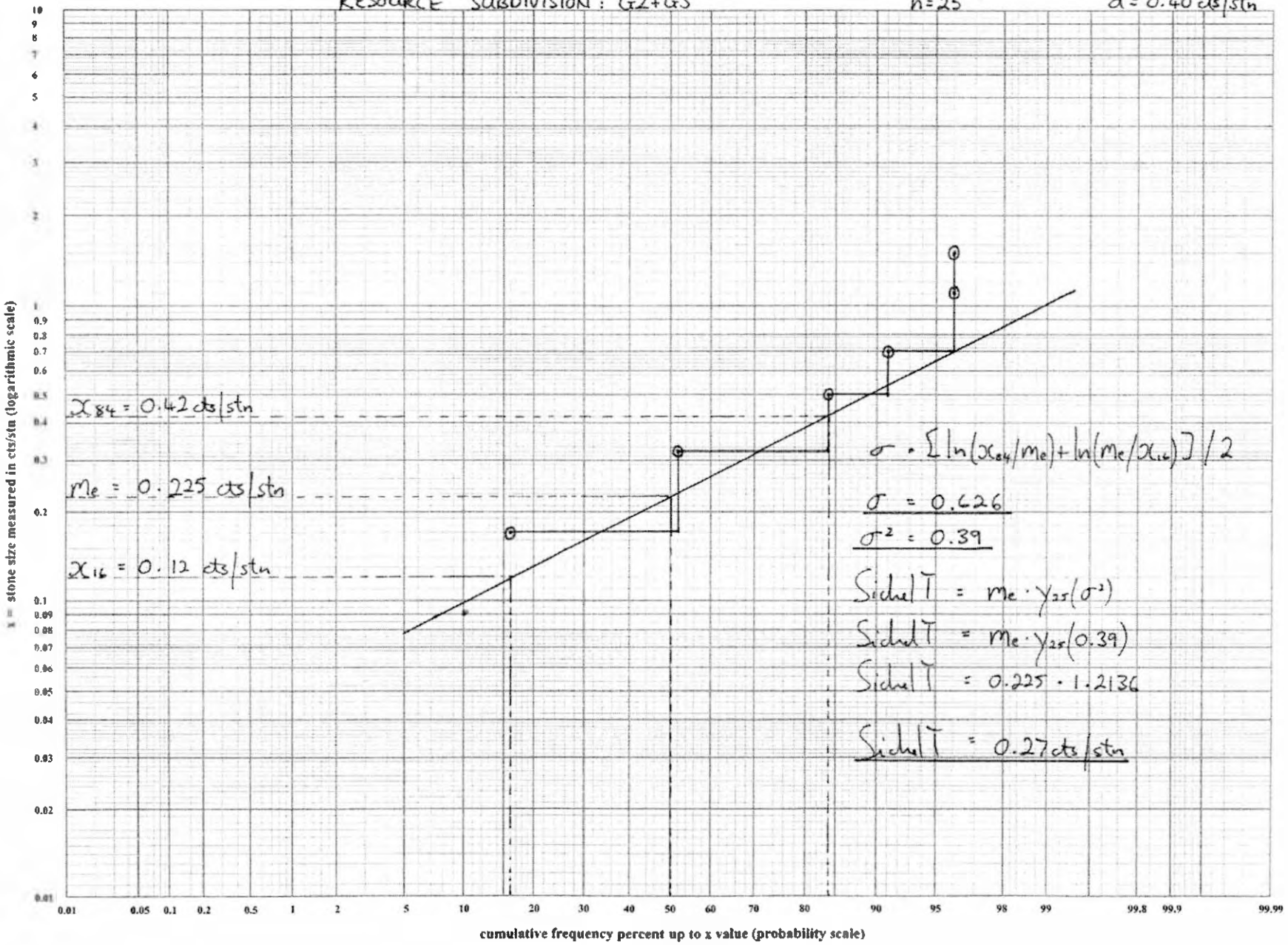
RESOURCE SUBDIVISION : G2+G3
n=25
$\bar{a}$ = 0.40 cts/stn
x_{84} = 0.42 cts/stn
m_e = 0.225 cts/stn
x_{16} = 0.12 cts/stn
$\sigma = [\ln(x_{84}/m_e) + \ln(m_e/x_{16})]/2$
σ = 0.626
σ^2 = 0.39
Sichel $\bar{T}$ = $m_e \cdot \gamma_{25}(\sigma^2)$
Sichel $\bar{T}$ = $m_e \cdot \gamma_{25}(0.39)$
Sichel $\bar{T}$ = 0.225 · 1.2136
Sichel $\bar{T}$ = 0.27 cts/stn
x = stone size measured in cts/stn (logarithmic scale)
cumulative frequency percent up to x value (probability scale)

RESOURCE SUBDIVISION : G3Sub1 $n = 36$ $\bar{a} = 0.29$ cts/stn

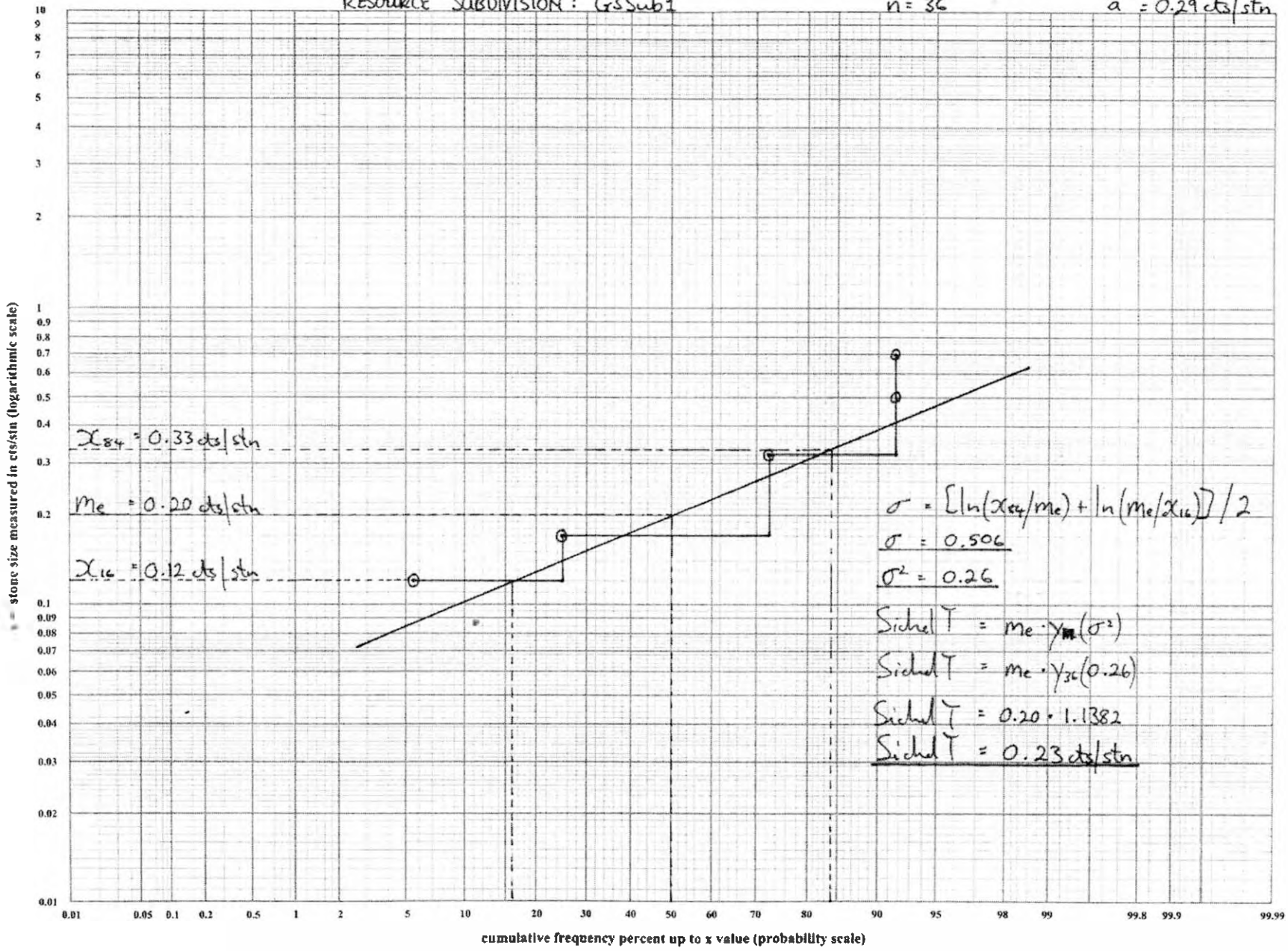

$\sigma = [\ln(x_{84}/m_e) + \ln(m_e/x_{16})]/2$

$\sigma = 0.506$

$\sigma^2 = 0.26$

Sichel $\bar{T} = m_e \cdot \gamma_m(\sigma^2)$

Sichel $\bar{T} = m_e \cdot \gamma_{36}(0.26)$

Sichel $\bar{T} = 0.20 \cdot 1.1382$

Sichel $\bar{T} = 0.23$ cts/stn

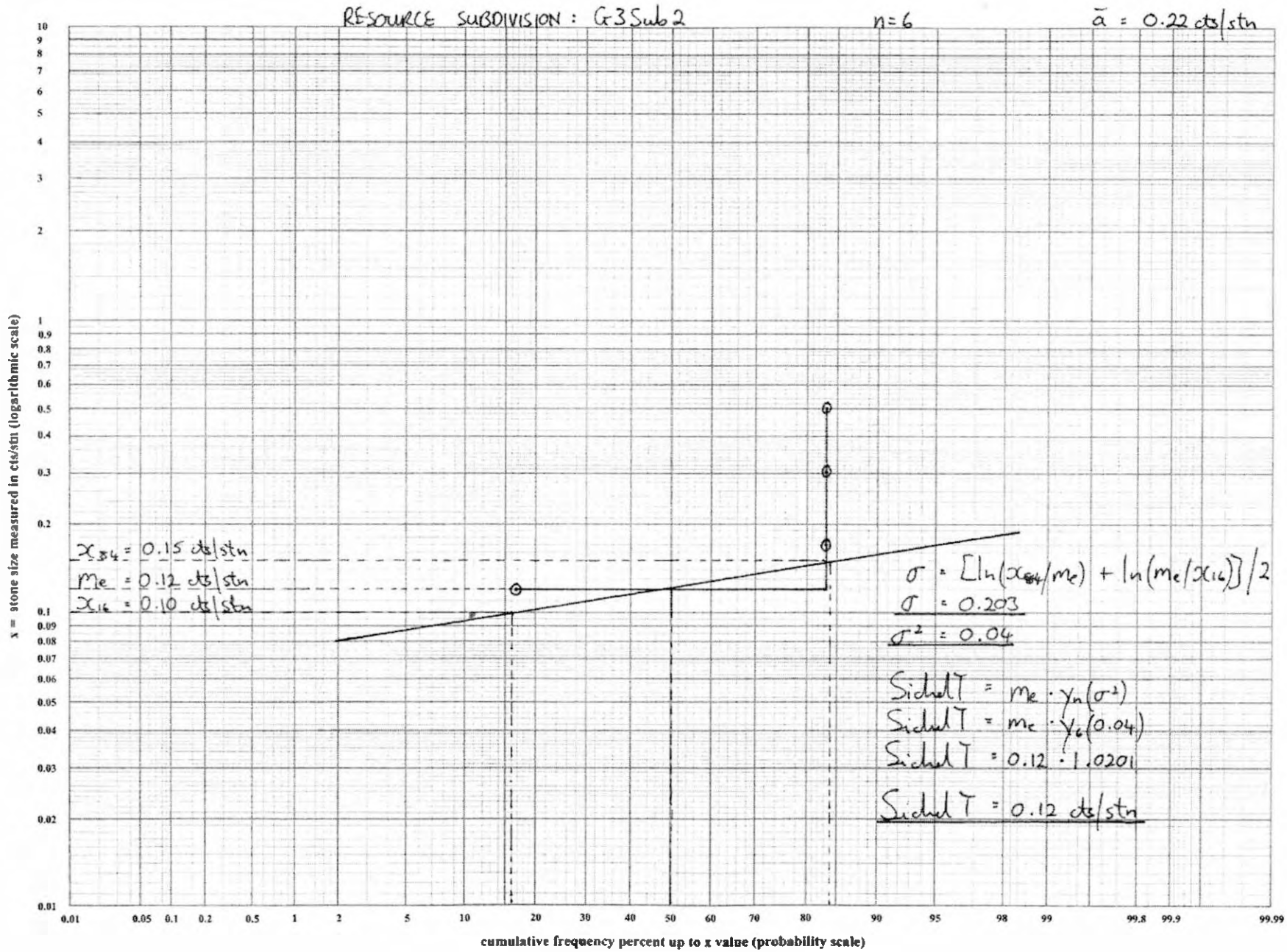
RESOURCE SUBDIVISION : G3Sub2
n=6
$\bar{a}$ = 0.22 cts/stn
x_{84} = 0.15 cts/stn
m_e = 0.12 cts/stn
x_{16} = 0.10 cts/stn
$\sigma = [\ln(x_{84}/m_e) + \ln(m_e/x_{16})]/2$
σ = 0.203
σ^2 = 0.04
SichdT = $m_e \cdot \gamma_n(\sigma^2)$
SichdT = $m_e \cdot \gamma_n(0.04)$
SichdT = 0.12 · 1.0201
SichdT = 0.12 cts/stn
x = stone size measured in cts/stn (logarithmic scale)
cumulative frequency percent up to x value (probability scale)

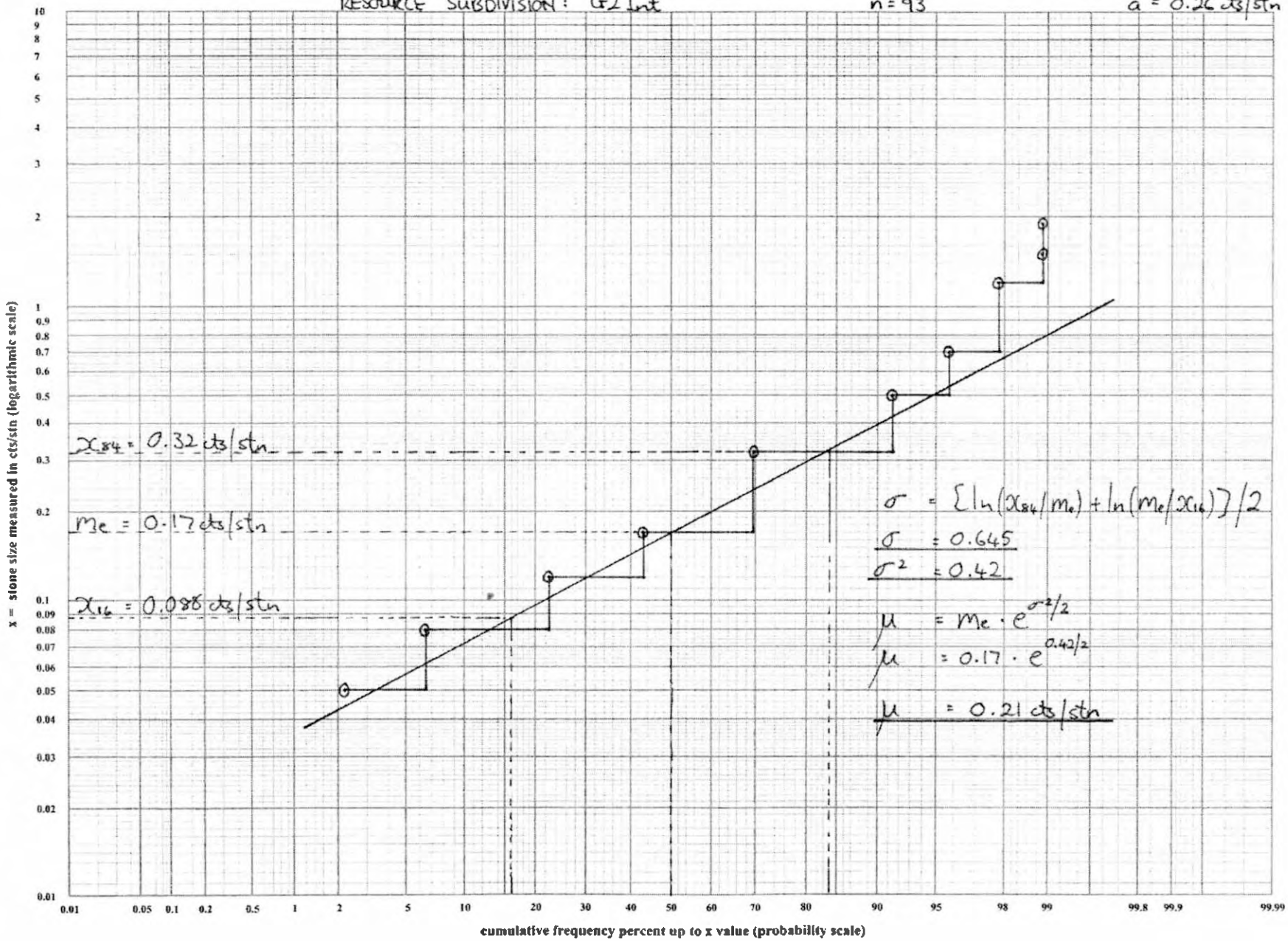
RESOURCE SUBDIVISION: G2 Int
n = 93
$\bar{a}$ = 0.26 cts/stn
x_{84} = 0.32 cts/stn
m_e = 0.17 cts/stn
x_{16} = 0.088 cts/stn
$\sigma = [\ln(x_{84}/m_e) + \ln(m_e/x_{16})]/2$
$\sigma = 0.645$
$\sigma^2 = 0.42$
$\mu = m_e \cdot e^{\sigma^2/2}$
$\mu = 0.17 \cdot e^{0.42/2}$
$\mu = 0.21$ cts/stn
x = stone size measured in cts/stn (logarithmic scale)
cumulative frequency percent up to x value (probability scale)

APPENDIX II – THE GRAPHICAL METHOD FOR LOGNORMAL DISTRIBUTIONS

A Graphical Method for the Calculation of m_e and σ for Lognormal Sample Populations

a) Divide the range of sample values into a suitable number of class intervals.

b) Calculate the cumulative frequency percentages for the sample population at each of the class intervals.

c) Plot the value of the upper limit of each class interval against the cumulative frequency percentage at that value, using log-probability graph paper. If the plotted points fall approximately on a straight line, then the sample population defines a two-parameter lognormal distribution.

d) Construct a set of lines, along the probability scale, from each plotted point to the cumulative percentage value of the next plotted point. Construct another set of lines, along the log scale, which link the first set of lines to the plotted point above. The result should be a step-shaped pattern extending downward from the line of the plotted points.

e) Construct a best-fit line, which is intermediate between the plotted points and the bottom vertices of the step pattern. More weight should be given to plotted points which represent greater increments in the frequency percentage. This best-fit line is a model of the two-parameter lognormal distribution defined by the sample population.

f) The value of m_e is the sample value, read off the best-fit line, at a cumulative frequency percentage of 50% (ie. $m_e = x_{50}$).

g) Read the value of x_{16} and x_{84} off the best-fit line.

h) Now, $\sigma = [\ln(x_{84}/m_e) + \ln(m_e/x_{16})] / 2$ (David, 1977)

APPENDIX III – SIMULATION RESULTS

	Lognormal Distribution Parameters for Simulation : μ = 0.20 cts/stn; σ^2 = 0.15									
	Distribution of the Lognormal Mean Estimates					Distribution of the Arithmetic Mean Estimates				
n	1st percentile (lower 98% central tendency limit)	5th percentile (lower 90% central tendency limit)	50th percentile (median)	95th percentile (upper 90% central tendency limit)	99th percentile (upper 98% central tendency limit)	1st percentile (lower 98% central tendency limit)	5th percentile (lower 90% central tendency limit)	50th percentile (median)	95th percentile (upper 90% central tendency limit)	99th percentile (upper 98% central tendency limit)
5	-36.7%	-27.8%	-1.8%	32.3%	50.7%	-36.7%	-27.5%	-1.8%	32.3%	50.7%
6	-32.0%	-24.2%	-0.7%	29.5%	44.2%	-32.1%	-24.2%	-0.8%	29.5%	43.8%
7	-29.6%	-21.6%	-1.0%	26.4%	42.3%	-29.6%	-21.6%	-1.1%	26.5%	42.1%
8	-28.3%	-21.6%	-1.0%	24.6%	36.2%	-28.4%	-21.6%	-1.0%	24.6%	36.1%
9	-26.7%	-20.0%	-1.1%	24.3%	38.5%	-26.7%	-20.3%	-1.3%	24.5%	38.4%
10	-24.8%	-19.1%	-0.6%	23.0%	33.1%	-24.8%	-18.9%	-0.8%	22.9%	33.7%
11	-24.7%	-18.8%	-0.8%	21.3%	33.4%	-24.7%	-18.8%	-0.8%	21.1%	33.4%
12	-23.8%	-17.5%	-0.8%	19.4%	30.2%	-23.7%	-17.7%	-0.8%	19.4%	30.3%
13	-22.5%	-16.7%	-0.5%	20.1%	30.1%	-22.2%	-16.9%	-0.5%	19.9%	29.7%
14	-19.9%	-15.8%	-0.8%	19.0%	27.1%	-20.0%	-15.6%	-0.9%	19.3%	27.2%
15	-21.2%	-15.9%	-1.1%	16.3%	25.1%	-21.5%	-16.2%	-1.1%	16.5%	25.2%
20	-18.3%	-13.8%	-0.9%	15.2%	23.1%	-18.3%	-13.7%	-0.8%	15.2%	23.7%
30	-15.9%	-11.5%	-0.6%	12.1%	17.7%	-15.8%	-11.4%	-0.6%	11.9%	17.9%
40	-14.3%	-10.2%	-0.3%	11.4%	16.8%	-14.1%	-10.2%	-0.3%	11.4%	16.8%
50	-13.1%	-9.2%	-0.4%	9.8%	13.6%	-13.0%	-9.2%	-0.3%	9.9%	13.9%
75	-10.4%	-7.7%	-0.2%	7.8%	11.1%	-10.5%	-7.7%	-0.2%	7.9%	11.0%
100	-8.9%	-6.1%	0.0%	6.8%	10.2%	-8.8%	-6.1%	0.0%	6.7%	10.2%
250	-5.9%	-4.2%	0.0%	4.3%	6.0%	-5.9%	-4.1%	0.0%	4.3%	5.9%
500	-4.0%	-2.9%	0.0%	2.9%	4.2%	-3.9%	-2.9%	0.1%	3.0%	4.3%

(grey numbers record the distribution of Sichel T estimates)

A summary of the the results of the sample campaign simulation over a two-parameter lognormal distribution, where μ = 0.20 cts/stn and σ^2 = 0.15.
This represents a case, for diamond size-frequency distribution, which is likely to occur at Site 3.
The distribution of the mean estimates, for each value of n, is defined by 1500 values resulting from 1500 sample campaign realisations.
Percentile values are expressed in terms of their percentage deviation from the actual mean of the population (ie. μ = 0.20 cts/stn).

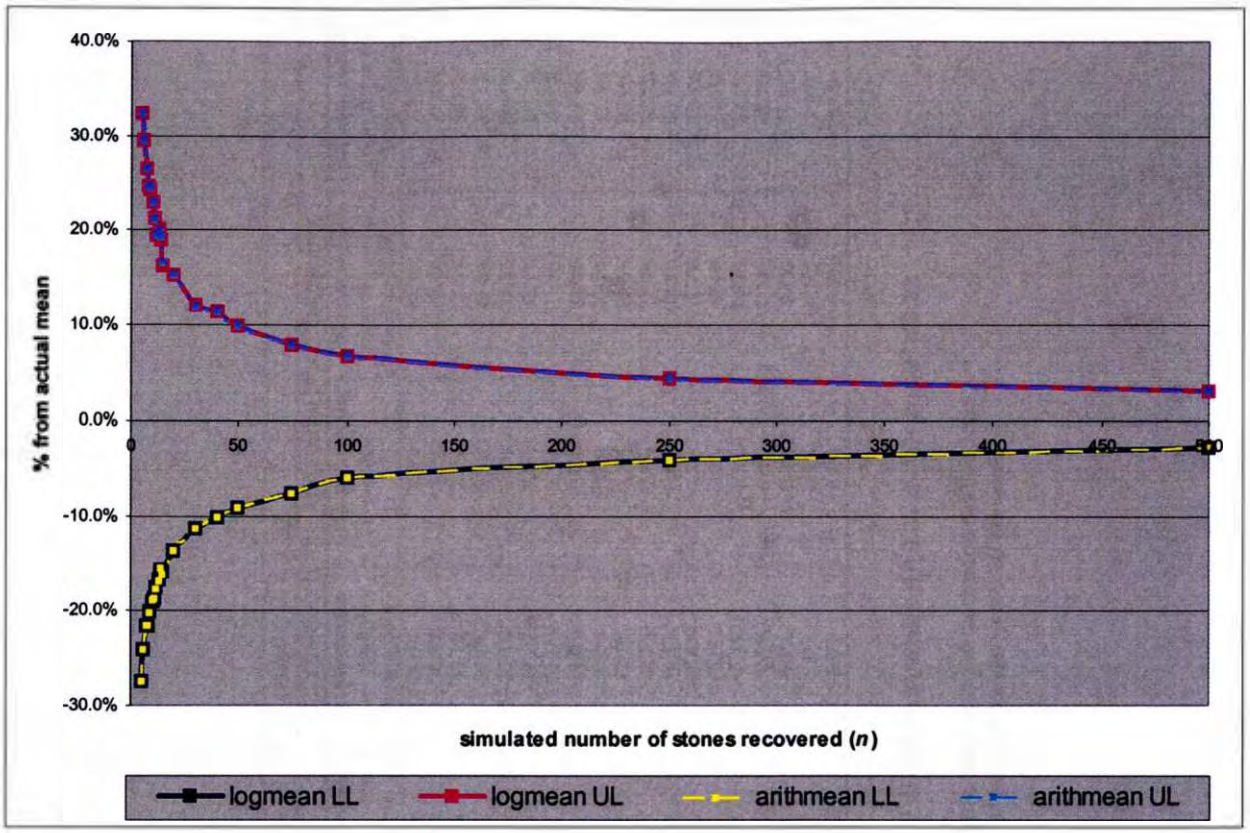

A graph of the 5th and 95th percentile values (90% central tendency limits) of the distributions of the mean estimates for the sample campaign simulation where μ = 0.20 cts/stn and σ^2 = 0.15. This represents a case, for diamond size-frequency distribution, which is likely to occur at Site 3. The 5th and 95th percentile values, for each value of *n*, are drawn from the distribution of 1500 values resulting from 1500 sample campaign realisations. Percentile values are expressed in terms of their percentage deviation from the actual mean of the population (ie. μ = 0.20 cts/stn).

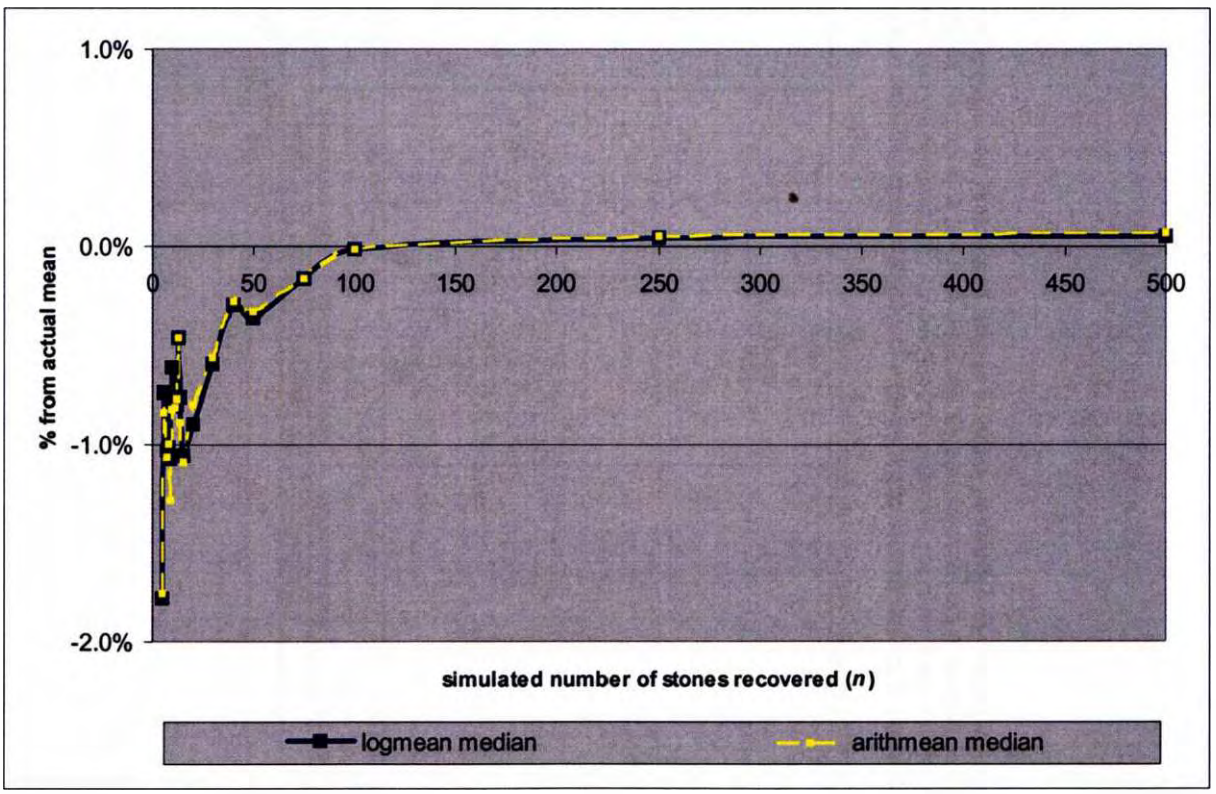

A graph of the 50th percentile values (medians) of the distributions of the mean estimates for the sample campaign simulation where μ = 0.20 cts/stn and σ^2 = 0.15. This represents a case, for diamond size-frequency distribution, which is likely to occur at Site 3. The 50th percentile values, for each value of *n*, are drawn from the distribution of 1500 values resulting from 1500 sample campaign realisations. Percentile values are expressed in terms of their percentage deviation from the actual mean of the population (ie. μ = 0.20 cts/stn).

	Lognormal Distribution Parameters for Simulation : μ = 0.20 cts/stn; σ^2 = 0.30									
	Distribution of the Lognormal Mean Estimates					Distribution of the Arithmetic Mean Estimates				
n	1st percentile (lower 98% central tendency limit)	5th percentile (lower 90% central tendency limit)	50th percentile (median)	95th percentile (upper 90% central tendency limit)	99th percentile (upper 98% central tendency limit)	1st percentile (lower 98% central tendency limit)	5th percentile (lower 90% central tendency limit)	50th percentile (median)	95th percentile (upper 90% central tendency limit)	99th percentile (upper 98% central tendency limit)
5	-46.6%	-35.6%	-2.3%	47.8%	77.5%	-46.6%	-35.4%	-2.3%	48.3%	77.0%
6	-44.3%	-36.0%	-2.9%	48.0%	75.4%	-44.5%	-36.0%	-3.2%	49.2%	77.4%
7	-38.7%	-30.7%	-2.4%	38.7%	60.6%	-38.7%	-30.7%	-2.6%	39.5%	68.0%
8	-38.7%	-30.5%	-2.2%	35.8%	56.9%	-38.3%	-30.6%	-2.5%	36.6%	58.7%
9	-36.0%	-29.9%	-2.3%	34.5%	53.6%	-36.0%	-30.3%	-2.3%	35.3%	54.7%
10	-36.0%	-27.1%	-2.3%	33.7%	55.7%	-36.0%	-27.2%	-2.2%	33.1%	55.1%
11	-34.2%	-26.0%	-2.0%	31.3%	46.9%	-34.3%	-25.9%	-2.1%	31.3%	48.5%
12	-32.5%	-25.1%	-1.9%	32.7%	51.4%	-32.4%	-24.9%	-2.0%	32.3%	50.1%
13	-32.2%	-24.5%	-1.5%	29.4%	47.0%	-32.4%	-24.3%	-1.2%	29.0%	47.4%
14	-31.1%	-22.5%	-1.4%	28.5%	42.5%	-31.0%	-22.7%	-1.3%	28.8%	42.9%
15	-30.2%	-22.0%	-1.1%	27.4%	39.6%	-30.2%	-22.7%	-0.8%	27.4%	42.1%
20	-26.0%	-19.2%	-0.4%	22.8%	35.9%	-26.3%	-19.4%	-0.6%	22.8%	36.7%
30	-21.7%	-16.4%	-1.1%	17.3%	24.1%	-21.8%	-16.4%	-1.1%	17.7%	23.8%
40	-18.3%	-13.7%	-0.7%	16.4%	24.2%	-17.9%	-13.8%	-0.8%	16.4%	24.7%
50	-17.6%	-12.9%	-0.2%	14.6%	21.3%	-17.4%	-12.7%	-0.3%	14.6%	20.3%
75	-14.4%	-10.6%	-0.5%	11.1%	16.3%	-14.4%	-10.9%	-0.6%	11.0%	16.1%
100	-12.7%	-9.4%	-0.3%	9.8%	13.8%	-12.8%	-9.3%	-0.3%	9.7%	14.5%
250	-8.4%	-5.9%	-0.1%	6.3%	9.2%	-8.2%	-5.9%	-0.1%	6.3%	9.1%
500	-6.3%	-4.4%	-0.1%	4.4%	5.9%	-6.3%	-4.4%	-0.2%	4.3%	6.0%

(grey numbers record the distribution of Sichel T estimates)

A summary of the the results of the sample campaign simulation over a two-parameter lognormal distribution, where μ = 0.20 cts/stn and σ^2 = 0.30.
This represents a case, for diamond size-frequency distribution, which is likely to occur at Site 3.
The distribution of the mean estimates, for each value of n, is defined by 1500 values resulting from 1500 sample campaign realisations.
Percentile values are expressed in terms of their percentage deviation from the actual mean of the population (ie. μ = 0.20 cts/stn).

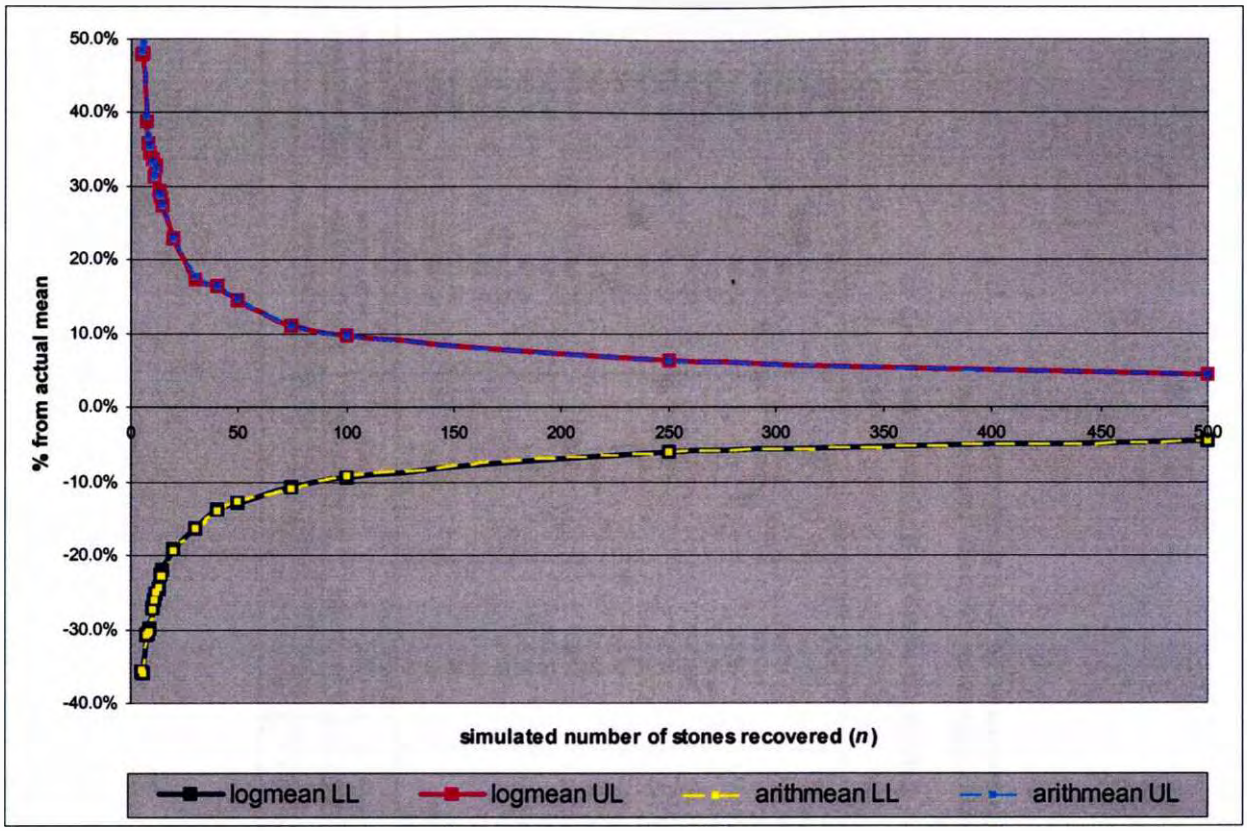

A graph of the 5th and 95th percentile values (90% central tendency limits) of the distributions of the mean estimates for the sample campaign simulation where μ = 0.20 cts/stn and σ^2 = 0.30. This represents a case, for diamond size-frequency distribution, which is likely to occur at Site 3. The 5th and 95th percentile values, for each value of *n*, are drawn from the distribution of 1500 values resulting from 1500 sample campaign realisations. Percentile values are expressed in terms of their percentage deviation from the actual mean of the population (ie. μ = 0.20 cts/stn).

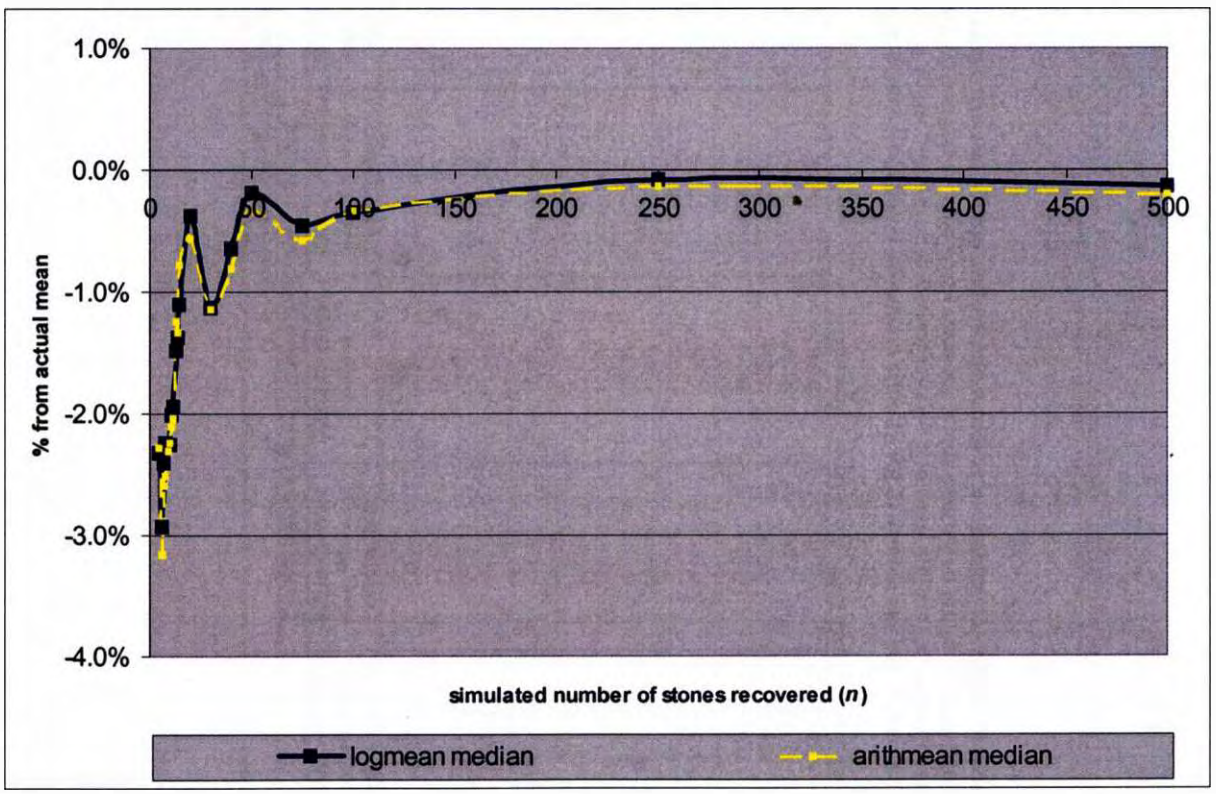

A graph of the 50th percentile values (medians) of the distributions of the mean estimates for the sample campaign simulation where μ = 0.20 cts/stn and σ^2 = 0.30. This represents a case, for diamond size-frequency distribution, which is likely to occur at Site 3. The 50th percentile values, for each value of *n*, are drawn from the distribution of 1500 values resulting from 1500 sample campaign realisations. Percentile values are expressed in terms of their percentage deviation from the actual mean of the population (ie. μ = 0.20 cts/stn).

	Lognormal Distribution Parameters for Simulation : μ = 0.20 cts/stn; σ^2 = 0.45									
	Distribution of the Lognormal Mean Estimates					Distribution of the Arithmetic Mean Estimates				
n	1st percentile (lower 98% central tendency limit)	5th percentile (lower 90% central tendency limit)	50th percentile (median)	95th percentile (upper 90% central tendency limit)	99th percentile (upper 98% central tendency limit)	1st percentile (lower 98% central tendency limit)	5th percentile (lower 90% central tendency limit)	50th percentile (median)	95th percentile (upper 90% central tendency limit)	99th percentile (upper 98% central tendency limit)
5	-52.1%	-44.8%	-7.0%	61.1%	106.8%	-55.8%	-44.8%	-7.1%	61.1%	106.8%
6	-49.2%	-40.7%	-5.2%	58.2%	93.5%	-49.0%	-41.1%	-5.0%	56.4%	90.0%
7	-50.2%	-39.4%	-4.8%	52.0%	85.0%	-50.5%	-39.6%	-4.9%	52.1%	85.0%
8	-45.0%	-35.9%	-3.4%	47.3%	74.3%	-45.0%	-36.1%	-3.5%	48.4%	76.8%
9	-45.9%	-35.5%	-3.6%	41.7%	71.9%	-45.3%	-35.2%	-3.3%	42.3%	70.1%
10	-44.0%	-33.9%	-2.3%	40.3%	64.2%	-43.7%	-33.9%	-2.3%	40.1%	62.6%
11	-41.6%	-31.4%	-2.9%	40.5%	65.8%	-41.5%	-31.6%	-3.2%	42.9%	66.9%
12	-38.9%	-30.6%	-1.8%	39.3%	59.5%	-39.1%	-31.2%	-1.7%	39.5%	61.2%
13	-38.0%	-29.3%	-2.4%	37.9%	59.0%	-37.5%	-29.7%	-2.6%	38.6%	61.0%
14	-37.0%	-28.8%	-1.9%	35.4%	56.3%	-36.9%	-28.6%	-2.1%	35.7%	56.4%
15	-36.3%	-28.5%	-2.3%	33.4%	52.9%	-36.5%	-28.4%	-2.8%	34.7%	49.7%
20	-32.4%	-25.4%	-1.6%	27.7%	48.5%	-32.6%	-25.7%	-1.7%	27.8%	49.6%
30	-26.7%	-20.3%	-1.6%	23.7%	32.9%	-27.2%	-20.9%	-1.8%	22.8%	34.2%
40	-23.6%	-18.5%	-0.6%	22.1%	32.3%	-22.9%	-18.4%	-0.6%	22.6%	32.4%
50	-21.7%	-16.3%	-0.5%	18.9%	29.0%	-22.3%	-16.8%	-0.5%	19.5%	29.1%
75	-17.4%	-13.5%	-0.7%	14.5%	22.7%	-18.1%	-13.6%	-0.8%	14.9%	23.0%
100	-15.2%	-11.8%	-0.3%	12.8%	19.2%	-15.1%	-12.0%	-0.3%	12.8%	19.8%
250	-10.1%	-7.6%	-0.2%	7.8%	10.9%	-10.3%	-7.5%	-0.1%	7.7%	10.9%
500	-7.3%	-5.3%	0.3%	5.6%	8.0%	-7.5%	-5.4%	0.3%	5.7%	7.9%

(grey numbers record the distribution of Sichel T estimates)

A summary of the the results of the sample campaign simulation over a two-parameter lognormal distribution, where μ = 0.20 cts/stn and σ^2 = 0.45.
This represents a case, for diamond size-frequency distribution, which is likely to occur at Site 3.
The distribution of the mean estimates, for each value of n, is defined by 1500 values resulting from 1500 sample campaign realisations.
Percentile values are expressed in terms of their percentage deviation from the actual mean of the population (ie. μ = 0.20 cts/stn).

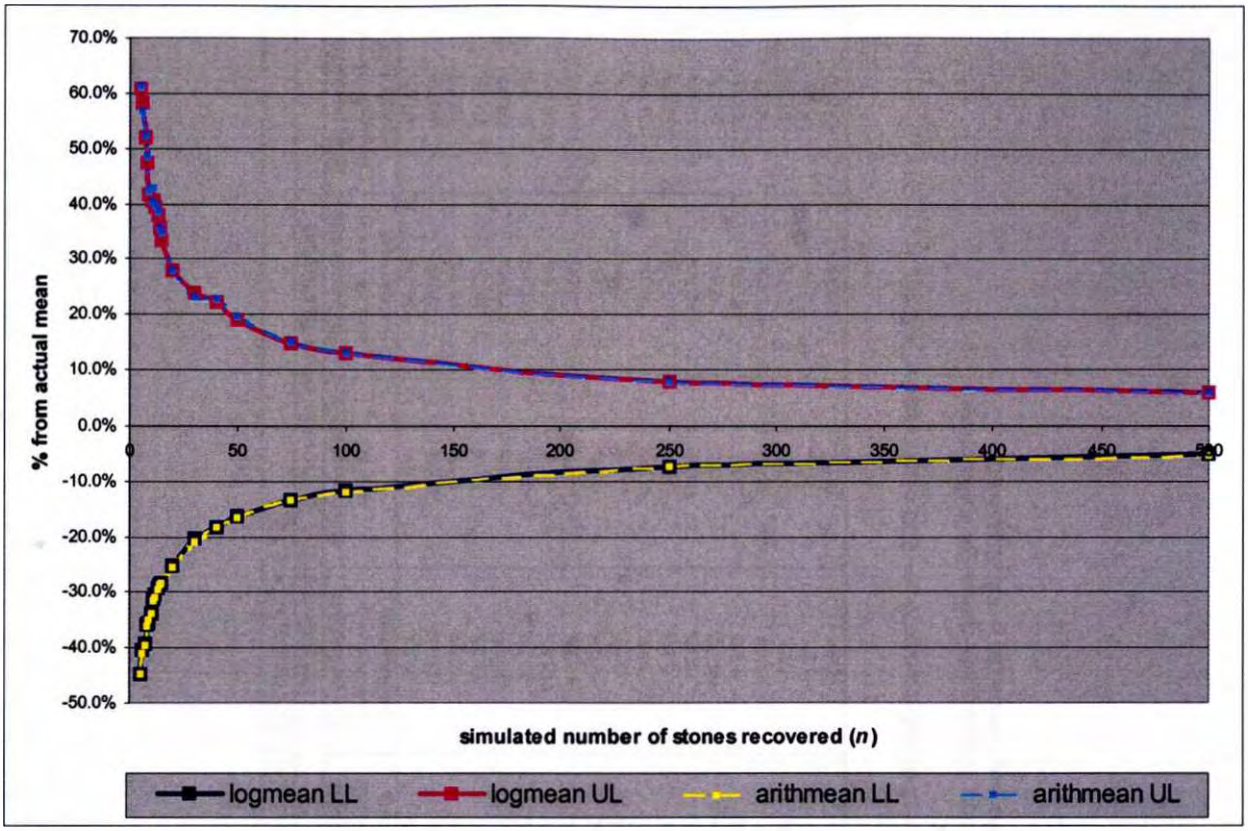

A graph of the 5th and 95th percentile values (90% central tendency limits) of the distributions of the mean estimates for the sample campaign simulation where μ = 0.20 cts/stn and σ^2 = 0.45. This represents a case, for diamond size-frequency distribution, which is likely to occur at Site 3. The 5th and 95th percentile values, for each value of *n*, are drawn from the distribution of 1500 values resulting from 1500 sample campaign realisations. Percentile values are expressed in terms of their percentage deviation from the actual mean of the population (ie. μ = 0.20 cts/stn).

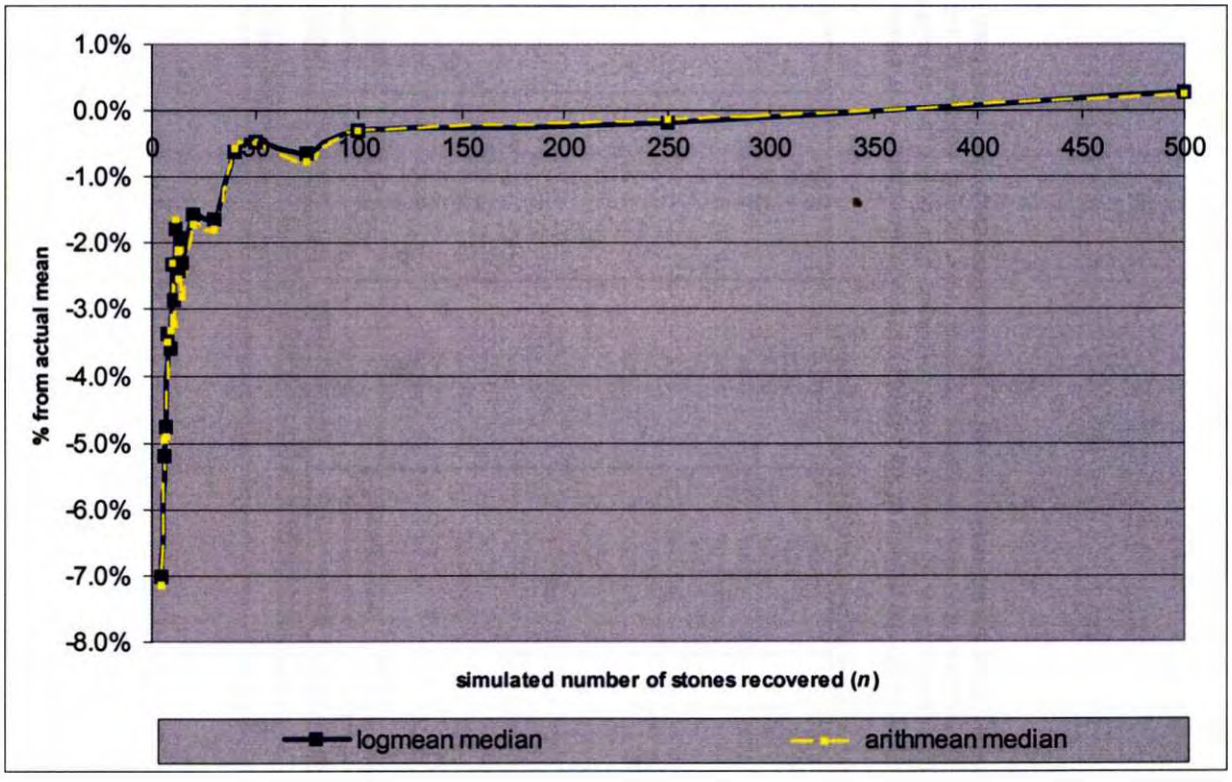

A graph of the 50th percentile values (medians) of the distributions of the mean estimates for the sample campaign simulation where μ = 0.20 cts/stn and σ^2 = 0.45. This represents a case, for diamond size-frequency distribution, which is likely to occur at Site 3. The 50th percentile values, for each value of *n*, are drawn from the distribution of 1500 values resulting from 1500 sample campaign realisations. Percentile values are expressed in terms of their percentage deviation from the actual mean of the population (ie. μ = 0.20 cts/stn).

	Lognormal Distribution Parameters for Simulation : μ = 0.30 cts/stn; σ^2 = 0.15									
	Distribution of the Lognormal Mean Estimates					Distribution of the Arithmetic Mean Estimates				
n	1st percentile (lower 98% central tendency limit)	5th percentile (lower 90% central tendency limit)	50th percentile (median)	95th percentile (upper 90% central tendency limit)	99th percentile (upper 98% central tendency limit)	1st percentile (lower 98% central tendency limit)	5th percentile (lower 90% central tendency limit)	50th percentile (median)	95th percentile (upper 90% central tendency limit)	99th percentile (upper 98% central tendency limit)
5	-35.2%	-28.1%	-1.4%	28.7%	43.2%	-36.5%	-28.1%	-1.4%	28.6%	43.6%
6	-33.9%	-23.7%	-1.6%	29.6%	46.4%	-33.9%	-23.8%	-1.5%	29.6%	46.9%
7	-29.5%	-22.9%	-1.1%	27.9%	43.0%	-29.6%	-22.8%	-1.1%	28.1%	43.5%
8	-27.4%	-22.2%	-1.0%	23.8%	37.8%	-27.3%	-22.2%	-1.0%	24.0%	37.7%
9	-27.4%	-20.1%	-1.4%	23.3%	33.2%	-27.1%	-20.0%	-1.4%	23.4%	33.9%
10	-25.8%	-20.1%	-1.0%	21.0%	31.6%	-25.8%	-20.2%	-0.9%	21.1%	32.2%
11	-25.8%	-18.1%	-0.5%	20.7%	27.7%	-26.1%	-18.3%	-0.5%	20.9%	28.3%
12	-23.9%	-17.3%	-0.6%	20.2%	29.6%	-23.9%	-17.3%	-0.6%	20.5%	30.3%
13	-22.0%	-17.3%	-1.1%	17.2%	26.6%	-21.9%	-17.2%	-1.0%	17.4%	26.8%
14	-22.1%	-15.7%	-0.7%	18.5%	26.4%	-22.3%	-15.8%	-0.6%	18.8%	25.7%
15	-23.2%	-16.3%	-0.2%	18.4%	25.5%	-23.1%	-16.4%	-0.3%	18.3%	26.3%
20	-20.1%	-14.1%	-0.6%	15.1%	22.7%	-20.1%	-13.8%	-0.7%	15.2%	22.5%
30	-15.4%	-11.1%	0.1%	12.3%	18.1%	-15.2%	-11.1%	0.0%	12.0%	18.2%
40	-14.0%	-10.1%	0.0%	10.6%	14.4%	-13.8%	-10.0%	0.0%	10.5%	14.2%
50	-12.0%	-9.4%	0.0%	9.6%	13.8%	-12.0%	-9.3%	0.0%	9.5%	13.8%
75	-9.5%	-6.9%	0.0%	8.1%	10.7%	-9.5%	-6.8%	-0.1%	8.0%	10.7%
100	-9.2%	-6.2%	0.2%	6.8%	9.8%	-9.1%	-6.2%	0.2%	6.8%	10.2%
250	-6.3%	-4.2%	0.0%	4.1%	5.6%	-6.4%	-4.2%	0.0%	4.2%	5.8%
500	-3.9%	-2.9%	0.1%	2.9%	4.3%	-3.9%	-2.9%	0.1%	3.0%	4.2%

(grey numbers record the distribution of Sichel T estimates)

A summary of the the results of the sample campaign simulation over a two-parameter lognormal distribution, where μ = 0.30 cts/stn and σ^2 = 0.15.
This represents a case, for diamond size-frequency distribution, which is likely to occur at Site 3.
The distribution of the mean estimates, for each value of n, is defined by 1500 values resulting from 1500 sample campaign realisations.
Percentile values are expressed in terms of their percentage deviation from the actual mean of the population (ie. μ = 0.30 cts/stn).

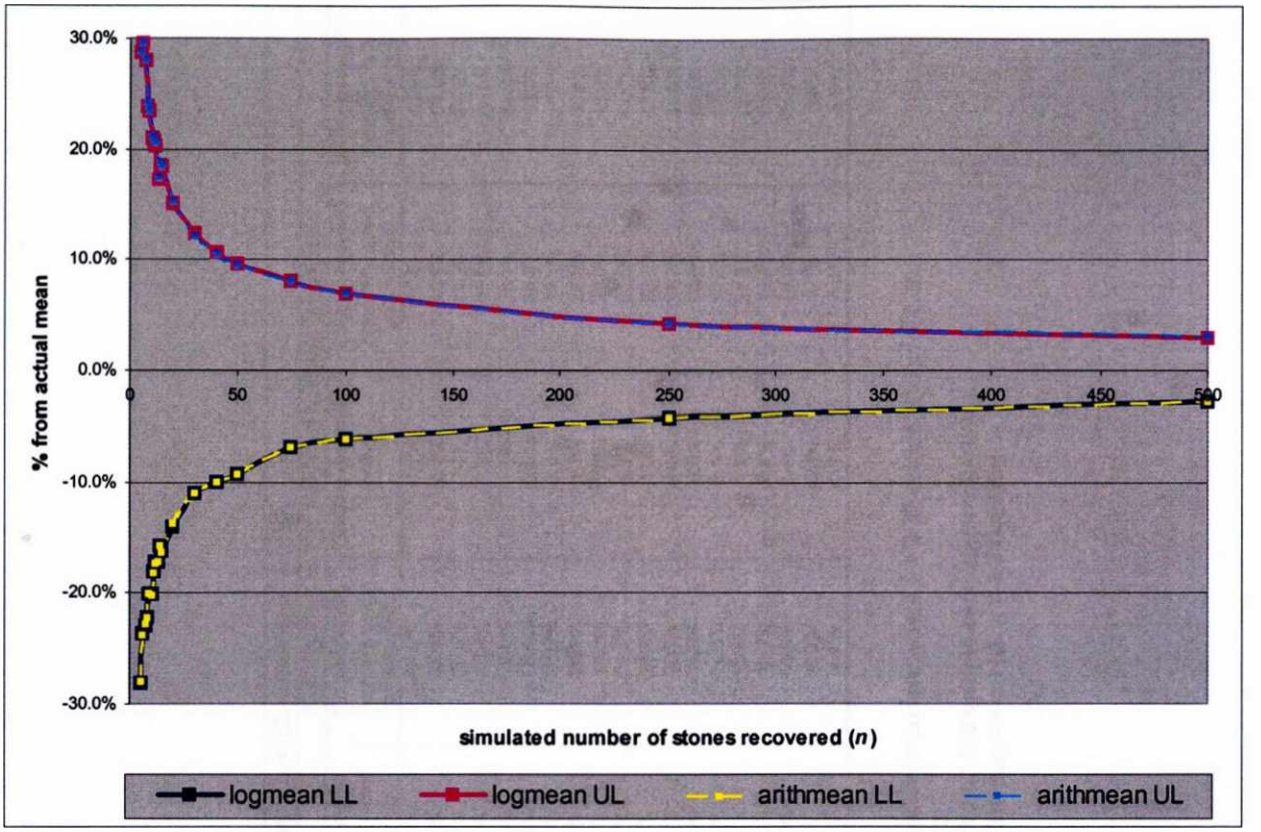

A graph of the 5th and 95th percentile values (90% central tendency limits) of the distributions of the mean estimates for the sample campaign simulation where μ = 0.30 cts/stn and σ^2 = 0.15. This represents a case, for diamond size-frequency distribution, which is likely to occur at Site 3. The 5th and 95th percentile values, for each value of *n*, are drawn from the distribution of 1500 values resulting from 1500 sample campaign realisations. Percentile values are expressed in terms of their percentage deviation from the actual mean of the population (ie. μ = 0.30 cts/stn).

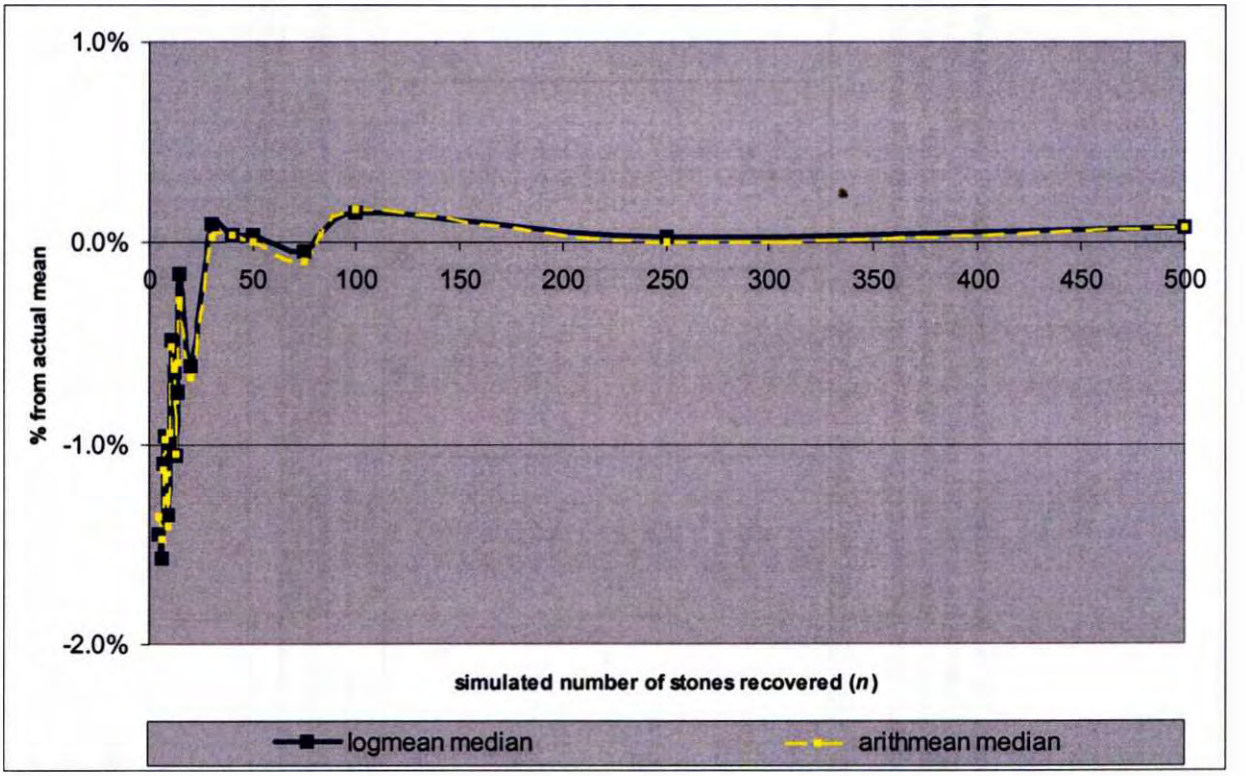

A graph of the 50th percentile values (medians) of the distributions of the mean estimates for the sample campaign simulation where μ = 0.30 cts/stn and σ^2 = 0.15. This represents a case, for diamond size-frequency distribution, which is likely to occur at Site 3. The 50th percentile values, for each value of *n*, are drawn from the distribution of 1500 values resulting from 1500 sample campaign realisations. Percentile values are expressed in terms of their percentage deviation from the actual mean of the population (ie. μ = 0.30 cts/stn).

	Lognormal Distribution Parameters for Simulation : μ = 0.30 cts/stn; σ^2 = 0.30									
	Distribution of the Lognormal Mean Estimates					Distribution of the Arithmetic Mean Estimates				
n	1st percentile (lower 98% central tendency limit)	5th percentile (lower 90% central tendency limit)	50th percentile (median)	95th percentile (upper 90% central tendency limit)	99th percentile (upper 98% central tendency limit)	1st percentile (lower 98% central tendency limit)	5th percentile (lower 90% central tendency limit)	50th percentile (median)	95th percentile (upper 90% central tendency limit)	99th percentile (upper 98% central tendency limit)
5	-44.8%	-37.1%	-3.0%	50.0%	78.4%	-45.3%	-37.0%	-3.0%	49.8%	78.4%
6	-41.8%	-33.9%	-3.1%	44.3%	69.1%	-41.8%	-34.3%	-2.8%	45.6%	69.6%
7	-40.8%	-30.6%	-2.0%	39.2%	61.9%	-40.8%	-30.5%	-2.1%	39.2%	61.5%
8	-38.2%	-30.3%	-2.3%	36.5%	53.2%	-38.0%	-30.4%	-2.6%	37.0%	54.2%
9	-34.5%	-28.9%	-1.6%	36.5%	56.8%	-34.8%	-29.0%	-1.4%	38.1%	59.2%
10	-34.9%	-26.2%	-0.4%	35.6%	52.8%	-34.9%	-26.5%	-0.5%	35.8%	48.6%
11	-34.7%	-26.4%	-3.3%	33.1%	50.6%	-35.0%	-26.8%	-3.4%	33.1%	50.5%
12	-31.5%	-25.7%	-1.7%	30.0%	49.3%	-31.6%	-25.9%	-1.7%	29.5%	50.4%
13	-32.1%	-23.9%	-1.2%	29.9%	47.2%	-32.7%	-24.2%	-1.3%	29.5%	48.0%
14	-32.0%	-23.9%	-1.1%	27.3%	41.3%	-32.1%	-24.1%	-1.2%	27.5%	41.3%
15	-28.3%	-22.7%	-1.1%	28.8%	43.2%	-28.4%	-22.6%	-1.0%	29.0%	47.0%
20	-26.6%	-20.4%	-1.4%	22.6%	33.2%	-26.4%	-20.7%	-1.4%	23.1%	34.6%
30	-21.6%	-15.8%	-0.4%	18.7%	27.4%	-21.8%	-15.9%	-0.5%	19.0%	28.5%
40	-19.5%	-14.5%	-0.5%	16.5%	23.2%	-19.4%	-14.6%	-0.4%	16.5%	23.0%
50	-18.7%	-13.6%	-0.8%	14.7%	20.9%	-18.6%	-13.6%	-0.8%	14.3%	20.6%
75	-14.5%	-10.4%	0.0%	11.9%	17.2%	-14.6%	-10.2%	-0.1%	12.0%	18.4%
100	-13.4%	-9.7%	-0.1%	9.9%	15.3%	-13.3%	-10.0%	0.0%	10.0%	14.7%
250	-8.8%	-5.9%	-0.1%	6.3%	8.6%	-8.9%	-6.0%	-0.2%	6.1%	8.8%
500	-5.7%	-4.2%	-0.1%	4.5%	6.5%	-5.8%	-4.1%	-0.1%	4.5%	6.5%

(grey numbers record the distribution of Sichel T estimates)

A summary of the the results of the sample campaign simulation over a two-parameter lognormal distribution, where μ = 0.30 cts/stn and σ^2 = 0.30.
This represents a case, for diamond size-frequency distribution, which is likely to occur at Site 3.
The distribution of the mean estimates, for each value of n, is defined by 1500 values resulting from 1500 sample campaign realisations.
Percentile values are expressed in terms of their percentage deviation from the actual mean of the population (ie. μ = 0.30 cts/stn).

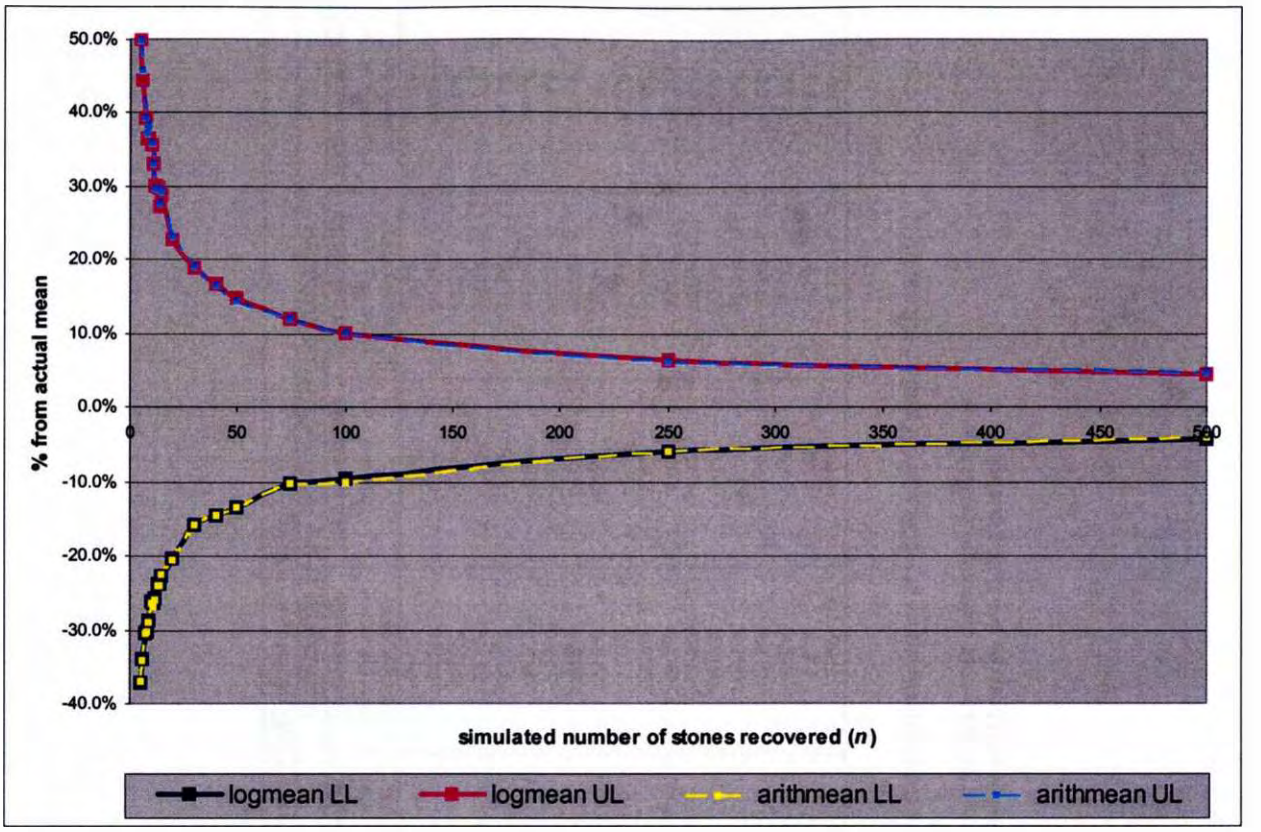

A graph of the 5th and 95th percentile values (90% central tendency limits) of the distributions of the mean estimates for the sample campaign simulation where μ = 0.30 cts/stn and σ^2 = 0.30. This represents a case, for diamond size-frequency distribution, which is likely to occur at Site 3. The 5th and 95th percentile values, for each value of *n*, are drawn from the distribution of 1500 values resulting from 1500 sample campaign realisations. Percentile values are expressed in terms of their percentage deviation from the actual mean of the population (ie. μ = 0.30 cts/stn).

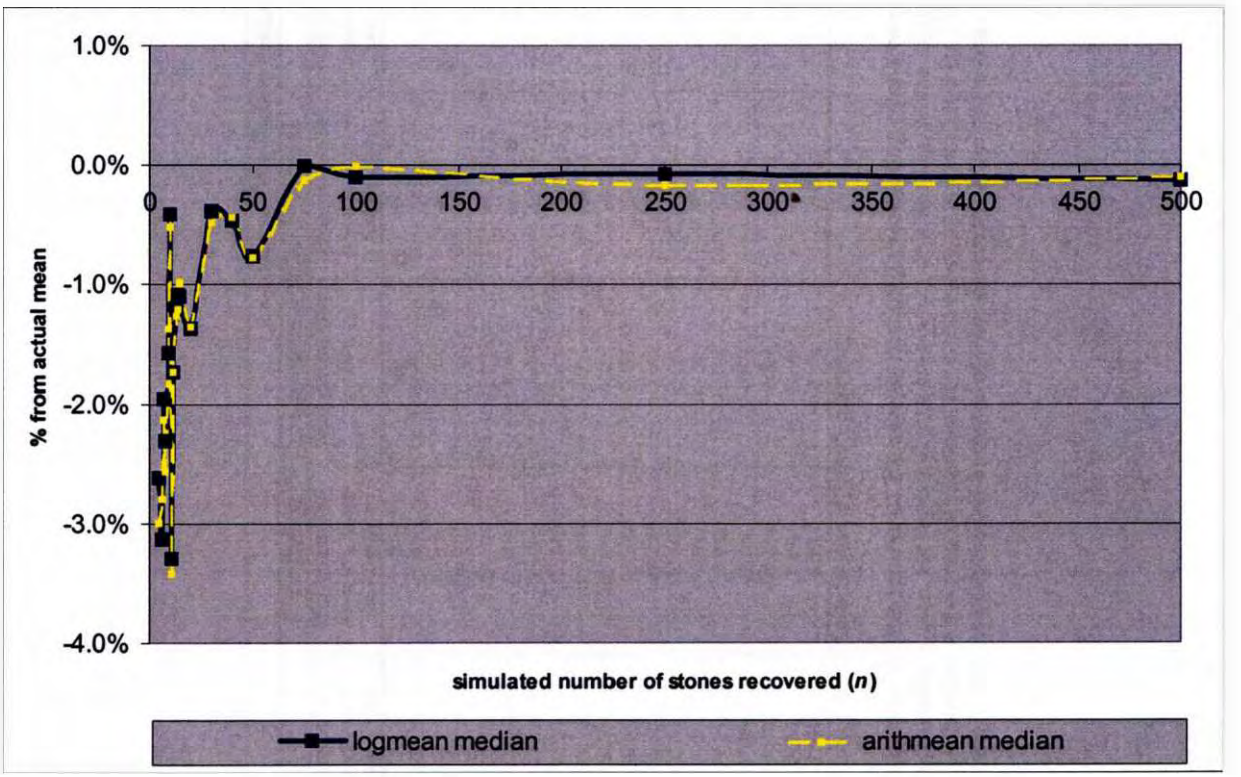

A graph of the 50th percentile values (medians) of the distributions of the mean estimates for the sample campaign simulation where μ = 0.30 cts/stn and σ^2 = 0.30. This represents a case, for diamond size-frequency distribution, which is likely to occur at Site 3. The 50th percentile values, for each value of *n*, are drawn from the distribution of 1500 values resulting from 1500 sample campaign realisations. Percentile values are expressed in terms of their percentage deviation from the actual mean of the population (ie. μ = 0.30 cts/stn).

	Lognormal Distribution Parameters for Simulation : μ = 0.30 cts/stn; σ^2 = 0.45									
	Distribution of the Lognormal Mean Estimates					Distribution of the Arithmetic Mean Estimates				
n	1st percentile (lower 98% central tendency limit)	5th percentile (lower 90% central tendency limit)	50th percentile (median)	95th percentile (upper 90% central tendency limit)	99th percentile (upper 98% central tendency limit)	1st percentile (lower 98% central tendency limit)	5th percentile (lower 90% central tendency limit)	50th percentile (median)	95th percentile (upper 90% central tendency limit)	99th percentile (upper 98% central tendency limit)
5	-55.4%	-44.4%	-5.1%	59.2%	[illegible]	-55.7%	-44.5%	-5.6%	58.7%	95.8%
6	-50.7%	-40.4%	-4.7%	54.1%	94.9%	-50.9%	-40.3%	-5.2%	54.7%	90.6%
7	-47.0%	-38.1%	-3.0%	45.7%	75.4%	-47.1%	-38.2%	-3.1%	47.2%	80.0%
8	-45.7%	-35.3%	-3.1%	47.3%	71.7%	-44.3%	-35.1%	-3.1%	46.7%	74.2%
9	-43.7%	-34.1%	-2.8%	46.0%	70.9%	-44.4%	-33.8%	-3.5%	45.8%	76.1%
10	-42.3%	-33.8%	-3.7%	44.3%	83.1%	-42.5%	-34.1%	-3.9%	44.3%	79.1%
11	-40.7%	-31.2%	-2.9%	39.6%	64.7%	-40.5%	-31.3%	-3.0%	40.7%	65.8%
12	-40.0%	-30.3%	-2.0%	39.6%	58.0%	-40.2%	-30.5%	-2.0%	40.2%	59.1%
13	-39.7%	-28.9%	-1.7%	38.6%	57.1%	-38.3%	-29.3%	-2.0%	39.7%	62.9%
14	-36.5%	-27.0%	-2.8%	36.2%	55.6%	-36.7%	-27.0%	-2.5%	37.0%	56.9%
15	-36.5%	-28.0%	-2.5%	34.4%	51.6%	-37.2%	-27.8%	-2.4%	34.4%	54.2%
20	-32.7%	-24.2%	-1.6%	29.4%	46.1%	-32.9%	-24.2%	-1.4%	30.6%	48.3%
30	-26.6%	-20.6%	-1.2%	25.1%	38.5%	-26.4%	-21.0%	-1.2%	25.1%	39.0%
40	-24.5%	-18.9%	-1.0%	20.3%	29.2%	-24.8%	-19.0%	-1.1%	20.5%	29.9%
50	-21.2%	-15.8%	-0.4%	18.9%	26.8%	-20.8%	-15.7%	-0.3%	19.3%	27.2%
75	-17.6%	-13.0%	-0.4%	14.7%	21.9%	-17.9%	-13.2%	-0.5%	15.2%	23.8%
100	-16.1%	-11.8%	-0.6%	12.7%	17.4%	-16.8%	-12.2%	-0.6%	13.0%	18.3%
250	-9.7%	-7.1%	-0.1%	8.1%	10.7%	-10.4%	-7.3%	-0.2%	8.2%	11.5%
500	-7.2%	-5.1%	-0.1%	5.5%	8.1%	-7.4%	-5.1%	-0.1%	5.7%	8.2%

(grey numbers record the distribution of Sichel T estimates)

A summary of the the results of the sample campaign simulation over a two-parameter lognormal distribution, where μ = 0.30 cts/stn and σ^2 = 0.45.
This represents a case, for diamond size-frequency distribution, which is likely to occur at Site 3.
The distribution of the mean estimates, for each value of n, is defined by 1500 values resulting from 1500 sample campaign realisations.
Percentile values are expressed in terms of their percentage deviation from the actual mean of the population (ie. μ = 0.30 cts/stn).

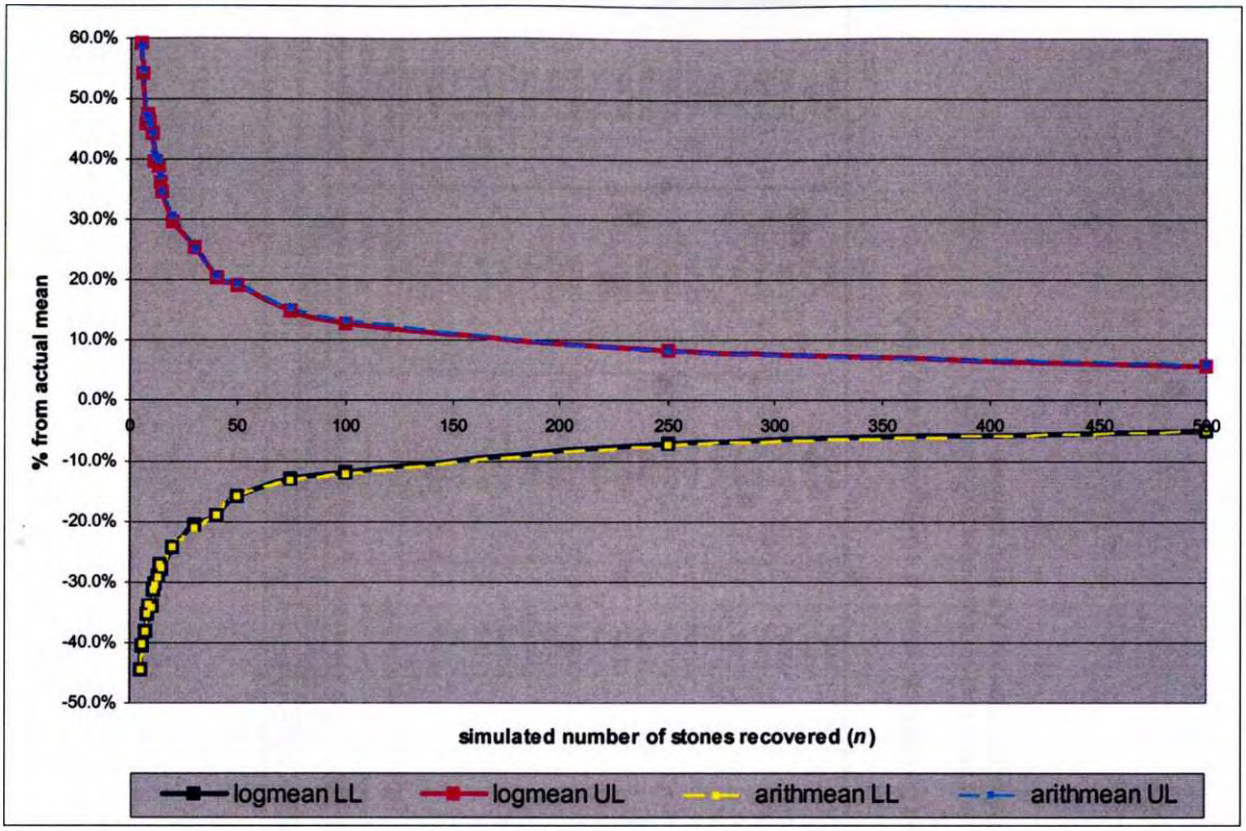

A graph of the 5th and 95th percentile values (90% central tendency limits) of the distributions of the mean estimates for the sample campaign simulation where μ = 0.30 cts/stn and σ^2 = 0.45. This represents a case, for diamond size-frequency distribution, which is likely to occur at Site 3. The 5th and 95th percentile values, for each value of *n*, are drawn from the distribution of 1500 values resulting from 1500 sample campaign realisations. Percentile values are expressed in terms of their percentage deviation from the actual mean of the population (ie. μ = 0.30 cts/stn).

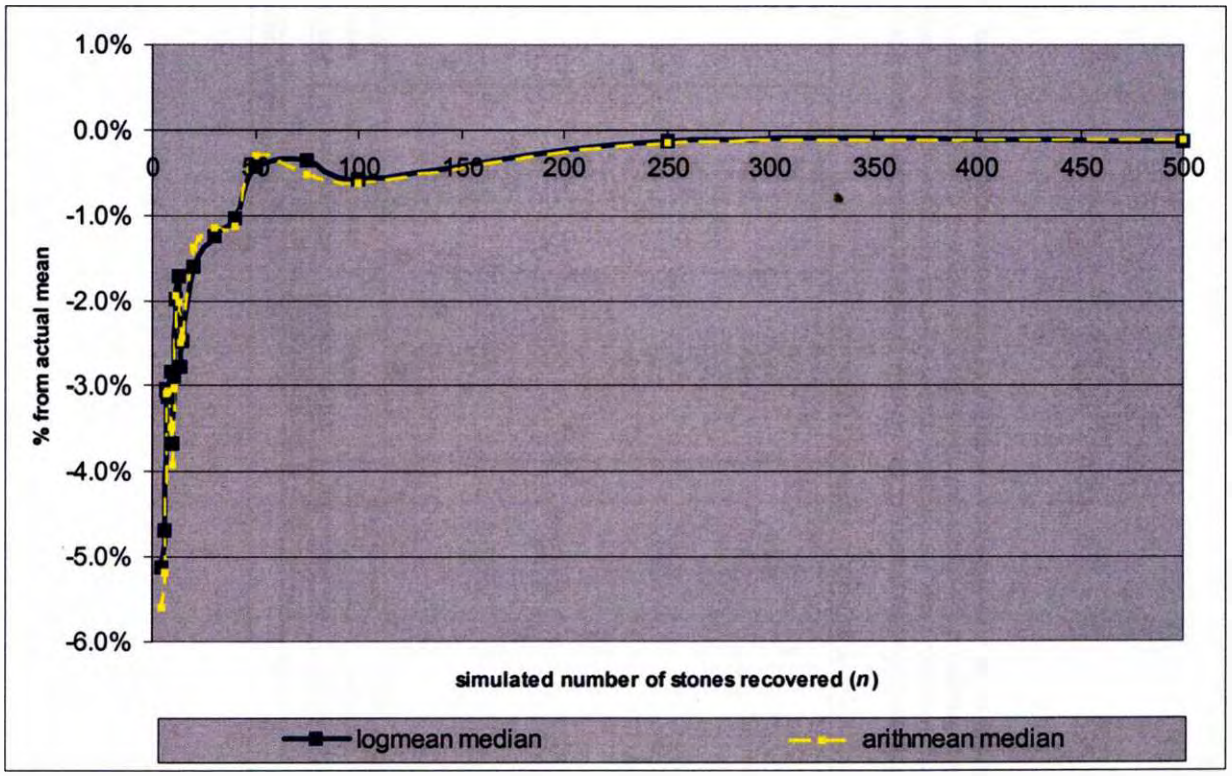

A graph of the 50th percentile values (medians) of the distributions of the mean estimates for the sample campaign simulation where μ = 0.30 cts/stn and σ^2 = 0.45. This represents a case, for diamond size-frequency distribution, which is likely to occur at Site 3. The 50th percentile values, for each value of *n*, are drawn from the distribution of 1500 values resulting from 1500 sample campaign realisations. Percentile values are expressed in terms of their percentage deviation from the actual mean of the population (ie. μ = 0.30 cts/stn).

	Lognormal Distribution Parameters for Simulation : μ = 0.40 cts/stn; σ^2 = 0.15									
	Distribution of the Lognormal Mean Estimates					Distribution of the Arithmetic Mean Estimates				
n	1st percentile (lower 98% central tendency limit)	5th percentile (lower 90% central tendency limit)	50th percentile (median)	95th percentile (upper 90% central tendency limit)	99th percentile (upper 98% central tendency limit)	1st percentile (lower 98% central tendency limit)	5th percentile (lower 90% central tendency limit)	50th percentile (median)	95th percentile (upper 90% central tendency limit)	99th percentile (upper 98% central tendency limit)
5	-34.1%	-26.3%	-1.8%	31.0%	52.1%	-34.1%	-26.3%	-1.8%	31.3%	52.1%
6	-30.3%	-24.5%	-1.4%	29.2%	46.2%	-30.3%	-24.5%	-1.4%	30.1%	46.5%
7	-30.0%	-23.1%	-0.9%	26.9%	40.6%	-30.1%	-23.2%	-0.9%	26.8%	40.1%
8	-27.8%	-21.5%	0.1%	24.1%	35.1%	-27.6%	-21.5%	0.1%	23.9%	35.8%
9	-26.0%	-19.8%	-1.2%	21.9%	33.7%	-25.9%	-19.9%	-1.0%	22.0%	33.2%
10	-26.2%	-19.3%	-1.0%	21.2%	33.5%	-26.4%	-19.3%	-1.0%	21.3%	33.3%
11	-24.9%	-18.6%	-0.8%	20.9%	31.0%	-24.3%	-18.6%	-0.8%	20.9%	31.2%
12	-23.2%	-17.8%	-1.0%	19.4%	29.8%	-23.0%	-17.8%	-0.8%	19.8%	30.2%
13	-23.7%	-17.7%	-0.4%	19.5%	31.4%	-24.4%	-17.7%	-0.1%	19.6%	31.7%
14	-22.2%	-16.3%	-0.3%	18.3%	27.1%	-21.9%	-16.4%	-0.4%	18.4%	26.9%
15	-21.0%	-14.8%	-0.6%	18.0%	26.3%	-21.0%	-14.8%	-0.6%	18.5%	26.7%
20	-19.3%	-14.3%	-0.5%	15.5%	22.4%	-18.7%	-14.3%	-0.5%	15.6%	21.9%
30	-15.5%	-12.0%	-0.2%	12.2%	17.8%	-15.4%	-12.1%	-0.2%	12.3%	18.0%
40	-13.8%	-10.7%	0.0%	10.9%	15.4%	-13.9%	-10.8%	0.0%	10.7%	16.0%
50	-11.8%	-8.9%	-0.2%	10.2%	14.8%	-11.7%	-8.8%	-0.2%	10.0%	14.8%
75	-10.2%	-7.4%	0.1%	8.0%	11.4%	-10.1%	-7.5%	0.1%	8.1%	11.5%
100	-8.8%	-6.5%	-0.3%	7.0%	10.1%	-8.9%	-6.5%	-0.3%	7.0%	10.1%
250	-5.5%	-4.0%	0.0%	4.3%	6.0%	-5.6%	-4.0%	0.0%	4.4%	6.0%
500	-4.0%	-2.9%	0.0%	2.9%	4.1%	-4.1%	-3.0%	0.0%	2.9%	4.0%

(grey numbers record the distribution of Sichel T estimates)

A summary of the the results of the sample campaign simulation over a two-parameter lognormal distribution, where μ = 0.40 cts/stn and σ^2 = 0.15.
This represents a case, for diamond size-frequency distribution, which is likely to occur at Site 3.
The distribution of the mean estimates, for each value of n, is defined by 1500 values resulting from 1500 sample campaign realisations.
Percentile values are expressed in terms of their percentage deviation from the actual mean of the population (ie. μ = 0.40 cts/stn).

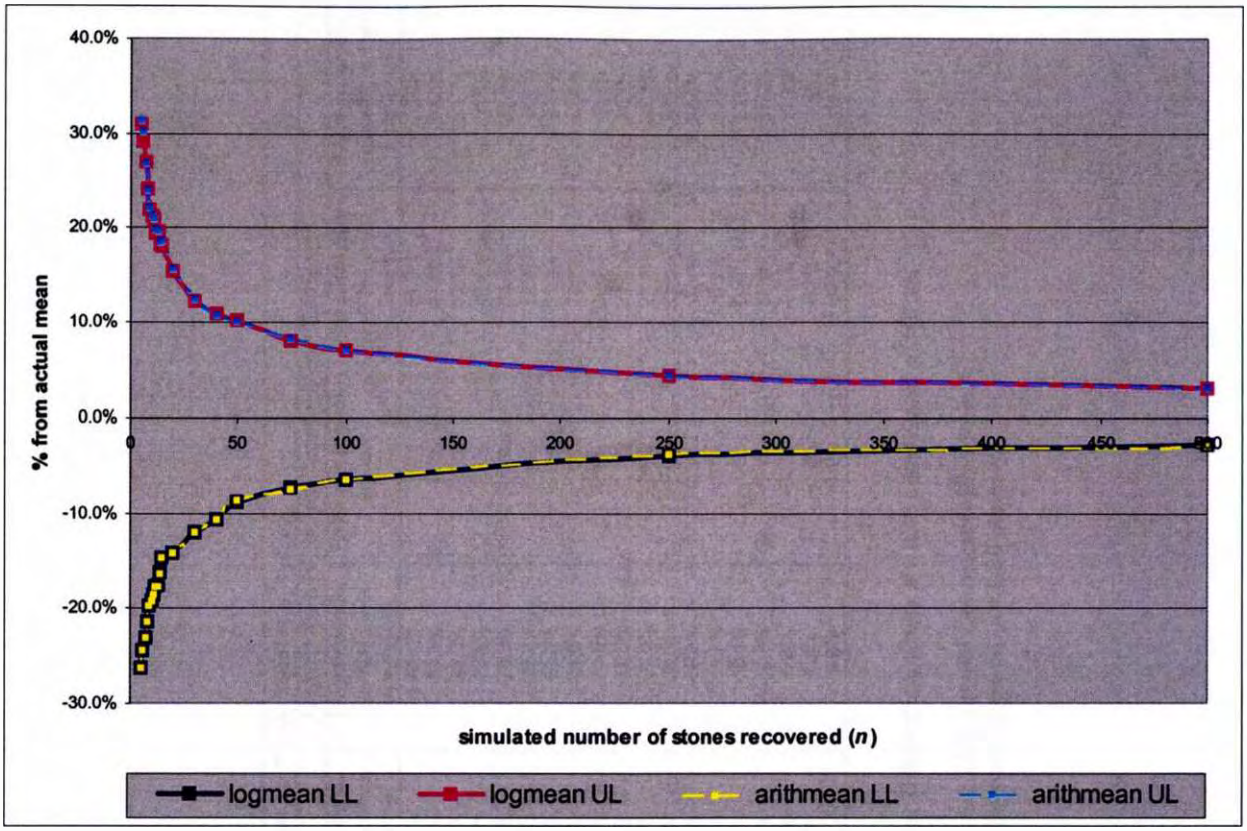

A graph of the 5th and 95th percentile values (90% central tendency limits) of the distributions of the mean estimates for the sample campaign simulation where μ = 0.40 cts/stn and σ^2 = 0.15. This represents a case, for diamond size-frequency distribution, which is likely to occur at Site 3. The 5th and 95th percentile values, for each value of n, are drawn from the distribution of 1500 values resulting from 1500 sample campaign realisations. Percentile values are expressed in terms of their percentage deviation from the actual mean of the population (ie. μ = 0.40 cts/stn).

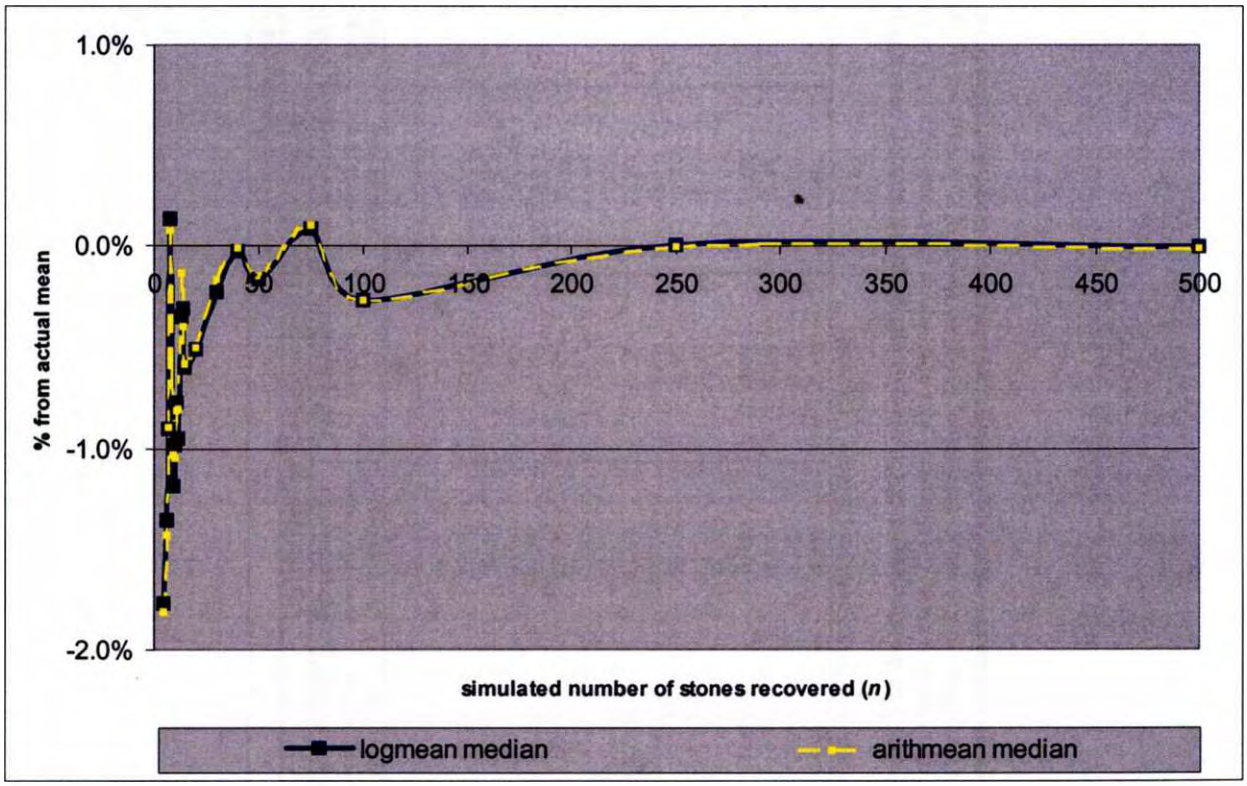

A graph of the 50th percentile values (medians) of the distributions of the mean estimates for the sample campaign simulation where μ = 0.40 cts/stn and σ^2 = 0.15. This represents a case, for diamond size-frequency distribution, which is likely to occur at Site 3. The 50th percentile values, for each value of n, are drawn from the distribution of 1500 values resulting from 1500 sample campaign realisations. Percentile values are expressed in terms of their percentage deviation from the actual mean of the population (ie. μ = 0.40 cts/stn).

	Lognormal Distribution Parameters for Simulation : μ = 0.40 cts/stn; σ^2 = 0.30									
	Distribution of the Lognormal Mean Estimates					Distribution of the Arithmetic Mean Estimates				
n	1st percentile (lower 98% central tendency limit)	5th percentile (lower 90% central tendency limit)	50th percentile (median)	95th percentile (upper 90% central tendency limit)	99th percentile (upper 98% central tendency limit)	1st percentile (lower 98% central tendency limit)	5th percentile (lower 90% central tendency limit)	50th percentile (median)	95th percentile (upper 90% central tendency limit)	99th percentile (upper 98% central tendency limit)
5	-44.9%	-38.3%	-3.8%	44.3%	71.1%	-45.2%	-36.8%	-3.7%	47.0%	73.0%
6	-42.8%	-35.1%	-3.8%	43.8%	67.3%	-42.8%	-34.7%	-4.1%	44.0%	68.8%
7	-39.2%	-31.8%	-2.5%	38.7%	63.4%	-40.2%	-32.0%	-2.6%	39.1%	63.7%
8	-39.3%	-29.7%	-2.1%	38.2%	62.1%	-39.1%	-29.8%	-2.4%	38.6%	60.5%
9	-38.4%	-28.6%	-1.7%	37.6%	57.0%	-37.6%	-28.3%	-2.0%	36.9%	57.0%
10	-33.8%	-26.6%	-0.8%	32.9%	51.2%	-33.9%	-26.5%	-0.9%	32.3%	49.6%
11	-34.6%	-26.0%	-1.7%	32.9%	50.0%	-35.4%	-26.0%	-1.8%	31.8%	50.7%
12	-32.5%	-26.3%	-1.2%	28.0%	42.8%	-32.4%	-26.0%	-1.5%	27.7%	43.6%
13	-32.2%	-24.6%	-2.4%	27.5%	45.3%	-33.1%	-24.8%	-2.5%	28.5%	44.7%
14	-30.2%	-23.9%	-0.8%	27.5%	41.7%	-30.3%	-24.0%	-0.8%	27.4%	44.7%
15	-31.1%	-23.0%	-0.7%	25.6%	38.3%	-31.0%	-23.0%	-0.8%	25.7%	38.3%
20	-27.4%	-20.4%	-0.8%	21.4%	32.6%	-27.2%	-20.3%	-0.8%	21.6%	32.2%
30	-22.7%	-16.7%	-0.4%	18.7%	26.8%	-22.9%	-16.8%	-0.3%	19.1%	27.0%
40	-18.9%	-14.6%	-0.5%	15.7%	23.5%	-19.0%	-14.7%	-0.6%	16.1%	23.2%
50	-16.9%	-12.9%	-0.5%	14.5%	20.9%	-16.9%	-13.1%	-0.4%	14.8%	20.6%
75	-14.6%	-10.6%	-0.4%	11.6%	16.5%	-14.6%	-10.8%	-0.4%	11.6%	17.2%
100	-11.5%	-8.6%	0.0%	10.3%	13.7%	-11.7%	-8.8%	-0.2%	9.9%	13.7%
250	-7.9%	-5.9%	-0.2%	6.1%	8.5%	-7.8%	-6.0%	-0.2%	6.2%	8.4%
500	-5.9%	-4.1%	-0.1%	4.4%	6.5%	-6.1%	-4.2%	-0.1%	4.5%	6.5%

(grey numbers record the distribution of Sichel T estimates)

A summary of the the results of the sample campaign simulation over a two-parameter lognormal distribution, where μ = 0.40 cts/stn and σ^2 = 0.30.
This represents a case, for diamond size-frequency distribution, which is likely to occur at Site 3.
The distribution of the mean estimates, for each value of n, is defined by 1500 values resulting from 1500 sample campaign realisations.
Percentile values are expressed in terms of their percentage deviation from the actual mean of the population (ie. μ = 0.40 cts/stn).

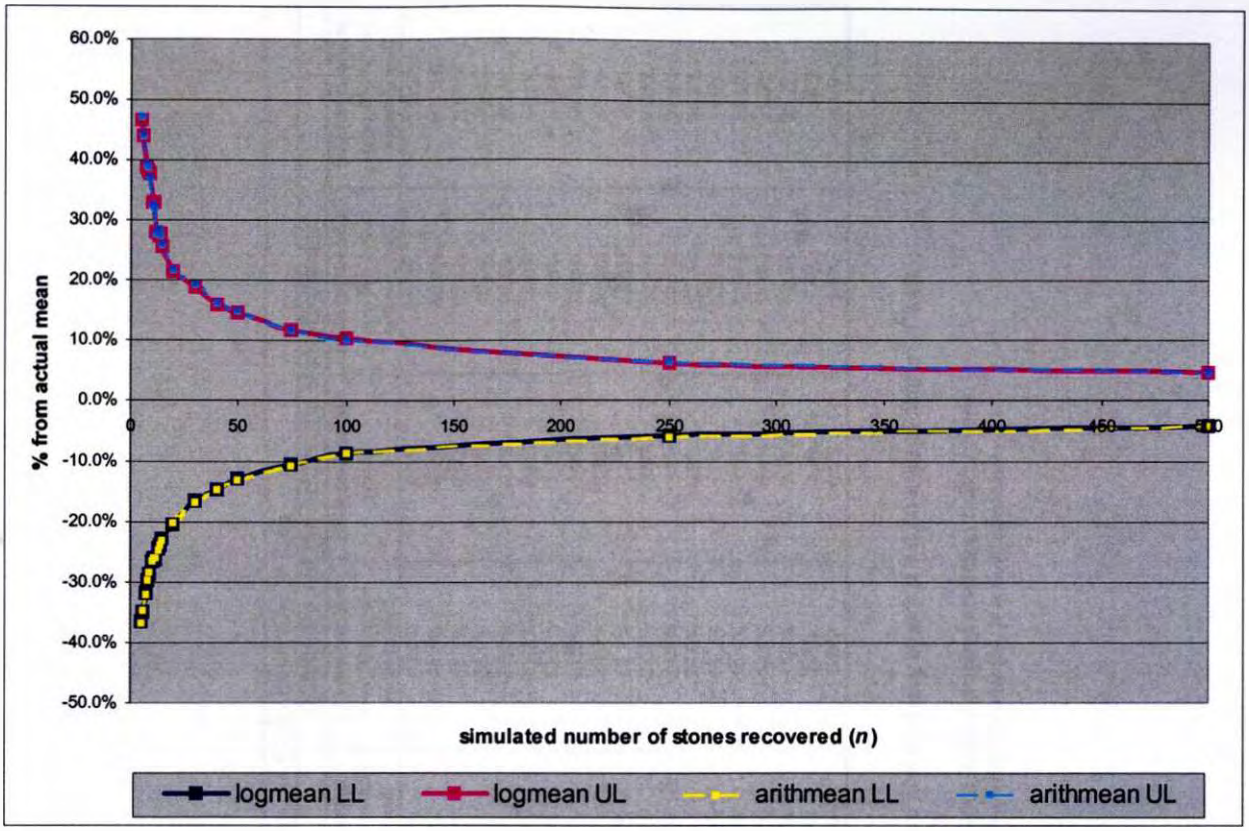

A graph of the 5th and 95th percentile values (90% central tendency limits) of the distributions of the mean estimates for the sample campaign simulation where μ = 0.40 cts/stn and σ^2 = 0.30. This represents a case, for diamond size-frequency distribution, which is likely to occur at Site 3. The 5th and 95th percentile values, for each value of n, are drawn from the distribution of 1500 values resulting from 1500 sample campaign realisations. Percentile values are expressed in terms of their percentage deviation from the actual mean of the population (ie. μ = 0.40 cts/stn).

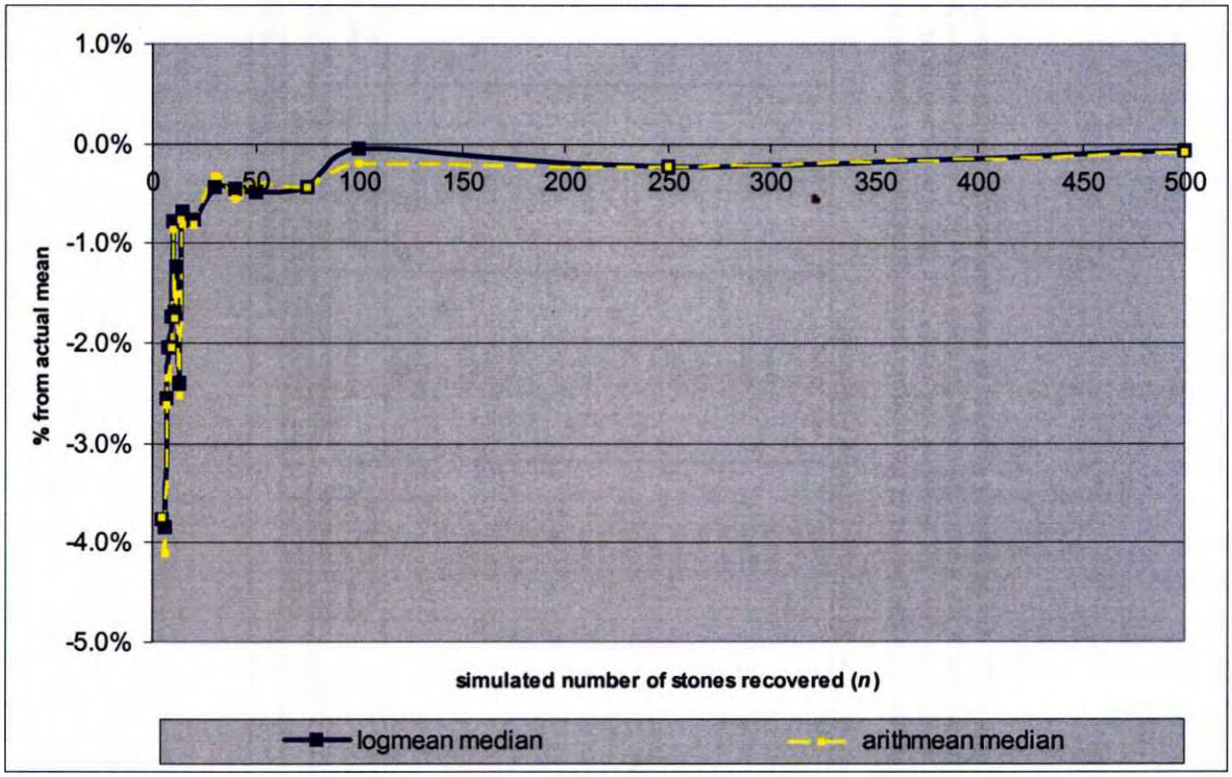

A graph of the 50th percentile values (medians) of the distributions of the mean estimates for the sample campaign simulation where μ = 0.40 cts/stn and σ^2 = 0.30. This represents a case, for diamond size-frequency distribution, which is likely to occur at Site 3. The 50th percentile values, for each value of n, are drawn from the distribution of 1500 values resulting from 1500 sample campaign realisations. Percentile values are expressed in terms of their percentage deviation from the actual mean of the population (ie. μ = 0.40 cts/stn).

	Lognormal Distribution Parameters for Simulation : μ = 0.40 cts/stn; σ^2 = 0.45									
	Distribution of the Lognormal Mean Estimates					Distribution of the Arithmetic Mean Estimates				
n	1st percentile (lower 98% central tendency limit)	5th percentile (lower 90% central tendency limit)	50th percentile (median)	95th percentile (upper 90% central tendency limit)	99th percentile (upper 98% central tendency limit)	1st percentile (lower 98% central tendency limit)	5th percentile (lower 90% central tendency limit)	50th percentile (median)	95th percentile (upper 90% central tendency limit)	99th percentile (upper 98% central tendency limit)
5	-54.1%	-43.6%	-4.5%	66.9%	122.5%	-54.0%	-43.6%	-4.5%	66.9%	122.5%
6	-52.4%	-41.0%	-4.2%	59.0%	97.4%	-52.7%	-41.1%	-4.2%	60.0%	101.1%
7	-49.9%	-38.0%	-2.5%	56.0%	85.1%	-50.0%	-38.1%	-2.8%	56.4%	84.6%
8	-45.1%	-35.4%	-2.6%	45.5%	70.2%	-45.5%	-35.6%	-2.9%	46.0%	76.9%
9	-43.8%	-33.8%	-2.2%	46.9%	70.1%	-43.3%	-34.0%	-2.4%	46.3%	66.8%
10	-42.2%	-33.3%	-2.7%	44.9%	74.0%	-42.1%	-33.2%	-2.9%	45.9%	78.5%
11	-41.2%	-32.4%	-2.7%	39.6%	58.4%	-41.7%	-32.4%	-2.7%	40.8%	58.6%
12	-39.5%	-31.5%	-2.4%	38.0%	58.8%	-40.3%	-31.7%	-2.6%	39.0%	59.4%
13	-39.0%	-29.4%	-2.9%	38.3%	57.2%	-38.7%	-29.9%	-2.8%	39.1%	60.1%
14	-38.0%	-28.8%	-2.7%	33.3%	57.2%	-38.7%	-29.1%	-2.8%	33.6%	57.5%
15	-35.6%	-27.0%	-0.7%	33.4%	51.8%	-36.0%	-27.3%	-0.8%	33.7%	53.9%
20	-32.6%	-23.8%	-0.9%	31.7%	48.0%	-32.6%	-23.6%	-1.1%	32.7%	50.4%
30	-28.5%	-20.8%	-1.0%	23.5%	34.8%	-29.5%	-21.0%	-0.9%	23.3%	36.3%
40	-22.4%	-17.1%	-0.7%	20.4%	29.7%	-22.9%	-17.2%	-1.0%	20.5%	31.9%
50	-22.2%	-16.1%	-0.7%	18.3%	27.8%	-22.4%	-16.4%	-0.5%	18.7%	28.8%
75	-19.3%	-13.8%	-0.2%	15.6%	22.1%	-19.1%	-13.7%	-0.4%	15.8%	21.9%
100	-15.6%	-11.5%	-0.1%	13.1%	19.6%	-15.7%	-11.4%	-0.1%	13.3%	20.2%
250	-11.3%	-7.6%	-0.3%	7.7%	12.5%	-11.3%	-7.8%	-0.3%	7.8%	12.4%
500	-7.5%	-5.1%	0.0%	5.9%	8.2%	-7.3%	-5.3%	-0.1%	5.9%	8.2%

(grey numbers record the distribution of Sichel T estimates)

A summary of the the results of the sample campaign simulation over a two-parameter lognormal distribution, where μ = 0.40 cts/stn and σ^2 = 0.45.
This represents a case, for diamond size-frequency distribution, which is likely to occur at Site 3.
The distribution of the mean estimates, for each value of n, is defined by 1500 values resulting from 1500 sample campaign realisations.
Percentile values are expressed in terms of their percentage deviation from the actual mean of the population (ie. μ = 0.40 cts/stn).

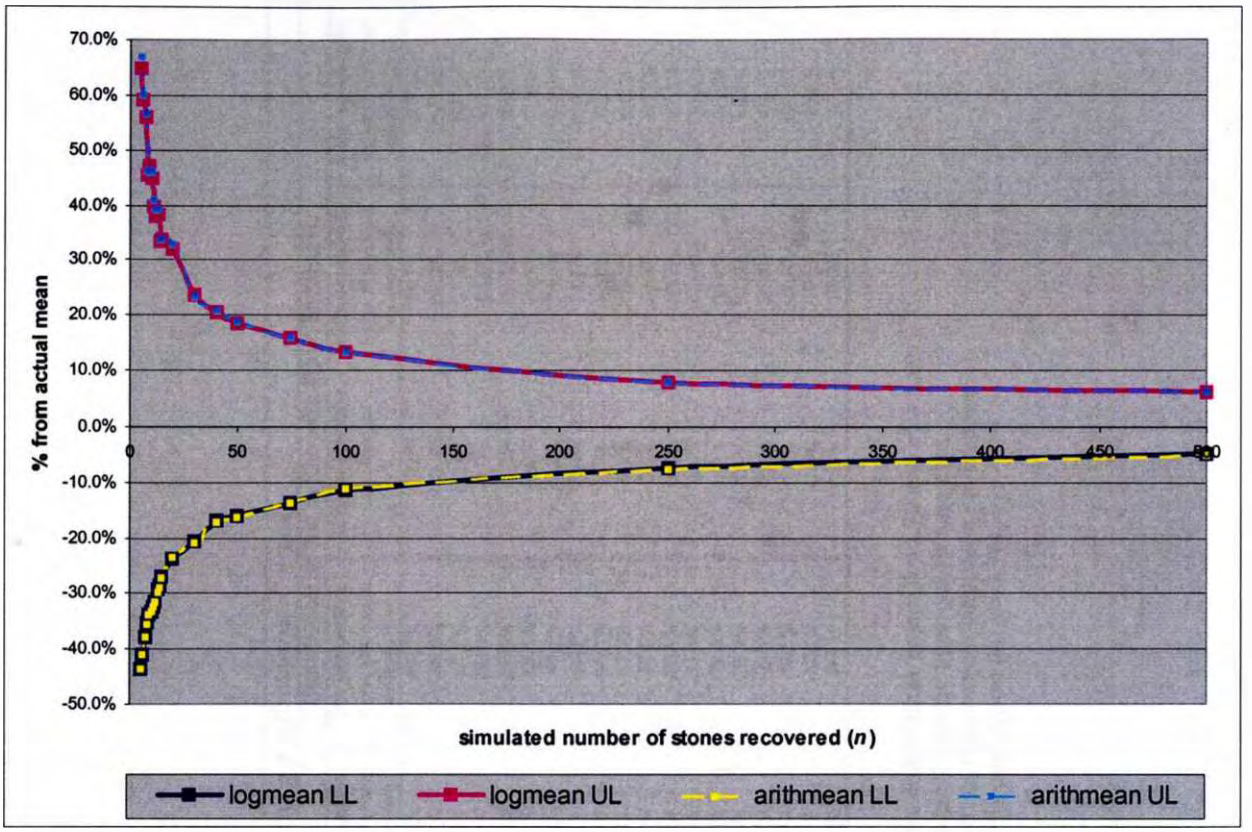

A graph of the 5th and 95th percentile values (90% central tendency limits) of the distributions of the mean estimates for the sample campaign simulation where μ = 0.40 cts/stn and σ^2 = 0.45. This represents a case, for diamond size-frequency distribution, which is likely to occur at Site 3. The 5th and 95th percentile values, for each value of *n*, are drawn from the distribution of 1500 values resulting from 1500 sample campaign realisations. Percentile values are expressed in terms of their percentage deviation from the actual mean of the population (ie. μ = 0.40 cts/stn).

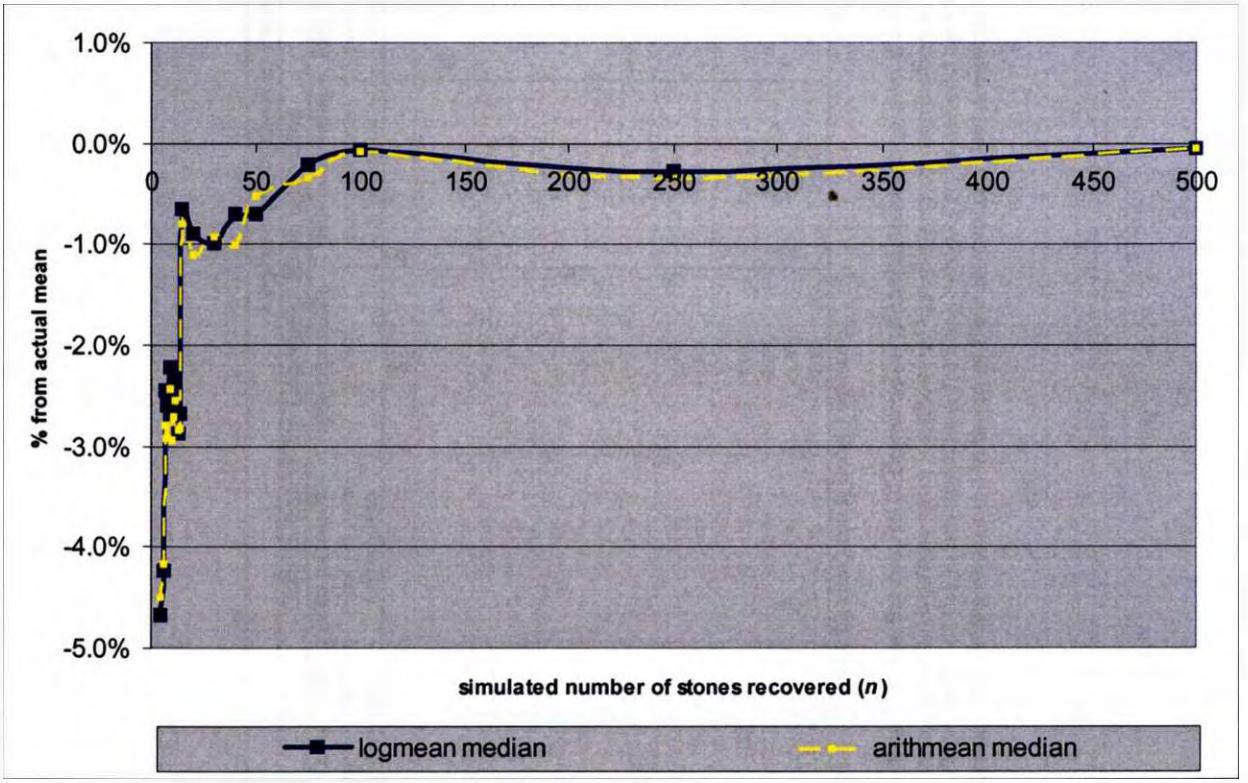

A graph of the 50th percentile values (medians) of the distributions of the mean estimates for the sample campaign simulation where μ = 0.40 cts/stn and σ^2 = 0.45. This represents a case, for diamond size-frequency distribution, which is likely to occur at Site 3. The 50th percentile values, for each value of *n*, are drawn from the distribution of 1500 values resulting from 1500 sample campaign realisations. Percentile values are expressed in terms of their percentage deviation from the actual mean of the population (ie. μ = 0.40 cts/stn).

	Lognormal Distribution Parameters for Simulation : μ = 1.70 cts/stn; σ^2 = 1.00									
	Distribution of the Lognormal Mean Estimates					Distribution of the Arithmetic Mean Estimates				
n	1st percentile (lower 98% central tendency limit)	5th percentile (lower 90% central tendency limit)	50th percentile (median)	95th percentile (upper 90% central tendency limit)	99th percentile (upper 98% central tendency limit)	1st percentile (lower 98% central tendency limit)	5th percentile (lower 90% central tendency limit)	50th percentile (median)	95th percentile (upper 90% central tendency limit)	99th percentile (upper 98% central tendency limit)
5	-75.4%	-62.2%	-11.8%	95.0%	203.5%	-75.3%	-62.7%	-12.4%	94.7%	201.9%
6	-68.2%	-56.2%	-10.4%	93.1%	194.0%	-68.4%	-58.0%	-10.4%	97.3%	191.2%
7	-66.6%	-57.2%	-13.0%	79.5%	159.5%	-66.3%	-57.7%	-12.6%	81.6%	157.5%
8	-63.7%	-53.2%	-7.9%	82.7%	148.1%	-65.0%	-52.8%	-9.0%	86.6%	147.3%
9	-61.2%	-49.4%	-6.6%	86.6%	136.4%	-61.0%	-50.1%	-6.7%	90.1%	159.6%
10	-58.4%	-48.4%	-7.3%	73.8%	135.2%	-58.7%	-49.1%	-7.2%	78.1%	136.9%
11	-57.4%	-47.4%	-7.3%	69.6%	124.0%	-57.6%	-47.5%	-7.2%	73.5%	132.8%
12	-54.9%	-44.4%	-6.1%	68.7%	121.0%	-55.8%	-44.7%	-6.9%	71.7%	124.5%
13	-55.5%	-44.0%	-6.9%	63.2%	115.9%	-55.9%	-44.1%	-7.3%	63.8%	122.2%
14	-52.7%	-42.9%	-4.6%	62.8%	98.0%	-53.4%	-43.2%	-5.4%	68.3%	105.3%
15	-51.2%	-42.7%	-5.0%	60.1%	101.1%	-52.7%	-43.9%	-5.4%	62.2%	99.2%
20	-46.0%	-36.2%	-3.7%	49.2%	80.2%	-46.8%	-36.1%	-3.8%	50.7%	87.3%
30	-39.6%	-32.1%	-2.4%	39.9%	68.9%	-40.6%	-32.6%	-2.6%	45.1%	71.4%
40	-36.5%	-28.6%	-2.4%	34.9%	54.0%	-37.7%	-29.4%	-3.3%	36.2%	55.8%
50	-32.5%	-25.0%	-1.5%	28.8%	44.1%	-33.1%	-26.2%	-1.9%	32.2%	48.1%
75	-27.1%	-21.1%	-1.6%	25.4%	36.4%	-28.6%	-22.1%	-2.2%	26.9%	43.1%
100	-23.4%	-17.8%	-0.8%	21.1%	31.3%	-23.5%	-18.5%	-1.4%	23.0%	36.3%
250	-16.9%	-12.0%	-0.6%	13.2%	19.4%	-17.3%	-12.2%	-0.6%	14.5%	20.6%
500	-11.7%	-8.7%	-0.3%	9.6%	14.2%	-12.2%	-9.1%	-0.3%	10.0%	15.6%

(grey numbers record the distribution of Sichel T estimates)

A summary of the the results of the sample campaign simulation over a two-parameter lognormal distribution, where μ = 1.70 and σ^2 = 1.00.
This represents an extreme case for diamond size-frequency distribution in the marine gravel deposits of the Sperrgebiet coastline.
The distribution of the mean estimates, for each value of *n*, is defined by 1500 values resulting from 1500 sample campaign realisations.
Percentile values are expressed in terms of their percentage deviation from the actual mean of the population (ie. μ = 1.70).

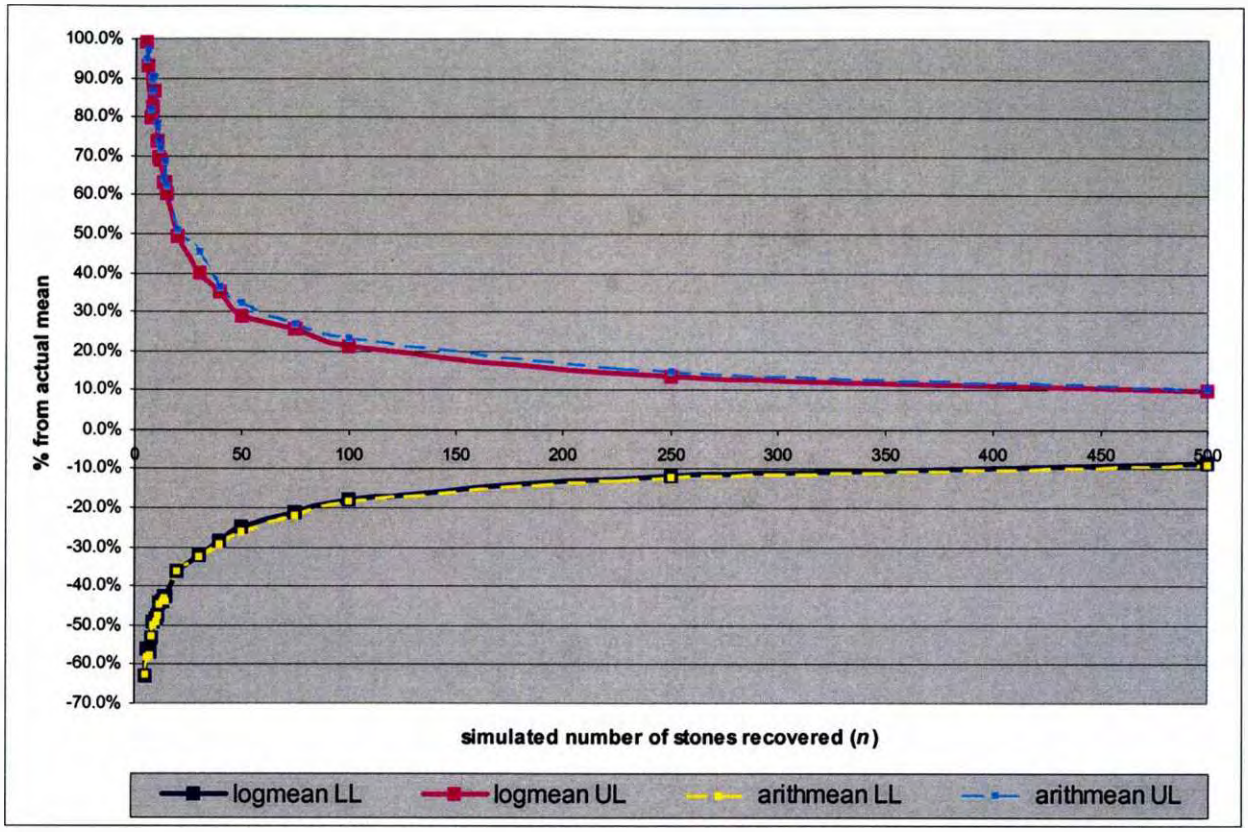

A graph of the 5th and 95th percentile values (90% central tendency limits) of the distributions of the mean estimates for the sample campaign simulation where μ = 1.70 cts/stn and σ^2 = 1.00. This represents an extreme case for diamond size-frequency distribution in the marine gravels of the Sperrgebiet, drawn from a sample of the linear gravel beaches in the south of MA1. The 5th and 95th percentile values, for each value of *n*, are drawn from the distribution of 1500 values resulting from 1500 sample campaign realisations. Percentile values are expressed in terms of their percentage deviation from the actual mean of the population (ie. μ = 1.70 cts/stn).

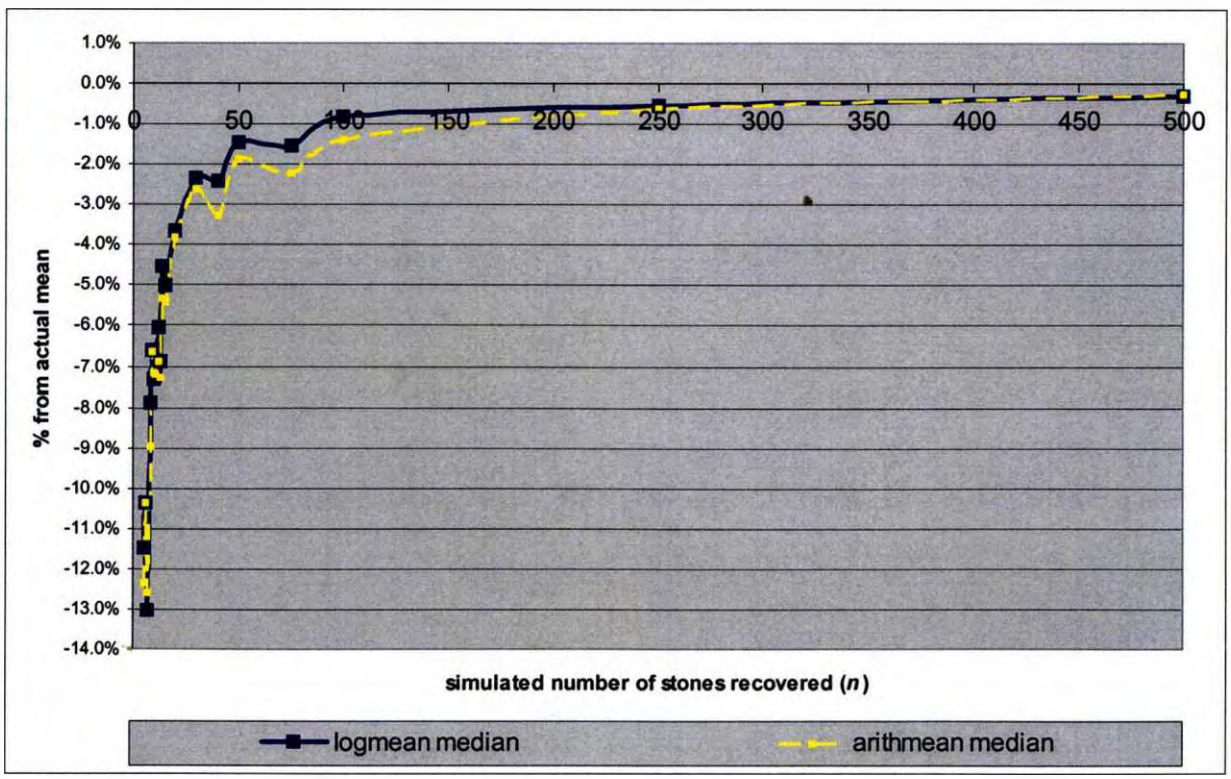

A graph of the 50th percentile values (medians) of the distributions of the mean estimates for the sample campaign simulation where μ = 1.70 cts/stn and σ^2 = 1.00 This represents an extreme case for diamond size-frequency distribution in the marine gravels of the Sperrgebiet, drawn from a sample of the linear gravel beaches in the south of MA1. The 50th percentile values, for each value of *n*, are drawn from the distribution of 1500 values resulting from 1500 sample campaign realisations. Percentile values are expressed in terms of their percentage deviation from the actual mean of the population (ie. μ = 1.70 cts/stn).